Faculty of Resource Science and Technology

Synthesis and Characterisation of Conjugated Bis-Schiff Base and The Boron Difluoride Complexes as Dye-Sensitiser for Dye Sensitised Solar Cell (DSSC) Application

Nursyafira Adzira Binti Halmi

Master of Science
2023

Synthesis and Characterisation of Conjugated Bis-Schiff Base and The Boron Difluoride Complexes as Dye-Sensitiser for Dye Sensitised Solar Cell (DSSC) Application

Nursyafira Adzira Binti Halmi

A thesis submitted

In fulfillment of the requirements for the degree of Master of Science

(Inorganic Chemistry)

Faculty of Resource Science and Technology
UNIVERSITI MALAYSIA SARAWAK
2023

DECLARATION

I declare that the work in this thesis was carried out in accordance with the regulations of Universiti Malaysia Sarawak. Except where due acknowledgements have been made, the work is that of the author alone. The thesis has not been accepted for any degree and is not concurrently submitted in candidature of any other degree.

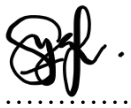

……

Signature

Name: Nursyafira Adzira Binti Halmi

Matric No.: 19020014

Faculty of Resource Science and Technology

Universiti Malaysia Sarawak

Date: 31 August 2023

ACKNOWLEDGEMENT

First and foremost, I would like to give my greatest thanks to Allah S.W.T. for His blessing and guidance to me throughout my up-and-down journey to complete this master's degree. Without His will, this will never happen at all. To my dear self, thank you so much for not giving up despite all those hardships and challenges you have been through in this journey. Although sometimes things seem impossible and you almost giving up so many times, thank you for still standing up and continue this journey.

Next, my sincere thanks go to my supervisor Associate Professor Dr Tay Meng Guan for his continuous guidance, invaluable assistance, and knowledge that he has shared with me during my research. This work would not have been possible without the constant support and encouragement from my supervisor. All his help and constructive comments have been so much help throughout the experimental and theses writing to the success of this research.

To my beloved family, especially my parents, thank you for your endless support, love, prayers, and encouragement. Thank you for always supporting me in whatever path I choose in life. To my siblings, although you guys never show it, I know I will always have your supports in whatever I do in life. Thank you for your helps directly or indirectly. I appreciate it so much.

To my friend and best co-worker, Sya, thank you so much for being there throughout my journey since degree year until my master's year. Without you, this journey will not be as fun as it is. Thank you for our lunches, playtime, mall time. During my ups and down you were always there by my side encouraging and supporting me. For sharing your every bit of knowledge with me and all your help thank you. I will cherish these memories forever. Also,

not forgetting my dearest colleagues, Kak Choomie, Victoria, Ciki, Aina, Michelle, Kak Seha for all the fun time we had together. Although it was only for a short time before you guys go on your own separate journeys, thank you for the friendship and memories that I will not forget. My sincere thanks to my best buddies for life, Amm, Noi, Nana, Uul, and Yaya for their emotional supports to me throughout my study journey especially for being good listener for me during my stressful times. Another circle of friends who have been there from since degree time, Nisa, Pjot, Nisa your support was always there with me and Sya even if we were far apart, thank you.

In addition, not to forget our UNIMAS technical staffs and lab assistant, Encik Ismadi, Encik Rajuna, Kak Ros, Kak Leida, Encik Raymond, Kak Yati, Encik Leo, Encik Wahab and Encik Ben for all their assistance and guidance in the instrumentation and lab supplies.

Finally, sincere gratitude to Zamalah UNIMAS and Yayasan Sarawak for providing financial helps throughout my study. Also, thank you to Universiti Malaysia Sarawak and Hexagon Highs for the opportunity to be appointed as the research assistance for their projects under the research grants [GL/F07/HEXA/2021] and [GL/F07/HEXA/02/2021]. Thank you to UNIMAS for providing facilities for my study since foundation up until today.

ABSTRACT

Schiff base and their metal complexes have been widely used as photovoltaic materials due to their excellent π-electron transfer properties along the molecule. In this study, a total of eleven conjugated symmetrical bis-Schiff base and its complexes with different π-spacers have been synthesised and spectroscopically characterised in order to investigate their conversion efficiency in dye-sensitiser solar cell (DSSC). All compounds were substituted either without any substituent or with hydroxy (-OH) or methoxy (-OMe) as the electron donor and difluoro boron (BF2) as the electron acceptor. The symmetrical bis-Schiff base compounds (**1a** – **4c**) were synthesised by using condensation reaction and further proceeded to undergo complexation with boron trifluoride diethyl ether to produce boron difluoride complexes (**1d** and **2d**). All compounds were adapted with some modifications from existing works but have not been tested as dye-sensitiser for DSSC. All the synthesised compounds were applied as dye-sensitiser in DSSC using titanium (IV) oxide (TiO_2) coated on a fluoride doped tin oxide (FTO) glass as the working electrode and electric paint containing carbon black and graphite coated indium tin oxide (ITO) glass as the counter electrode. The power conversion efficiencies (PCE) of the eleven bis-Schiff base compounds were tested using a 100W LED light with multimeter and resistance set up. The efficiencies result was compared to N3 Dye as the benchmark standard. The results showed that the compound with aromatic ring bridge as the π-spacer in *para*- position and methoxy (-OMe) substituent gave the highest efficiency at 0.0691% whereas compound with aromatic ring and difluoro boron (BF_2) gave the lowest efficiency at 0.0012%. The presence of strong electron donor and extended π-conjugation effect in the structure allows effective charge transfer along the molecule which affects the conversion efficiency of DSSC device.

Keywords: Conversion efficiency, dye-sensitised solar cells, dye-sensitiser, symmetrical bis-Schiff-base, π-conjugated system

Sintesis dan Pencirian Bes-Schiff Simetri yang Berkonjukasi serta Kompleks Boron Difluorida sebagai Pewarna Foton untuk Sel Solar Peka Pewarna

ABSTRAK

*Bes Schiff serta kompleks logamnya telah digunakan dengan meluas sebagai bahan fotovolta kerana sifat perpindahan elektron-π di sepanjang molekul. Sejumlah sebelas bes Schiff simetri terkonjugat dan kompleksnya dengan penjarak-π yang berbeza telah disintesis dan dicirikan secara spektroskopi untuk mengkaji kecekapan penukaran mereka di dalam sel solar peka pewarna. Kesemua sebatian telah digantikan sama ada tanpa apa-apa bahan ganti atau dengan hidroksi (-OH) atau metoksi (-OMe) sebagai penderma elektron dan boron difluorida sebagai penerima elektron. Sebatian bes Schiff simetri (**1a** – **4c**) telah disintesis melalui tindak balas pemeluwapan dan seterusnya manjalani pengkompleksan dengan boron trifluorida dietil eter untuk menghasilkan kompleks boron difluorida (**1d** dan **2d**). Kesemua sebatian telah diadaptasikan dengan sedikit ubah suai dari karya sedia ada tetapi belum diuji sebagai pewarna foton untuk DSSC. Kesemua sebatian yang telah disintesis telah digunakan sebagai pewarna foton untuk DSSC menggunakan titanium dioksida (TiO_2) yang disalut di atas kaca oksida timah terdop fluorida (FTO) sebagai elektrod kerja dan cat elektrik yang mengandungi hitam karbon dan grafit disalut di atas kaca oksida indium timah sebagai elektrod pembalas. Kecekapan penukaran kuasa (PCE) bagi kesebelas bes Schiff telah diuji menggunakan persediaan lampu LED 100W dengan multimeter beserta rintangan. Hasil kecekapan telah dibandingkan dengan pewarna N3 sebagai tanda aras piawai. Keputusan menunjukkan bahawa sebatian yang mengandungi titian gelang aromatik sebagai penjarak-π diposisi para- beserta bahan ganti metoksi (-OMe) memberikan kecekapan tertinggi sebanyak 0.0691% manakala sebatian yang mengandungi titian gelang dan boron difluorida (BF_2) memberikan kecekapan terendah*

sebanyak 0.0012%. Kehadiran penderma elektron yang kuat beserta kesan konjugasi-π yang diperpanjangkan di dalam struktur mengizinkan perpindahan cas yang berkesan disepanjang molekul mempengaruhi kecekapan penukaran peranti DSSC.

Kata kunci: *Kecekapan penukaran, sel solar peka perwarna, pewarna foton, bes Schiff simetri, sistem π-konjugasi*

TABLE OF CONTENTS

LIST OF TABLES

LIST OF FIGURES

LIST OF SCHEMES

Page

LIST OF ABBREVIATIONS

%	Percent
°C	Degree celcius
^{13}C	Carbon
^{1}H	Proton
Ag	Silver
AM	Air mass
BF_2	Boron difluoride
$BF_3.Et_2O$	Boron trifluoride diethyl ether
Br	Bromine
Br^-	Bromide
C	Carbon
C=N	Azomethine
C=O	Carbonyl
Cd	Cadmium
$CDCl_3$	Deuterated chloroform
CdO	Cadmium oxide
$-CH_3$	methyl
$CHCl_3$	Chloroform
Cl	Chlorine
Co	Cobalt
-COOH	Carboxyl
CSP	Concentrated solar power
d	Doublet

DAMN	Diaminomaleonitrile
DCM	Dichloromethane
DIPEA	*N*,*N*-Diisopropylethylamine
DMSO	Dimethyl sulfoxide
DSSC	Dye-sensitised solar cell
e^-	electron
EL	electroluminescent
eV	Electronvolt
F	Fluorine
FF	Fill factor
fs	Femtosecond
FTIR	Fourier-transform infrared
FTO	Fluorine-doped tin oxide
g	Gram
G	global
Ga_2O_3	Gallium(III) oxide
GC/MS	Gas chromatogram/Mass spectroscopy
H_2O_2	Hydrogen peroxide
Hg	Mercury
HOMO	Highest occupied molecular orbital
Hz	Hertz
I^-/ I_3^-	Iodide/triiodide
I_2	Iodine
ICT	Intramolecular charge transfer
In_2O_3	Indium(III) oxide

IR	Infrared
ITO	Indium tin oxide
J_{sc}	Short circuit current
KBr	Potassium bromide
KOH	Potassium hydroxide
kWh/m^2	Kilowatt hours per square metre
LED	Light-emitting diode
LUMO	Lowest unoccupied molecular orbital
m	Multiplet
m/z	Mass-to-charge ratio
mA	Milliampere
MeOH	Methanol
MHz	Megahertz
ml	Millilitre
mmol	Millimole
mV	Millivolt
N	Nitrogen
N_2O_2	Dinitrogen dioxide
NaOH	Sodium hydroxide
Nb_2O_5	Niobium pentoxide
Ni	Nickel
NLO	Non linear optics
nm	Nanometre
NMR	Nuclear magnetic resonance
O	Oxygen

o	Ortho
O_2	Oxygen
-OH	Hydroxyl
OLED	Organic light-emitting diode
OMe	Methoxy
p	Para
p.m.	Post meridiem
PCE	Power conversion efficiency
Pd	palladium
ppm	Part per million
p-Subst.	*Para*-substituent
Pt	platinum
PV	Photovoltaic
Ru	Ruthenium
s	Singlet
Sn	Tin
SnO_2	Tin(IV) oxide
t	Triplet
TCO	Transparent conducting oxide
TEA	Triethylamine
TiO_2	Titanium(IV) dioxide
TMS	Trimethylsilane
UV	Ultraviolet
UV-Vis	UV-Visible
W/m^2	Watt per square metre

Zn	Zinc
ZnO	Zinc oxide
π	Pi
π^*	Anti-pi
Ω	ohm
Ω/cm^2	Ohm per square centimetre

CHAPTER 1

INTRODUCTION

1.1 Solar energy

Many developing countries are emerging rapidly due to the increasing population, urbanisation and modernisation and continue in fast growing. The rise in energy demand caused many countries to source for the renewable energies in order to replace those conventional and non-renewable energy sources such as gas and coal. Solar, wind, biomass and geothermal energies are often the alternative renewable energy sources, which can be used to produce energy repeatedly with zero or almost zero emissions to the environment (Panwar et al., 2011).

Solar energy, like other renewable energy sources, is a promising and readily available source of energy to deal with long-term concerns in the energy crisis. Among other available renewable energy sources, solar energy is the most freely and highly available energy at almost everywhere at our planet. In average, around 342 W/m^2 of solar energy is absorbed in Earth atmosphere of which around 30% is dispersed and reflected back to space, leaving approximately 70% (239 W/m^2) available for harvesting and capture. Annual effective solar irradiance received by Earth ranges from 60 – 250 W/m^2 (Kabir et al., 2018).

Malaysia has a diverse range of energy resources, including oil, natural gas, coal in which renewable energy include biomass, hydro and solar. Despite having abundant natural resources, Malaysia mostly reliant on fossil fuels for industrial and transportation sectors. For Malaysia's long-term sustainable energy development, renewable sources became more appealing in which the most notable sources are biomass and solar energy (Shafie et al.,

2011). Since Malaysia is a country surrounded by sea and located near the equator, Malaysia naturally received daily solar irradiations of 4.21 kWh/m^2 to 5.56 kWh/m^2 according to Malaysian Meteorological Department. In average, Malaysia received about 6 hours of sunlight per day and the highest recorded solar radiation was 6.8 kWh/m^2 in August and November (Shafie et al., 2011). On the other hand, the highest temperature recorded is 37.5 °C in 2018 whereas the average peak direct radiation is around 297 W/m^2 at 12 p.m. and the absolute peak direct radiation is 865 W/m^2 at 2 p.m. Thus, the climatic conditions of Malaysia make it favourable for the development of solar energy. However, as Zulkifli (2021) stated that in Malaysia, despite solar photovoltaics has been considered as a long-term renewable energy source in the country, it was accounted for less than 1% of total power generation in 2018. This could be due to the price of the solar panel which is much higher than conventional energy supply, and the duration of solar panel. In many cases, the solar panel and its' batteries were encountered with malfunctions which have limited use of solar energy in our Malaysian households.

1.2 Photovoltaics technology

There are two main techniques that usually being used in solar technologies which are concentrated solar power (CSP) and photovoltaics (PV). CSP techniques provide power by focusing the energy collected from sun to water or any other working medium whereas PV techniques provides electricity by depending on photoelectric effect (Dong et al., 2012).

Photovoltaics energies are categorised as 3 different major generations. The first generation of PV are crystal silicon wafer-based cells which is currently the dominant cell technology account for 90% of commercial global solar cells market (Gul et al., 2016; Milichko et al., 2016; Shubbak et al., 2019). This type of solar cells is the oldest and most

widely used technology owing to their high efficiencies. While the first generation silicon based solar cells continue to lead the market, second generation of PV technologies begin to emerge when researchers all around the world start looking and exploring various other options to produce power more efficiently using solar cells (Pandey et al., 2016). Second generation solar cells technology is thin-film technology which require less or no silicon during the production process (Gul et al., 2016). In thin film technology, the thin layers of semiconductors materials are deposited into a large sheet of glass which act as a supporting substrate or superstrate as shown in Figure 1.1. To compare, this technology only requires less than a micron thickness of semiconductor material which is around 100-1000 times lesser than silicon wafer (Green, 2000). Despite the changes brought by the second generation solar cells, it turned out that this technology was not successful as the second generation solar cell only occupies 10% of the market. This is because the second generation solar cell only generates average 15% efficiency and resulted in no significant growth (Milichko et al., 2016). Another reason is that this technology produces high toxicity from the multicomponent semiconductors as well as from some of the starting materials.

Figure 1.1: Thin film technology

The improvement stage to solve these known problems has brought up the development of third generation solar cells. These types of solar cells are different from the former generation where the light absorption and charge transport functions are separated at different part of the devices (Rawal et al., 2015). This generation solar cells which includes

Organic, Perovskites and Dye-Sensitised Solar Cells (DSSC) are still in the development and still uncommercialised technology (Nain & Kumar, 2021). These technologies are highly promising but not yet commercially proven (Mohanta et al., 2015). Among the solar cell technologies from third generation, dye sensitised solar cells are one of the most developed third generation solar cell types. Due to their improved properties, many researchers are doing extensive research to produce this technology (Nain & Kumar, 2021). Dye-sensitised solar cells (DSSC) are developed based on dye molecules sandwiched between two electrodes where electron hole pairs of the dye molecules are transferred through TiO_2 nanoparticles (Mohanta et al., 2015). DSSCs are made up of nanostructured metal-oxide electrodes such as nanoporous TiO_2, dyes, iodide/triiodide electrolytes and counter electrode stack together like a sandwich. According to Mohanta (2015), DSSC recorded a maximum efficiency of only 11.9% but offered a cheap and flexible cell. Even so, there are a few major disadvantages that many researchers are currently trying to look for other variety of options to improve this technology. This include the usage of liquid electrolytes which are prone to leakage and vaporisation under high temperature (Venkatesan et al., 2019). Nevertheless, DSSC is still a promising improved technology that have a bright future ahead.

Referring to Figure 1.2, solar cells from first and second generation started being developed around 1970s and the first generation solar cells offer the highest efficiencies followed by second generation till date (National Renewable Energy Laboratory, 2017). As for the emerging PV technology, it started around 1990s and still have the lowest efficiency compared to other technology. However, despite having the lowest efficiency so far, it can be seen from the chart that the trend for emerging PV increase more rapidly in few years' times (Shelke et al., 2013).

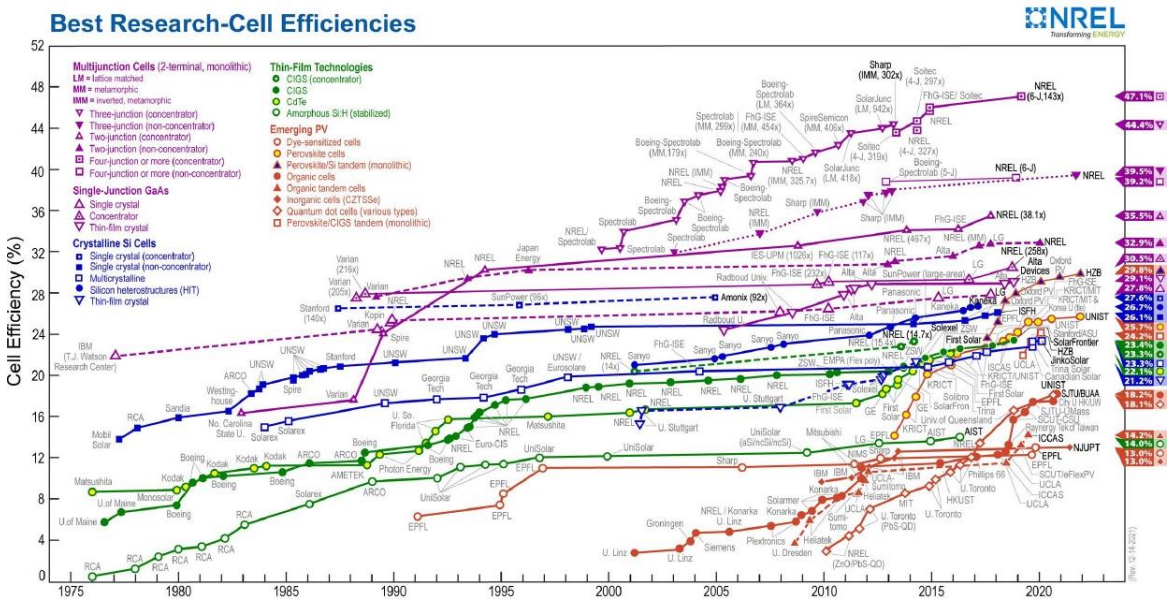

Figure 1.2: Best research cell efficiencies obtained from NREL (Retrieved from https://www.nrel.gov/pv/)

1.3 Operation principle of DSSC

DSSC device consists of two electrodes, one of which a nanocrystalline semiconductor material with a large band gap such as titanium dioxide (TiO_2) sensitised with dye and the other of which a platinum doped, or graphite coated working electrode (Figure 1.3) (Shelke et al., 2013). The gap in between those electrodes is filled with electrolyte solution to complete the composition.

When sunlight hits the DSSC device, the monolayer of the charge-transfer dye that were sensitised to the nanocrystalline semiconductor material absorbs photons and undergo photoexcitation resulting to the injection of electron into the conductor band of the oxide. Across the semiconductor interface, charge separation occurs where the electron from the dye moved into the TiO_2 leaving a hole in the oxidised dye molecule. The electrons propagate through the TiO_2 porous network until reaching the working electrode which is where the charge collection and charge extraction take place. Extracted charge will then travel across

the external circuit to perform electrical work and return to the counter electrode where reduction occur. The electrolyte located between the dye and counter electrode are served to reduce the oxidised dye restoring the dye to its original state. The regeneration of the dye to its original state intercepts the dye from recapturing of the electron from the conduction band (Grätzel, 2003). Continuous injection of electron from the photo-excited dye into the semiconductors resulted in the current flows in the circuit. Overall, the devices do not suffer any permanent chemical transformation when generating electric power from light (Hagfeldt et al., 2010).

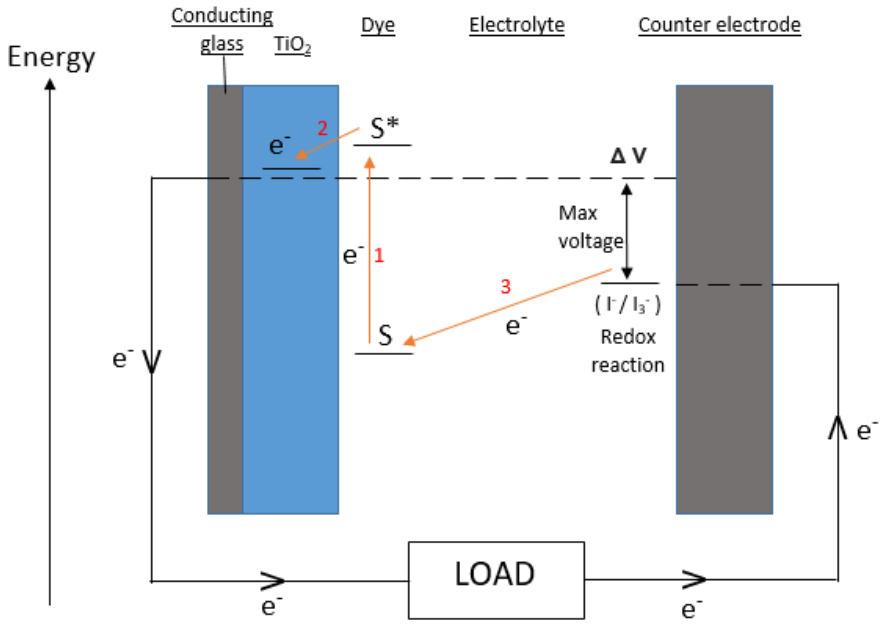

Figure 1.3: Simple energy level diagram for DSSC operation principle

The lowest unoccupied molecular orbital (LUMO) energy of the used photosensitiser should be larger than the conduction band of the semiconductor in order to allow successful injection of electron. Meanwhile, the highest occupied molecular orbital (HOMO) energy of the photosensitiser should be smaller than the electrolyte (Yahya et al., 2021). In addition,

the excited state of the photosensitiser should be higher than the conduction band to ensure the electron transfer process can take place while its oxidised state level should be more positive than redox potential of electrolyte for the dye to be regenerated back to its original state (Hagfelt et al., 2010). Yahya and co-workers (2021) also stated that the rate of electron injection should be faster that the degeneration of the dye from its excited state to its relaxed state. Therefore, a successful electron injection and dye regeneration can be attained.

1.4 Essential requirements of dye sensitiser for DSSC

Dye sensitiser is one of the most important components in DSSC. It acts as a photosensitiser, which in charge of the absorption of light and converting it into electrical energy (Semalti & Sharma, 2020). The performance of DSSC is mostly determined by the dye used as the photosensitiser (Alhamed et al., 2012). To serve their purposes efficiently, typical photosensitiser should have the following criteria such as: (1) a deep, broad and strong absorbance that cover the whole visible region and near-infrared (NIR) region of the solar spectrum which resulting in a high molar absorbance coefficient; (2) strong absorption of the dye particles that bind deeply onto the semiconductor surface; (3) anchoring group such as -COOH, -OH, or -O to bind with semiconductor to increase the rate of electron transfer; (4) rate of transfer of electron injection must be faster than the decay of the dye; (5) higher energy level of the dye excited state than the conduction band of semiconductor to ensure the electron injection process can take place; (6) more positive oxidised state energy level of the dye than the redox potential of the electrolyte; (7) more positive potential and small energy gap of the HOMO level of the dye than the valence band level of semiconductor as well as larger LUMO energy than the conductor band level which allow successful injection into semiconductor; (8) avoid undesirable dye aggregation on the semiconductor surface so that non-radiative decay on the excited state to the ground state can be avoided;

and (9) good photostability, thermal stability and electrochemical stability (Hagfelt et al., 2010; Shalini et al., 2016; Semalti & Sharma, 2020; Yahya et al., 2021). In this study, the synthesised compounds possess some of the required criteria such as criteria; (1), (2), (3), (4) and (9) to be applied as dye sensitiser in DSSC.

Chemical dyes, organic dyes and natural dyes have been widely used and studied as a photosensitiser for DSSC device. Most well-known chemical dyes in this field are Ru-based dyes which was developed by Grätzel and his team (2003). It is recorded that these Ru-based dyes has achieved efficiency of near 11-12%. However, due to the ruthenium toxicity, less accessibility, uneconomical and unfavourable procedure, many researchers are looking for alternatives dyes that does not require heavy metals such as ruthenium (Richhariya & Kumar, 2018).

Metal-free dyes which include natural dyes and organic dyes are being researches as an alternative to Ru-based dyes. Research of Ru-free dyes intensifies as they offer a low cost, environmentally friendly process, design versatility and have broad and intense absorption properties (Naik et al., 2018). Besides, they also have a better molar extinction coefficient and a diverse molecular structure (Shalini et al., 2016). These types of dyes have recorded an efficiency of 9.8% (Semalti & Sharma, 2020). However, both metal-free organic dyes and natural dyes have several drawbacks which include a shorter excited state excitation lifespan than metal complexes and aggregation-induced self-quenching in the visible range (Mahadevi & Sumathi, 2020).

It is discovered that Schiff base and their complexes is easy to prepare and has a favourable optoelectronic property, greater stability in the oxidised state, and photochromic behaviour. Therefore, in the past few years, many researchers are gaining interest on Schiff

base as an alternative sensitiser in DSSC to overcome the disadvantages of Ru-based dyes and metal-free organic sensitisers as mentioned above (Mahadevi & Sumathi, 2020).

1.5 Introduction and applications of Schiff base and its' metal complexes

Schiff base was first found by a scientist named Hugo Schiff in 1864 when he described the condensation reaction between an aldehyde or ketone and an amine (Cozzi, 2004; Ashraf et al., 2011). Schiff base is a compound with the structure of azomethine group (-C=N-). They are usually synthesised by condensation reaction of aldehyde or ketone with a primary amine usually under acids or base catalysis or also with heat (Scheme 1.1) (Sinha et al., 2008; Xavier & Srividhya, 2014). Basically, Schiff base are formed when the carbonyl group of aldehyde or ketones are replaced by the nitrogen group of an amine in a condensation reaction (Goel et al., 2014). The resulting imines are the one that can bind to the metal ions via the lone pair electron of nitrogen (Gupta & Sutar, 2008). Aromatic Schiff base are known to be more stable especially those that have a good conjugation system mean while aliphatic Schiff bases are unstable and prone to polymerisation. In addition, Schiff base are more readily formed with aldehyde compared to ketone (Xavier & Srividhya, 2014).

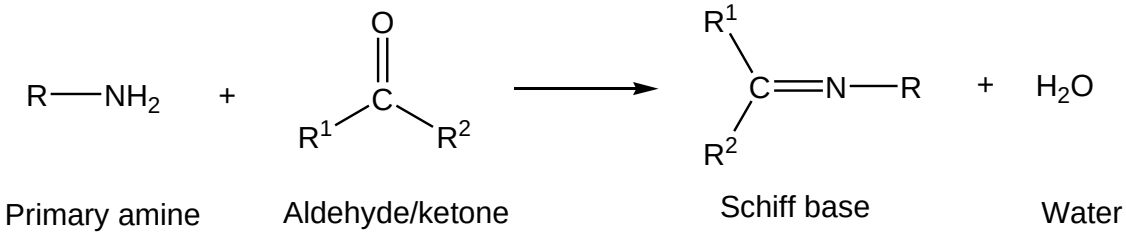

Scheme 1.1: The formation of Schiff base

Until now, Schiff base have been extensively used for industrial purposes as pigments and dyes, catalysts, active transport, liquid-liquid extraction, as an intermediate in organic synthesis and also as polymer stabilisers (Da Silva et al., 2011; Al Zoubi et al., 2017).

Besides, in most literature, it has been reported that Schiff base is also biologically important for example, as an antimicrobial, antifungal, antibacterial, anti-inflammatory and antitumor activity (Sinha et al., 2008; Da Silva et al., 2011; Sinthuja et al., 2018; Kuddushi et al., 2018). The presence of the imine group in the compound has contribute to the important use in biological activities (Da Silva et al., 2011). Kuddushi and coworkers (2008) in their work stated that complexation of Schiff bases with variety of metal ions also hold a very important role in the development of coordination chemistry field. Complexes of Schiff bases also have good properties in anticorrosion (Elemike et al., 2019) and anti-microbial (Pervaiz et al., 2021). Some of the complexes have been widely used for insecticides, herbicides, and fungicides (Zhu et al., 2000; Xu et al., 2017; Shakdofa et al., 2018).

Schiff base is considered as "privileged ligands" (Cozzi, 2004) because Schiff base complexation with almost all metals is stable and most of synthesised Schiff base complexes have shown excellent catalytic activity in various reactions even at elevated temperature and in presence of moisture. Schiff bases metal complexes have been studied widely over the past few years as the photosensitiser for DSSC due to their high thermal and moisture stabilities. Many soluble extended π-conjugated materials based on Schiff base metal complexes have been studied as sensitisers for wide-bandgap oxide semiconductors like TiO_2 and have shown a good degree of conversion of an incident photon to electric current (Mahadevi & Sumathi, 2020). An array of energy applications has been found for them, including light/electricity signal converters in organic light-emitting diodes and dye-sensitised solar cells, energy storage, and possible conductive thermoelectric materials (Zhang et al., 2018). According to Lokhande and coworkers (2019), one of the reasons for Schiff bases can be utilised as dye-sensitiser for DSSC is that they can absorb visible radiation and undergo charge transitions.

Salicylaldehyde and diamine-derived transition metal complexes of N_2O_2 Schiff base have sparked a lot of interest as a promising class of luminous materials. For example, *N,N'*-bis(salicylimine)-1,2-ethylenediamine (salen) [Figure 1.4 (a)] and *N*,*N*'-bis(salicylimine)-1,2-phenylenediamine (salphen) [Figure 1.4 (b)] which have fascinating electroluminescent (EL), nonlinear optical (NLO), and catalytic capabilities (Zhang et al.,2018).

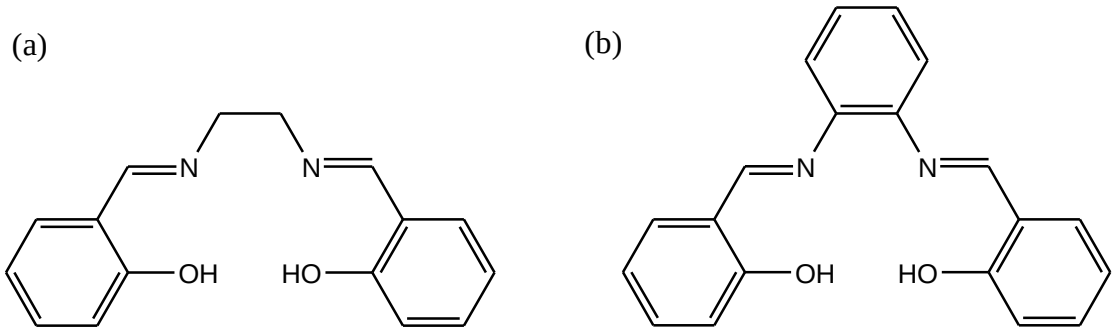

Figure 1.4: Structure of metal complex of (a) salen and (b) salphen

When [M(salen)] is utilised as a photosensitiser in a DSSC cell, rapid electron transfer from the excited state of [M(salen)] to the band zone of TiO_2 occurs instead of reaction with O_2 (Zhang et al., 2018). Because of their electron transfer behaviour, salen metal complexes have peculiar qualities such as ease of synthesis and chemical modification, high stability assured by chelating ligand, variable magnetic, optical, and redox activity (Tsaturyan et al., 2018).

1.6 Boron difluoride complexes

The design and synthesis of boron-containing compounds with prospective applications in functional materials, such as organic light-emitting devices (OLEDs), nonlinear optics, fluorescent and fluoride ion sensors, and biomolecular probes, has recently received a lot of attention (Hou et al., 2007; Shanmugapriya et al., 2016; Zhao et al., 2019).

In terms of luminescent materials, boron-containing complexes, in particular N,N-, O,O- and N,O-chelated difluoroboron complexes, are desirable fluorophores because of the easily tuneable ligand structure, high molar absorption coefficients, large Stokes shift, high fluorescence quantum yields in solutions and solid states, and photochemical stability (Zhao et al., 2018). Such complexes can have their optical characteristics modified primarily by selecting the suitable ligand to act as a chromophore. There is a broad range of potential structures, but among them, borinic complexes with (O,N) chelating ligands have received the most attention, probably because they typically have a high degree of stability (Wesela-Bauman et al., 2015).

It is known that boron is a strong electrophilic as it can complete the octet by filling the vacant orbital. Owing to that fact, in general, organoboron compounds are more stable compared to organometallic compounds because the covalency of B–O and B–N bonds has increased (Hou et al., 2007). In addition, the boron atom function is to stabilise an anionic chelating (O,N)-ligand which explains why the lowering of the LUMO level. As a result, to maintain the desired optical properties of a compound, the stability of B-N and B-O bonds is important (Wesela-Bauman et al., 2015). Following to the stabilisation of B-N and B-O bonds, boron complexes also may offer additional stability to overcome the instability of imine (C=N) bonds in Schiff base structure as emitting materials (Hou et al., 2007).

According to Agren and co-workers (2020), organic fluorescent dyes are perceived as promising materials due to its transdisciplinary uses in various industries such as bioimaging, chemosensors, Organic light emitting diodes (OLED), explosives detection as well as DSSC. The importance of heterocyclic coordination centers with N, O, π-conjugated ligands has led to the development of several novel luminous dye families. These

chromophores' exceptional fluorescent colour is due to the extent of their π bond conjugated system. Notably, it is known that four coordinated boron complexes have shown an outstanding fluorescent properties (Chaabene et al., 2019; Agren et al., 2020). Interestingly, four-coordinate boron(III) complex are reported to be more stable than tri-coordinate boron compounds (Shanmugapriya et al., 2016).

1.7 Problem statement

According to the properties of a Schiff base metal complexes stated in the previous section, Schiff base has met the criteria of a typical photosensitiser as stated in (1), (2), (3), (4) and (9) in Section 1.4. A vast number of Schiff base compounds have been studied as a dye sensitiser in DSSC but the recorded PCE still have not reach efficiency needed to be commercialised. However, Bis-Schiff base analogue with two imine group (-C=N-) still not gaining many interests from the scientists to be applied as dye sensitiser. In addition, the application of boron-containing compounds in functional materials such as OLED, fluorescent and non-linear optics has been receiving a lot of attention however it was discovered that there has not been enough research on the complexation of bis-Schiff base derivatives with boron difluoride, and there haven't been many published articles about their use in DSSC. Therefore, as Schiff bases compound well known for its ease of preparation, modification, and complexation, it can be easy to design the structure according to the ideal criteria needed by a photosensitiser such as the presence of extended aromatic structure for better conjugation effect. The presence of an extended conjugated materials and good electron donor in the structure of Schiff base facilitates the electron movement along the structure which can improve the charge carrier mobility thus increasing the degree of conversion of an incident photon to electric current. Thus, in this research, four series of

conjugated bis-Schiff base derivatives (Figure 1.5) with different substituent and π-spacer were synthesised in order to investigate their effect to the conversion efficiency in DSSC.

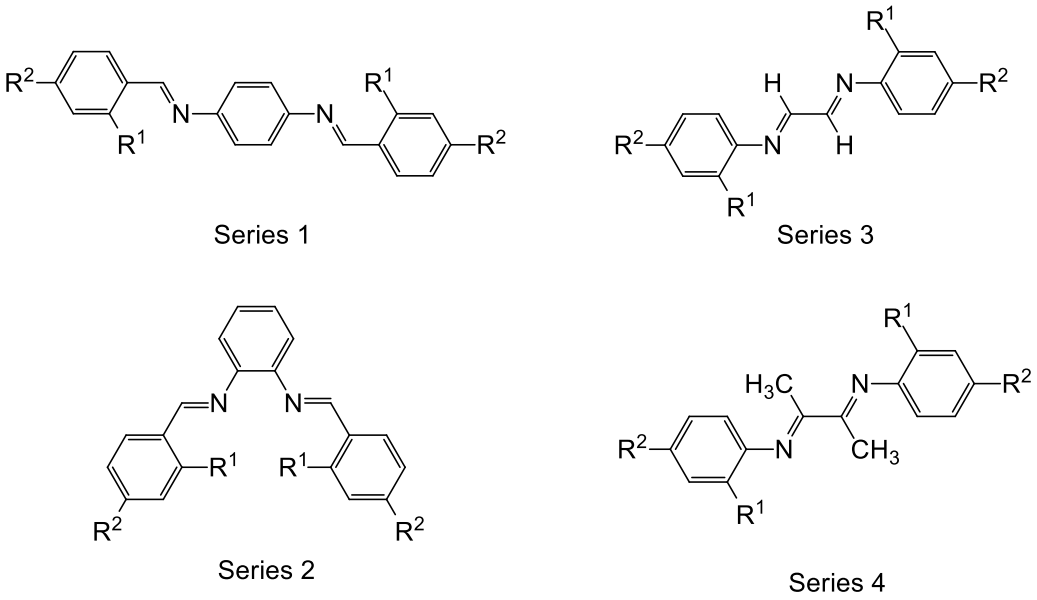

where, 1a/2a/3a/4a : R^1 = H, R^2 = H
1b/2b/3b/4b : R^1 = OH, R^2 = H
1c/2c/3c/4c : R^1 = H, R^2 = -OMe
1d/2d/3d/4d : R^1 = H, R^2 = -COOMe

Figure 1.5: Four series of Schiff base derivatives with different substituent

1.8 Objectives

This research was aimed to carry out the following objectives based on the hypothesis that the conversion efficiency in solar cells can be improved by changing the molecular structure and its substituent of the molecule:

i. To synthesise and characterise four series of Schiff bases with different molecular structure and substituent and its boron difluoride complexes.

ii. To fabricate all the synthesised Schiff bases and its complexes using thin film method as dye sensitiser in DSSC.

iii. To determine and elucidate the power conversion efficiency of the synthesised compounds and its relation to molecular structure.

1.9 Scope of the thesis

To convey the work of this research, the thesis is divided into five chapters. The first chapter in this thesis start with the Introduction which discusses the importance of solar energy as an alternative source of renewable energy, the trend of photovoltaics energy, DSSC mechanism and its dye sensitiser essential requirements and introduction of Schiff base. Next, the second chapter of this thesis is the Literature Review which discusses about the component of a DSSC cell and its role in solar conversion efficiency followed by the synthesis pathway of a Schiff base compounds and complexes as well as its application.

Meanwhile, the third chapter of this thesis described the methodology and the spectroscopic data of the synthesised compounds as well as the fabrication of DSSC and its calculation method. In chapter 4, all the analysis of the data and results of synthesis part and fabrication part are discussed. The spectroscopic data and efficiency data are presented in this chapter as well. Finally, the last chapter of this thesis is Chapter 5 which includes the conclusion of the whole project and suggestion for future works.

CHAPTER 2

LITERATURE REVIEW

2.1 Components of DSSC and their vital role in solar conversion efficiency

Based on the principle described earlier, a complete set of a DSSC device is made up of a transparent conductive oxide (TCO), a semiconductor, a dye-sensitiser, redox electrolyte, and a counter electrode arranged in a sandwich-like arrangement (Figure 2.1). Each of the materials have their own functions that allow electron to complete the circuit and generate energy. Therefore, it is critical for each component to play its vital role in order to successfully convert visible light into electrical power. In the following sub-chapters, studies on the materials used in each component are examined and addressed.

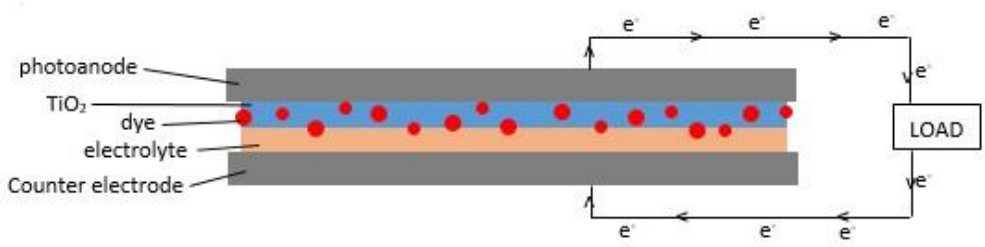

Figure 2.1: Arrangement of DSSC device

2.1.1 Glass substrate material

The conventional electrode used in DSSCs is made of transparent conducting oxides which are usually known as TCO, coated with glass substrates to which they are assembled (Ikpesu et al., 2020). TCO has been widely employed in DSSCs because it combines the physical features of visible light transmittance for light harvesting with electrical conductivity for current collection (Wang et al., 2009). Furthermore, TCOs are commonly

used in DSSCs due to their inexpensive cost, abundance, and good optical transparency in the visible and infrared regions of the sun spectrum (Ikpesu et al., 2020). TCO component is crucial because it is responsible for transmitting incoming light and collecting electrons that are transferred through the TiO_2 nanostructure (Yoo et al., 2010). According to Suhaimi and his coworkers (2015), highly transparent TCO substrates (transparency > 80%) are important to allow the most amount of sunlight reaching the active region.

As a photoanode for DSSCs, TCO should have low electrical resistance, high optical transmittance and high photoelectrical responsiveness (Kwak et al., 2011; Noh et al., 2012). To make TCO electrically conductive, they are doped with metal oxide semiconductor that have a broad band gap (~3 eV) such as SnO_2, In_2O_3, ZnO, CdO and Ga_2O_3 (Noh et al., 2012). Among the listed semiconductor, Sn-doped In_2O_3 (ITO) and F-doped SnO_2 (FTO) are well-known and widely used (Suhaimi et al., 2015; Kwak et al., 2011). In addition, ITO films have a transmittance of over 80% in the visible region and a sheet resistance of around 18 Ω/cm^2 meanwhile FTO films have a transmittance of about 75% and a sheet resistance of 8.5 Ω/cm^2 (Suhaimi et al., 2015). Notably, in the standard preparation of a DSSC device, the semiconductor (TiO_2) needs to be sintered on the TCO substrates at a high temperature (400-500 ℃) in order to eliminate any organic compounds in the TiO_2 and for a good adhesion between TCO substrates and TiO_2. Any reduction of the sintering temperature can affect the efficiency of the cell. (Sheehan et al., 2015). Between FTO and ITO, FTO are more preferred as a TCO because of its heat-resistance properties compare to ITO which are less preferred as it has a lesser heat resistance (Yoo et al., 2010). A study also has been done to compare between FTO and ITO in which both are sintered at 450 ℃. The results shows that the sheet resistance of ITO increase from 18 Ω/cm^2 to 52 Ω/cm^2 after sintering meanwhile sheet resistance of FTO remained unchanged and the overall efficiencies are 9.4% and 2.4% for

FTO and ITO respectively (Suhaimi et al., 2015). Therefore, FTO are the most recommended TCO substrates to be used in DSSC because of its stability at high temperature, conduction properties, stable sheet resistance temperature, stable in acid temperature, low-cost and good optical and electrical properties (Ikpesu et al., 2020; Noh et al., 2012; Sheehan et al., 2015; Suhaimi et al., 2015).

2.1.2 Metal oxide semiconductor

Metal oxide semiconductor is a thick nanoparticle layer is located at the middle part of DSSC. It provides a wide surface area for light-harvesting absorption molecules which accept electrons from photoexcitation of dye sensitiser (Suhaimi et al., 2015). To form a photoanode, the TCO glass substrates are deposited with a nano structed metal oxide semiconductor. Electronic conduction is enabled by the interconnection of these molecules (Suhaimi et al., 2015; Ikpesu et al., 2020). Some examples of common metal oxide used in DSSC is TiO_2, ZnO, SnO_2, Nb_2O_5 and more.

In the DSSC, the presence of an oxide semiconductor layer is critical for converting light energy into electrical energy. Furthermore, the interaction between the dye and the semiconductor oxide particles will be critical in deciding how light energy is converted into electrical energy (Sofyan et al., 2018). The oxide film binds the dye molecules, collects photogenerated electrons from the dye molecules' LUMO level, and provides a passage for the electrons to be transported to the TCO (Lee & Yang, 2011). Therefore, it is important for a metal oxide semiconductor to have a large surface area to bind a large amount of dye, high light-harvesting efficiency, high and rapid electron movement, low electron recombination, conduction energy level located in between LUMO level of dye-sensitiser and redox level or electrolyte and chemical stability (Lee & Yang, 2011; Pan et al., 2013).

In addition, it is also important for it to have a nanoporous film because it is widely known in nanomaterials fields that the smaller the particle size is, the surface area to volume ratio of a material will be greater (Sofyan et al., 2018). Thus, the smaller the particles of metal oxide semiconductor are, the higher surface interaction and faster electron injection can be achieved, hence, improve the device efficiency (Lei et al., 2010; Sofyan et al., 2018).

Most common metal oxide semiconductor that is widely used in DSSC is titanium dioxide (TiO_2) and zinc oxide (ZnO). Due to its high efficiency, low cost, stability, ease of preparation and catalytic activity, TiO_2 is more preferred than ZnO (Kumar et al., 2020; Sofyan et al., 2018). Furthermore, according to Pan and coworkers (2013), TiO_2 also possesses excellent physicochemical qualities, including heat resistance, a high refractive index, and a large band gap. These properties satisfy the needed properties to enhance DSSC performance. Although ZnO are found to be an excellent alternative to TiO_2 due to similarity in its properties, ZnO dissolves in iodide/triiodide electrolyte which lower the efficiency (Kumar et al., 2020).

TiO_2 is further categorised in 3 polymorphs phase which is rutile, anatase and brookite. To date, anatase TiO_2 are more preferred as it satisfies the requirements needed. Among all three, anatase phase are more stable chemically as it has a high conduction band energy (3.2 eV) meanwhile rutile approximately has conduction band of 3 eV. Plus, previous study also stated that anatase nanoparticle can load more dye sensitiser and has a higher electron diffusion coefficient as well as can generate 30% more short circuit current than rutile (Lee & Yang, 2011; Suhaimi et al., 2015). Thus, anatase TiO_2 are better metal oxide semiconductor to be used in DSSC devices.

2.1.3 Dye-sensitiser

The active material that attached to the layer on semiconductor is known as dye sensitiser. Sensitiser acts as the solar light harvester in the DSSC which is one of the most important components in DSSC as it affects the light harvesting efficiency and photoelectric conversion efficiency in overall (Alhamed et al., 2012). Aside from being a light harvester, a sensitiser also helps pumping the electron from the excited dye into the conduction band of the TiO_2 layer along with accepting electron from redox electrolyte to complete the cycle (Shalini et al., 2016).

In addition, the placements of the energy levels at the oxide/dye/electrolyte interference are critical to the DSSC's function (Hagfeldt et al, 2010). A sensitiser should possess a HOMO and LUMO level of an excited dye around 0.2-0.3 eV above the conduction band of TiO_2. The energy level of LUMO should be higher than the energy level of semiconductor conduction band meanwhile the energy level of HOMO must be lower than redox couple (Figure 2.2) This is to avoid back reaction from happening as the activation energy level for the dye to undergo reduction increase thus leads to less competition with dye regeneration by the redox electrolyte (Shalini et al., 2016; Yahya et al., 2021).

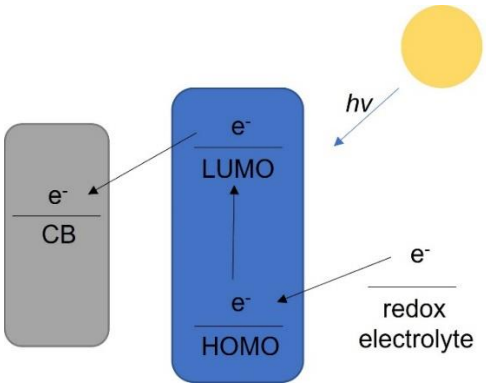

Figure 2.2: Energy level of electron movement in DSSC

Furthermore, the presence of anchoring group in the dye structure helps it to bind deeply onto the surface of TiO_2 semiconductor (Yahya et al., 2021). When the dye bind to the surface of TiO_2, it forms a monomolecular layer which ensure the probability of relaxation of the dye increases (Shalini et al., 2016). Few examples of commonly used anchoring group is -COOH, -OH, -O. Carboxylate group (-COOH) form ester bond with TiO_2 thus allowing better electron movement throughout the process. (Shalini et al., 2016).

Rate of charge injection and charge recombination also affect the cell efficiency. To compare, the rate of electron injection to conduction band occurs in femtosecond (fs) to picosecond time scale meanwhile charge recombination occur in micro to milliseconds. Thus, reverse reaction of the electron from conduction band into the oxidised dye can be prevent since the reaction is much slower than reduction from redox electrolyte. (Shalini et al., 2016). Apart from that, the stability of the sensitiser should be enough to sustain about 10^8 turnover cycles without having significant degradation in about 20 years of exposure to solar light in order to be durable for a long time outdoors (Grätzel, 2003; Hagfeldt et al., 2010; Shalini et al., 2016).

There is numerous dye sensitiser have been synthesised including organic, inorganic, synthetic or natural dye. Organic materials, such as photovoltaics, are also showing significant promise in the growth of this subject, whereas inorganic materials have so far proven to be quite promising (Wesley et al., 2014). One of the compounds that can fulfil the above requirements is Schiff base compound as their structure is easily modified to the desired structure. Schiff bases with high π-conjugated system (-N=C-C=C-) can be achieved by choosing the appropriate starting materials considering that Schiff bases ligands can be easily synthesised as well as stable to form complexes with metal ions (Gupta & Sutar,

2008). In addition, according to Xavier & Srividhya (2014), Schiff bases that is made up of aromatic aldehydes together with effective conjugation system is very stable. This is because the conjugation effect across the ligand would be more extended when the phenylene bridge replaced the ethylene bridge (Tong et al., 2014). It is a general finding that the molecule will be more stable the more conjugated the system is. Efficiency of DSSC device can be enhanced with the introduction of conjugated system as they help in increasing electron transport ability in throughout the molecule (Gondia & Sharma, 2017; Mahadevi & Sumathi, 2020). Other than that, extended π-conjugated structure also reduces the energy gap between HOMO and LUMO of the molecule which is then enhance the electrical conductivity (Ye et al., 2021). As mentioned before, Schiff base structure can easily be modified by changing starting materials needed. Thus, choosing a starting material that have good anchoring group such as -COOH or -OH are crucial to ensure good anchoring of dye to the TiO_2 surface.

In 2017, Teo and co-workers (2017) in his work reported that their conversion efficiency of DSSC can be boost by introducing a π-conjugated system in their bis-chalcone molecules. Apart from that, they also discovered that the molecule with a *meta*-position on the central phenyl ring had a 20% poorer conversion efficiency than the one with a *para*-position on the central phenyl ring (Figure 2.3). This is due to meta-branching in the molecule structure can break the π-conjugation system which resulted in lower conversion efficiency (Teo et al., 2017).

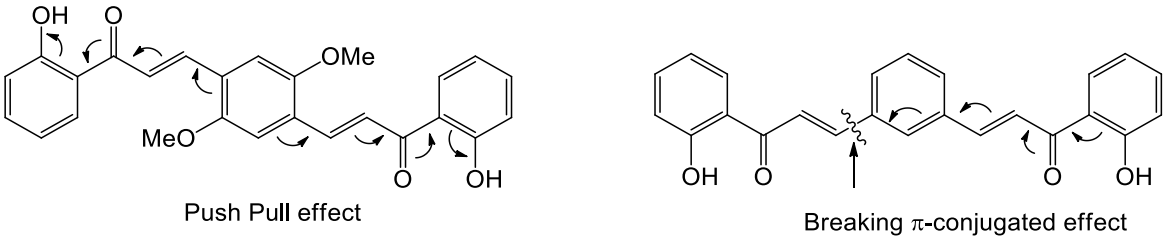

Figure 2.3: Chemical structure of the bis-chalcone compounds with para- and meta-position of central phenyl ring (Teo et al., 2017)

Wang and co-workers (2017) in his paper stated that the photoelectric characteristics of complexes are governed by the scale of the π-conjugated system on the ligands. In their study, they found out that as the conjugation system increase, the electron density also increases. Thus, enhancing the conjugated delocalised system. Furthermore, the gaps between HOMO and LUMO also can be reduced following the increasing conjugation system which is related with the broadening absorbance band of the dye (Yang et al., 2012; Zhang et al., 2015). Previous research by Zhang and co-workers (2018) has synthesised series of Schiff base having different type of π-spacer in between (Figure 2.4). They reported that phenylene ring demonstrate red shift emission as it replaces ethylene bridge which is consistent with theoretical studies.

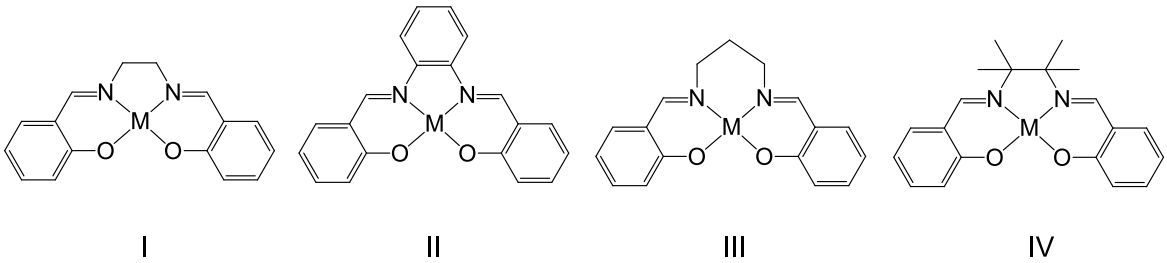

Figure 2.4: Prototype of Schiff bases with different bridge in between (Zhang et al., 2018)

2.1.4 Electrolyte

Electrolyte is also one of important component in DSSC device as it completes the electron cycle. They supply the internal electric ion conductivity inside the device by diffusing within the mesoporous TiO_2 layer (Shalini et al., 2016). In addition, in between electrode and metal oxide layer, electrolyte is the one who accountable for the internal charge-carrier transport. During the whole operation, electrolyte continually regenerate the dyes and itself by redox couple reaction (Semalti & Sharma, 2020). The oxidised electrolyte redox couple is first reduced at the counter electrode and then the reduced electrolyte component is used to regenerate the photo oxidised dye (Yu et al., 2010). A few requirements needed for electrolyte to achieve greater efficiencies include long term stability, can reduce oxidised dye rapidly, does not degrade and cause desorption at the oxide surface and also have fast diffusion to sustain light energy conversion (Su'ait et al., 2015).

According to Iftikhar and coworkers (2019), there are variety of electrolyte types are being investigated in order to achieve optimal performance such as liquid electrolyte, gel electrolyte, quasi-solid electrolyte, solid state electrolyte and others. However, most common and most efficient one is liquid electrolyte which so far recorded the highest efficiencies, approaching 14% efficiencies under full sunlight illumination. Liquid electrolytes offer various advantages compare to other types of electrolytes such as low viscosity, high conductivity, simple preparation methods, strong connectivity at electrode and electrolyte interface, non-porous structure and same phase charge carriers (Su'ait et al., 2015; Iftikhar et al., 2019). To note, there are some problems in using liquid electrolytes such and leakage, evaporation and instability. However, there researchers are still looking for suitable sealing material to overcome the problems (Iftikhar et al, 2015; Semalti & Sharma, 2020).

Among several redox electrolyte that have been used in DSSC devices such as hydroquinone and bromine (Br^-/Br_2), iodide/triiodide (I^-/I_3^-) redox couple is the most extensively used and studied for DSSC device (Ye et al., 2014; Su'ait et al., 2015). This is because I^-/I_3^- redox couple offers several interesting qualities such as slow back electron transfer (recombination) from TiO_2 to I_3^- due to complicated multi electron transfer process. In addition, they are also highly soluble in variety of solvents, high diffusion coefficient and relatively low light absorbance so that there is less competition with dye. Plus, they also quite stable and does not decompose under condition needed to operate the device (Su'ait et al., 2015). Ye and coworkers (2014) in their work also stated that I^-/I_3^- redox couple have favorable kinetic properties such as fast oxidation, excellent infiltration, high stability, low cost and easy to prepare. Therefore, although variety of alternatives have been proposed and studied so far, I^-/I_3^- redox couple have shown the best performances and maximum efficiencies in DSSC devices operation.

2.1.5 Counter electrode

Counter electrode plays an important role in DSSC device because it is the one who responsible for reducing the materials involved for the redox process which is then regenerate the oxidised dye after electron injection (Ikpesu et al., 2020). The electrons that are arrived from external circuit are transported back into the redox electrolyte system by the counter electrode (Suhaimi et al., 2015). Counter electrodes are made of TCO glass substrate coated with platinum (Pt), silver (Ag) or carbon (C) onto the glass to provide a reversible transfer of electrons coming from the external circuit back to electrolyte (Semalti & Sharma, 2020; Yahya et al., 2021). In addition, they also catalyse the I_3^- ions formed in the electrolyte by the reduction of I^- ions (Shalini et al., 2015). An excellent counter electrode should fulfill important requirement which includes having a high catalytic activity, low

electrical resistance, chemically inert, low charge transfer resistance, high exchange current density for reduction process, stable and transparent (Shalini et al., 2015; Semalti & Sharma, 2020; Yahya et al., 2021).

The best material to date, having an excellent electro-catalytic activity, is Pt coated counter electrode. However, due to their high cost, lack of resource, high temperature needed for sintering process and low stability in electrolyte researchers are looking for another alternative to replace Pt (Shalini et al., 2015; Semalti & Sharma, 2020). Carbon has been appealing low-cost option as it offers enough conductivity and heat resistance, as well as corrosion resistance and electrocatalytic activity for reduction of I_3^- (Suhaimi et al., 2015). Carbonaceous materials such as carbon black, carbon nanotubes, activated carbon, graphite and graphene have been attempted to be use as alternative counter electrode materials. Despite they show low catalytic activity compared to Pt-based counter electrode, increasing the active surface area of the catalytic layer can compensate the limitations (Shalini et al., 2015).

2.2 Synthesis of Schiff base

Synthesizing Schiff base undergo condensation reaction in which the carbonyl group of aldehyde or ketones (C=O) are being replaced by the imine group in primary amine (Al Zoubi et al., 2018; Abu-Dief & Mohamed, 2015). There are a few syntheses technique to synthesise Schiff base compounds depending on the desired final product needed. The few available and used technique are discussed in the next subtopic.

2.2.1 Conventional methods

Among all the available techniques, conventional methods are the most traditional and widely used technique to synthesise Schiff base compounds. The conventional synthetic

methods include heating a mixture of metal salt and ligands selected in a solvent system (Sharma et al., 2018).

2.2.1.1 Two-steps technique

Two-step synthesis technique is a preferred technique to synthesis unsymmetrical Schiff base because it is a straightforward, and effective way to obtain unsymmetrical product (Roth et al., 2007; Schmidt et al., 2016). This technique is usually chosen to synthesise unsymmetrical product because it is difficult to be obtain directly (Nartop & Öğütcü, 2020). The procedure includes isolating the intermediate precursor formed by condensation of two reagents and further reacting the isolated compound with another different components (Schmidt et al., 2016). Roth and co-workers (2007) have synthesised unsymmetric Schiff base using two-steps synthesis as shown in Scheme 2.1, where the group synthesised unsymmetric Schiff base via two-step reaction in alcoholic solution at 0 °C. The by-products (Hphmb) obtained was isolated by using size exclusion chromatography (SEC) with good yield (>80%) and then further reacted with second primary amine forming unsymmetrical compound (H_2pmptsc) without any further purification.

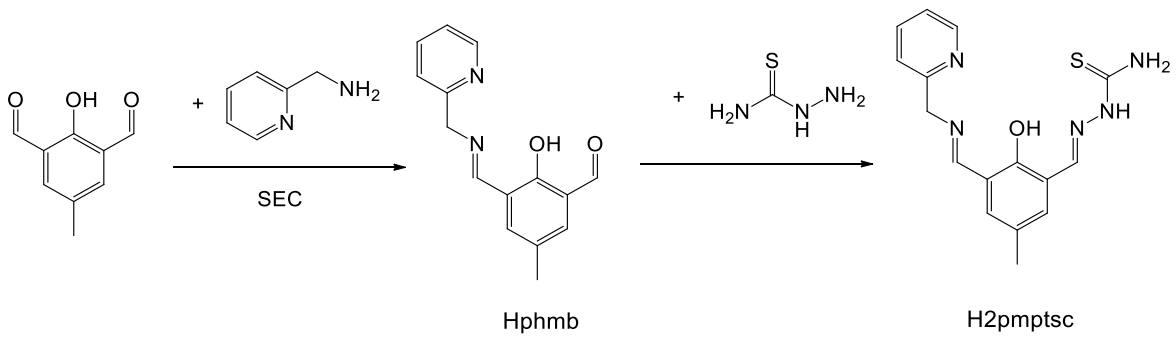

Scheme 2.1: Synthesis of the ligands H_2pmptsc (Roth et al., 2007)

2.2.1.2 One-pot technique

Recently, a method called multi-component reactions or one-pot reactions were introduced where the reactions involve 3 or more reactants at once (Deshineni et al., 2016). The methods are simple and easy to handle which all the reagents needed are added at once or adding the second reagents into the first rection without isolation part (Abdalhadi et al., 2020). There are many advantages of synthesizing using this method which includes reduction in synthesis time, high structural diversity, simple operation, reducing purification cost and reducing waste products (Deshineni et al, 2016; Abdalhadi et al., 2020).

In 2010, a one pot, three-component reaction involving aldehydes, malononitrile, and 4-hydroxycoumarin in the presence of a catalytic quantity of hexamethylenetetramine was reported by Wang and co-workers (2010) as an efficient and convenient technique for synthesis of dihydropyrano[3,2-c]chromene derivatives. Within a short period of time, high to exceptional yields of dihydropyrano[3,2-c]chromene derivatives were produced. The reaction was done in ethanol solvent and stirred under reflux for appropriate time in 89% yield (Scheme 2.2).

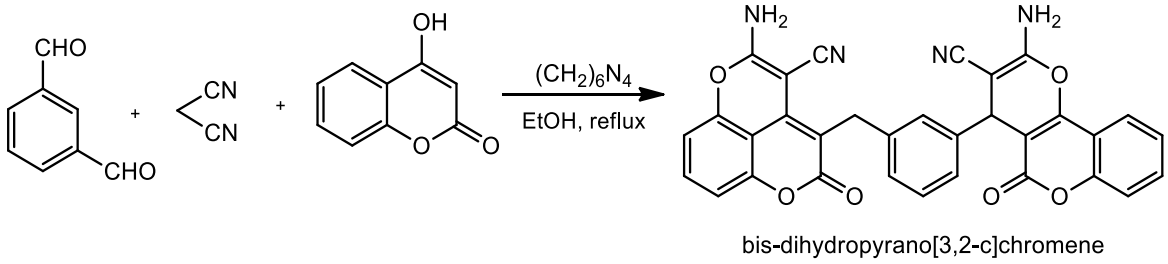

Scheme 2.2: Synthesis pathway of dihydropyrano[3,2-c]chromene in one-pot (Wang et al., 2010)

In addition, Ebrahimi and co-workers (2013) also have reported a novel and simple green one-pot synthesis method of anthranilamide. This method provides a green way to

make sirtinol, a medicinally significant Schiff base, and other bioactive anthranilamide Schiff bases. The described Schiff bases are made without the need of any catalysts by reacting isatoic anhydride, amines, and aromatic aldehydes in water at room temperature (Scheme 2.3). In this approach, no cyclisation toward 2,3-dihydro-4(1H)-quinazolinones happened, and only anthranilamide Schiff bases were generated (Ebrahimi et al., 2013).

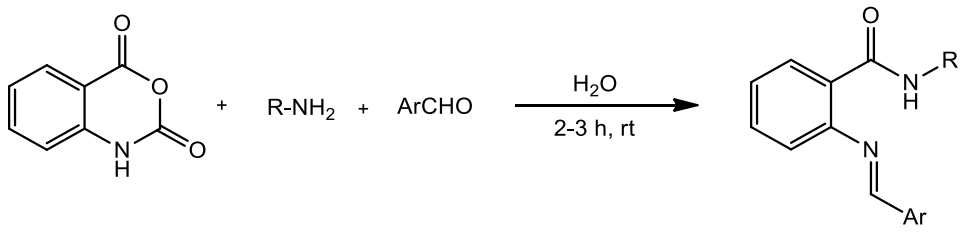

Scheme 2.3: General pathway for one-pot synthesis of anthranilamide Schiff base (Ebrahimi et al., 2013)

According to Radi and co-workers (2015), synthesis of Schiff base using one-pot method offers good and excellent yield. Abdalhadi and co-workers (2020) has synthesised a 2,3-diaminomaleonitrile (DAMN) derivatives using a one-pot method in ethanol solution in the presence of acetic acid. The reaction was running for 5 hours at 80 ℃ in nitrogen atmosphere (Scheme 2.4). Their works have shown a considerable reduction in synthesis time and cost of purification.

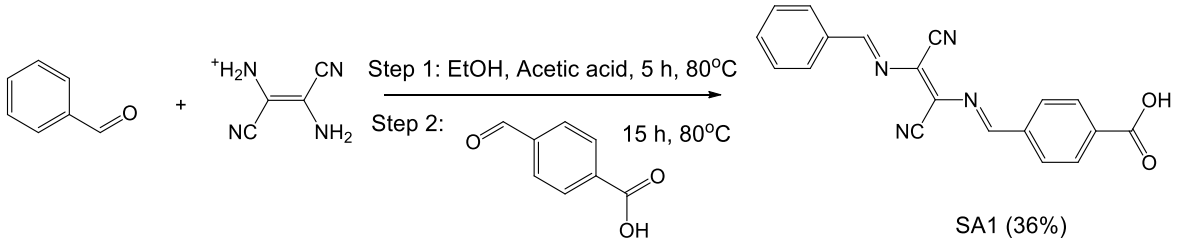

Scheme 2.4: Synthesis scheme of SA1 (Abdalhadi et al., 2020)

Another paper that described the synthesis of anthranilamide bearing 4-aminoquinoline in one-pot reaction was published in 2017 by Salve and co-workers. The synthesised compound was for *Mycobacterium tuberculosis* gyrase inhibitors. The reaction was started by mixing isatoic anhydride **(1)**, 7-chloro-4-hydrazinylquinoline **(2)**, and substituted aromatic and/or heteroaromatic aldehydes **(3)** in water at room temperature, yielding the product **(4a-u)** in high yields (Scheme 2.5). They have tried several tests to find the optimum reaction conditions in which the shortest reaction time yielding maximum yield was in water solvent and without catalyst (Salve et al., 2017).

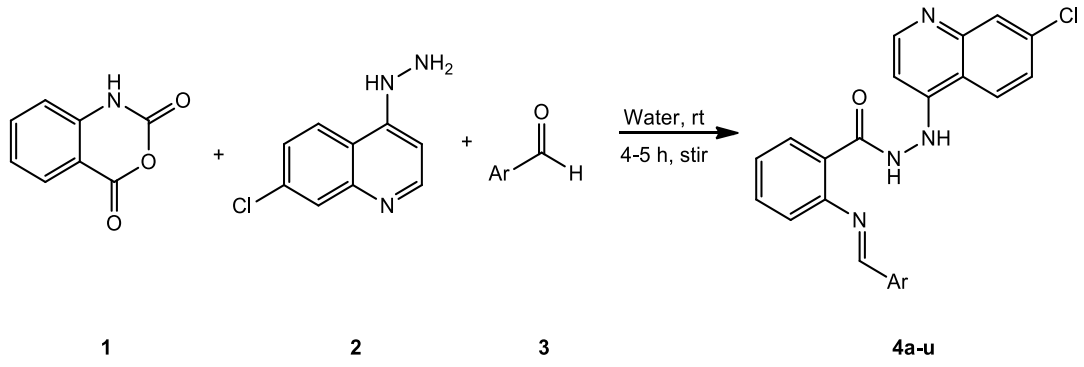

Scheme 2.5: One-pot three component synthesis of target compounds 4a-u (Salve et al., 2017)

However, there are several drawbacks in using this method in which the product from the final steps is irreversible. In addition, functional groups on the side-branches of the components are usually incompatible, requiring the use of more or less expensive protection techniques. Furthermore, the conversion of the components in the reactor does not occur simultaneously in a single step but rather conduct multiple sub-reactions of two components, resulting in products and by-products in their final products (Ugi et al., 1994; Ugi et al, 1998). Moreover, Kuan (2021) in her work reported that incorporating electron acceptor substituent especially in *para* position of aromatic ring is tedious and difficult to achieve. This is due to destabilisation of ionic resonance contributor and reduced the single bond

character of the C=N bond. Also, the nucleophilic attack of amine to carbonyl moiety also reduced by the strong electron withdrawing compound.

2.2.2 Microwave irradiation method

Another method which is considered as green chemical method is microwave irradiation method which use microwave irradiation as the heat source (Shntaif & Rashid, 2016). Microwave irradiation as a nonconventional energy source for synthesizing organic and inorganic compounds has piqued researchers' interest because of its clean, convenient, and cost-effective nature (Kassim et al., 2019). This method offers many advantages such as high chemical reaction rate, high yield, easy workup, less hazard and high purity without the need to isolate and purify steps (Haque et al., 2018; Kassim et al., 2019). The general method is quite straightforward where the mixture of starting materials and added into the same conical flask or beaker and inputted inside microwave oven and irradiated for few minutes (Shntaif & Rashid, 2016). The heating of the reaction utilising microwave irradiation by "in-core" heating not only reduces reaction time but also improves product yield and purity by eliminating unwanted side reactions (Kassim et al., 2019). The general pathway of synthesizing Salicylaldazine *via* microwave irradiation under ethanolic solutions done by Kassim and his co-workers (2019) are shown in Scheme 2.6.

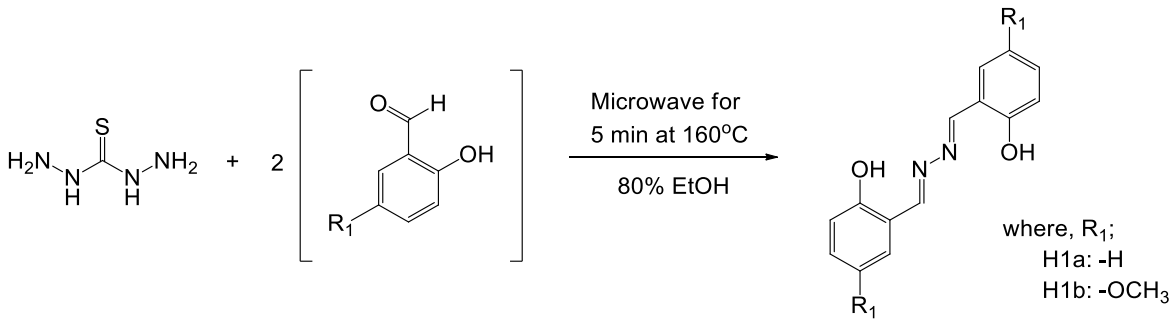

Scheme 2.6: General pathway of Salicylaldazine via microwave irradiation (Kassim et al., 2019)

Even so, this method has a few shortcomings such as it is difficult to performed reaction monitoring course and time-monitoring particle growth of some inorganic species. Furthermore, compared to glassware equipment used in conventional methods, microwave synthesis reactor is much expensive as well as the scale-up production using microwave-mediated has yet to achieve the production quantities of "classical" reactors (Ambrozic et al., 2011).

2.3 Complexation of Schiff base

In the evolution of coordination chemistry, metal complexes of Schiff bases play a crucial role because of the ease of Schiff base ligands coordinate with metal center through the imine nitrogen (C=N) moiety and another group which can stable a wide range of metals in various oxidation states (Samani & Mehranpour, 2021).

Among many boron complexes that have been synthesised, it has been reported that complexation of boron complexes using boron trifluoride diethyl ether ($BF_3.Et_2O$) have shown an excellent effect on electrochemical properties of a molecules. This is shown by the lowering of energy gap after complexation with $BF_3.Et_2O$, showing the accuracy of the electrochemical determination of LUMO and HOMO energy levels. These numbers are the

variables that explain the molecule's prospective charge transfer interaction (Chaabene et al., 2019).

Phan and co-workers (2019) have synthesised a series of unsymmetrical bis-chalcone with Cl or OMe as the electron donor side and its complexation with $BF_3.Et_2O$ and Ru(II)-DMSO (Figure 2.5) as the electron acceptor side to demonstrate the effect of push pull effect and π-conjugated system. In their work, it was recorded that compounds with BF_2 shows higher efficiency than with Ru(II)-DMSO. This is due to sufficient π-electron delocalisation and push-pull effects generated in the molecule with BF_2 comparing to Ru(II)-DMSO compounds (Phan et al. 2019).

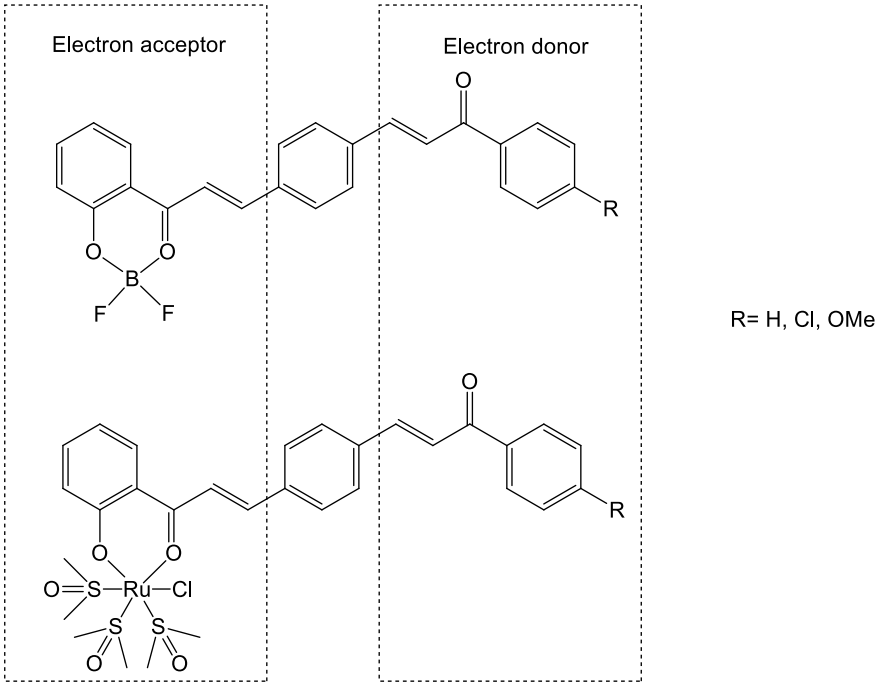

Figure 2.5: The unsymmetrical bis-chalcone with different electron donors and acceptors (Phan et al., 2019)

The preparation of boron complexes is quite straightforward where strong bases such as potassium hydroxide (KOH) and sodium hydroxide (NaOH) or weak base such as

triethylamine (TEA) and *N*,*N*-diisopropylethylamine (DIPEA) is added in order to deprotonate the -OH in the molecule and then reacted with BF_3•Et_2O, usually in inert condition to get the desired complexes compound. In 2016, Shanmugapriya and co-workers (2016) have synthesised and describe boranil fluorescent dye for hydrogen peroxide detection and successfully applied for H_2O_2 imaging in HeLa cells. The imine derivatives were treated with $BF_3.Et_2O$ in presence of triethylamine (TEA) in DCM solvent for 4 hours (Scheme 2.7).

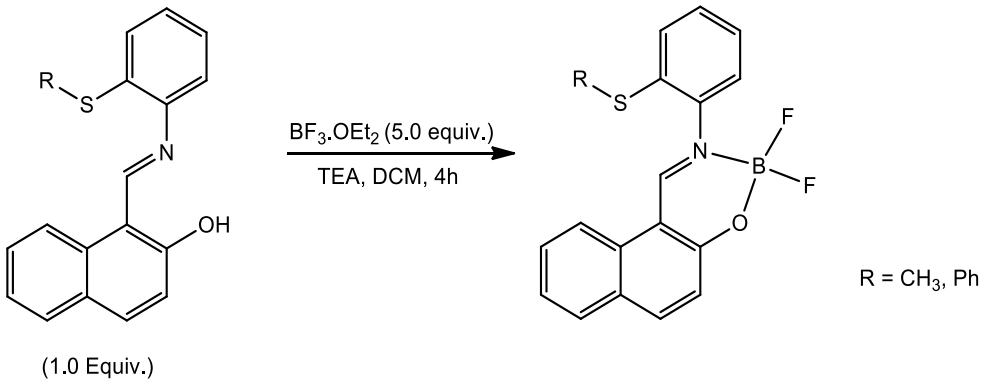

Scheme 2.7: Preparation of boranil complex (Shanmugapriya et al., 2016)

Sun and co-workers (2017) have reported the synthesis of difluoro boron complex of Schiff bases (Figure 2.6). The reaction was first refluxed with TEA in dichloroethane for 30 minutes under nitrogen atmosphere. Then, $BF_3.Et_2O$ were added slowly and continue refluxed for 8 hours. Interestingly, this compound shows reversible changes of colour emitted according to it states. Crystalline states of this complex emit a strong yellow light. However, after being grind, changing its states into amorphous, its powder emits orange red light. The fluorescence could be recovered when the powder was heated.

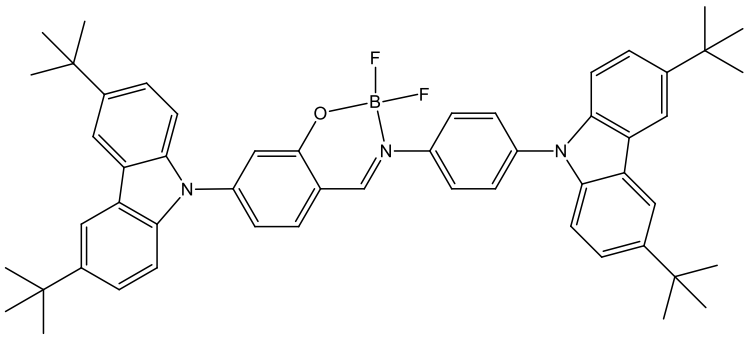

7-(3,6-Di-tert-butyl-9H-carbazol-9-yl)-3-(4-(3,6-di-tert butyl-9H-carbazol-9-yl)phenyl)-2,2-difluoro-2H-2l4,3l4-benzo[e][1,3,2]oxazaborinine (TPOB)

Figure 2.6: Structure of difluoro boron complex of Schiff base reported by Sun and co-workers (2017)

In addition, a difluoroboron compound of a novel imine-based tripodal ligand was developed and produced by Sen (2019) (Scheme 2.8). Like previous example, the preparation of boron complex is similar except for TEA were replaced by DIPEA for the same function which is to deprotonate the -OH. According to the results, the produced boron complex showed powerful emission with substantial Stokes shifts in the range of 83 nm to 96 nm. Plus, it has been discovered to have high quantum yield values of up to 48%. The huge Stokes shifts and high efficiency emissions in boron complex solutions make it a valuable fluorophore for materials science applications (Sen, 2019).

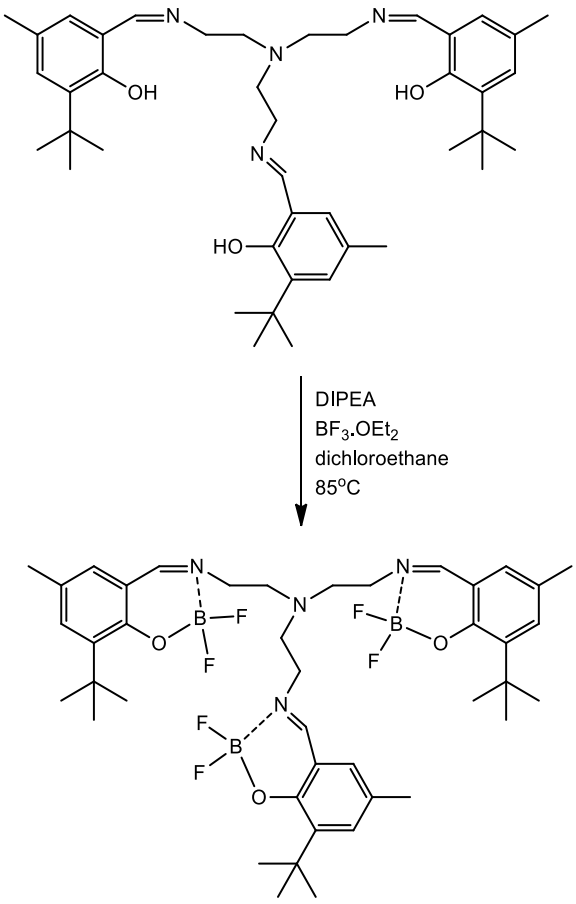

Scheme 2.8: Formation of the trinuclear fluoroborate complex (Sen, 2019)

Lately, a new difluoro boron complexes of Schiff base based on N,O-chelating has been synthesised by Sen and co-workers (2020) to study their photophysical and electrochemical properties (Scheme 2.9). The Schiff base was first added with TEA and stirred for 15 minutes at 50℃. After that, $BF_3.Et_2O$ was added dropwise into the solution and maintained for 4 hours at 85℃ under argon atmosphere.

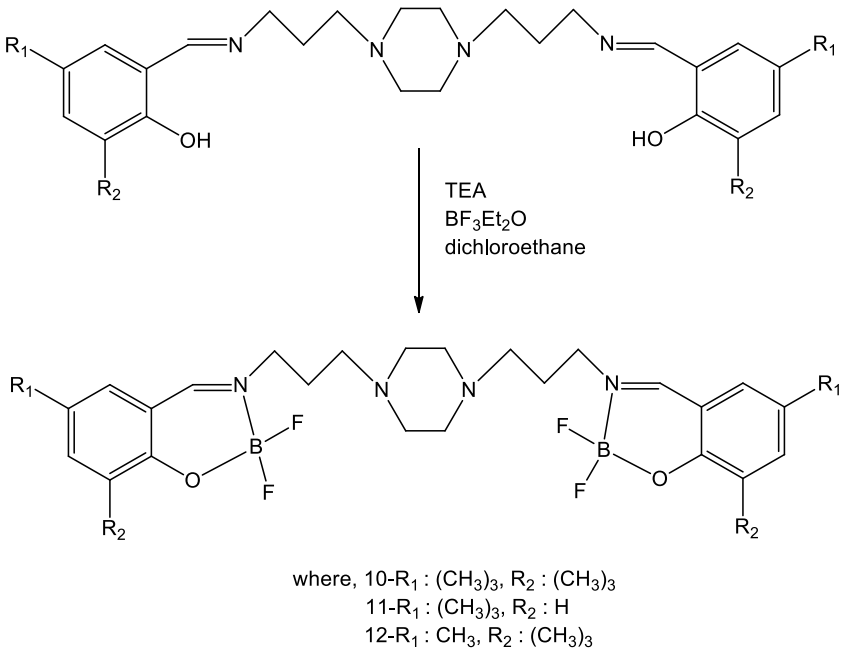

Scheme 2.9: Structure of difluoro boron complex of Schiff base based on N,O-chelating (Sen et al., 2020)

Large Stokes shifts were observed in the region of 92 nm to 115 nm due to the flexible dinuclear boron complexes linked by a flexible carbon chain. These characteristics make these compounds valuable for use in fluorescent materials. Due to its potential applications in numerous domains such as organic light-emitting diodes (OLEDs), laser dyes, fluorescence imaging probes, solar cells, and as photosensitiser dyes in photodynamic treatment, luminous organic and organometallic compounds are the focus of current intense research (Sen et al., 2020).

2.4 Schiff base metal complexes as sensitiser

Schiff base and their metal complexes have been used widely as photovoltaic materials as they have the potential photovoltaic characteristics. Besides, Schiff base is biodegradable, non-toxic, have a good electrical conductivity in conjugated compound, cheaper and easy to produce. These advantages made Schiff base became very promising in

the application of DSSC (Wesley et al., 2014). In addition, Schiff base transition metal complexes are useful as photosensitisers because of their high thermal and moisture stabilities. Many soluble extended π-conjugated materials based on Schiff base metal complexes have been investigated as sensitisers for wide-bandgap oxide semiconductors like TiO_2 and have found a decent amount of conversion of an incident photon to electric current over the last few years (Mahadevi & Sumathi, 2020). In fact, substantial research has shown that metal complexation of Schiff bases has a significant impact on their activity as well as their optoelectronic properties. As a result, they could be used as sensitisers and acceptors in dye-sensitised solar cells (Chouk et al., 2019).

According to Wesley et al (2014), even though that organic dye has many advantages, they are still lacking in term of efficiency. To compare with organic dye, inorganic metal complexes have a higher stability in term of thermal and chemical, have intense absorption in visible region have strong adsorption onto semiconductor surface, have efficient electron injection onto conduction band of semiconductor. Therefore, by combining organic compounds with metal ions the compounds can have both properties such as improved properties and higher efficiency.

Aside from being the sole compound as the sensitiser, Schiff base metal complex also can be used as co-sensitiser of another available dye as reported by Wang and co-workers (2017). In their work, they have synthesised few asymmetric Zn(II), Cd(II) and Hg(II) benzimidazole-based complexes **1**-**4** (Figure 2.7) and it is reported that the complexes have shown a significant influence in their DSSC performances when used as co-sensitiser of N719 dye (Figure 2.8), which is a typical representative of organic dye for DSSC. The increase in efficiency is due to the fact that these complexes were able to overcome the

limitations of N719 absorption in the visible spectrum over a short wavelength interval, keeping it from aggregating, counteract competitive visible light absorption of I_3^-, and suppress charge recombination by forming an effective cover layer of dye molecules on the TiO_2 surface.

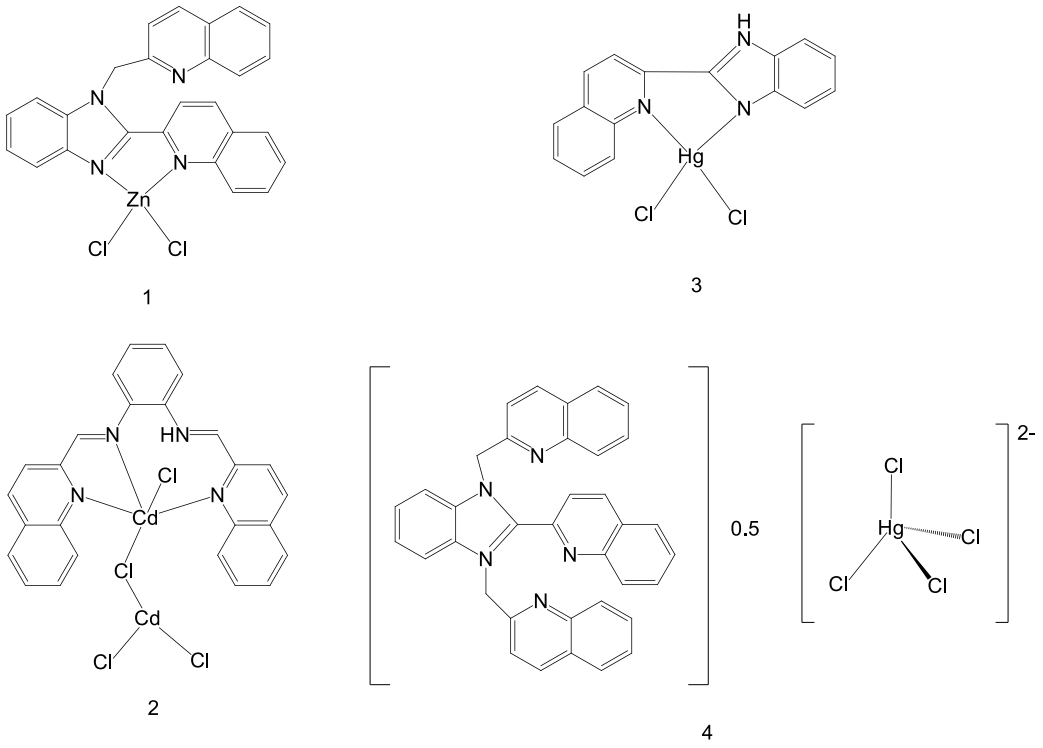

Figure 2.7: The structure of asymmetric Zn(II), Cd(II) and Hg(II) benzimidazole-based complexes (Wang et al., 2017)

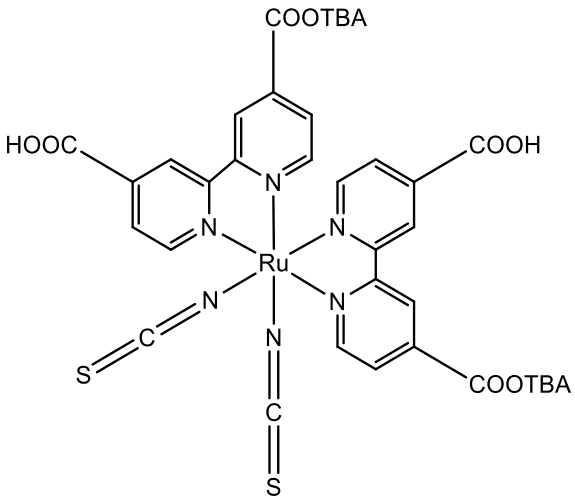

Figure 2.8: The structure of N719 dye

In 2018, Gencer Imer and co-workers (2018) have synthesised symmetrical Schiff base ligand based on pyridine and its complexation with Co(II), Ni(II) and Pd(II) transition metal complexes (Figure 2.9). The general process for the complexation is the methanolic solution of respective metal salt was added dropwise into the ligand solution in mixture of MeOH/$CHCl_3$ (1:1). The mixture was the refluxed for 1 hour at 80 ℃. The metal bind onto the ligands through phenolic -OH and azomethine nitrogen. The photovoltaics properties of the compounds were investigated, and they reported that all the photon to current conversion values except for Ni(II) complex is higher than the value of its free ligand. This demonstrates that adding transition metal to the ligand can improve the dye's overall efficacy as a dye sensitiser.

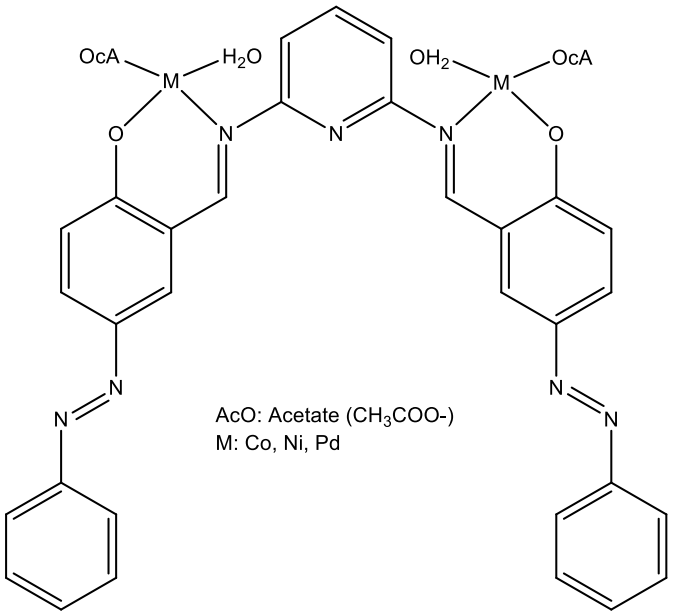

Figure 2.9: The general structure of pyridine-based Schiff base ligand and their metal complexes (Gencer Imer et al., 2018)

In another work, a Zn(II) metal Schiff base complex (Figure 2.10) was synthesised and used as sensitiser in DSSC devices (Kilinc et al., 2019). The cost-effective chemical precipitation approach was used to synthesise the complex. They can be made using simple and affordable chemical process where the ligand and the metal salt were mixed in ethanolic solution in equal molar amounts and refluxed for 60 minutes. The resulting solution was condensed to reduce the volume into 15-20 mL and left to cool to room temperature. The recorded efficiency of the Zn(II) metal Schiff base was calculated as 0.73%. This finding suggests that the metal Schiff-base complex of Zn(II) plays an important role in electron transport. As a result, it's possible that a low-cost Zn (II) metal Schiff-base combination could be used as a sensitiser in DSSC (Kilinc et al., 2019).

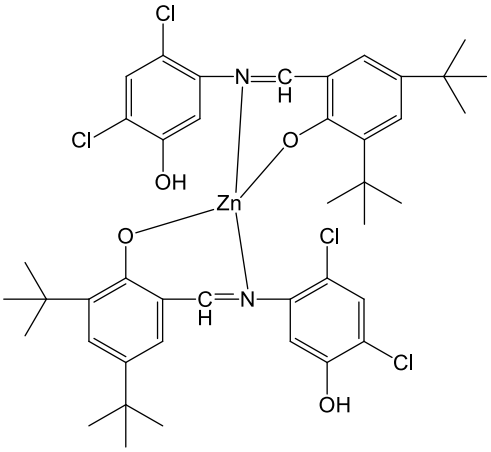

Figure 2.10: The chemical structure of Zn(II) metal Schiff base complex (Kilinc et al., 2019)

CHAPTER 3

METHODOLOGY

3.1 Materials and reagent

Chemicals namely *p*-phenylenediamine (MERCK), *o*-phenylenediamine (Fluka Chemica), glyoxal (MERCK), diacetyl (MERCK), 2-hydroxybenzaldehyde (MERCK), benzaldehyde (Bendosen), *p*-tolualdehyde (ALDRICH), *p*-anisaldehyde (ALDRICH), methyl-4-formylbenzoate (MERCK), aniline (R&M Chemicals), 2-aminophenol (MERCK), *p*-toluidine (MERCK), *p*-anisidine (MERCK), methyl-4-aminobenzoate (ALDRICH), boron trifluoride diethyl ether (MERCK), triethylamine (MERCK), polyethylene glycol (ALDRICH), polyethylene glycol 20000 (MERCK), titanium (IV) oxide anatase (ALDRICH), Potassium iodide (MERCK), iodine resublimed (R&M Chemicals), *cis*-Bis(isothiocyanato)bis(2,2'-bipyridyl-4,4'-dicarboxylato) ruthenium(II), N3, dye (ALDRICH) and triton X-100 (ACROS Organics) were used as received without further purification otherwise stated.

Ethanol was purified by refluxing 900 mL of ethanol with 3.5 g of magnesium granular and 1.5 g of iodine until the solution turned colorless. Then the purified ethanol was collected via distillation.

3.2 Characterisation

The Fourier-transform infra-red (FT-IR) analysis were conducted by using Thermo Scientific Nicolet iS10 FTIR spectrophotometer in KBr disc at the wavelength of 400 – 4000 cm^{-1}. The ^{1}H, ^{13}C NMR spectra were obtained from JEOL ECA-500 MHz NMR spectrophotometer with appropriate deuterated solvent ($CDCl_3$: 7.26 ppm, DMSO-d_6: δH

2.50 ppm) at room temperature and tetramethylsilane (TMS) was used as the internal standard reference. The molecular weights of the compounds were recorded using Agilent 5977 GC/MS, under the following operating conditions: injector temperature at 280 °C, detector temperature 280 °C, the oven temperature increased at the rate 10 °C/min from 50-280 °C. Helium gas was used as the carrier gas. The percentage of carbon, hydrogen and nitrogen were recorded by using Thermo Scientific Flash*Smart* CHNS Analyser. Lastly, the UV-Vis spectra were carried out using Agilent Cary 60 UV-Vis spectrophotometer with a 1 cm quartz cuvette in the range of 200–800 nm.

3.3 Preparation of symmetrical bis-Schiff base ligands

3.3.1 (*N*^{1}*E*,*N*^{4}*E*)-*N*^{1},*N*^{4}-dibenzylidenebenzene-1,4-diamine, (1a)

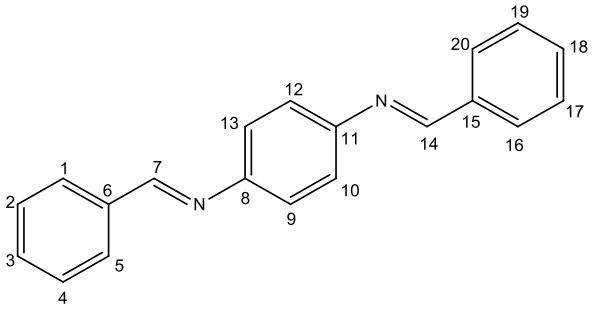

Benzaldehyde (10 mmol, 1.061 g) in 20 mL ethanol was added into *p*-phenylenediamine (5 mmol, 0.541 g) and refluxed while stirred for 2 hours at 80 °C. The precipitate formed was then filtered and washed a few times with 15 mL cold ethanol each time. The yellow precipitate was purified by *via* slow diffusion of hexane into dichloromethane solution of the product. This method was according to the method as published by Sun & Yao (2011). Yield: 1.391 g, 98%. IR (KBr, cm^{-1}) υ: 3055.11 (C-H aromatic), 2884.38 (C-H stretching), 1615.70 (C=N stretching), 1574.49, 1492.07 (C=C aromatic), 1362.55 (C-N stretching). ^{1}H NMR (500 MHz, DMSO-d_6, δ ppm) H: 8.69 (s, 2H, HC=N, H-7, 14), 7.96 (d, 4H, *J* = 9 Hz, $H_{aromatic}$, H-1, 5, 16, 20), 7.53 (m, 6H, $H_{aromatic}$, H- 2, 3, 4, 17, 18, 19), 7.37 (s, 4H, $H_{aromatic}$,

H-9, 10, 12, 13). ^{13}C NMR (125 MHz, DMSO- d_6, δ ppm) C: 160.62 (C-7, 14), 149.99 (C-8, 11), 136.61 (C-6, 15), 131.90 (C-3, 18), 129.30 (C-1, 5, 20, 16), 129.11 (C-2, 4, 17, 19), 122.44 (C-9, 10, 12, 13). UV-Vis (DCM) (λ_{max}/nm): 273 and 355. Anal. Calcd. For $C_{20}H_{16}N_2$: C, 84.48; H, 5.67; N, 9.85. Found: C, 84.43; H, 5.53; N, 9.62. MS (*m/z*): 284 [M].

3.3.2 2,2'-((1*E*,1'*E*)-(1,4-phenylenebis(azanylylidene))bis(methanylylidene))diphenol, (1b)

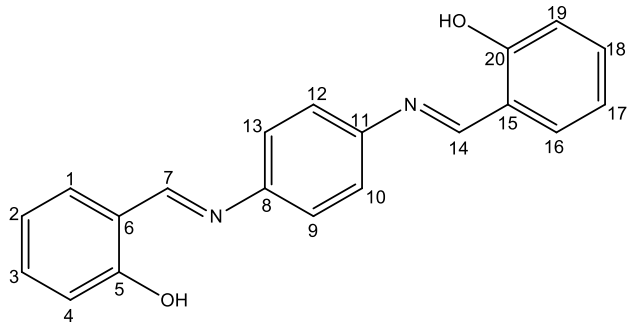

2-hydroxybenzaldehyde (10 mmol, 1.22 g) in 20 mL ethanol was added into 20 mL ethanolic solution of *p*-phenylenediamine (5 mmol, 0.541 g). The mixture then refluxed while stirred for 1 hour. Brown precipitate formed was then filtered and wash a few times using cold ethanol. Bright orange crystal was obtained *via* slow diffusion of hexane into dichloromethane solution of the powder. This method was according to the method as published by Sun & Yao (2011). Yield: 1.493 g, 95%. IR (KBr, cm^{-1}) υ: 3375.55 (OH), 2983.82 (C-H aromatic), 2868.77 (C-H stretching), 1600.45 (C=N stretching), 1567.58, 1485.40 (C=C aromatic), 1364.86 (C-N stretching), 1268.99 (C-O stretching). ^{1}H NMR (500 MHz, DMSO-d_6, δ ppm) H: 9.03 (s, 2H, HC=N, H-7, 14), 7.68 (d, 2H, *J* = 7 Hz, $H_{aromatic}$, H-1, 16), 7.55 (s, 4H, $H_{aromatic,}$ H-9, 10, 12, 13), 7.43 (t, 2H, *J* = 8 Hz, $H_{aromatic,}$ H-3, 18), 6.99 (m, 4H, $H_{aromatic,}$ H-2, 4, 17, 19). ^{13}C NMR (125 MHz, DMSO- d_6, δ ppm) C: 163.74 (C-5, 20), 160.82 (C-7, 14), 147.15 (C-8, 11), 133.90 (C-3, 18), 133.00 (C-1, 16), 123.10 (C-9, 10,

12, 13), 119.90 (C-2, 17), 119.75 (C-6, 15), 117.06 (C-4, 19). UV-Vis (DCM) (λ_{max}/nm): 274 and 370. Anal. Calcd. For $C_{20}H_{16}N_2O_2$: C, 75.93; H, 5.10; N, 8.86. Found: C, 75.72; H, 4.95; N, 8.74. MS (*m/z*): 316 [M].

3.3.3 (*N*^{1}*E*,*N*^{4}*E*)-*N*^{1},*N*^{4}-bis(4-methoxybenzylidene)benzene-1,4-diamine, (1c)

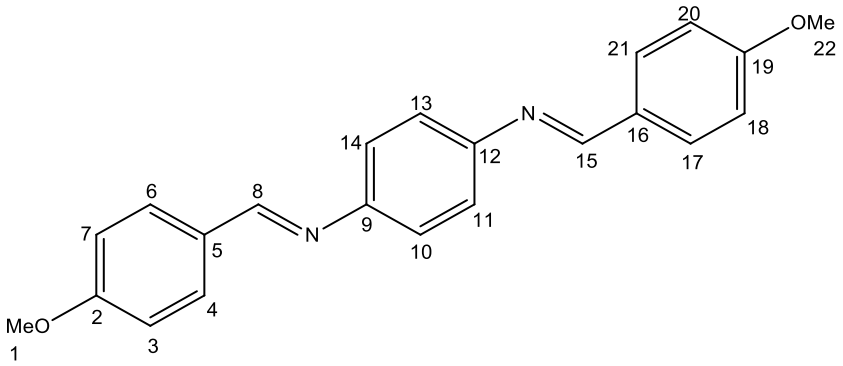

The procedure was similar to **1a** but benzaldehyde was replaced with *p*-anisaldehyde (10 mmol, 1.362 g). The yellow precipitate formed was purified *via* recrystallisation by using vapour diffusion of hexane into dichloromethane. This method was according to the method as published by Mohan & Kumar (2005). Yield: 1.669 g, 97%. IR (KBr, cm^{-1}) υ: 2955.03 (C-H aromatic), 2840.23 (C-H stretching), 1603.92 (C=N stretching), 1568.60, 1509.73 (C=C aromatic), 1300.74 (C-N stretching), 844.48 (*para*-Subst.). ^{1}H NMR (500 MHz, DMSO-d_6, δ ppm) H: 8.59 (s, 2H, HC=N, H-8, 15), 7.90 (d, 4H, *J* = 9 Hz, $H_{aromatic,}$ H-3, 7, 18, 20), 7.30 (s, 4H, $H_{aromatic,}$ H-10, 11, 13, 14), 7.08 (d, 4H, *J* = 9 Hz, $H_{aromatic,}$ H-4, 6, 17, 21), 3.84 (s, 6H, H-1, 22). ^{13}C NMR (125 MHz, DMSO- d_6, δ ppm) C: 163.26 (C-2, 19), 160.00 (C-8, 15), 133.02 (C-9, 12), 131.54 (C-4, 6, 17, 21), 130.26 (C-5, 16), 122.77 (C-10, 11, 13, 14), 115.22 (C-3, 7, 18, 20), 56.45 (C-1, 22). UV-Vis (DCM) (λ_{max}/nm): 290 and 359. Anal. Calcd. For $C_{22}H_{20}N_2O_2$: C, 76.72; H, 5.85; N, 8.13. Found: C, 76.84; H, 5.71; N, 7.74. MS (*m/z*): 344 [M].

3.3.4 (*N*^{1}*E*,*N*^{2}*E*)-*N*^{1},*N*^{2}-dibenzylidenebenzene-1,2-diamine, (2a)

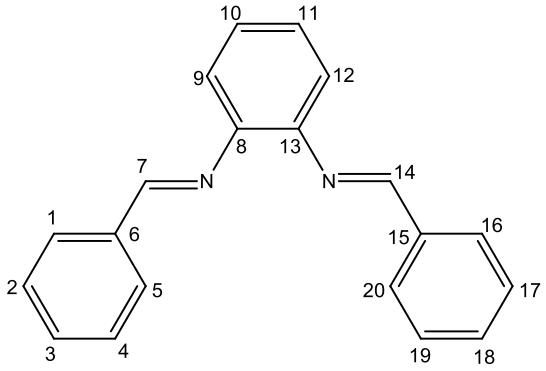

Ethanolic solution of benzaldehyde (10 mmol, 1.061 g) was added into ethanolic solution of *o*-phenylenediamine (5 mmol, 0.541 g). The mixture was refluxed for 8 hours at 80 ℃. Then, the solvent was reduced until ~15 mL by using rotary evaporator. The dark concentrated mixture was left at room temperature until precipitate formed. The cream-coloured precipitate formed was then isolated and washed with cold ethanol a few times. This method was according to the method as published by Akila et al. (2012) with slight modification. Yield: 0.687 g, 54%. IR (KBr, cm^{-1}) υ: 3057.78 (C-H aromatic), 2957.97 (C-H stretching), 1603.19 (C=N stretching), 1488.14, 1447.05 (C=C aromatic), 1392.26 (C-N stretching). ^{1}H NMR (500 MHz, DMSO-d_6, δ ppm) H: 7.88 (s, 1H, HC=N, H-7), 7.87 (s, 1H, HC=N, H-14), 7.69 (d, 2H, *J* = 7 Hz, $H_{aromatic,}$ H-1, 20), 7.45 (m, 4H, $H_{aromatic,}$ H-9, 10, 11, 12), 7.26 (m, 6H, $H_{aromatic}$, H-2, 3, 4, 17, 18, 19), 7.09 (d, 2H, *J* = 7 Hz, $H_{aromatic,}$ H-5, 16). ^{13}C NMR (125 MHz, $CDCl_3$, δ ppm) C: 154.16 (C-7), 142.88 (C-14), 136.40 (C-8), 136.06 (C-13), 130.17 (C-12), 129.91 (C-6, 15), 129.41 (C-1, 16), 129.21 (C-2, 17), 128.93 (C-5, 20), 127.66 (C-9), 126.09 (C-4, 19), 123.31 (C-3), 122.98 (C-18), 119.99 (C-10), 110.72 (C-11).UV-Vis (DCM) (λ_{max}/nm): 292. Anal. Calcd. For $C_{20}H_{16}N_2$: C, 84.48; H, 5.67; N, 9.85. Found: C, 84.03; H, 5.67; N, 10.08. MS (*m/z*): 284 [M].

3.3.5 2,2'-((1*E*,1'*E*)-(1,2-phenylenebis(azanylylidene))bis(methanylylidene))diphenol, (2b)

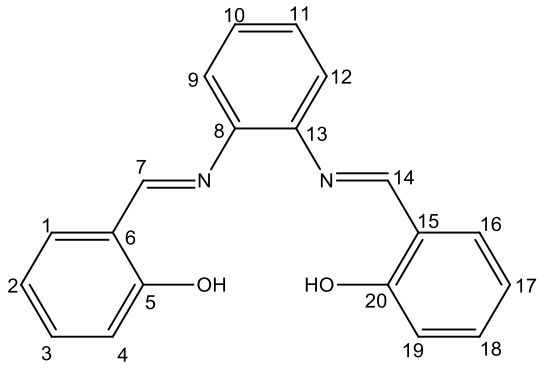

The procedure was similar to **1b** but *p*-phenylenediamine was replaced by *o*-phenylenediamine (5 mmol, 0.541 g). The orange crystal was obtained *via* slow evaporation of the precipitate in chloroform:ethanol (10:1) mixture of solvent. This method was according to the method as published by Akila et al. (2012) with slight modification. Yield: 1.455 g, 92%. IR (KBr, cm^{-1}) υ: 3320.03 (OH), 2925.59 (C-H aromatic), 2887.33 (C-H stretching), 1606.87 (C=N stretching), 1556.83, 1480.29 (C=C aromatic), 1365.49 (C-N stretching), 1274.24 (C-O stretching). ^{1}H NMR (500 MHz, DMSO-d_6, δ ppm) H: 8.90 (s, 2H, HC=N, H-7, 14), 7.63 (d, 2H, *J* = 9 Hz, $H_{aromatic,}$ H-1, 16), 7.40 (m, 6H, $H_{aromatic,}$ H-3, 9, 10, 11, 12, 18), 6.93 (m, 4H, $H_{aromatic,}$ H-2, 4, 17, 19). ^{13}C NMR (125 MHz, DMSO- d_6, δ ppm) C: 164.57 (C-5, 20), 160.91 (C-7, 14), 142.79 (C-8, 13), 132.97 (C-1, 16), 132.99 (C-9, 12), 128.35 (C-10, 11), 120.28 (C-3, 18), 120.01 (C-2, 17), 119.62 (C-6, 15), 117.20 (C-4, 19). UV-Vis (DCM) (λ_{max}/nm): 270 and 335. Anal. Calcd. For $C_{20}H_{16}N_2O_2$: C, 75.93; H, 5.10; N, 8.86. Found: C, 75.83; H, 4.80; N, 8.94.

3.3.6 (N^1E,N^2E)-N^1,N^2-bis(4-methoxybenzylidene)benzene-1,2-diamine, (2c)

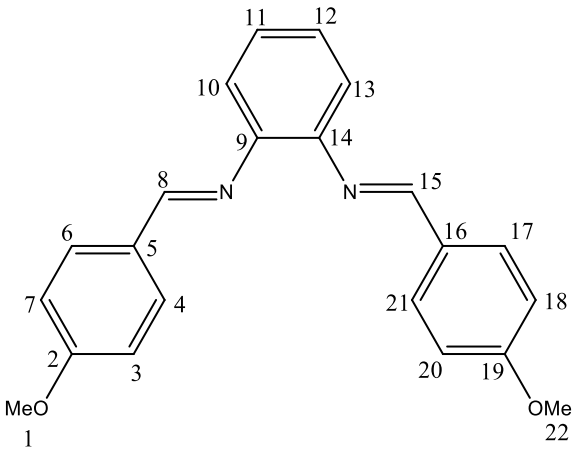

The procedure was similar to **1c** but *p*-phenylenediamine was replaced with *o*-phenylenediamine (5 mmol, 0.541 g). The solvent of the mixture solution was reduced until ~15 mL and left to precipitate at room temperature. The white precipitate formed was collected and wash with cold ethanol for a few times. Purification of the product was done *via* slow vapour diffusion of hexane into dichloromethane solution of the product. This method was according to the method as published by Pansuriya et al. (2007) with slight modification. Yield: 1.549 g, 90%. IR (KBr, cm^{-1}) υ: 3013.90 (C-H aromatic), 2831.40 (C-H stretching), 1606.87 (C=N stretching), 1509.73, 1456.75 (C=C aromatic), 1291.91 (C-N stretching), 826.82 (*para*-Subst.). ^{1}H NMR (500 MHz, $CDCl_3$, δ ppm) H: 7.88 (s, 1H, HC=N, H-8), 7.86 (s, 1H, HC=N, H-15), 7.65 (d, 2H, *J* = 8 Hz, $H_{aromatic,}$ H-6, 17), 7.23 (d, 2H, *J* = 7 Hz, $H_{aromatic,}$ H-11, 12), 7.03 (d, 2H, *J* = 8 Hz, $H_{aromatic,}$ H-4, 21), 6.97 (d, 2H, *J* = 8 Hz, $H_{aromatic,}$ H-7, 18), 6.86 (d, 2H, *J* = 8 Hz, $H_{aromatic,}$ H-3, 20), 5.40 (s, 2H, $H_{aromatic,}$ H-10, 13), 3.85 (s, 3H, H-1), 3.78 (s, 3H, H-22). ^{13}C NMR (125 MHz, $CDCl_3$, δ ppm) C: 161.02 (C-2), 159.24 (C-19), 154.24 (C-8), 143.28 (C-15), 136.20 (C-9), 130.81 (C-14), 128.60 (C-5), 127.33 (C-16), 122.85 (C-11, 12), 122.64 (C-10, 13), 119.82 (C-7, 3), 114.54 (C-21, 17), 114.30 (C-20, 18), 110.54 (C-6, 4), 55.48 (C-1), 55.41 (C-22). UV-Vis (DCM) (λ_{max}/nm):

285 and 336. Anal. Calcd. For $C_{22}H_{20}N_2O_2$: C, 76.72; H, 5.85; N, 8.13. Found: C, 76.38; H, 5.63; N, 7.96. MS (*m/z*): 344 [M].

3.3.7 (*N*,*N*'*E*,*N*,*N*'*E*)-*N*,*N*'-(ethane-1,2-diylidene)dianiline, (3a)

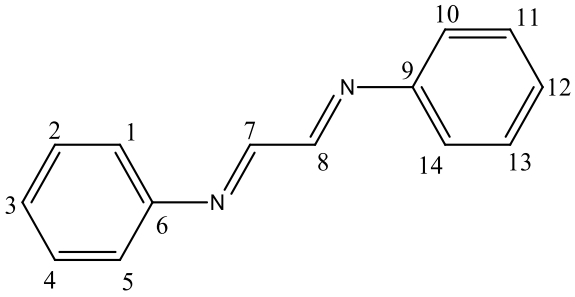

Aniline (10 mmol, 0.931 g) in 20 mL of ethanol was added into glyoxal (5 mmol, 0.290g) in 10 mL of ethanol. The solution was stirred at room temperature for 4 hours. The resulting pale yellow precipitate was collected and washed with cold ethanol and diethyl ether for a few times. This method was according to the method as published by Nourmohammadian & Gholami (2012) with slight modification. Yield: 0.541 g, 52%. IR (KBr, cm^{-1}) υ: 3390.68 (NH stretching), 3049.22 (C-H aromatic), 2899.10 (C-H stretching), 1595.09 (C=N stretching), 1497.96, 1427.31 (C=C aromatic), 1280.13 (C-N stretching). ^{1}H NMR (500 MHz, $CDCl_3$, δ ppm) H: 8.40 (s, 2H, HC=N, H-7, 8), 7.44 (t, 4H, *J* = 7 Hz, $H_{aromatic}$, H-2, 4, 11, 13), 7.31 (m, 6H, $H_{aromatic,}$ H-2, 3, 4, 11, 12, 13). ^{13}C NMR (125 MHz, $CDCl_3$, δ ppm) C: 159.84 (C-7, 8), 157.65 (C-6, 9), 143.06 (C-3, 12), 123.11 (C-2, 4, 11, 13), 114.68 (C-1, 5, 10, 14). UV-Vis (DCM) (λ_{max}/nm): 284 and 340. MS (*m/z*): 208 [M].

3.3.8 2,2'-((1*E*,1'*E*)-ethane-1,2-diylidenebis(azanylylidene))diphenol, (3b)

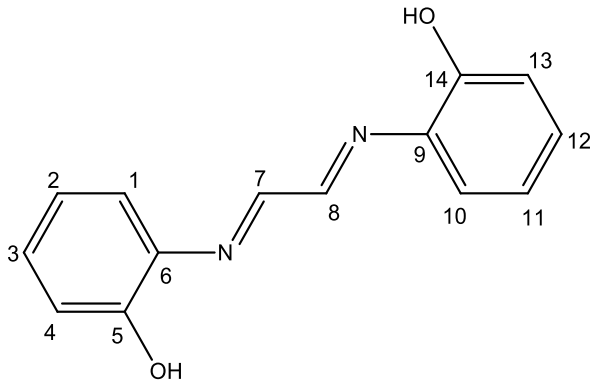

2-aminophenol (10 mmol, 1.091 g) in 20 mL ethanol was added into glyoxal (5 mmol, 0.290 g) in 10 mL ethanol. The mixture was refluxed for 2 hours at 80 °C. The precipitate formed was isolated *via* filtration and wash using cold ethanol for few times. This method was modified from the method as published by Nourmohammadian & Gholami (2012). Yield: 0.997 g, 83%. IR (KBr, cm^{-1}) υ: 3373.02 (NH stretching), 2928.54 (C-H aromatic), 2881.44 (C-H stretching), 1600.98 (C=N stretching), 1495.01, 1436.14 (C=C aromatic), 1341.95 (C-N stretching), 1247.75 (C-O stretching). ^{1}H NMR (500 MHz, DMSO-d_6, δ ppm) H: 7.29 (s, 2H, NH), 6.74 (t, 2H, *J* = 7 Hz, $H_{aromatic,}$ H-2, 11), 6.68 (d, 2H, *J* = 8 Hz, $H_{aromatic,}$ H-1, 10), 6.65 (d, 2H, *J* = 8 Hz, $H_{aromatic,}$ H-4, 13), 6.60 (t, 2H, *J* = 7 Hz, $H_{aromatic,}$ H-3, 12), 5.25 (s, 2H, H-7, 8). ^{13}C NMR (125 MHz, DMSO-d_6, δ ppm) C: 141.25 (C-5, 14), 130.11 (C-6, 9), 121.35 (C-2, 11), 118.60 (C-3, 12), 116.03 (C-1, 10), 114.14 (C-4, 13), 75.24 (C-7, 8). UV-Vis (DCM) (λ_{max}/nm): 293. MS (*m/z*): 240 [M].

3.3.9 (*N*,*N*'*E*,*N*,*N*'*E*)-*N*,*N*'-(ethane-1,2-diylidene)bis(4-methoxyaniline), (3c)

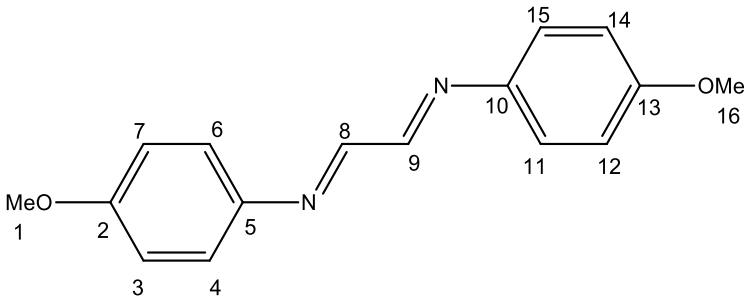

The procedure was similar to **3a** but aniline was replaced with *p*-anisidine (10 mmol, 1.23 g). The dark green needle precipitate was form and isolated *via* filtration and washed with cold ethanol few times. The product was in high purity and no purification steps needed. This method was according to the method as published by Tay et al. (2019). Yield: 1.034 g, 97%. IR (KBr, cm^{-1}) υ: 3016.84 (C-H aromatic), 2828.45 (C-H stretching), 1603.92 (C=N stretching), 1583.31, 1492.07 (C=C aromatic), 1280.13 (C-N stretching), 816.99 (*p*-Subst.). ^{1}H NMR (500 MHz, $CDCl_3$, δ ppm) H: 8.42 (s, 2H, H-8, 9), 7.33 (d, 4H, *J* = 7 Hz, H-4, 6, 11, 15), 6.95 (d, 4H, *J* = 7 Hz, H-3, 7, 12, 14), 3.84 (s, 6H, H- 1, 16). ^{13}C NMR (125 MHz, $CDCl_3$, δ ppm) C: 159.90 (C-2, 13), 157.72 (C-8, 9), 143.12 (C-5, 10), 123.19 (C-4, 6, 11, 15), 114.74 (C-3, 7, 12, 14), 55.67 (C-1, 16). UV-Vis (DCM) (λ_{max}/nm): 296 and 376. Anal. Calcd. For $C_{16}H_{16}N_2O_2$: C, 71.62; H, 6.01; N, 10.44. Found: C, 71.20; H, 5.74; N, 10.14. MS (*m/z*): 267 [M].

3.3.10 (*N*,*N*'*E*,*N*,*N*'*E*)-*N*,*N*'-(butane-2,3-diylidene)dianiline, (4a)

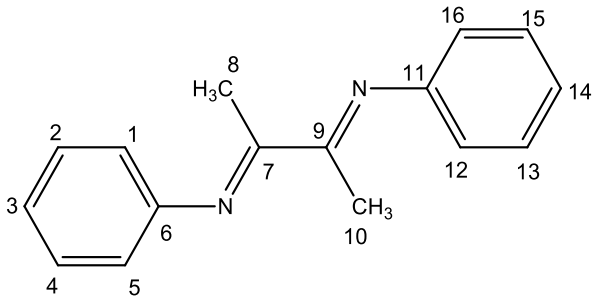

Diacetyl (5 mmol, 0.430 g) was added into a beaker. Then, 5 drops of glacial acetic acid, aniline (10 mmol, 0.931 g) and 1 mL of ethanol was added into the beaker containing diacetyl. The mixture was stirred at room temperature until yellow precipitate comes out. The formed precipitate was isolated *via* filtration and wash with cold ethanol and diethyl ether. This method was according to the method as published by Haddleton (2001) with slight modification. Yield: 0.221 g, 18%. IR (KBr, cm^{-1}) υ: 3061.00 (C-H aromatic), 2960.92 (C-H stretching), 1630.42 (C=N stretching), 1586.21, 1480.29 (C=C aromatic), 1366.44 (C-N stretching). ^{1}H NMR (500 MHz, $CDCl_3$, δ ppm) H: 7.38 (t, 4H, *J* = 14 Hz, H-2, 4, 13, 15), 7.12 (t, 2H, *J* = 15 Hz, H-3, 14), 6.80 (d, 4H, *J* = 10 Hz, H-1, 5, 12, 16), 2.16 (s, 6H, H-8, 10). ^{13}C NMR (125 MHz, $CDCl_3$, δ ppm) C: 168.36 (C-7, 9), 151.06 (C-6, 11), 129.07 (C-2, 4, 13, 15), 123.91 (C-3, 14), 118.75 (C-1, 5, 12, 16), 15.53 (C-8, 10). UV-Vis (DCM) (λ_{max}/nm): 334. Anal. Calcd. For $C_{16}H_{16}N_2$: C, 81.32; H, 6.82; N, 11.85. Found: C, 81.64; H, 6.47; N, 11.77. MS (*m/z*): 236 [M].

3.3.11 2,2'-((1*E*,1'*E*)-butane-2,3-diylidenebis(azanylylidene))diphenol, (4b)

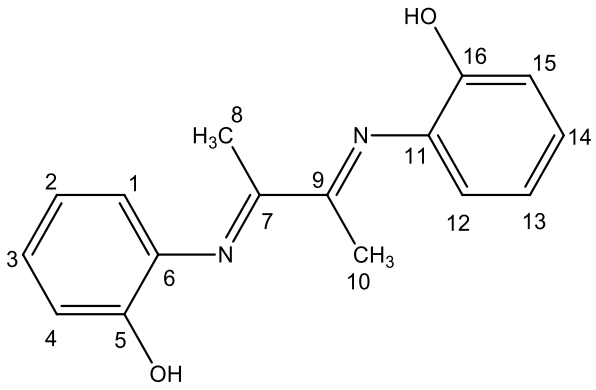

The procedure was similar to **3b** but the glyoxal was replaced with diacetyl (5 mmol, 0.430 g). Yield: 1.074 g, 80%. IR (KBr, cm^{-1}) υ: 3337.57 (NH stretching), 3031.47 (C-H aromatic), 2995.15 (C-H stretching), 1603.98 (C=N stretching), 1489.19, 1427.38 (C=C aromatic), 1383.23 (C-N stretching), 1227.24 (C-O stretching). ^{1}H NMR (500 MHz, DMSO-d_6, δ ppm) H: 7.18 (s, 2H, NH), 6.70 (m, 4H, $H_{aromatic,}$ H-1, 2, 10, 11), 6.58 (m, 4H, $H_{aromatic}$, H-3, 4, 12, 13), 1.40 (s, 6H, H-15, 16). ^{13}C NMR (125 MHz, DMSO-d_6, δ ppm) C: 141.55 (C-5, 14), 130.17 (C-6, 9), 120.70 (C-2, 11), 118.77 (C-3, 12), 115.96 (C-1, 10), 114.13 (C-4, 13), 81.92 (C-7, 8), 20.99 (C-15, 16). UV-Vis (DCM) (λ_{max}/nm): 293. MS (*m/z*): 268 [M].

3.3.12 (*N*,*N*'*E*,*N*,*N*'*E*)-*N*,*N*'-(butane-2,3-diylidene)bis(4-methoxyaniline), (4c)

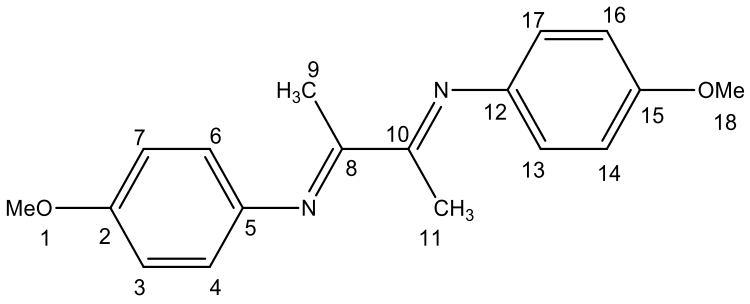

The procedure was also similar to **3c** but glyoxal was replaced with diacetyl (5 mmol, 0.430 g). The dark green precipitate was formed and isolated *via* filtration and washed with cold ethanol few times. The product was in high purity and no purification steps needed. This method was according to the method as published by Tay et al. (2019). Yield: 1.407 g, 95%. IR (KBr, cm^{-1}) υ: 2999.18 (C-H aromatic), 2834.34 (C-H stretching), 1630.42 (C=N stretching), 1600.91, 1497.96 (C=C aromatic), 1353.72 (C-N stretching), 838.59 (*p*-Subst.). ^{1}H NMR (500 MHz, DMSO-d_6, δ ppm) H: 6.96 (d, 4H, *J* = 9 Hz, H-4, 6, 13, 17), 6.80 (d, 4H, *J* = 9 Hz, H-3, 7, 14, 16), 3.76 (s, 6H, H-1, 18), 2.08 (s, 6H, H-9, 11).^{13}C NMR (125 MHz, DMSO- d_6, δ ppm) C: 168.61 (C-2, 15), 156.55 (C-8, 10), 144.19 (C-5, 12), 120.70 (C-4, 6, 13, 17), 114.39 (C-3, 7, 14, 16), 55.61 (C-1, 18), 15.55 (C-9, 11). UV-Vis (DCM) (λ_{max}/nm): 291 and 354. Anal. Calcd. For $C_{18}H_{20}N_2O_2$: C, 72.95; H, 6.80; N, 9.45. Found: C, 73.35; H, 6.52; N, 9.03. MS (*m/z*): 296 [M].

3.4 Preparation of symmetrical bis-Schiff base ligands boron complex

3.4.1 3,3'-(1,4-phenylene)bis(2,2-difluoro-2H-benzo[e][1,3,2]oxazaborinin-3-ium-2-uide), (1d)

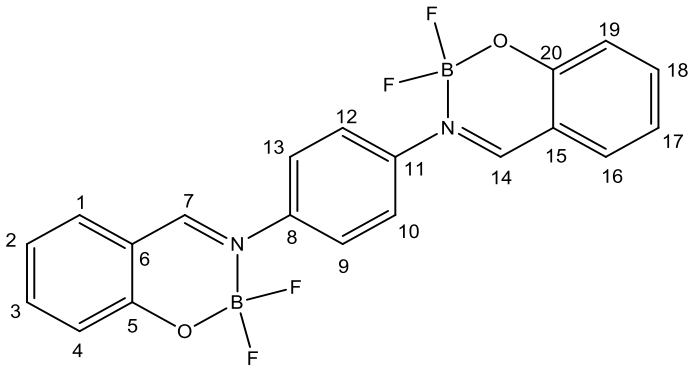

Ligand **1b** (0.63 mmol, 0.199 g) in 30 mL of dry dichloromethane was added into round bottom flask. Then, triethylamine (6.3 mmol, 0.637 g) was added into the solution. The mixture was degassed *via* freeze-pump-thaw technique and added with nitrogen gas and stirred for 15 minutes at 50 ℃. After that, boron difluoride diethyl ether (12.6 mmol, 1.788 g) was added slowly *via* syringe and degassed the mixture again *via* freeze-pump-thaw technique. The mixture was then refluxed while stirred for 4 hours at 85 ℃ to afford bright yellow precipitate. The formed precipitate was collected *via* filtration and washed with water and diethyl ether 15 mL each time for several times. This method was according to the method as published by Sen et al. (2020) with slight modification. Yield: 0.219 g, 84%. IR (KBr, cm^{-1}) υ: 3069.83 (C-H aromatic), 3037.45 (C-H stretching), 1618.64 (C=N stretching), 1550.94 (C=H aromatic), 1315.45 (C-N stretching), 1212.43, 1044.64 (B-F), 1153.56, 1097.63 (B-O). UV-Vis (DCM) (λ_{max}/nm): 293 and 387. Anal. Calcd. For $C_{20}H_{14}B_2F_4N_2O_2$: C, 58.31; H, 3.43; N, 6.80. Found: C, 58.34; H, 3.09; N, 6.66.

3.4.2 3,3'-(1,2-phenylene)bis(2,2-difluoro-2H-benzo[e][1,3,2]oxazaborinin-3-ium-2-uide), (2d)

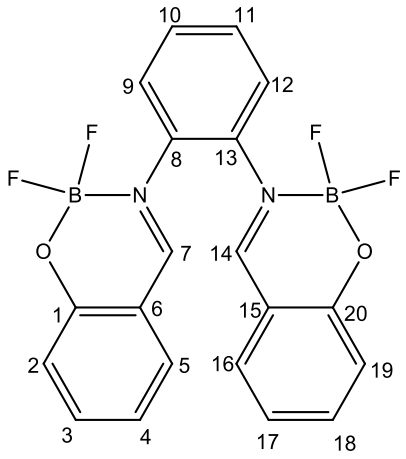

The procedure was similar to **1e** but ligand **2b** (0.63 mmol, 0.199 g) was used instead of ligand **1b**. The bright yellow precipitate was formed and collected *via* filtration and washed for a few times by using water and diethyl ether. Yield: 0.236 g, 91%. IR (KBr, cm^{-1}) υ: 3078.66 (C-H aromatic), 3046.28 (C-H stretching), 1618.64 (C=N stretching), 1459.69 (C=H aromatic), 1383.16 (C-N stretching), 1218.32, 1062.31 (B-F), 1130.01, 1085.85 (B-O). UV-Vis (DCM) (λ_{max}/nm): 279 and 364. Anal. Calcd. For $C_{20}H_{14}B_2F_4N_2O_2$: C, 58.31; H, 3.43; N, 6.80. Found: C, 57.95; H, 3.05; N, 6.66.

3.5 Fabrication of dye-sensitised solar cell (DSSC)

The method for DSSC fabrication was referring to method published by Phan (2019) with some modifications. In this work, the working electrode was made from FTO glass (ALDRICH) coated by TiO_2 layer meanwhile the counter electrode was made from ITO glass coated with conductive paint by Bare Conductive containing carbon black and graphite. The complete assembly of the device is shown in Figure 3.1. The preparation of each component is described in the following sub-section.

Figure 3.1: Complete assembly of DSSC

3.5.1 Preparation of TiO_2 working electrode

Titanium(IV) oxide anatase (TiO_2) (1 g) and polyethylene glycol (0.8 g) was added with 2 mL ethanol and 1 mL deionised water in a mortar. Then the mixture was ground using pestle until the texture of the mixture became a paste-like mixture. After that, three drops of triton X-100 were added into the mixture and grinded again for a while.

The FTO and ITO glass was rinsed and sonicated in acetone, methanol and deionised water for 5 minutes each time respectively. Then, the FTO and ITO glass was dried at 45 ℃ for 20 minutes and then exposed under UV light for 30 minutes. After that, adhesive tape was pasted on the FTO glass surface to make 1 cm x 2 cm dimension and TiO_2 was immediately onto the surface *via* doctor blade technique. After TiO_2 paste was dried a little bit, the tape was removed and the coated FTO glass was sintered at 460 ℃ for 15 minutes and then cooled to room temperature.

3.5.2 Preparation of N3 standard dye

A standard ruthenium dye used for DSSC device, *cis*-Bis(isothiocyanato)bis(2,2'-bipyridyl-4,4'-dicarboxylato) ruthenium(II), or commonly known as N3 dye (0.03 mmol, 0.0223 g) was added with 50 mL methanol and 50 mL acetonitrile in 250 mL beaker. The beaker was covered with aluminium foil to avoid any light exposure and sonicated for 30 minutes. The preparation was done in a dark room as N3 dye is sensitive to light.

3.5.3 Preparation of symmetrical bis-Schiff base ligands and complexes as dye sensitiser

All the respective bis-Schiff base ligands and boron difluoride complexes (0.03 mmol) was dissolved in 7 mL of dichloromethane. The dissolved compound was closed and sonicated for 10 minutes.

3.5.4 Preparation of working electrode

The coated FTO glass was immersed into the prepared N3 dye in a dark room and was placed in the oven at 45 ℃ for 120 minutes. Then, the FTO glass was taken out and wash with acetonitrile and air dried before assembling.

As for the bis-Schiff base ligands and boron difluoride complexes, the coated FTO glass was immersed into the prepared solution and put into the oven at 39 ℃ for 24 hours. Then the FTO glass was taken out and air dried.

3.5.5 Preparation of counter electrode

The counter electrode was done by using ITO glass. The cleaned ITO glass was also pasted with adhesive tape in the dimension of 1 cm x 2 cm. Then, the ITO glass was immediately coated with electric paint by Bare Conductive *via* doctor blade technique and left to dried at room temperature. After dried, the tape was removed and ready to be assembled.

3.5.6 DSSC electrolyte

Iodine sublimed (0.127 g) and 0.83 g potassium iodide was added into a 10 mL vial. Then, 10 mL ethylene glycol was added into the vial and the mixture was stirred for 30 minutes. The vial was wrapped with aluminium foil to avoid direct light exposure.

3.5.7 DSSC assembly

The prepared working electrode and counter electrode was put together face-to-face where the coated area face each other. The cell was then clipped together using binder clips at both sides and offset the edges to apply multimeter probes. After that, the iodide/triiodide redox electrolyte was dropped about 2-3 drops from the edges and the binder clips was squeezed a few times to make the electrolyte covered all the dye area and the cell was ready to be tested. The graphical diagram of DSSC assembling process is described in Figure 3.2.

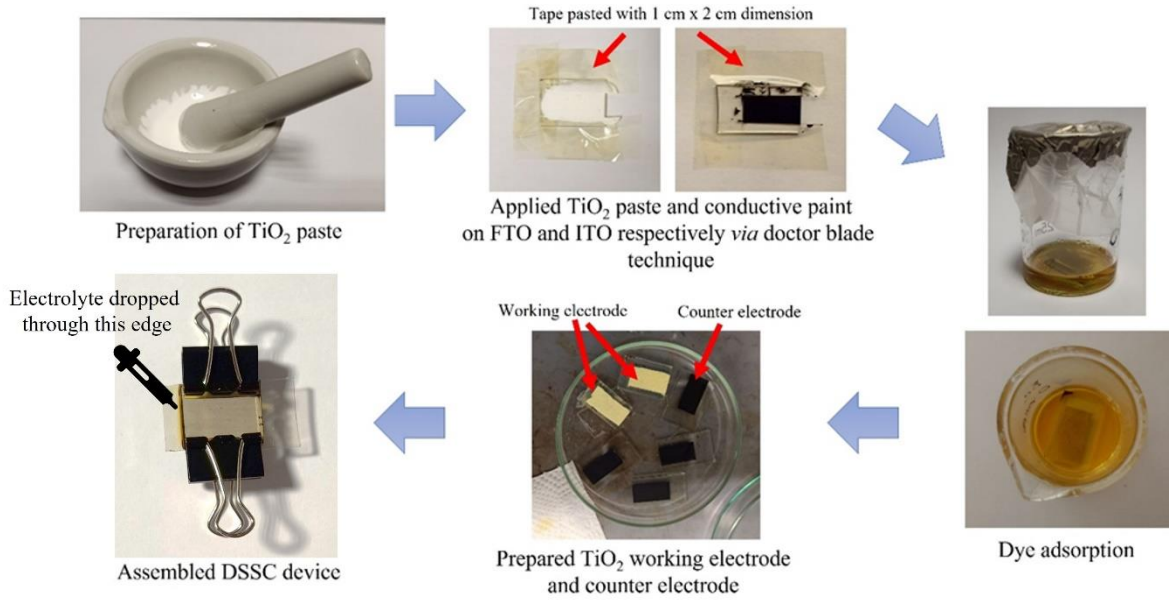

Figure 3.2: Graphical representation of DSSC assembling process

3.5.8 Photoelectrochemical measurement

Prior to testing the bis-Schiff base ligands and its boron complexes, *cis*-Bis(isothiocyanato)bis(2,2'-bipyridyl-4,4'-dicarboxylato) ruthenium (II), commonly known as N3 dye was tested first to make sure that the fabrication method and measurements were correct and consistent. The fabricated DSSC were tested with 100W LED lamp with resistor box (Shanghai Domao; Model: ZX21) and multimeter (XEOLE, China; Model: XL830L) to record the current-voltage (I-V) characteristics. An arrangement of 31.6 cm x 28.6 cm x 23.8 cm box was made for the measurements. Light intensity of the LED lamp was measured using light meter (Sunche Light Meter HS 1010) at the cell location point meanwhile the active area of the cell (2 cm^2) was measured with ruler.

From the I-V curves, the fill factor (FF) and the power conversion efficiency (η%) of the cell was calculated using the equation as shown in Equation 3.1 and Equation 3.2 respectively:

$$FF = \frac{J_{MP} \, X \, V_{MP}}{J_{SC} \, X \, V_{OC}}$$ Equation 3.1

J_{MP} = maximum current (mA)

V_{MP} = maximum voltage (mV)

J_{SC} = short-circuit currents (mA)

V_{OC} = open-circuit voltages (mV)

$$\eta = \frac{Jsc \, x \, Voc \, x \, FF}{Pin} \, x \, 100\%$$ Equation 3.2

Jsc = solar circuit current density (mA/cm^2)

Voc = open circuit photovoltage (V)

FF = fill factor (%)

Pin = incident light intensity (W/cm^2)

A = cell area (cm^2)

η = power conversion efficiency (%)

CHAPTER 4

RESULTS AND DISCUSSIONS

4.1 Synthesis of symmetrical bis-Schiff base compounds

4.1.1 Synthesis pathway and mechanism of bis-Schiff base compounds

A total of eleven conjugated symmetrical bis-Schiff base and their complexes have been synthesised. For the conjugated symmetrical bis-Schiff base, there are four different series that have different π-spacer as shown in Figure 4.1. The π-spacers as the connector of the two phenyl rings to allow the π-electron transfer from one side to another side along the bis-Schiff base molecule.

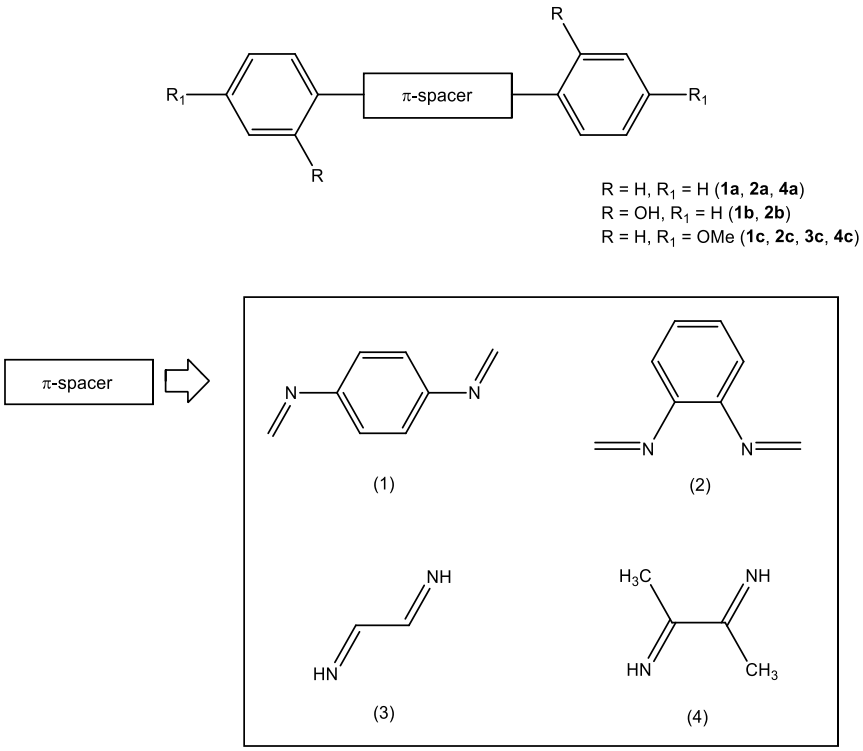

Figure 4.1: Four series of conjugated symmetrical bis-Schiff base compounds

The formation mechanism of bis-Schiff base molecule is as shown in Scheme 4.1 but due to variety of compounds that have been synthesised, compound **1a** has been chosen to represent the conjugated symmetrical bis-Schiff base formation.

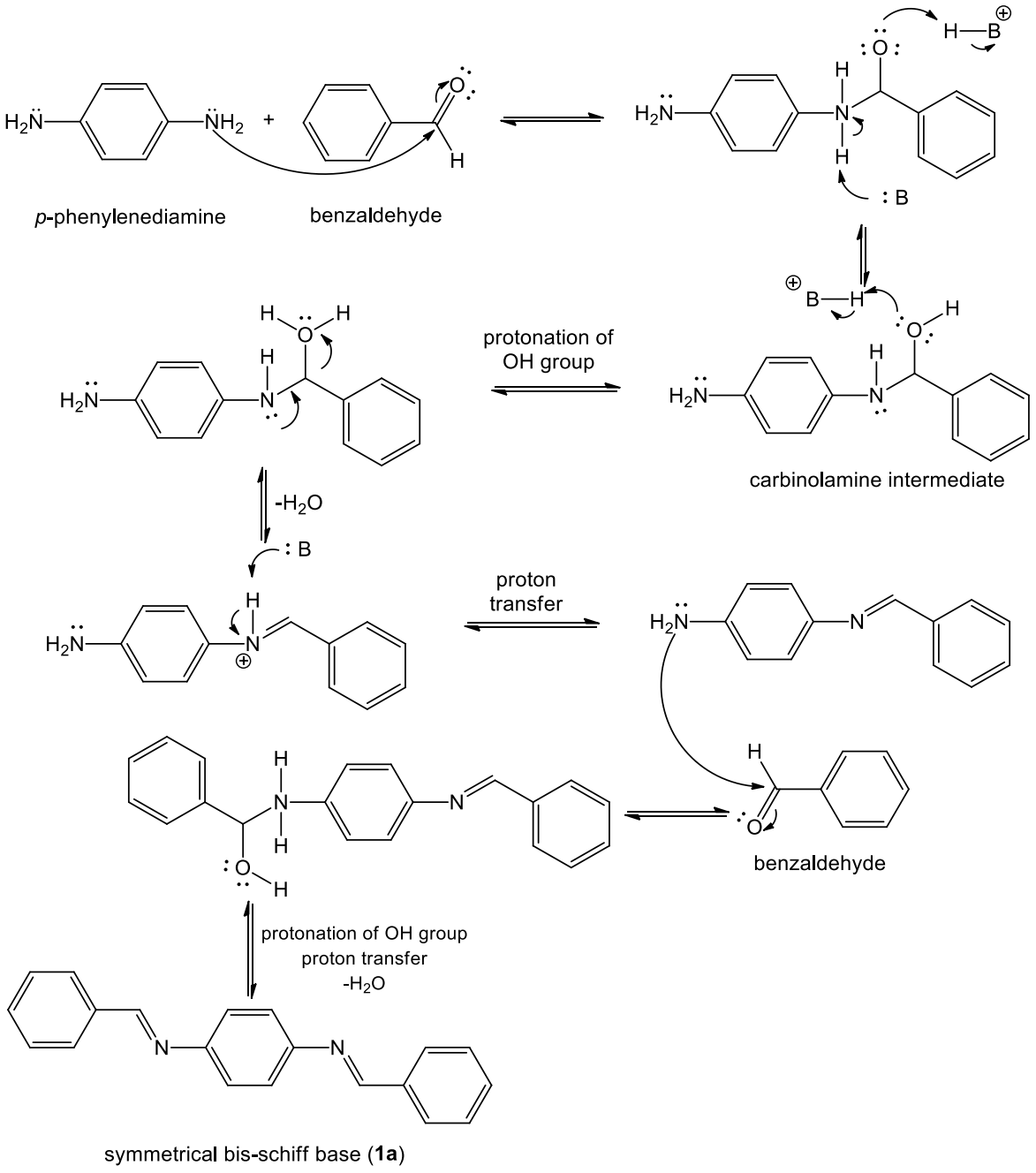

Scheme 4.1: Conjugated symmetrical bis-Schiff base compound formation mechanism (**1a**)

From Scheme 4.1 the carbonyl (C=O) group of the aldehyde/ketone is a good electrophile meanwhile the amine is a good nucleophile. Nucleophilic attack of lone pair electron from amine to the carbonyl group of aldehyde/ketone generate a tetrahedral intermediate which then undergo deprotonation from bases (denoted with B) and forming carbinolamine intermediate. The hydroxyl (-OH) group in the carbinolamine intermediate then undergo another protonation to become water molecule which is a good leaving group. Lone pair from the adjacent nitrogen helps to facilitate the departure of the leaving group generating another intermediate which is a protonated Schiff base. Deprotonation of hydrogen molecule to remove the positive charge will then generate the final form of Schiff base.

4.1.2 Synthesis and characterisation of conjugated symmetrical bis-Schiff base compounds

All the compounds were successfully synthesised except for compounds **3a**, **3b** and **4b** as shown in Figure 4.2. Compound **3a** was failed to be synthesised because of the instability of imine (C=N) bond. The instability of imine bond causes the hydrolysis of the structure which makes the starting materials still present in the final product. The formation of by-products instead of Schiff base in the synthesis of **3b** and **4b** was the reason causing the failure to synthesise these two compounds. The by-products undergo cyclisation with the -OH substituent. Despite this, the following sub-topics will go into further detail into the attempts and outcomes of those compounds. Despite that, the attempts and results of those compounds will be discussed further in the following sub-topics.

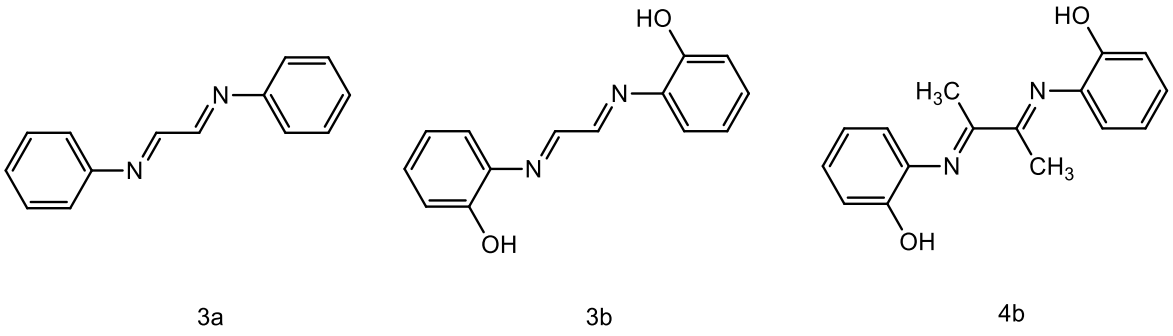

3a 3b 4b

Figure 4.2: Chemical structure of compound **3a**, **3b** and **4b**

Compound **1a** was synthesised by reacting *p*-phenylenediamine with benzaldehyde in 1:2 ratio respectively (Scheme 4.2). Ethanol was used as the solvent and the reaction was carried out by refluxing the mixture for 2 hours at 80 ℃ while stirred. In order to follow green synthesis route, no acid catalyst was added in the reaction as the reaction still proceed in the absence of acid. At the end of the reaction, yellow precipitate formed and isolated *via* filtration and washed with cold ethanol to remove impurities. Vapour diffusion method of hexane into dichloromethane solution of the product was used to crystallise the product to further purify the end product. Similar method was used to synthesise the rest of the compounds except for compound **2a** and **4a**.

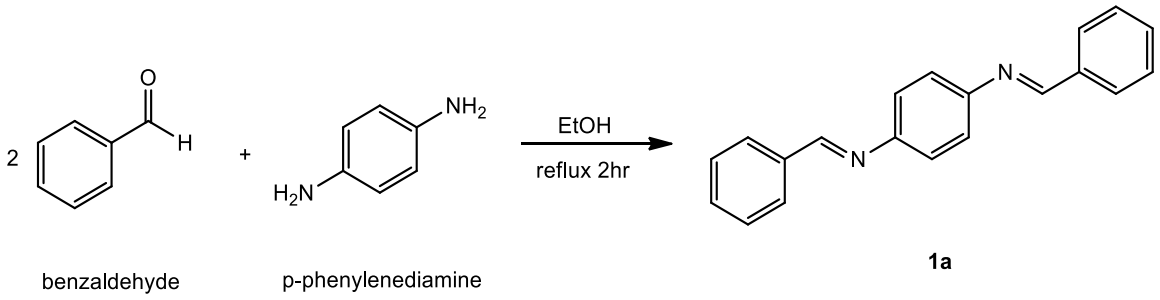

benzaldehyde p-phenylenediamine

Scheme 4.2: Chemical reaction of compound **1a**

For compound **2a**, *o*-phenylenediamine and benzaldehyde was reacted similarly for the refluxing part, but no precipitate was formed even after the reaction was completed (Scheme 4.3). To induce the precipitate, the amount of solvent was reduced to ~15 mL using rotary evaporator. The concentrated mixture was left to precipitate at room temperature. Other method to induce precipitation such as adding insoluble solvent into the mixture to reduce solubility resulting in the formation of benzimidazole instead of Schiff base compound. However, when the concentrated mixture was left to precipitate on its own, its result in the formation of Schiff base by-product as shown in the gas chromatogram in Figure 4.3. This is because the reaction between *o*-phenylenediamine and aldehyde faces selectivity problem due to the competitive formation of Schiff base compounds (I), 2-disubstituted benzimidazole (II) and 1,2-substituted benzimidazole (III) as shown in Scheme 4.4 (Yu et al., 2016).

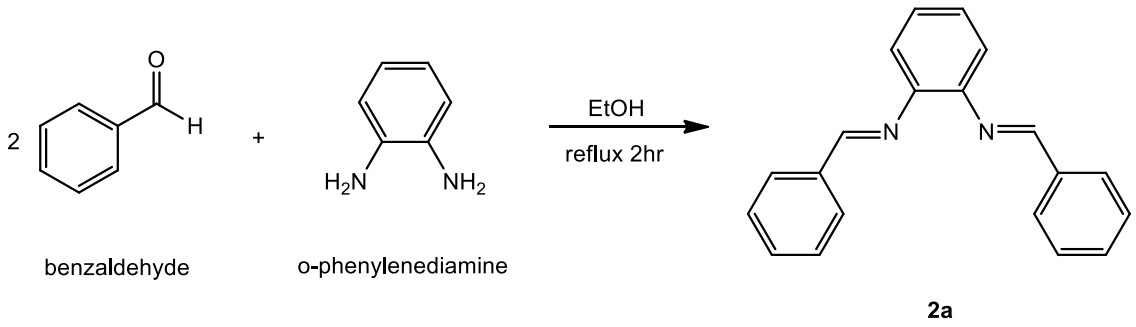

Scheme 4.3: Chemical reaction of compound 2a

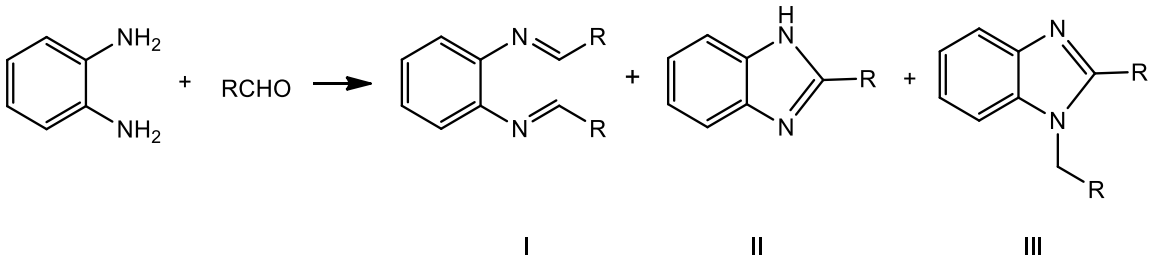

Scheme 4.4: Possible formation of reaction between *o*-phenylenediamine and aldehydes

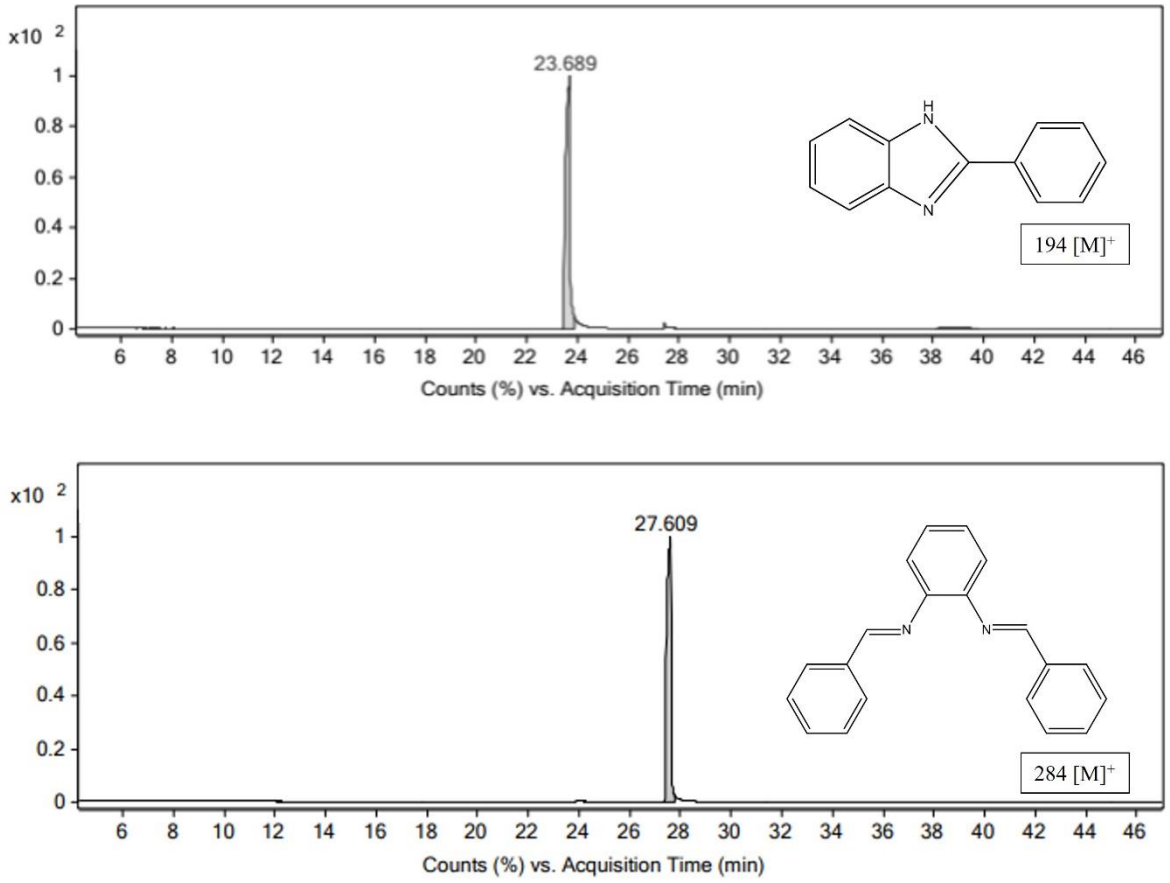

Figure 4.3: Gas chromatogram of benzimidazole and Schiff base formation of **2a**

Compound **3a** was synthesised using the same procedure for compound **1a** as mentioned in Scheme 4.2. At the end of the procedure, a pale-yellow precipitate was obtained after being filtering and washed using cold ethanol and diethyl ether. From IR spectroscopy data (Figure 4.4), a strong peak at 1595.09 cm^{-1} is found indicating the presence of C=N group of the imine group in Compound **3a**. Apart from that, another two strong

stretching bands are found at 1497.96 cm^{-1} and 1427.31 cm^{-1} which indicate the presence of C=C of the aromatic rings of the molecule. The vibration bands of 1280.13 cm^{-1} and 3049.22 cm^{-1} were found indicate the presence of C-N and C-H aromatic, respectively. However, the presence of vibration bands at 3390.68 cm^{-1} and 3364.19 cm^{-1} belong to N-H group of aniline, which proved that the starting materials was still present in the product. The band for primary amine occurs at the range of 3500-3300 cm^{-1} and present in two band (Pavia et al., 2014).

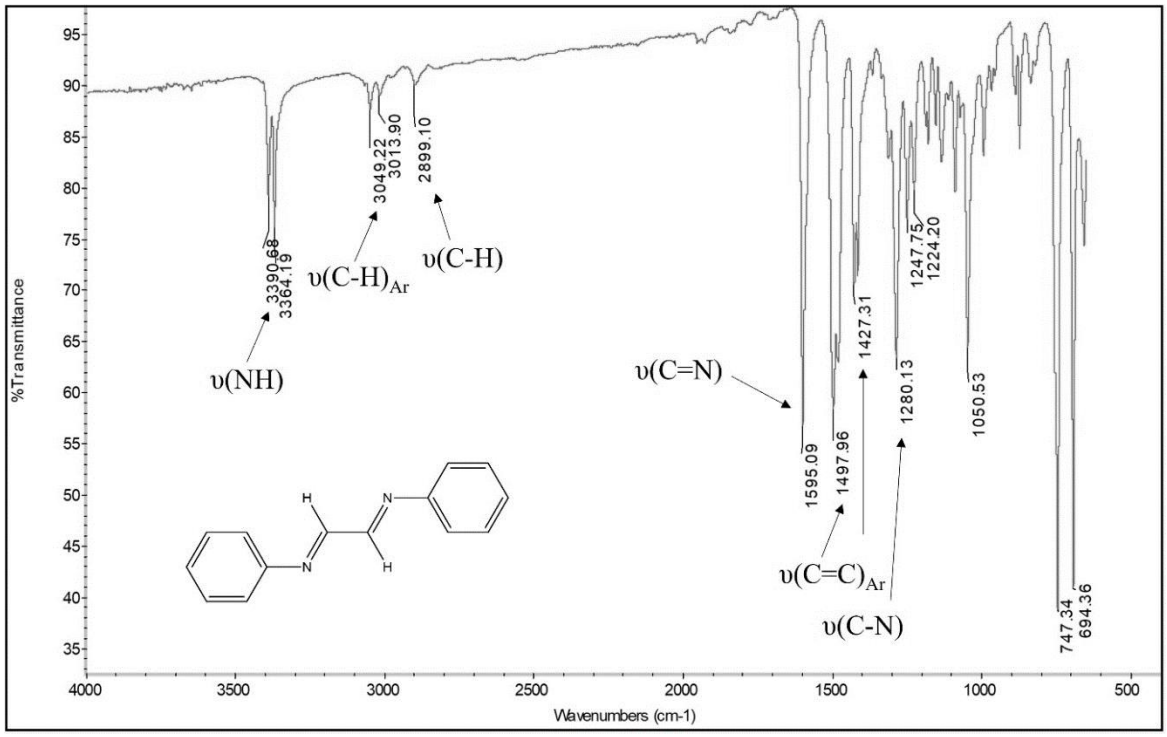

Figure 4.4: IR spectrum of compound **3a**

^{1}H NMR spectrum of compound **3a** (Figure 4.5) also indicate the presence of starting material at δH 3.69 which correspond to the NH group from aniline. A singlet resonance peak at δH 8.40 ppm is assigned to the imine proton (-C=N-) indicating the successful formation of diimine compound (Abdalhadi et al., 2020). Apart from that, a triplet at δH 7.44 ppm and a multiplet at δH 7.31 which is due to the overlapping of a doublet and triplet

is also found attributed to the aromatic protons of the diamine compound. In addition, two triplets at δH 7.15 ppm and δH 6.75 ppm due to the aromatic protons from aniline as well. The ^{13}C NMR spectrum also indicate the presence of aniline which can be found in Appendix 20.

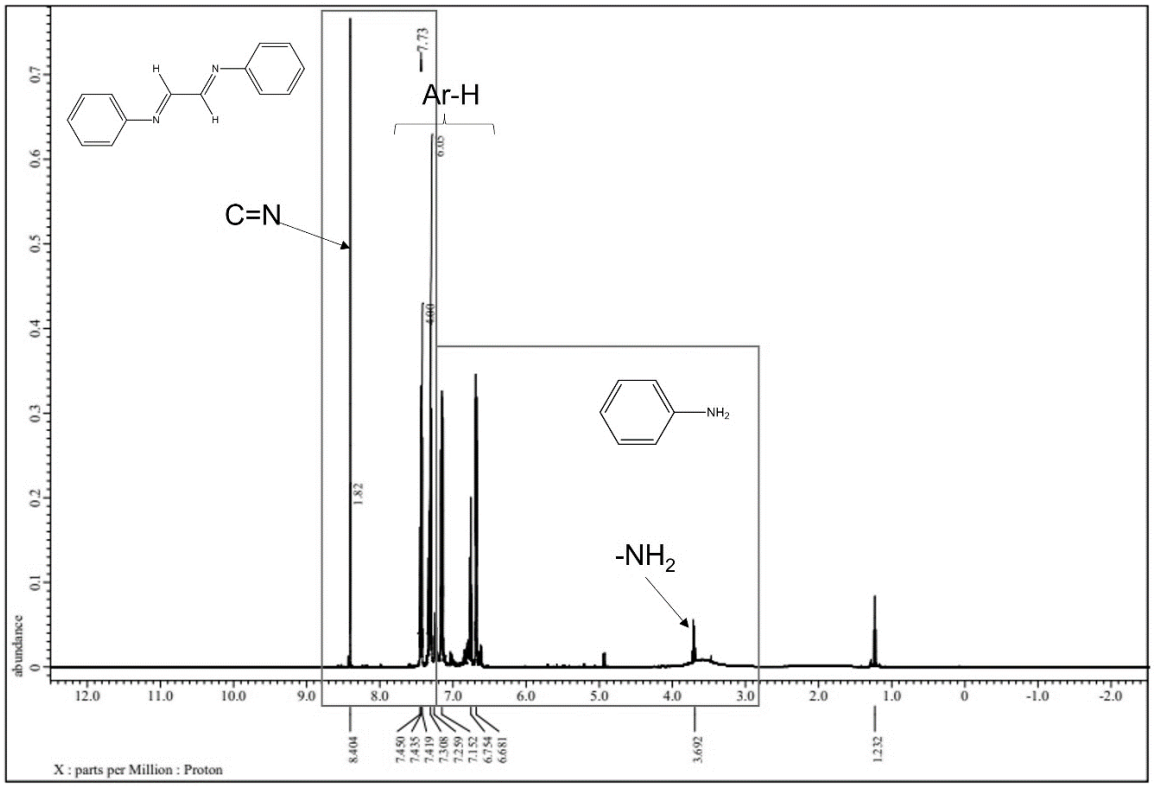

Figure 4.5: ^{1}H NMR spectrum compound **3a**

In addition, GC-MS data as shown in Figure 4.6 also shows extra peak assigned to aniline peak aside from the Schiff base peak. The peak present at 21.252 minutes retention time with 60.7% area belongs to compound **3a** whereas the peak at 8.445 minutes retention times with 39.3% area belongs to the starting material aniline.

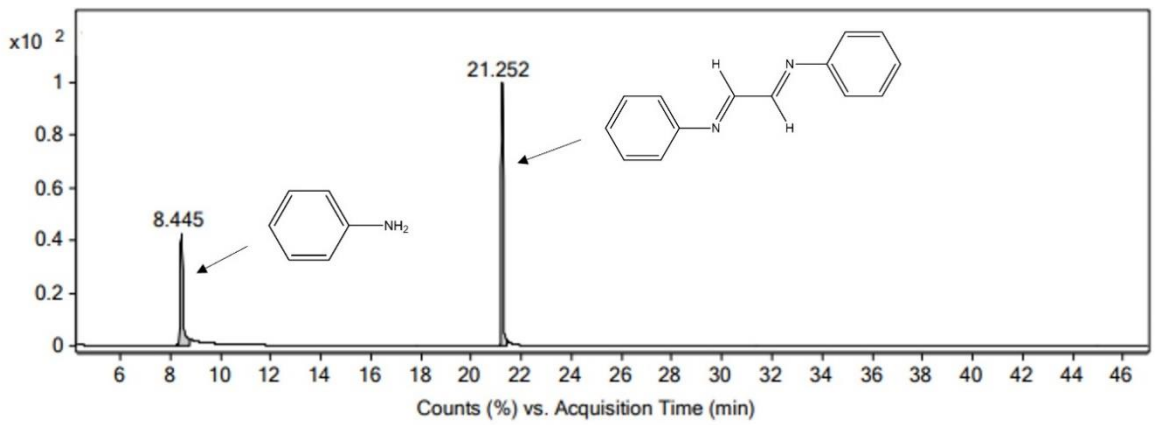

Figure 4.6: Gas chromatogram of compound **3a**

Referring to mass spectrum of in Figure 4.7 below, the top mass spectrum is belonged to the starting material aniline that has base peak of m/z= 93. Meanwhile, the bottom mass spectrum is the spectrum of compound **3a.** Base peak value of m/z 207 is indicated to the parent compound **3a**. The fragment ion at peak m/z = 104 is due to the loss of half of the structure which include a benzene ring and imine group from the parent molecule that form $C_7H_6N^+$ ion. Another peak at m/z = 77 is due to the benzene ring after the loss of imine group generating $C_6H_5^+$.

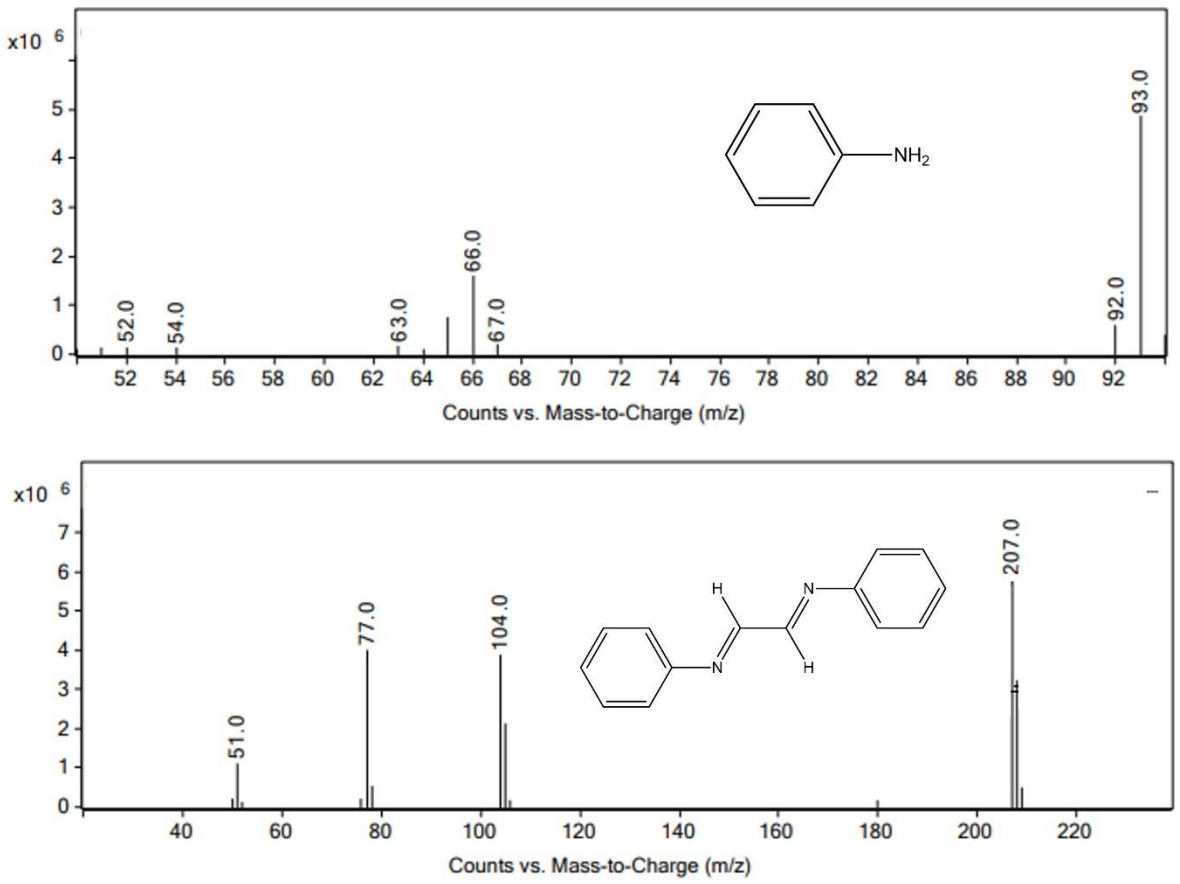

Figure 4.7: Mass spectrum of compound **3a** and aniline

The UV-visible absorption spectrum (Figure 4.8) was obtained by using DCM solvent in room temperature. From the spectrum, two distinct absorption bands are observed at λ = 284 nm and λ = 340 nm which are assigned to the electronic transition of $\pi \rightarrow \pi^*$ of the aromatic rings and $n \rightarrow \pi^*$ of the imine group respectively.

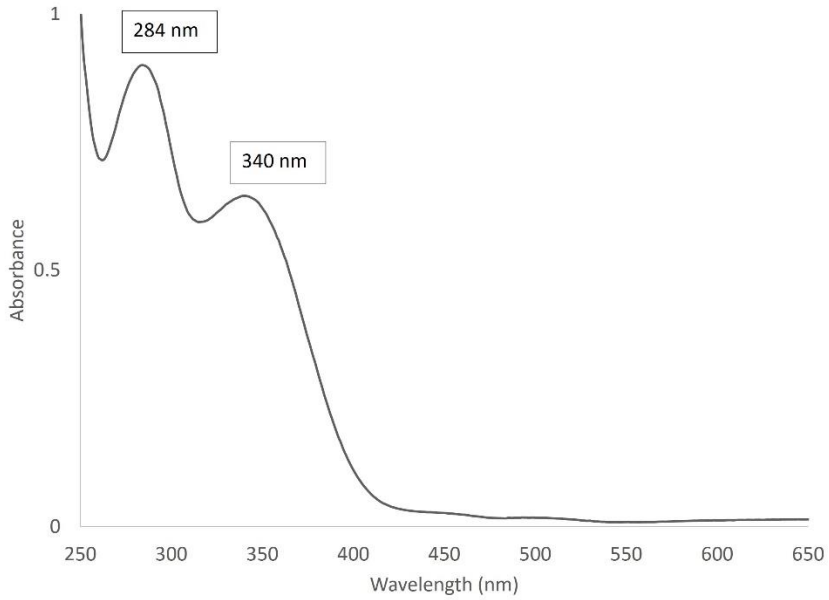

Figure 4.8: UV-visible spectrum of compound **3a**

The presence of starting materials aniline in the compound can be due to the instability of the imine bond (-C=N-) which cause hydrolysis of compound **3a**. A longer reaction duration (4 – 5 hours) was also tried in order to get rid of aniline by completing the reaction but aniline still remained in the final product. This suggested that the reaction's incompletion might not be the reason. Several other methods such as recrystallisation and column chromatography to purify and isolate compound **3a** were not successful and aniline still remained in the final product. For this reason, the pure form of compound **3a** was not successfully obtained.

As for compound **4a** (Figure 4.9), similar attempts at synthesis fail to form any precipitate. Therefore, another method by Haddleton (2001) was modified and tested in which compound **4a** was able to be synthesised. The preparation method only needs to stir both starting materials in a little amount of ethanol (1 mL) with the addition of glacial acetic acid (5 drops) as the catalyst. The yellow precipitate formed almost immediately, and it was then filtered and washed with ethanol and diethyl ether.

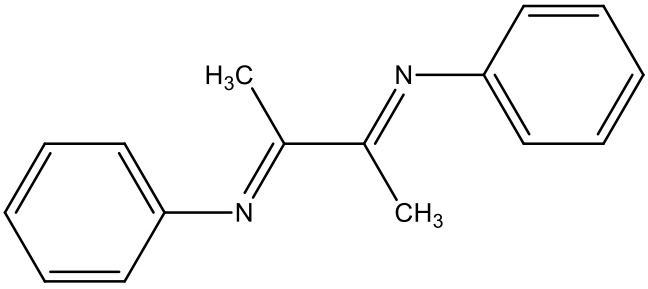

Figure 4.9: The chemical structure of (*N,N'E,N,N'E)-N,N'-*(butane-2,3-diylidene)dianiline (**4a**)

Compounds **3b** and **4b** (Figure 4.10) were also attempted but after a few trial and method modifications, the compounds were still failed to be synthesise as it does not form a Schiff base structure but instead the reaction underwent cyclisation to form bibenzoxazoline (Figure 4.11). The product of condensation reaction of *o*-aminophenols with carbonyl groups could either produce an oxazolidine, which form rapidly, or a mixture of oxazolidine with Schiff base in equilibrium in which it is the most direct route of this reaction (Murase, 1959; Hajji et al., 2013). It is thought at first that the condensation product of glyoxal with aniline would provide **3b** but after a structural reinvestigation suggested that the final product is as shown in Figure 4.11 (Farfán et al., 1992). It is also reported that aniline are readily forms heterocycles as the amino and hydroxy group are adjacent to each other due to the stereo-selective transformation of glyoxal (Cinar et al 2020). According to Farfán (1992), this kind of condensation reaction determine by the steric factors of the dicarbonyl compounds, acidity of hydroxyl group as well as the basicity of the amino group. The NMR, IR spectroscopy and also crystalline analysis by Tauer (1986) & Niklas (2019) also showed the formation of bibenzoxazoline structure. The reaction of *o*-aminophenols with aniline or diacetyl is shown in Scheme 4.5.

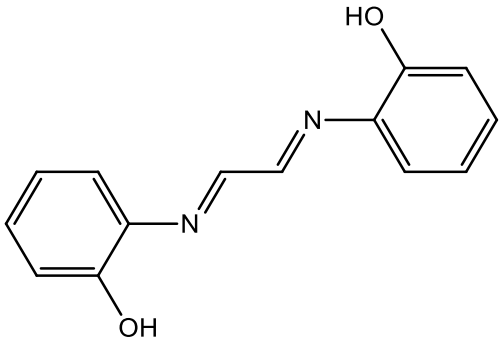

2,2'-((1*E*,1'*E*)-ethane-1,2-diylidenebis(azanylylidene))diphenol

3b

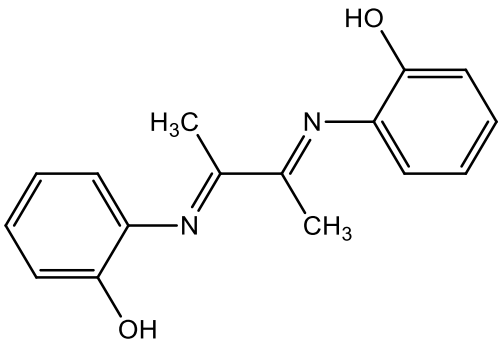

2,2'-((1*E*,1'*E*)-butane-2,3-diylidenebis(azanylylidene))diphenol

4b

Figure 4.10: Chemical structure of compounds **3b** and **4b**

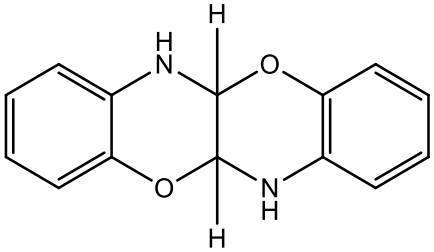

2,2'-bibenzoxazoline

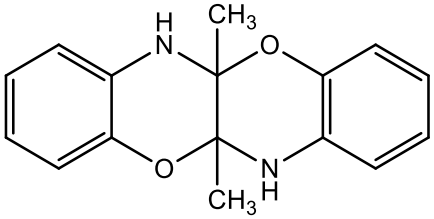

2,2'-dimethyl-2,2'-bibenzoxazoline

Figure 4.11: Chemical structure of cyclisation product

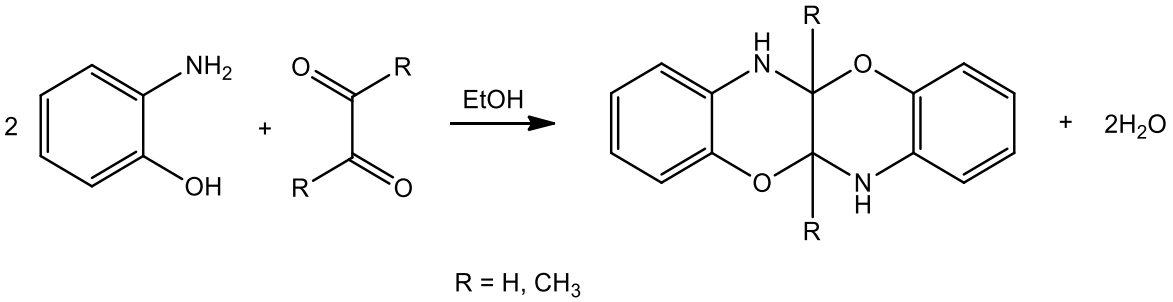

R = H, CH_3

Scheme 4.5: Reaction of 2-aminophenol with glyoxal (**3b**) and diacetyl (**4b**)

According to IR spectrum that is shown in Figure 4.12, a sharp peak was observed at 3372.02 cm^{-1} corresponding to -N-H- group from the cyclic part at the middle of the

structure. According to Pavia and co-workers (2014), the secondary amines appear as one band and weaker peak of aliphatic compounds comparing to aromatic compounds. Therefore, although both peaks appear at about the same frequency range (3300 cm^{-1}), it correspond to the N-H peak because N-H peak appears as a strong sharp peak whereas -OH peak appears as a strong broad peak (Pavia et al., 2014). In addition, another IR stretching at 1600.98 cm^{-1} is attributed to the -C=C- of cyclic alkene. C-N and C-O vibration bands are also found in the spectrum at 1391.45 cm^{-1} and 1209.48 cm^{-1} respectively. Apart from that, the presence of vibration bands at 1495.01 cm^{-1} and 1436.14 cm^{-1} are attributed to the C=C aromatic rings of the molecule. Similarly, IR spectrum for compound **4b** were found at around similar vibration bands as compound **3b** as shown in Figure 4.13.

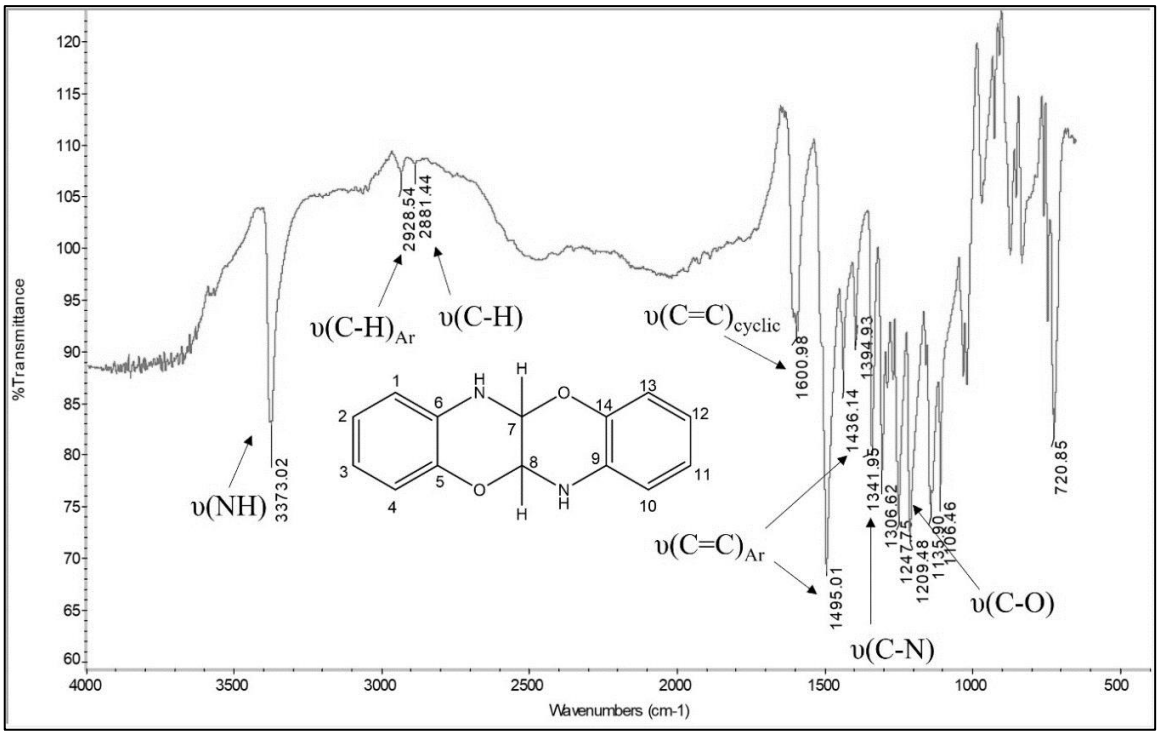

Figure 4.12: IR spectrum of compound **3b**

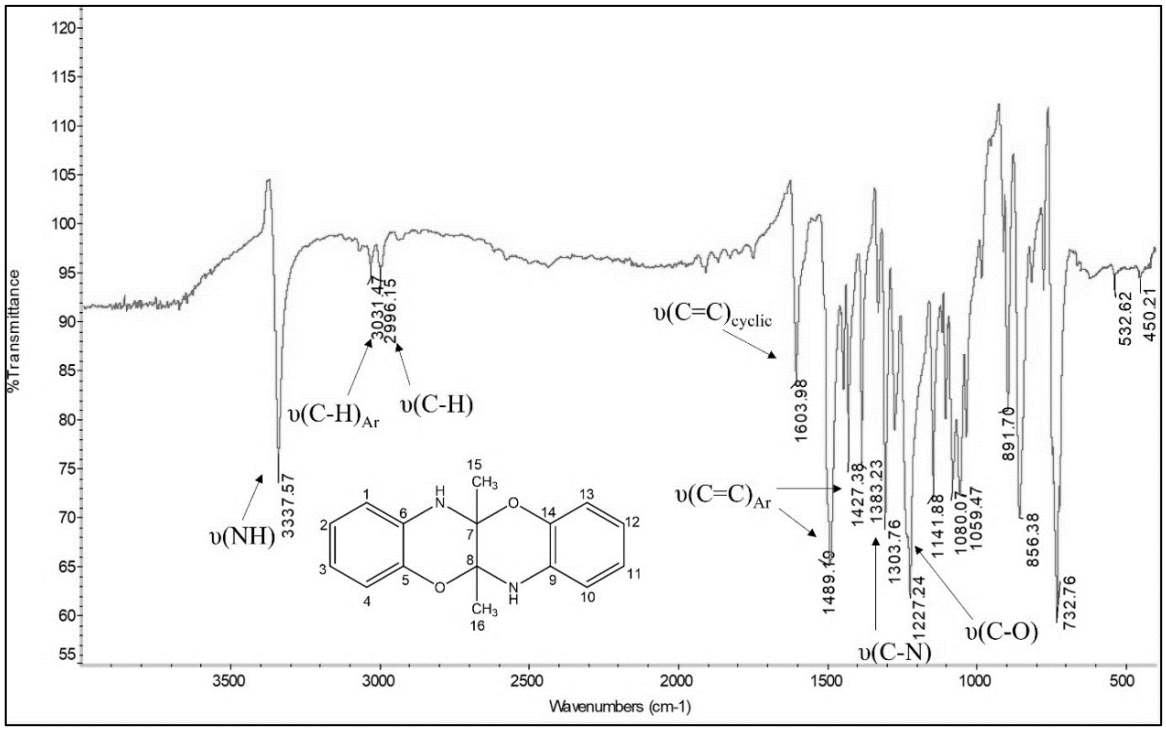

Figure 4.13: IR spectrum of compound **4b**

^{1}H NMR spectrum of compound **3b** (Figure 4.14) also indicates the formation of bibenzoxazoline instead of Schiff base compound. A singlet resonance peak at δH 7.29 ppm was attributed to the -NH group. In addition, two triplets and two doublets are observed at δH 6.74 ppm - δH 6.60 ppm correspond to the aromatic protons of the compound. Another singlet resonance as found at δH 5.25 ppm which correspond to aliphatic C-H of the cyclic alkene at the centre part of the molecule. Furthermore, ^{1}H NMR spectra for compound **4b** (Figure 4.15) observed peaks correspond to bibenzoxazoline as well. Referring to the spectrum, a singlet resonance peak at δH 7.18 ppm attributed to the -NH peak meanwhile peaks in the range of δH 6.70 - δH 6.58 ppm attributed to aromatic protons of the compound. Another singlet resonance at δH 1.40 ppm observed was correspond to the methyl (-CH_3)

peak at the centre of the compound structure. Therefore, it is confirmed that compound **3b** and **4b** does not form Schiff base as there is no imine proton was observed in the spectrum.

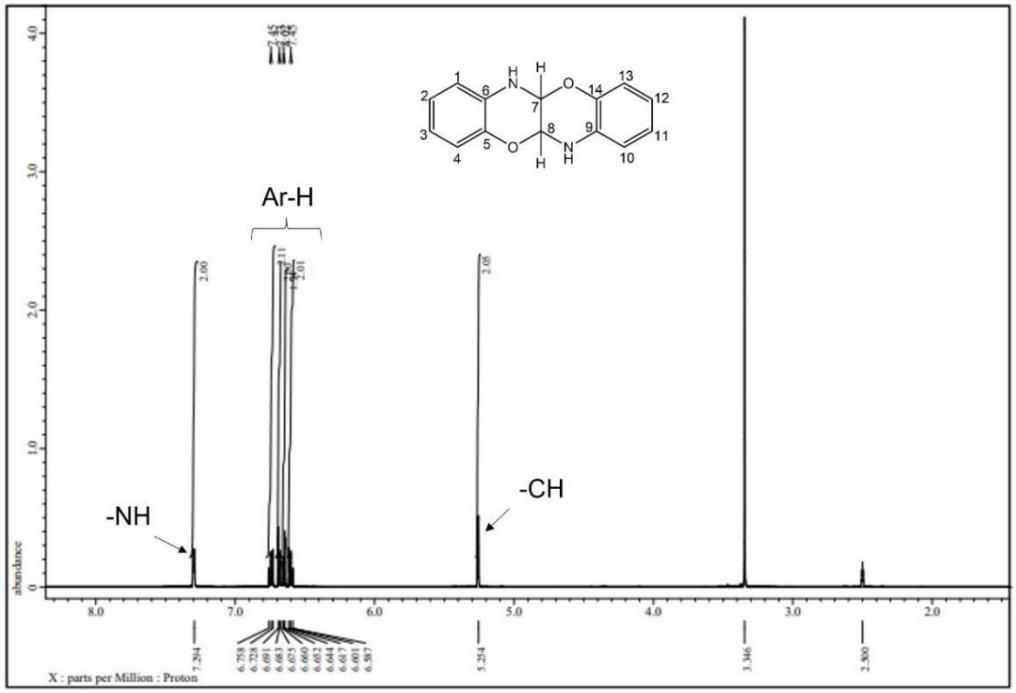

Figure 4.14: ^{1}H NMR spectrum of compound **3b**

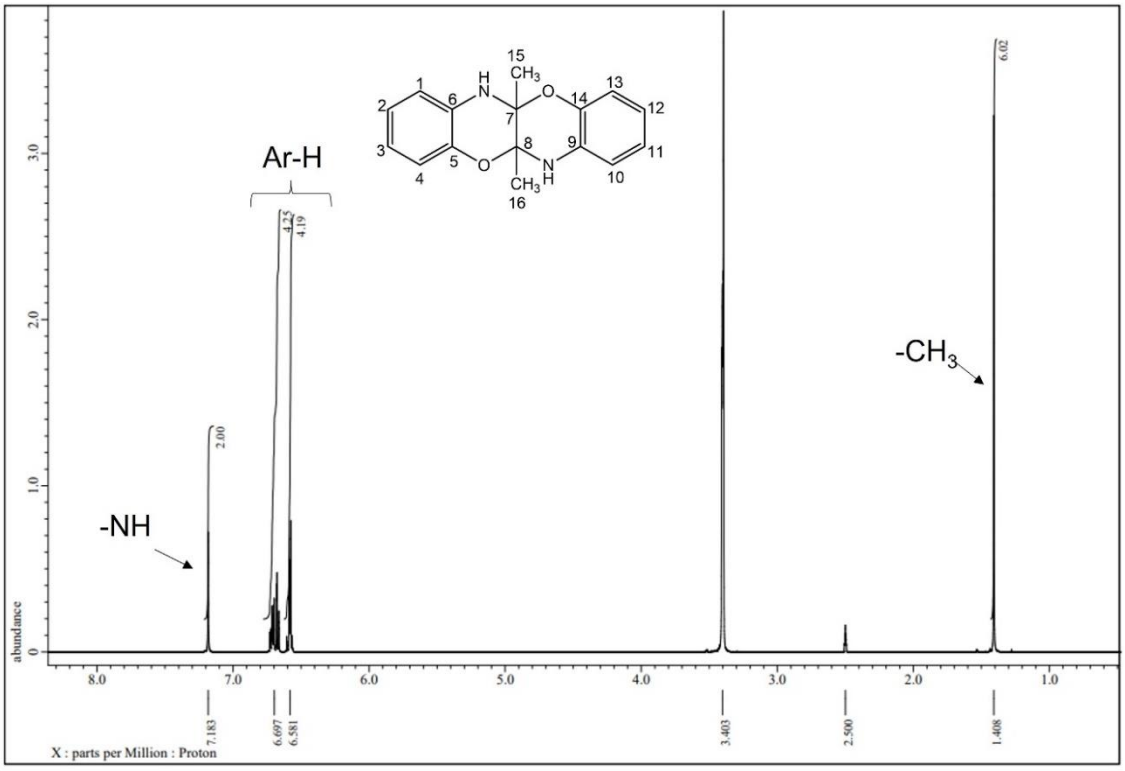

Figure 4.15: ^{1}H NMR spectrum of compound **4b**

The ^{13}C NMR spectra of compounds **3b** and **4b** can be found in Figure 4.16 and Figure 4.17 below respectively. Based on the ^{13}C NMR spectra, both compounds **3b** and **4b** show correct number of carbons accordingly to their structure. For ^{13}C NMR spectrum for compound **4b**, there are extra peak located at δC 20.99 ppm due to carbon of methyl group in the structure. Although both Schiff base compounds and bibenzoxazoline compounds both have the same number of carbons, the absence of peak at around δC 150 ppm – 160 ppm at both spectrum which should be correspond to C=N signal further prove that the compound formed was not Schiff base but indeed, it was bibenzoxazoline.

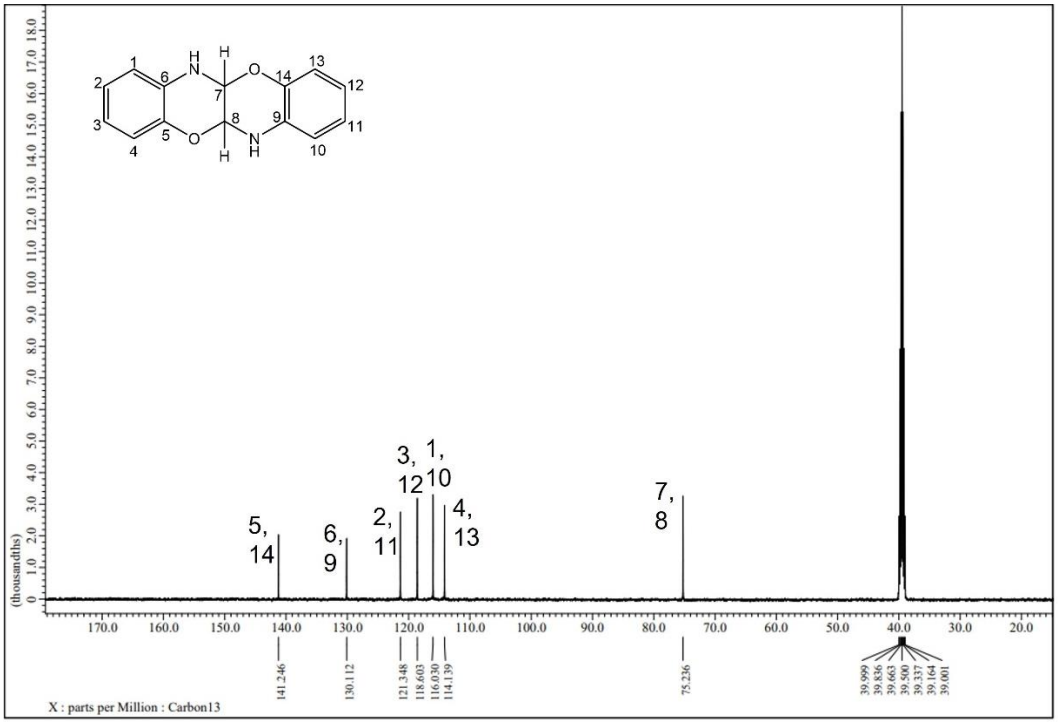

Figure 4.16: ^{13}C NMR spectrum of compound **3b**

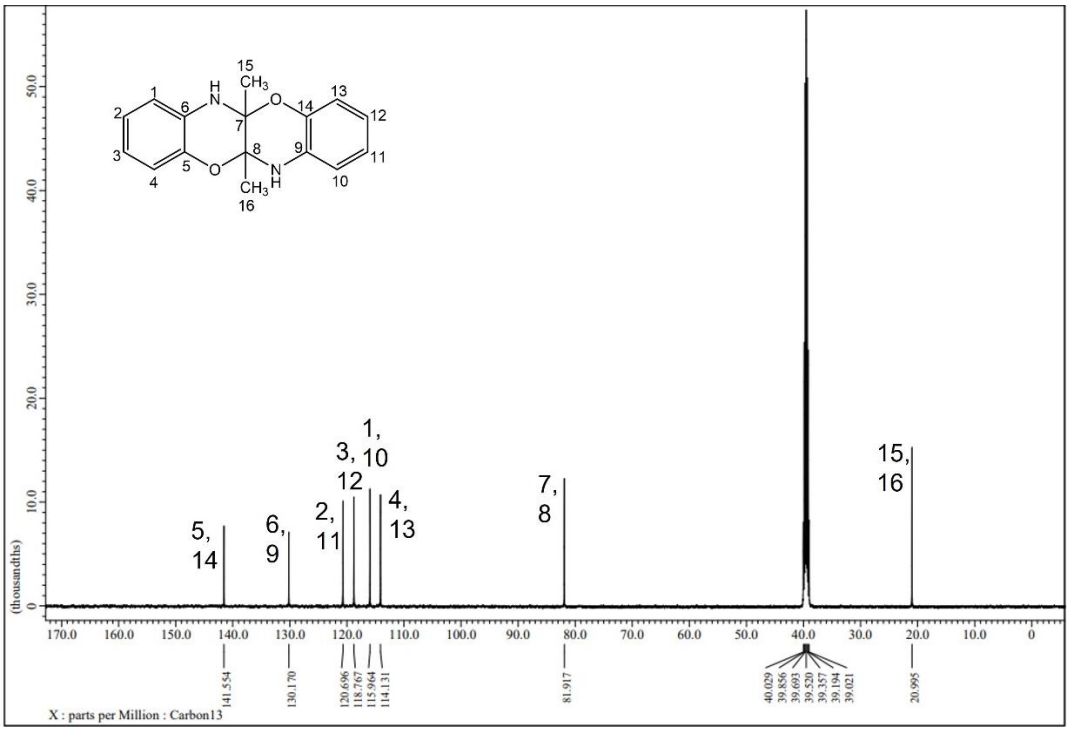

Figure 4.17: ^{13}C NMR spectrum of compound **4b**

Figure 4.18 shows the mass spectrum for compound **3b**. Based on the spectrum, base peak of m/z = 240 is the parent peak. The loss of half of the molecule gives ion peak of m/z = 133 ($C_8H_7NO^{2+}$) while the fragmentation of both NH-C bond corresponds to the ion peak of m/z = 120 ($C_7H_6NO^{3+}$).

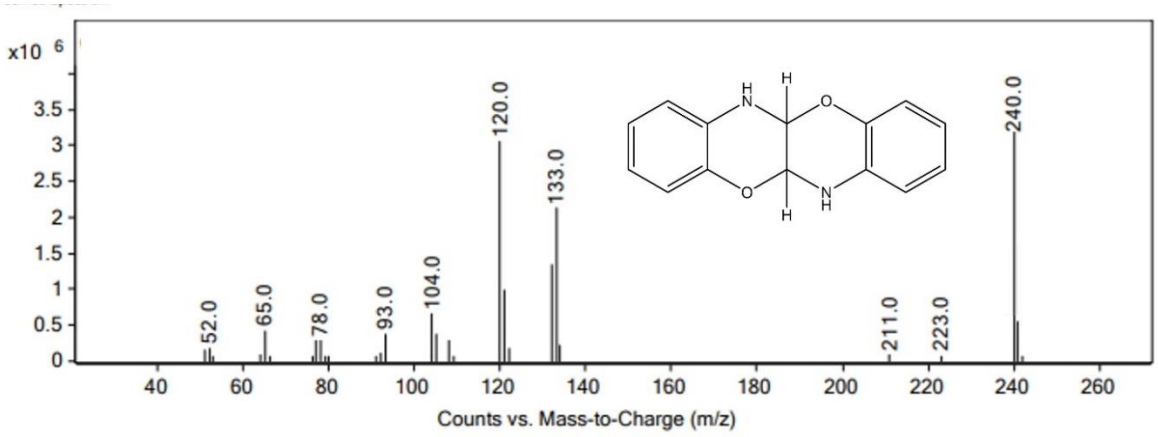

Figure 4.18: Mass spectrum of compound **3b**

Meanwhile, mass spectrum for compound **4b** is shown in Figure 4.19. The base peak of m/z = 268 is correspond to the original compound structure. Ion peak of m/z = 161 ($C_{10}H_{11}NO^{2+}$) is due to the loss of half of the structure while ion peak of m/z = 146 ($C_9H_8NO^{3+}$) is the mass fragment due to the loss of the methyl group.

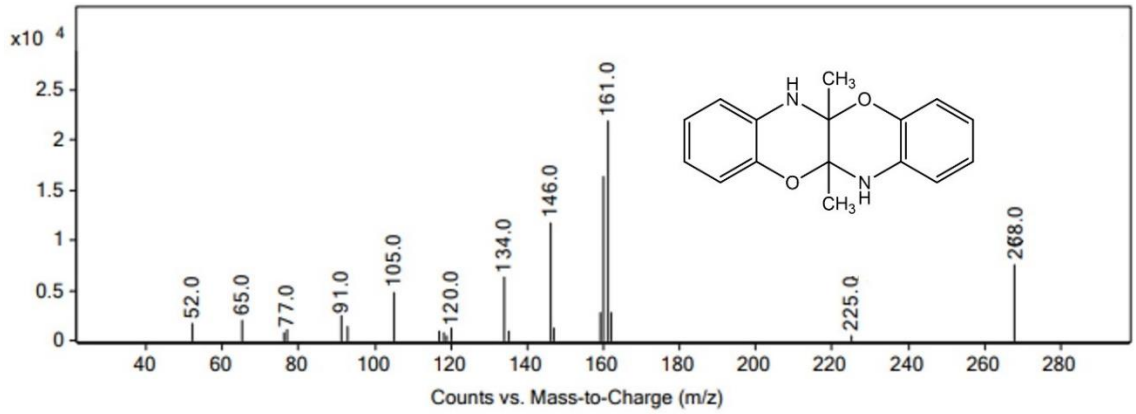

Figure 4.19: Mass spectrum of compound **4b**

4.1.3 IR spectra of conjugated symmetrical bis-Schiff base compounds

Out of the twelve bis-Schiff base compounds, only nine compounds have been successfully synthesised. However, only spectroscopic spectra of compound **1a** are presented in the discussion meanwhile the spectra for compounds **1b – 4c** (**3a**, **3b** and **4b** not included) can be found in the Appendices. The IR data of compounds **1a-4c** are tabulated in Table 4.1.

The formation of symmetrical bis-Schiff base compounds was confirmed mainly by the disappearance of C=O peak at around 1750-1700 cm^{-1} in the IR spectrum of the starting materials (glyoxal, diacetyl, 2-hydroxybenzaldehyde, benzaldehyde and *p*-anisaldehyde). Apart from that, there is also the disappearance of NH_2 peak of the starting materials (*p*-phenylenediamine, *o*-phenylenediamine, aniline, 2-aminophenol and *p*-anisidine) at around 1681 cm^{-1} from the IR spectra. Meanwhile, a new stretching band were found around 1630-1600 cm^{-1} which is attributed to C=N bond in a Schiff base structure. The absence of C=O and NH_2 peak and the appearance of C=N peak is the main indicator of the successful formation of Schiff base compound (Sönmez et al., 2010). The frequencies of the C=N bond were shifted to lower frequency than the normal range (1690-1640 cm^{-1}). Similarly, the C=C bond was also shifted to lower energy region at around ~1589 and ~1480 cm^{-1} compared its usual range at 1600 & 1475 cm^{-1}. This was due to the presence of -N=C-C=N- conjugation system along the molecule that facilitates the electron delocalisation in the molecule which shifted these band to the lower frequencies (Pavia et al., 2014). For compounds **1b** and **2b**, a broad band was found at around 3300 cm^{-1} are due to the presence of -OH group at the *ortho* position of the phenyl ring in the compound. The υ(OH) frequencies was found shifted at lower frequencies compare to the free -OH band of phenol which is around 3700-3584 cm^{-1} due to the intermolecular bonding that weakens the O-H bond. In addition, peak at

around 800 cm^{-1} was also found for compound **1c**, **2c**, **3c** and **4c** which attribute to the -OMe substituent presents at the *para* position at both side of the phenyl ring.

Table 4.1: Selected IR data of symmetrical bis-Schiff base compounds **1a-4c**

cmp	υOH (cm^{-1})	υC-H_{ar} (cm^{-1})	υC-H (cm^{-1})	υC=N (cm^{-1})	υC=C_{ar} (cm^{-1})	υC-N (cm^{-1})	υC-O (cm^{-1})	υ(*p*-Subst.) (cm^{-1})
1a	NA	3055.11	2884.38	1615.70	1574.49 1492.07	1362.55	NA	NA
1b	3375.55	2983.82	2868.77	1600.45	1567.58 1485.40	1364.86	1268.99	NA
1c	NA	2955.03	2840.23	1603.92	1568.60 1509.73	1300.74	NA	844.48
2a	NA	3057.78	2957.97	1603.19	1488.14 1447.05	1392.26	NA	NA
2b	3320.03	2925.59	2887.33	1606.87	1556.83 1480.29	1365.49	1274.24	NA
2c	NA	3013.90	2831.40	1606.87	1509.73 1456.75	1291.91	NA	826.82
3c	NA	3023.90	2854.34	1626.87	1589.38 1489.13	1297.19	NA	837.99
4a	NA	3061.00	2960.92	1630.42	1586.21 1480.29	1366.44	NA	NA
4c	NA	2999.18	2834.34	1630.42	1600.91 1497.96	1353.72	NA	838.59

*NA = Not Available

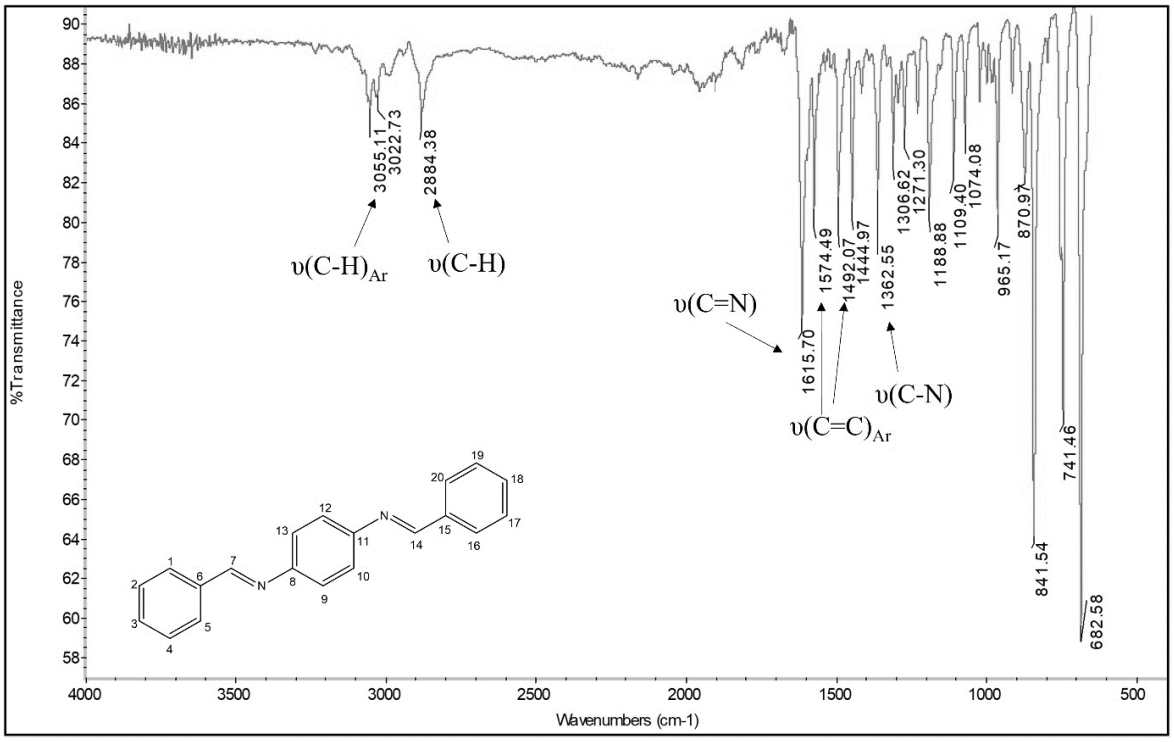

Figure 4.20: IR spectrum of symmetrical bis-Schiff base of compound **1a**

Comparing the C=N peak of aromatic π-spacer and aliphatic π-spacer, the position of C=N stretching band of aromatic π-spacer are shifted further to lower wavelength than of aliphatic π-spacer. The C=N stretching band of aliphatic π-spacer at around 1630 cm^{-1} is located closer to the normal range (1690-1640 cm^{-1}) while the stretching band of aromatic π-spacer is found at around 1600 cm^{-1}. In addition, the intensity of the C=N stretching band in both aromatic and aliphatic π-spacer also differ where aromatic π-spacer are more intense compared to aliphatic π-spacer. The aromatic nature of the π-spacer is more stable and gives more conjugation effects compare to aliphatic π-spacer due to the conjugation effect across the

molecule with phenylene bridge are more extended compare to ethylene bridge (Tong et al., 2014).

4.1.4 NMR spectra of conjugated symmetrical bis-Schiff base compounds

Table 4.2 shows the ^{1}H NMR data of symmetrical bis-Schiff base compounds **1a-4c**. Based on the table below, the ^{1}H and ^{13}C NMR spectra are also useful to confirm the formation of symmetrical bis-Schiff base compounds.

Table 4.2: ^{1}H NMR data of symmetrical bis-Schiff base compounds **1a-4c**

cmp	δ C=N (ppm)	δH aromatic (ppm)	δOCH_3 (ppm)	δCH_3 (ppm)
1a	8.69	7.96 (d,4H), 7.53 (m,6H), 7.37 (s,4H)	NA	NA
1b	9.03	7.68 (d, 2H), 7.55 (s, 4H), 7.55 (s, 4H), 7.43 (t, 2H), 6.99 (m, 4H)	NA	NA
1c	8.59	7.90 (d, 4H), 7.30 (s, 4H), 7.08 (d, 4H)	3.84 (s, 6H)	NA
2a	7.88, 7.87	7.69 (d, 2H), 7.45 (m, 4H), 7.26 (m, 6H), 7.09 (d, 2H)	NA	NA
2b	8.90	7.63 (d, 2H), 7.40 (m, 6H), 6.93 (m, 4H)	NA	NA
2c	7.88, 7.86	7.65 (d, 2H), 7.23 (d, 2H), 7.03 (d, 2H), 6.97 (d, 2H), 6.86 (d, 2H), 5.40 (s, 2H)	3.85 (s, 3H), 3.78 (s, 3H)	NA
3c	8.42	7.33 (d, 4H), 6.95 (d, 4H)	3.84 (s, 6H)	NA
4a	NA	7.38 (t, 4H), 7.12 (t, 2H), 6.80 (d, 4H)	NA	2.16 (s, 6H)
4c	NA	6.96 (d, 4H), 6.80 d, 4H)	3.76 (s, 6H)	2.08 (s, 6H)

*NA = Not Available

From the table above, the formation of Schiff base compounds was confirmed by the absence of CHO signal at around 10 ppm and the appearance of HC=N signal at the range of δH 7.88 –9.03 as singlets which indicates the successful formation of diimine compound. For compounds **2a** and **2c**, there are two singlet signals appeared next to each other in which one of it is attributed to imine signal (δH 7.87 ppm & δH 7.86 ppm respectively) and the

other (δH 7.88 ppm) are due to trace solvent of dimethylformamide left in the sample while trying to crystallise the product.

Moreover, the aromatic protons signal appeared at the range of δH 5.46 – δH 7.96 ppm as a doublet, triplet and multiplet due to overlapping signals. All signals were found in their expected range with correct splitting and integration. In addition, compounds **1c**, **2c**, **3c** and **4c** displayed an extra singlet signal at δH 3.76 – δH 3.84 ppm correspond to the methoxy group located at the *para* position of the aromatic ring. Besides, compound **4a** and **4b** recorded an important singlet signal at 2.16 ppm and 2.08 ppm respectively which assigned to the methyl group hydrogen ($\underline{H}_3$C-C=N) of attached at the π-spacer of both compounds.

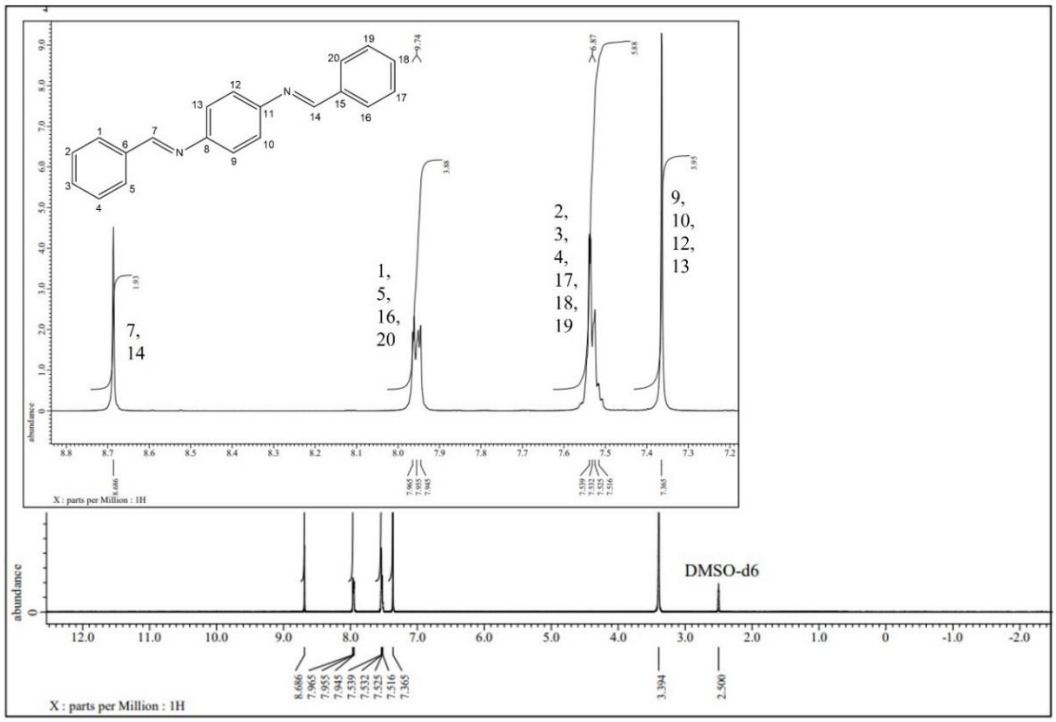

Figure 4.21: ^{1}H NMR spectrum of compound **1a**

Referring to Table 4.2, except for compounds **2a** and **2c** where they undergo arrangement, compound **3c** shows signals at higher field (δH 8.42 ppm) compared to signals from other compounds that contain aromatic π-spacer (δH 8.59 – 9.03 ppm). For compounds

4a and **4c** no proton signals were found for C=N due to the presence of methyl group at the carbon. The π-conjugation causes the proton signal was shifted to lower field. Therefore, it shows that aromatic π-spacer gives more π-conjugation effects compared to aliphatic π-spacer.

As for ^{13}C NMR, all the spectra were found corresponding to their respective carbon number as shown in Table 4.3. All the important peaks attributed to their respective functional groups are included in the table.

Table 4.3: ^{13}C NMR data of symmetrical bis-Schiff base compounds **1a-4c**

cmp	δC-OH (ppm)	δC=N (ppm)	δC-N (ppm)	δC=C (ppm)	δC-OCH_3 (ppm)	δOCH_3 (ppm)	δC-CH_3 (ppm)
1a	NA	160.62	149.99	136.61, 131.90, 129.30, 129.11, 122.44	NA	NA	NA
1b	163.74	160.82	147.15	133.90, 133.00, 123.10, 119.90, 119.75, 117.06	NA	NA	NA
1c	NA	160.00	133.02	131.54, 130.26, 122.77, 115.22	163.26	56.45	NA
2a	NA	154.16, 142.88	136.40, 136.06	130.17, 129.91, 129.41, 129.21, 128.93, 127.66, 126.09, 123.31, 122.98, 119.99, 110.72	NA	NA	NA
2b	164.57	160.91	142.79	132.97, 132.99, 128.35, 120.28, 120.01, 119.62, 117.20	NA	NA	NA
2c	NA	154.24, 143.28	136.20, 130.81	128.60, 127.33, 122.85, 122.64, 119.82, 114.54, 114.30, 110.54	161.02, 159.24	55.48, 55.41	NA
3c	NA	157.72	143.12	123.19, 114.74	159.90	55.67	NA
4a	NA	168.36	151.06	129.07, 123.91, 118.75	NA	NA	15.53
4c	NA	156.55	144.19	120.70, 114.39	168.61	55.61	15.55

*NA = Not Available

Based on the peaks found, it is confirmed that Schiff base compound was formed due to the absence of carbonyl (C=O) peak which usually found at around 190 – 220 ppm. Meanwhile, peaks correspond to imine group (C=N) was found in the range of 142 – 168 ppm showing the successful formation of Schiff base compound. Apart from that, for compounds **1b** and **2b**, peak at 163 and 164 ppm, respectively, were attributed to the carbon near -OH group. In addition, extra peaks at around 159 – 168 ppm was assigned to carbon connecting to methoxy (-OMe) and peaks around 55 – 56 ppm were assigned to carbon of methoxy group which are found in compounds **1c**, **2c**, **3c** and **4c** that have methoxy substituent in their structure. For compound **4a** and **4c**, peaks at 15 ppm found in both compounds are due to the methyl group attached at the π-spacer **(**H_3C-C=N)**.**

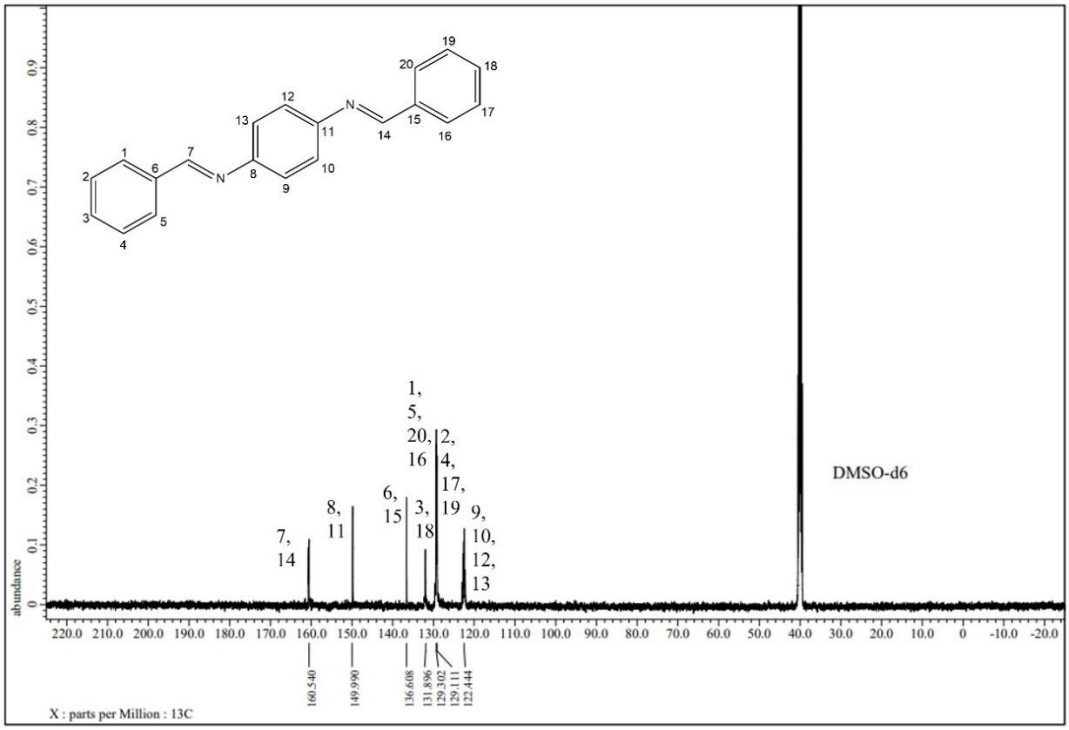

Figure 4.22: ^{13}C NMR spectrum of compound **1a**

4.1.5 UV-Visible of conjugated symmetrical bis-Schiff base compounds

The summary of UV-Visible data of compounds **1a** – **4c** are presented in Table 4.5. All of the compounds were dissolved in DCM and analysed using Agilent Cary 60 UV-Vis spectrophotometer with a 1 cm quartz cuvette in the range of 200–800 nm.

Table 4.4: UV-Visible absorption data of symmetrical bis-Schiff base compounds **1a-4c**

Compounds	π→π* (nm)	n→π* (nm)
1a	273	335
1b	274	370
1c	297	367
2a	270	335
2b	285	336
2c	290	359
3c	296	376
4a	290	340
4c	291	354

The absorption peaks of all compounds were found at the range of 245 – 376 nm whereby the absorption bands at 245 – 296 were assigned to the π→π* electronic transition of aromatic rings while the absorption bands at 296 – 376 nm were assigned to the n→π* electronic transition of the azomethine group (-C=N-) (Alattar et al., 2020). Normally, the absorption bands would appear at around 200 – 250 nm. However, due to the conjugation effect in the structure (-N=C-C=N-), all the absorption peaks shifted to the longer wavelength which also known as bathochromic shift or red shift. In addition, the presence of electron donating substituent attached at the molecule also causing the bathochromic shift of the compounds (Pavia et al., 2014). This is because the electron donating substituent donates electron to the molecule which increase the delocalisation of electrons in the molecule thus decrease the electronic transition energy. From the table above, the λ_{max} of the bathochromic shift increasing in the order of -H < -OH < -OMe substituent.

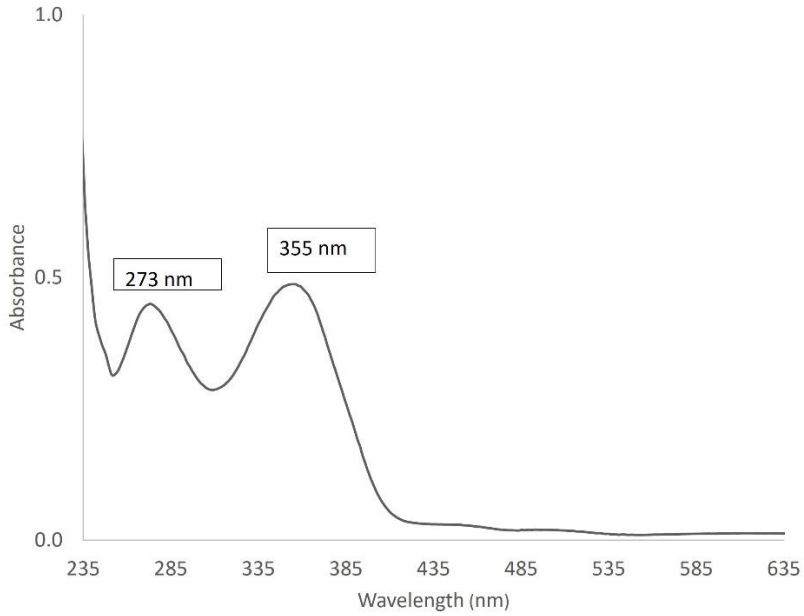

Figure 4.23: UV-Visible spectrum of compound **1a**

The results in Table 4.4 show that compound **1c** undergo more bathochromic shift compared to compound **2c** due to the aromatic π-spacer bridge in **1c** is in para- position which is known to have better π-conjugation system compared to aromatic π-spacer bridge with ortho-position (compound **2c**). This might be due to the steric hindrance of ortho-position which decrease the π-conjugation effect. In addition, for compound with aliphatic π-spacer bridge, the presence of methyl group from the backbone of π-spacer bridge causing a hypsochromic shift in compound **4c** thus the absorption peak was found at little bit shorter wavelength compared to compound **3c** where there is no methyl group at the π-spacer bridge backbone.

4.1.6 CHN analysis of conjugated symmetrical bis-Schiff base compounds

To further confirmed the successful formation of diimine compound as well as the purity, CHN elemental analyses were performed. The results obtained are tabulated in Table 4.5. The differences in the experimental values of the carbon, hydrogen and nitrogen

percentages and the calculated values for all compounds were in the range of ±0.4% which indicate the high purity of compounds **1a** – **4c**.

Table 4.5: CHN elemental analysis results of symmetrical bis-Schiff base compounds **1a-4c**

Compound	Formula	Found (Calculated)		
		C%	H%	N%
1a	$C_{20}H_{16}N_2$	84.43 (84.48)	5.53 (5.67)	9.62 (9.85)
1b	$C_{20}H_{16}N_2O_2$	75.72 (75.93)	4.95 (5.10)	8.74 (8.86)
1c	$C_{22}H_{20}N_2O_2$	76.84 (76.72)	5.71 (5.85)	7.74 (8.13)
2a	$C_{20}H_{16}N_2$	84.03 (84.48)	5.67 (5.67)	10.08 (9.85)
2b	$C_{20}H_{16}N_2O_2$	75.83 (75.93)	4.80 (5.10)	8.94 (8.86)
2c	$C_{22}H_{20}N_2O_2$	76.38 (76.72)	5.63 (5.85)	7.96 (8.13)
3c	$C_{16}H_{16}N_2O_2$	71.20 (71.62)	5.74 (6.01)	10.14 (10.44)
4a	$C_{16}H_{16}N_2$	81.64 (81.32)	6.47 (6.82)	11.77 (11.85)
4c	$C_{18}H_{20}N_2O_2$	73.35 (72.95)	6.52 (6.80)	9.03 (9.45)

4.1.7 GC-MS analysis of conjugated symmetrical bis-Schiff base compounds

In addition, the formation of compounds **1a** – **4c** is also further confirmed with gas chromatogram and mass spectrometry analysis. The GC-MS data is summarised in Table 4.6.

Table 4.6: GC-MS analysis of symmetrical bis-Schiff base compounds 1a-4c

Compound	Area (%)	Base peak (m/z)
1a	100	284
1b	100	316
1c	100	344
2a	100	284
2c	100	344
3c	100	267
4a	97.11	236
4c	100	296

*NA = Not Available

The GC-MS of all compounds **1a** – **4c** were found to be in high purity with all of it only shows only 1 peak except for compound **2b**. Compound **2b** were failed to be analysed

with GC-MS due to the hydrolysis of the compound at high temperature. The gas chromatogram for compound **1a** (Figure 4.24) shows only one peak present at retention time of 29.555 minutes with 100% of area which shows that the sample is in very high purity.

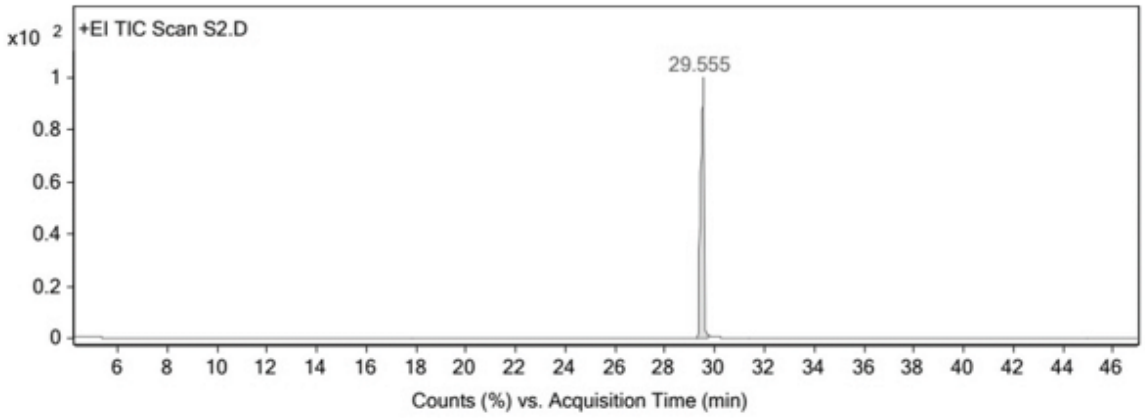

User Chromatogram Peak List

RT	Height	Normalized Height	Height %	Area	Area %	Area Sum %	Base Peak m/z	Symmetry	Width
29.555	20530349.44	99.82	100	196451428.75	100	100	284.2	0.15	0.437

Figure 4.24: Gas chromatogram of compound **1a**

Figure 4.25 shows the mass spectrum of compound **1a**. Referring to the spectrum, it shows a base peak of m/z 284. The fragmented molecule giving $C_{13}H_{10}N^+$ lead to an ion peak of m/z 180. Meanwhile, the loss of imine group (-C=N-) forming $C_6H_5^+$ generated ion peak of m/z 77. The mass spectra of compounds **1b** – **4c** can be found in Appendix 28 – 36.

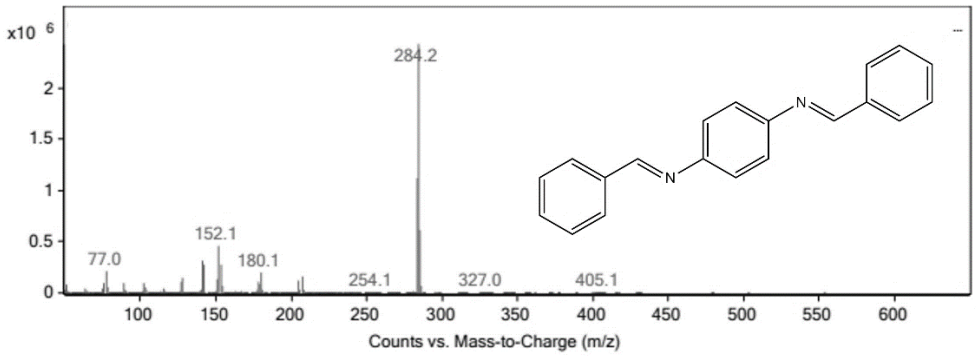

Figure 4.25: Mass spectrum of compound **1a**

4.2 Complexation of boron difluoride with symmetrical bis-Schiff base compounds

After confirmation of the bis-Schiff base formation, the next step was proceeded to the complexation reaction with boron difluoride (BF_2) as the electron acceptor. The complexation of boron difluoride with symmetrical bis-Schiff base compounds was based on the method by Sen and coworkers (2020) with some modifications. Compounds **1b** and **2b** were first deprotonated using a small amount of triethylamine (TEA) as the Lewis base for about 15 minutes. Then boron trifluoride diethyl ether was added slowly using a syringe into the mixture and continue stirring for another 4 hours. The reaction was carried out under inert condition using nitrogen gas *via* freeze-pump-thaw technique. The completion and purity of the precipitate was comfirmed using TLC where only one spot was observed. Then the precipitate was collected *via* filtration and washed using water and diethyl ether.

From the series, complexation can only be done from compounds **1b** and **2b** which is due to the presence of N atom from imine and O atom from hydroxy substituent in the compound acting as the coordinating chelating agents. Referring to Figure 4.26, the complexation with boron difluoride were successful with compound that contain N atom and

O atom in their structure while the complexation will not occur with only N atom present (b).

Both complexes (**1d** and **2d**) were synthesised successfully and analysed by using FTIR, CHN analysis and UV-Visible to confirm the structure. Unfortunately, compounds **1d** and **2d** have a very poor solubility in almost of all organic solvent. They are only slightly soluble in a very large amount of solvents (~0.001g in 10 mL DCM) even after heating and sonicating for more than 6 hours. Hence, ^{1}H NMR and ^{13}C NMR analysis could not be performed and recorded.

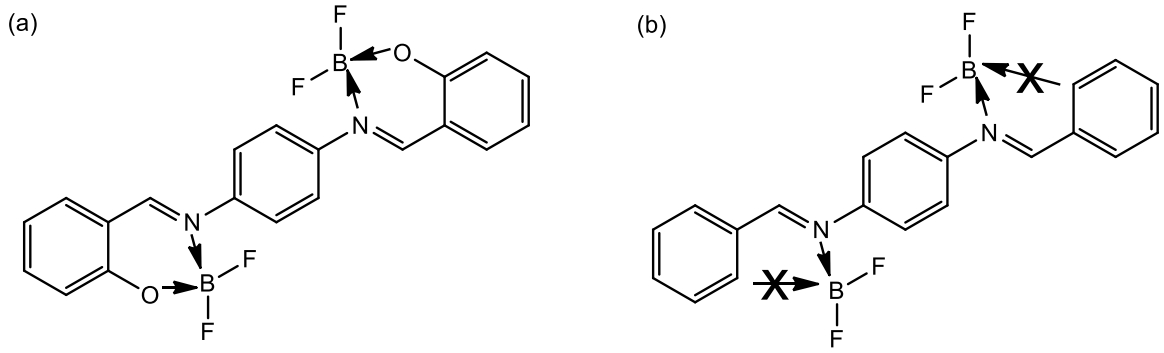

Figure 4.26: Successful formation of N,O- chelating boron difluoride complex (a) and unsuccessful formation of boron difluoride complex (b)

Like the previous characterisation discussion, only the spectroscopic analysis for compound **1d** is used as an example throughout the discussion and the analysis for compound **2d** can be retrieved in appendices.

4.2.1 IR spectra of boron difluoride symmetrical bis-Schiff base compounds

IR spectra for boron difluoride symmetrical bis-Schiff base complexes **1d** and **2d** were recorded using Thermo Scientific Nicolet iS10 FTIR spectrophotometer in KBr disc at the wavelength of 400 – 4000 cm^{-1}. The significant signals of IR analysis are summarised in Table 4.7 together with its free ligands as a comparison.

Table 4.7: FTIR analysis of symmetrical bis-Schiff base free ligands and boron difluoride complexes

cmp	υOH (cm^{-1})	υC-H_{ar} (cm^{-1})	υC-H (cm^{-1})	υC=N (cm^{-1})	υC=C_{ar} (cm^{-1})	υC-N (cm^{-1})	υB-F (cm^{-1})	υB-O (cm^{-1})
1b	3375.55	2983.82	2868.77	1600.45	1567.58 1485.40	1364.86	NA	NA
1d	NA	3069.83	3037.45	1618.64	1550.94 1503.84	1315.45	1212.43 1044.64	1153.56 1097.63
2b	3320.03	2925.59	2887.33	1606.87	1556.83 1480.29	1365.49	NA	NA
2d	NA	3078.66	3046.28	1621.59	1553.88 1474.41	1383.16	1218.32 1062.31	1130.01 1085.85

*NA = Not Available

The disappearance of OH peak of complexes **1d** and **2d** from its free ligand (**1b** and **2b**) shows that the OH from the free ligand has been deprotonated. The deprotonated hydroxyl oxygen can coordinate with boron difluoride ion. The C=N band of the free ligands (**1b** and **2b**) were shifted from 1600.45 cm^{-1} and 1606.87 cm^{-1} to a higher region at 1618.64 cm^{-1} and 1621.59 cm^{-1} (**1d** and **2d**) respectively. In addition, the vibration bands for C-H aromatic also shifted from 2983.82 cm^{-1} and 2925.59 cm^{-1} to 3069.83 cm^{-1} and 3078.66 cm^{-1} after complexation. This proves that the imines and phenolic protons took part in the coordination of the boron atoms (Sen et al., 2020).

Furthermore, new bands were observed at 1044.64 – 1218.32 cm^{-1} and 1085.85 – 1153.56 cm^{-1} assigned to B-F and B-O chelating bonds respectively (Kukharenko & Avramenko, 2001; Sen, 2019).

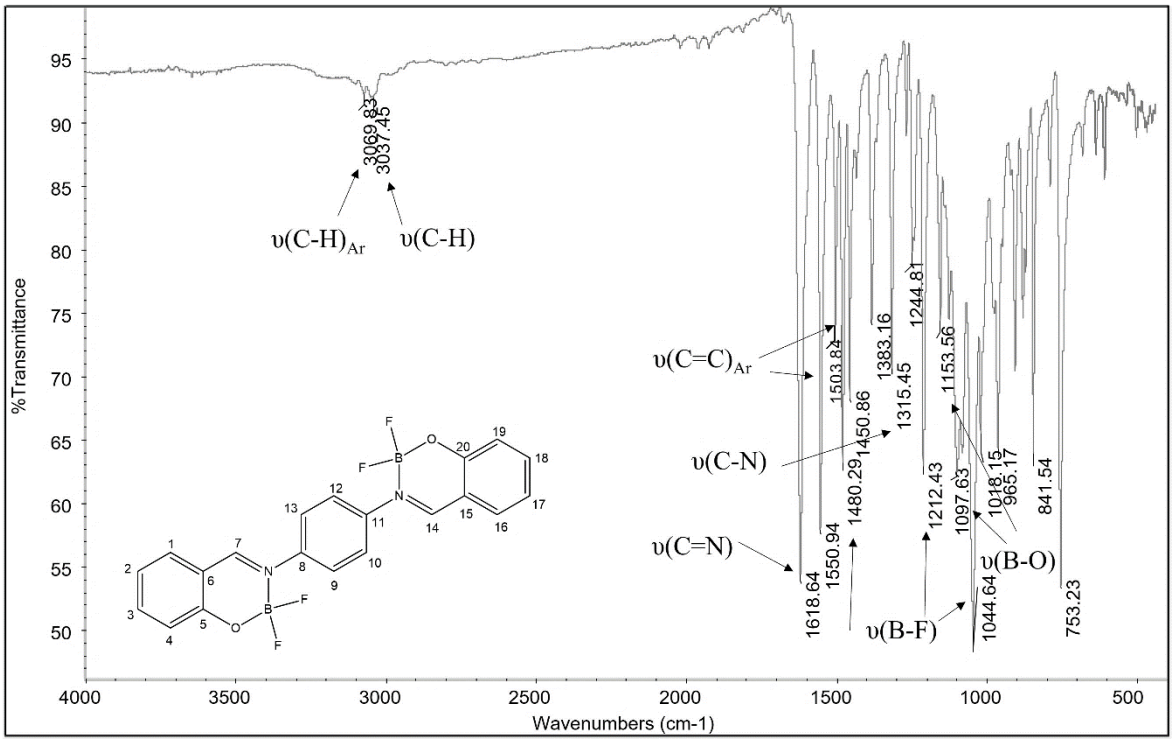

Figure 4.27: IR spectrum of compound **1d**

4.2.2 UV-Visible analysis of boron difluoride symmetrical bis-Schiff base compounds

UV-visible analysis for compound **1d** and **2d** was done by using Agilent Cary 60 UV-Vis spectrophotometer with a 1 cm quartz cuvette in the range of 200–800 nm in DCM solvent. Due to the poor solubility of boron difluoride complexes, the complexes were filtered several times until an almost clear solution was obtained. Table 4.8 shows the UV-Vis data for both free ligands and its boron difluoride complexes.

Table 4.8: UV-Visible analysis of symmetrical bis-Schiff base ligands and boron difluoride complexes

Compounds	π→π* (nm)	n→π* (nm)	Intramolecular charge transfer (ICT) (nm)
1b	274	370	NA
1d	297	385	442
2b	285	336	NA
2d	279	364	449

*NA = Not Available

The π→π* and n→π* electronic transitions for boron difluoride complexes (compounds **1d** and **2d**) shifted to a longer wavelength which is from 274 – 285 nm to 279 – 293 nm and 336 – 370 nm to 364 – 387 nm, respectively. This is due to the increase in the dipole moments (Sen, 2020). In addition, the red-shifts also occur due to the strong electron-withdrawing abilities of boron difluoride units (Sun et al., 2017). This reflects the common behaviour of boron difluoride complexes containing NO-bidentate ligands (Sen, 2019).

An extra absorption bands was observed at 442 nm and 449 nm of compound **1d** and **2d** respectively which represents the intramolecular charge transfer (ICT). This is due to the presence of boron difluoride which is a strong electron-withdrawing group causing a movement of π-electron towards to boron difluoride analogue (Sun et al., 2017; Xing & Jia, 2021).

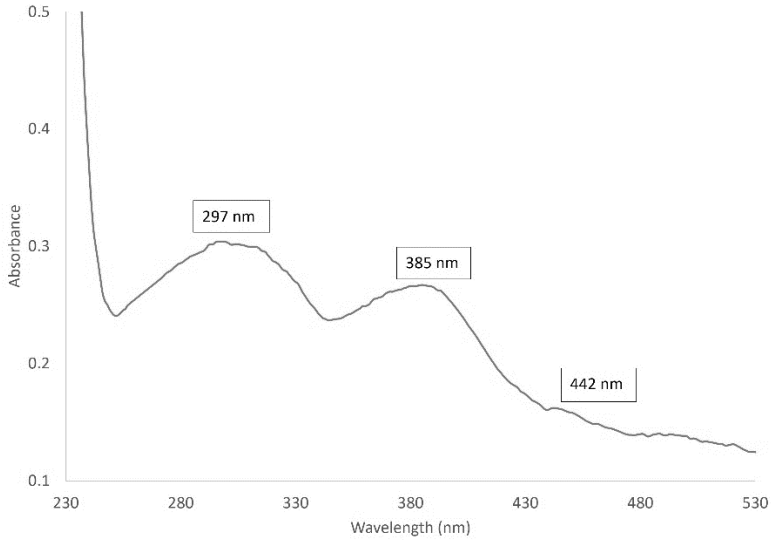

Figure 4.28: UV-Visible spectrum of compound **1d**

4.2.3 CHN analysis of boron difluoride symmetrical bis-Schiff base compounds

CHN analysis (Table 4.9) were also performed to confirm the complex structure as well as the purity. The differences in between the experimental values of carbon, hydrogen and nitrogen percentages and calculated values for all complexes were ±0.4%, which indicated the formation of boron difluoride complexes according to the postulated structure as shown in Figure 4.29 and the complexes were pure.

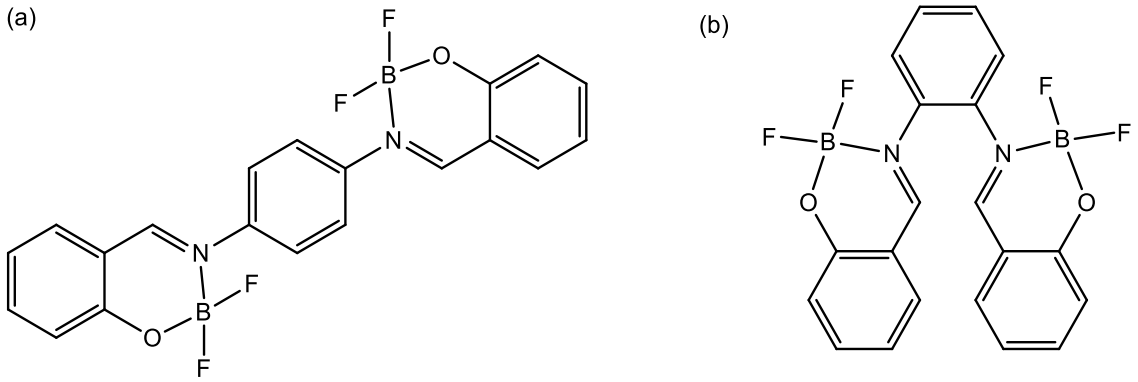

Figure 4.29: Postulated structure of **1d** (a) and **2d** (b)

Table 4.9: CHN analysis of symmetrical bis-Schiff base ligands and boron difluoride complexes

Compound	Formula	Found (Calculated)		
		C%	H%	N%
1d	$C_{20}H_{14}B_2F_4N_2O_2$	58.31 (58.34)	3.43 (3.09)	6.80 (6.66)
2d	$C_{20}H_{14}B_2F_4N_2O_2$	58.31 (57.95)	3.43 (3.05)	6.80 (6.66)

Unfortunately, due to the poor solubility of these complexes in almost all available organic solvents such as dichloromethane, chloroform, diethyl ether, dimethyl formamide, dimethyl sulfoxide, ethanol, methanol, ethyl acetate, hexane and other common laboratory organic solvents, the NMR data could not be obtained. Nevertheless, the IR, UV-Visible and CHN analysis are the evidence of the boron difluoride complexes formation.

4.3 Attempts synthesis of unsymmetrical bis-Schiff base with push pull effects

The formation of BF_2 complex with symmetrical bis-Schiff base was an exciting milestone for the study. After the complexation with symmetrical bis-Schiff base, we proceeded to unsymmetrical bis-Schiff base analogue in order to generate push-pull effect which is essential in improving the conversion efficiency of DSSC (Teo, 2017; Phan, 2019).

Attempts to synthesise unsymmetrical bis-Schiff base with an electron acceptor substituent at one side and electron donator substituent at the other side (Figure 4.30) in order to induce push pull effects along the molecule were unfortunately unsuccessful. This was due to the difficulty to isolate the compounds from the mixture of unsymmetrical and symmetrical products formed simultaneously in the same ratio.

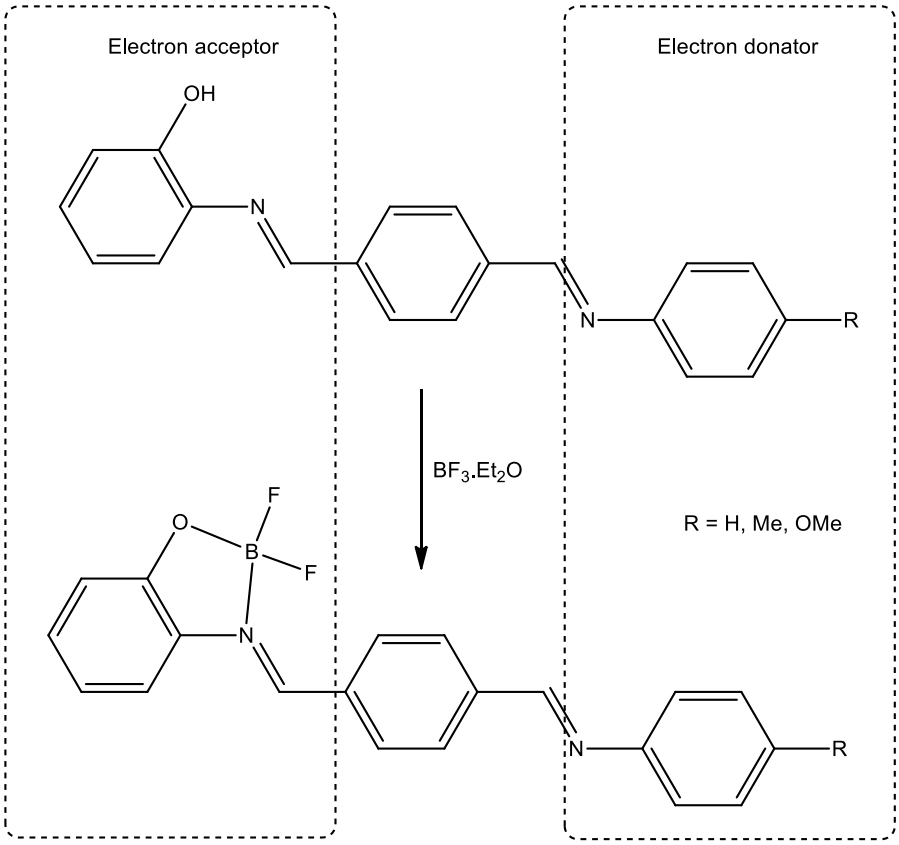

Figure 4.30: Proposed structure of unsymmetrical bis-Schiff base compound with push pull effects

Indeed, a few trials have been attempted in order to synthesise these compounds in which one of it is two-step method which forming intermediate mono-substituted Schiff base (M1) by reacting terephthaldehyde with 2-aminophenol in 1:1 ratio. But unfortunately, based on ^{1}H NMR and GCMS data, the reaction led to the formation of mixture of symmetrical

bis-Schiff base by-product and mono substituted Schiff base namely I-4-[{(2-hydroxyphenyl)imino}methyl]benzaldehyde (**M1**) (Scheme 4.6).

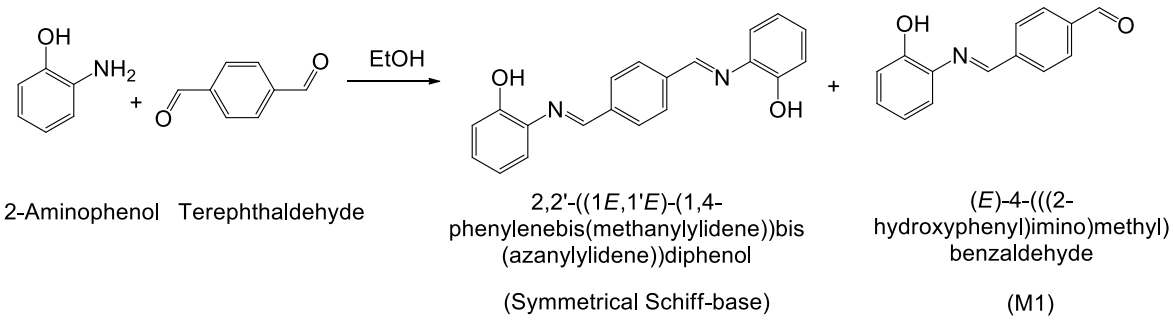

Scheme 4.6: Attempt of synthesizing intermediate M1 by reacting 2-aminophenol with terephthaldehyde

In addition, a few variables such as changing the ratio of the starting materials such as 1:1, 1:2, 1:3, 1:4 and 1:5, changing solvents such as ethanol, methanol and butanol, reaction temperature ranging from 30 minutes – 3 hours as well as temperature. However, none of these attempts succeed to give reasonable yield of **M1**.

Other than that, an attempt to synthesise unsymmetrical Schiff base using one pot technique also unsuccessful. In this procedure, all three starting materials which is 2-aminophenol, terephthaldehyde and aniline were added together in a flask and refluxed for 2 hours. As a result, the mixtures of unsymmetrical bis-Schiff base and two symmetrical Schiff base product were formed (S1, S2 and S3) as shown in Scheme 4.7. A few variables as mentioned before also have been done with this technique but gives no significant changes.

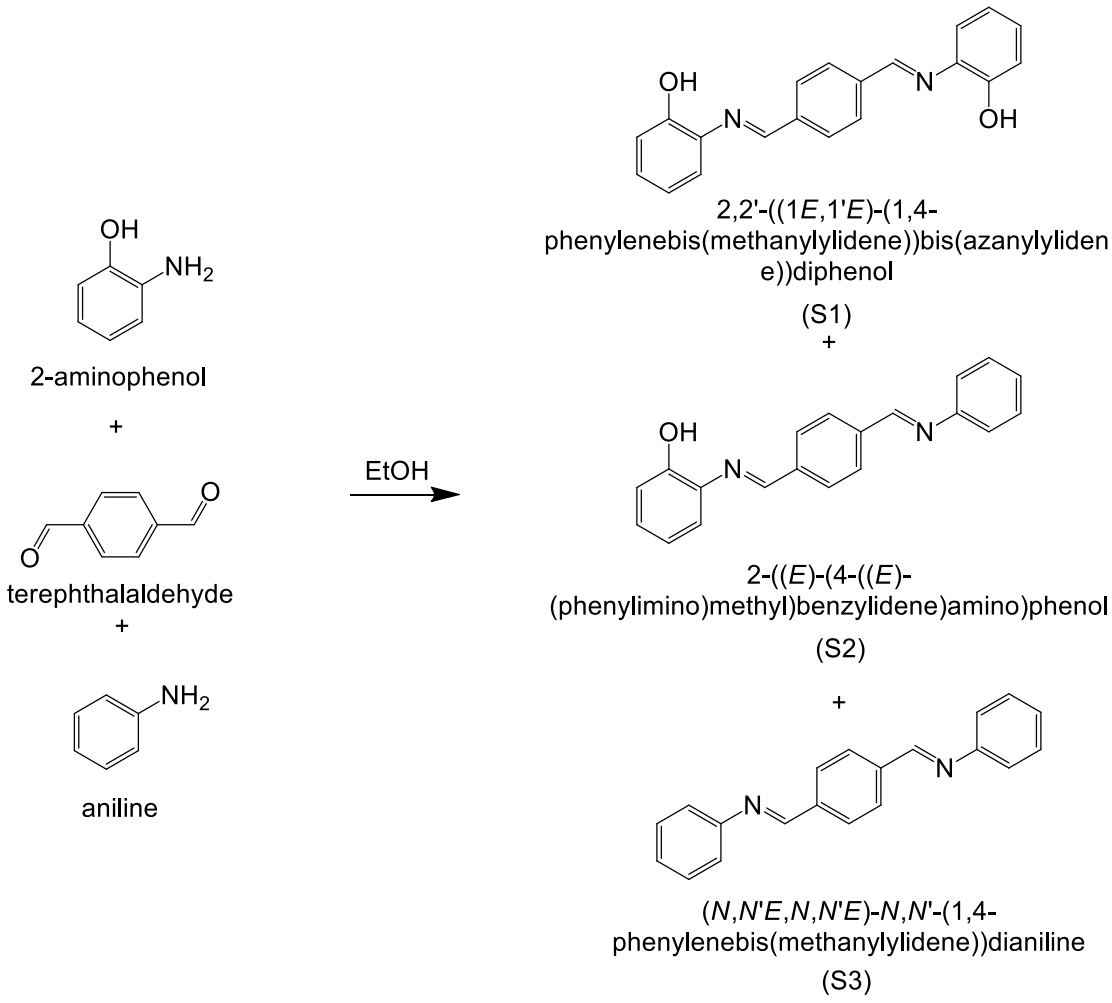

Scheme 4.7: Attempt of synthesizing unsymmetrical bis-Schiff base using one pot technique

It has been confirmed through GCMS and ^{1}H NMR spectra whereby the product gives three different compounds as stated above. As shown by ^{1}H NMR (Figure 4.31), a broad peak at δH 9.10 was found attributed to the -OH group with integral of 3 meaning that there were three -OH proton was found which is from **S1** and **S2**. Another peak at δH 8.80 and δH 8.70 correspond to the proton from imine group (HC=N) with integral of 4 and 2 respectively where four protons is from three symmetrical product (**S1** and **S3**) and two protons from unsymmetrical product (**S2**). In addition, peaks at δH 8.18 – δH 8.06 attributed

to the protons from centre aromatic ring where strong single peak is from **S1** and **S3** and the other is from **S1** with a total of 12 protons. Furthermore, at the range of δH 7.46 – δH 6.84 was due to the rest of aromatic protons in which has a total of 27 protons. Altogether, all 48 protons from **S1**, **S2** and **S3** was found correspond to their correct number of protons according to their structure.

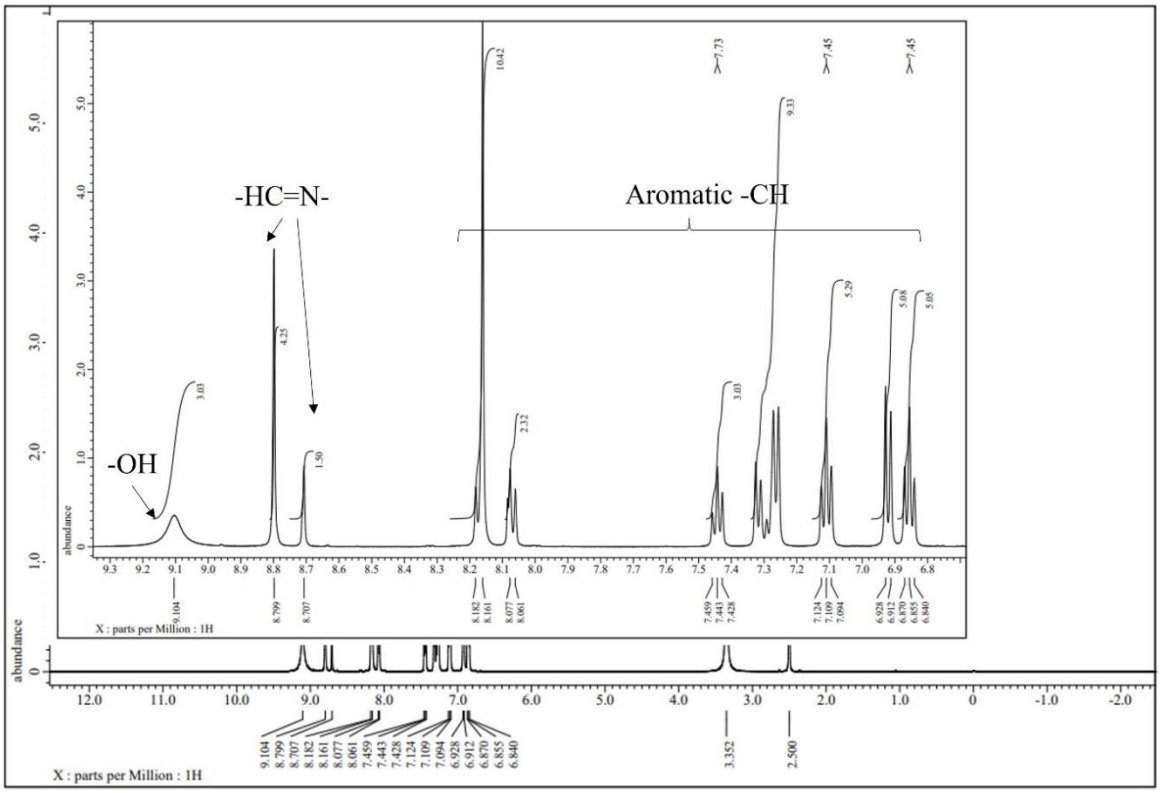

Figure 4.31: ^{1}H NMR of unsymmetrical bis-Schiff base attempt

Aside from that, results from GCMS also supports results from ^{1}H NMR. Referring to the GCMS spectra in Figure 4.32, the product of unsymmetric bis-Schiff base compound consists of the mixture of unsymmetrical and two symmetrical products. Although the desired product (**S2**) gives the highest percentage of products (63.54%), the challenges is to isolate **S2** from the mixture of product. Several separation and purification technique have been done to isolate **S2** however to no avail. This may be due to the almost similar properties

of all three compounds that it is difficult to isolate. The spots on TLC of the product also gives very near spot from each other that it overlapped even after changing to various types of eluents. In addition, isolation technique *via* column chromatography have also been done using silica gel using various types of eluents. However, it is failed to separate as all three compounds were still found in all fractions as well as few starting materials. This may be due to the reason that imine bond is prone to hydrolysis especially in the presence of acid or base. The silica gel that was used in column chromatography have acidic sites that causes the hydrolysis of imine bond. An attempt to deactivate silica by running through the column using triethylamine was also found to be unsuccessful. Therefore, column chromatography is usually not a good choice to isolate most of Schiff base compounds. The difficulties in getting unsymmetrical bis-Schiff base may be due to both reactive sites of terephthaldehyde are too reactive that both sites are reacting simultaneously during the reaction. Attempt was also done using glyoxal with aniline however unable to get unsymmetrical product due to the same reason as mentioned.

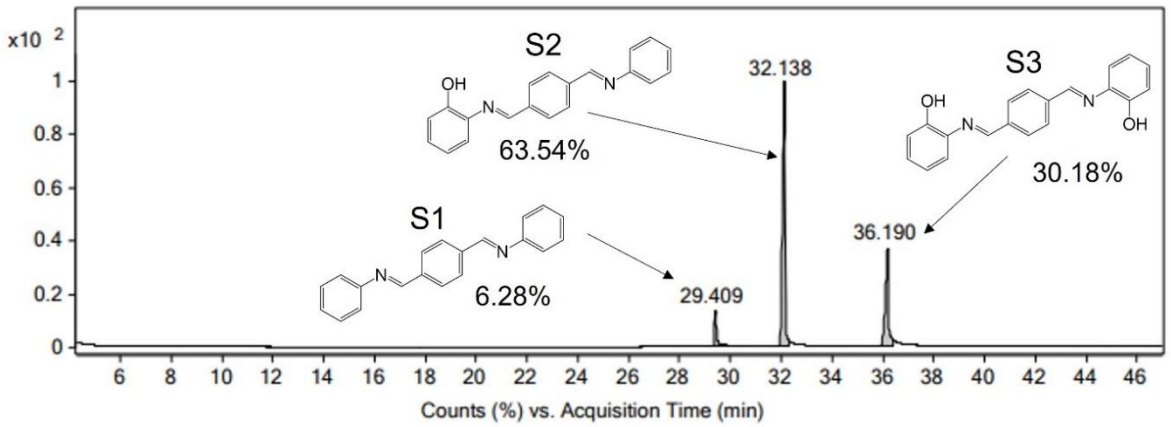

Figure 4.32: Gas chromatogram of unsymmetrical bis-Schiff base attempt

4.4 Application of symmetrical bis-Schiff base compounds and complexes in DSSC

All the successfully synthesised symmetrical bis-Schiff base compounds and boron difluoride bis-Schiff base complexes that have been discussed previously were applied as dye-sensitiser in DSSC device. It is worth to note that the DSSC conversion efficiency in this project was measured with respect to 100W LED light source and not to the standard solar simulator AM 1.5G under incident light intensity of 100 mW/cm^2 that were usually used. In an arrangement of 31.6 cm x 28.6 cm x 23.8 cm box, a LED light, and DSSC device connected to resistor box and multimeter was setup as shown in Figure 4.33.

Figure 4.33: Setup of photoelectrical measurement of DSSC

The DSSC device was connected to a resistor box (Shanghai Domao; Model: ZX21) and a multimeter (XEOLE, China; Model: XL830L) by using alligator clip and was placed at distance of 2 cm from light source. The LED light was set to the highest brightness to get high intensity (~100000 lux). The best condition is at a shorter distance with the highest

brightness (Figure 4.34). This condition was chosen in order to get the highest power possible in this indoor set up.

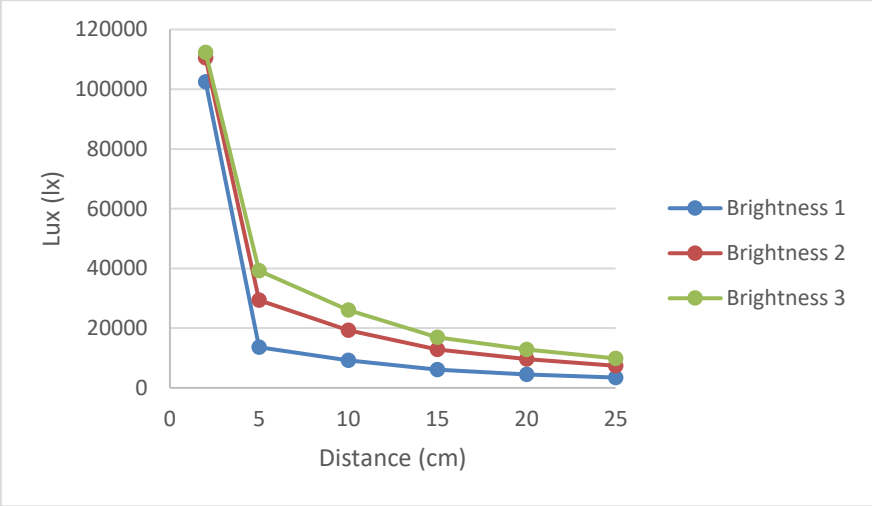

Figure 4.34: The distance and brightness intensity (lux) for DSSC measurement

To fabricate the DSSC, firstly, FTO and ITO glass was cleaned and sonicated thoroughly by using acetone, methanol and deionised water. FTO glass was used as the working electrode meanwhile ITO glass was used as the counter electrode. A titanium(IV) oxide anatase (TiO_2) paste was prepared by mixing with polyethlene glycol, ethanol, deionised water and triton X-100 which is then grinded by using mortar and pestle until paste-like texture. Then, onto the FTO glass, the TiO_2 mixture was coated *via* using doctor blade technique in a 1 cm x 2 cm dimension area. The coated side should be the side that has transparent conductive coating on it which can be find out using multimeter set to resistance. The corrected side should have resistance of 0 Ω. Next, the coated FTO glass was sintered at 460 °C for 15 minutes then cooled to room temperature. Meanwhile, the ITO glass was coated with electric paint using Bare Conductive which contain carbon black and graphite

as the main ingredients that was usually used in DSSC. The coating was also done in 1 cm x 2 cm area *via* doctor blade technique and left to dried at room temperature.

The N3 standard dye was prepared by dissolving it into methanol and acetonitrile and sonicated for 30 minutes. It is important to do the whole preparation of N3 standard dye in a dark room in order to avoid sunlight as it is very sensitive towards sunlight. Meanwhile, the symmetrical bis-Schiff base ligands and complexes that have been synthesised was prepared by dissolving it in dichloromethane and sonicated for 10 minutes.

On the other hand, iodide/triiodide electrolyte solution was also prepared using iodine and potassium iodide mixed in ethylene glycol and stirred for 30 minutes. The prepared electrolyte was stored in a vial and wrapped with aluminium foil to avoid light exposure. Ethylene glycol was used instead of other solvent such as acetonitrile or methanol to avoid the electrolyte from evaporating too fast while testing the device.

The preparation of working electrode was done by immersing the coated FTO glass into the prepared N3 dye and symmetrical bis-Schiff base ligands and complexes prepared beforehand. The immersed FTO glass was then put into oven at 45 ℃ for 120 minutes and 39 ℃ for 24 hours for N3 dye and symmetrical bis-Schiff base ligands and complexes respectively. After that, the immersed was taken out and air dried.

Lastly, assembling all the DSSC components by attaching the prepared working electrode and counter electrode face-to-face making sure the coated area facing each other and then clipped together by using binder clips. At both sides of the glass was left offset at around 0.5 cm in order to attach multimeter probes. Then, 2-3 drops of iodide/triiodide electrode were dropped from the edges and the binder clips was squeezed a few times to

make sure all coated surface was covered by electrolyte. This is to ensure that every surface area can take part in the dye regeneration process.

The setup for the photoelectrical measurement was done as shown in Figure 4.33. An arrangement of 31.6 cm x 28.6 cm x 23.8 cm box was made for the measurements. 100W LED lamp was attached vertically from above the box and the DSSC device was placed on a stable surface facing the LED light. Alligator clips was used to connect the device through a resistor to the multimeter probes. To get a stable reading, the DSSC device and also the set up should not be moved or interfere. In addition, the reading also should be taken without stopping in the middle of the measurements process in order to get the best results.

The current-voltage (J-V) and power-voltage (P-V) curves was calculated and generated from the data obtained (Figure 4.35). From these curves, the value of short-circuit currents (J_{SC}), open-circuit voltages (V_{OC}), maximum current (J_{MP}) and maximum voltage (V_{MP}) was calculated. Meanwhile, the value of fill factor (FF) and efficiency (η%) was calculated using Equations 4.1 and 4.2:

$$FF = \frac{J_{MP}\ X\ V_{MP}}{J_{SC}\ X\ V_{OC}} \qquad \text{Equation 4.1}$$

and

$$\eta\ = \frac{Jsc\ x\ Voc\ x\ FF}{Pin}\ x\ 100\% \qquad \text{Equation 4.2}$$

From the efficiency formula, the incident light intensity (P_{IN}) is usually measured using irradiance (lux). However, rather than irradiance, illuminance is a better way to quantify the light level for indoor environment but somehow illuminance creates conversion problems. This is because there is still no simple and easily obtained standard method to

convert illuminance (lux) into irradiance (W m^{-2}) and *vice versa* (Michael et al., 2020). To convert, different conversion factor is needed for every wavelength which can be determined from the spectral analysis of light composition. Unless the spectral composition of the light is known, it is not possible to make a conversion. Therefore, in order to get an approximate conversion factor for the incident light conversion in the formula, a wavelength is needed. As there are no equipment available to measure the exact wavelength of the light used, therefore the wavelength of the visible spectrum was used because illuminance only considers the spectrum of visible light. Given that the visible spectrum has the maximum peak of around 555 nm, as well as the peak of the eye-sensitivity curve particularly at 555 nm, the spectral irradiance of most indoor room light source also shows maximum peak approximately around 550 nm (Vignati, 2012; Alhorani et al., 2021). Therefore, for this wavelength, the corresponding value is 1.464 mW/m^2, which is then the conversion rule can be extracted as shown in Equation 4.3:

$$I_{IN}\ (W/m^2)\ = 1.464\ x\ 10^{-3}\ x\ I_{IN}\ (lx) \qquad \text{Equation 4.3}$$

where, I_{IN} = incident light intensity

Indeed, that based on the UV spectrum of symmetrical bis-Schiff base compounds and its complex does not show absorption at around 550 nm wavelength, however, the dye does gives values when tested with DSSC device meaning that the light also emits wavelength in the dye range. Therefore, as mentioned earlier, as there is no equipment to get the exact wavelength, only approximate conversion factor can be used.

To ensure the quality of the conversion efficiency measurement, N3 dye named *cis*-bis(isothiocyanato)bis(2,2'-bipyridyl-4,4'-dicarboxylato)ruthenium(II), which has been used as the standard dye sensitiser in DSSC, was used as the control standard. Figure 4.35

shows the plot of current and power vs voltage of N3 dye sensitiser that was measured under the setup as aforementioned.

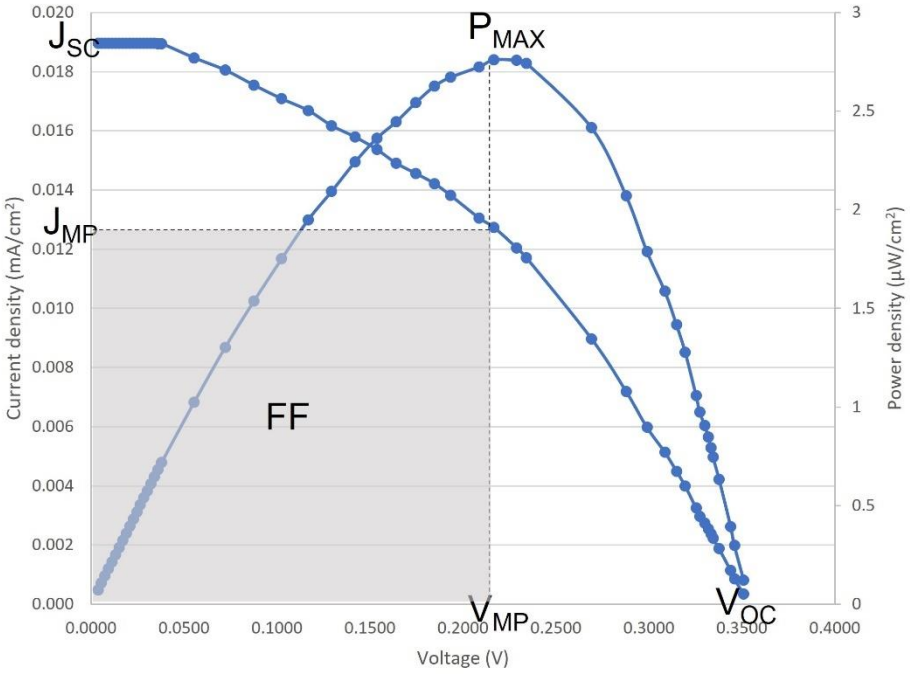

Figure 4.35: Current and power vs voltage curves of N3 dye sensitider

Indeed, DSSC efficiencies reports in many literatures are usually measured using solar simulators with typical irradiance of 1000 W/m^2 and Air Mass 1.5 Global (AM 1.5 G) that results with a spectrum that is similar to the solar spectrum. This value is about equivalent to sunny day, and it is very high compared to the irradiation levels indoor (Vignati, 2012). While using standard method such as solar simulator is necessary to compare solar cells that are intended to be commercialised for outdoor use, it is also necessary to investigate their efficiency to be use indoor using artificial light sources which are more often used than outdoor lights.

The power conversion efficiency results of the synthesised bis-Schiff base compounds and complexes are presented in Table 4.10 and the *J*/*V* curves are shown in Figure 4.36.

Table 4.10: Power conversion efficiency results of symmetrical bis-Schiff base ligands and boron difluoride complexes

Dye sensitiser	I_{IN}	I_{IN} (W/m^2)	J_{SC} (mA/cm^2)	V_{OC} (V)	J_{MP} (mA/cm^2)	V_{MP} (V)	FF	η%
N3 dye	112400	164.5536	0.0190	0.3510	0.0120	0.2289	41.4	0.1676
1a	102500	150.0600	0.0072	0.1560	0.0036	0.0687	22.2	0.0166
1b	107100	156.7944	0.0067	0.1511	0.0032	0.0969	30.9	0.0200
1c	112300	164.4072	0.0077	0.3453	0.0062	0.1846	42.9	0.0691
1d	101100	148.0104	0.0027	0.0444	0.0017	0.0149	20.3	0.0017
2a	114500	167.6280	0.0050	0.0453	0.0032	0.0317	44.4	0.0060
2b	114800	168.0672	0.0093	0.2119	0.0033	0.0977	16.1	0.0189
2c	113300	165.8712	0.0075	0.2877	0.0043	0.1280	25.3	0.0329
2d	108100	158.2584	0.0053	0.0159	0.0033	0.0059	22.8	0.0012
3c	114000	166.8960	0.0054	0.1000	0.0019	0.0741	25.6	0.0082
4a	112500	164.7000	0.0084	0.2751	0.0037	0.1118	18.0	0.0253
4c	112700	164.9928	0.0017	0.2200	0.0007	0.1257	24.9	0.0056

Note that the conversion efficiency of N3 dye in this study is much lower than other studies for example from Phan (2019) which is 5.165%. This is unfortunately because of restriction faced in this study where this study was done during Covid-19 period. The restriction is more to travel restriction to Taiwan to proceed with photoelectrical measurement which was originally planned. Therefore, a manual set up in our own lab was done to proceed with the photoelectrical measurement. Nevertheless, N3 standard dye was used to ensure the fabrication process was correct and consistent. Due to this reasoning, the number from the efficiency studies is not very significant to see the conversion efficiency

value of each compound but rather to see and compare which structure of the compound gives the best conversion power.

Referring to Table 4.10 and Figure 4.36, DSSC sensitised with **1c** showed the highest power conversion efficiency (PCE) of 0.0691% with current density of 0.0077 mA/cm^2, V_{OC} of 0.3453 V and FF value of 42.9. Meanwhile, the lowest dye sensitiser is compound **2d** where its PCE is 0.0012%, current density of 0.0053 mA/cm^2, V_{OC} of 0.0159 V and FF of 22.8. To note, the thickness of TiO_2, the electrolyte, the cell resistance, and the conversion of photocurrent absorbed by the dye are all elements that can influence the FF value. As a result of the dye sensitiser's improved absorption, more photons are absorbed, resulting in a higher photocurrent that can be delivered to the nanocrystalline TiO_2 layer, increasing overall performance (Teo et al., 2017). Compound **1c** shows the highest power due to the efficient electron delocalisation throughout its structure as well as the presence of a good electron donator (-OMe) while compound **2d** shows the least efficiency might be due to the difficulty of the dye to absorb itself to the TiO_2 surface because of its solubility problem in almost all available organic solvents. Theoretically, if boron complexes **1d** and **2d** is soluble, they might give a higher efficiency than Schiff base compounds.

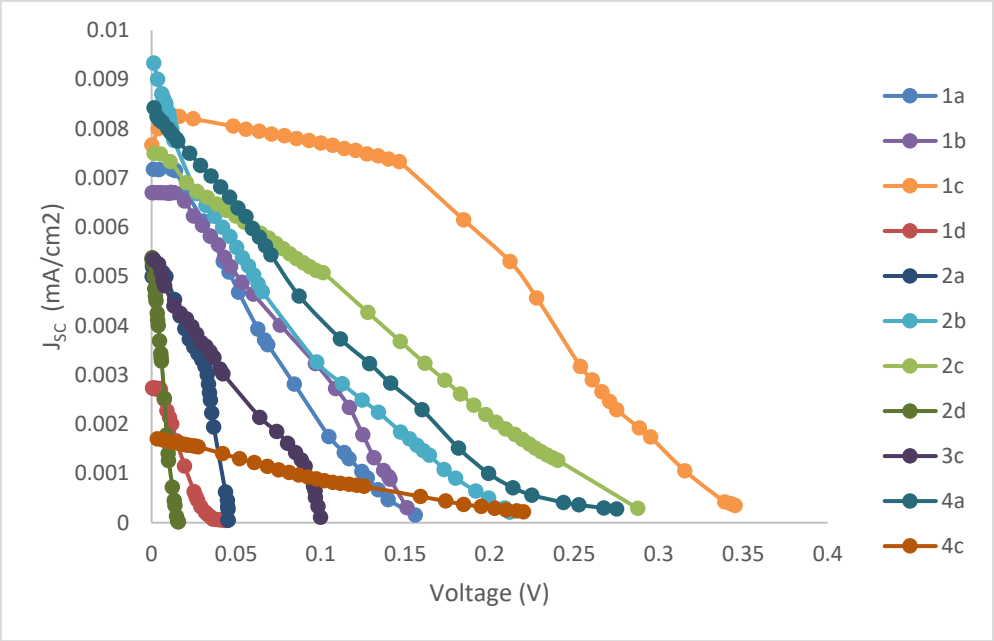

Figure 4.36: J/V measurement of symmetrical bis-Schiff base compounds and complexes as dye-sensitiser

The effect of different substituent in the molecule can be observed through the PCE values of the compound series as shown in Figure 4.37. Compounds **1c** and **2c** which contain -OMe substituent at both ends showed the highest efficiency for both series with 0.0691% (0.0077 mA/cm^2) and 0.0329% (0.0075 mA/cm^2) PCE, respectively. This is because -OMe groups donate electrons leading to a charge transfer within the molecule and delivered the electrons towards TiO_2. Interestingly, compounds **1b** and **2b** containing -OH substituent at both ends which shows luminescent properties under UV light shows lower PCE than -OMe substituents at 0.0200% (0.0067 mA/cm^2) and 0.0189% (0.0093 mA/cm^2), respectively. It is known that in terms of electron donor, -OMe is a stronger electron donor than -OH. Other substituents that are known to have higher conversion efficiencies are carboxylic acids (-COOH), phosphonic acids and sulphonic acids. This is because these substituents can anchor to the surface of TiO_2 as an effective binding site. For example, -COOH substituents can

form ester linkage with the TiO_2 surface which gives a strong bound dye that can allow better electronic communication between both parts (Ladomenou et al., 2014; Zhang & Cole, 2015).

Furthermore, in comparison to compounds without substituent (compounds **1a** and **2a**), its PCE was indeed lower than those with substituent. This is due to the absence of electron donor in the molecule. Compounds **1a** and **2a** gives PCE of 0.0166% (0.0072 mA/cm^2) and 0.0060% (0.0050 mA/cm^2) respectively. However, for compounds **1d** and **2d**, which are the boron difluoride complexes showed the lowest efficiency of the series at 0.0017% (0.0027 mA/cm^2) and 0.0012% (0.0053 mA/cm^2) of PCE respectively. This may be due to the poor solubility of complexes **1d** and **2d** in solvent system which can be seen by the reformation of its precipitates on top of TiO_2 during the fabrication process. This causes the increase in the thickness of the layer of working electrode as well as increases the direct contact of working electrode with counter electrode which results in the increase of cell resistance affecting the efficiency of the cell (Teo et al., 2017).

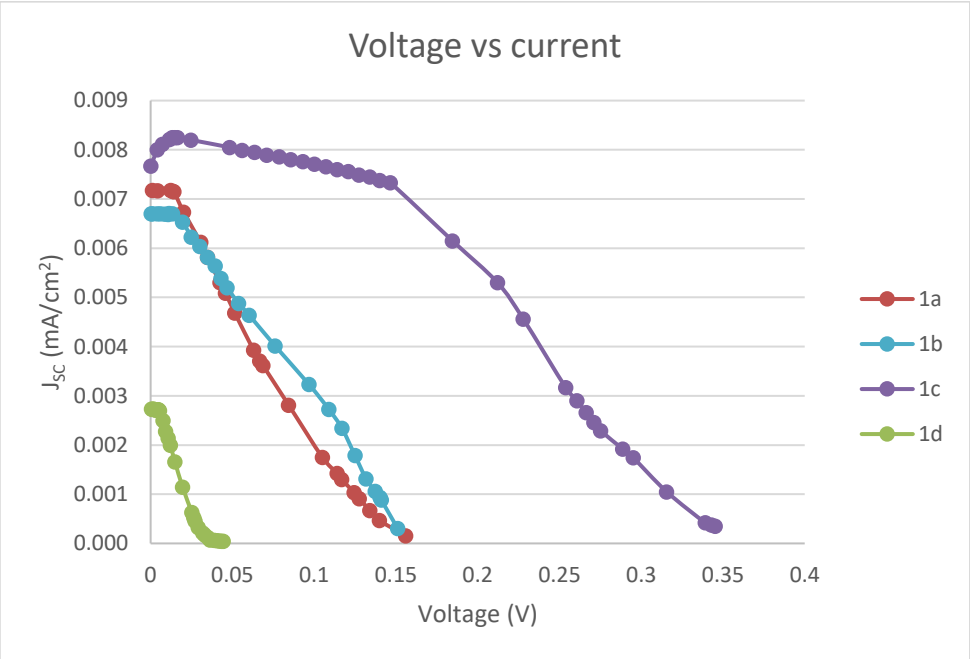

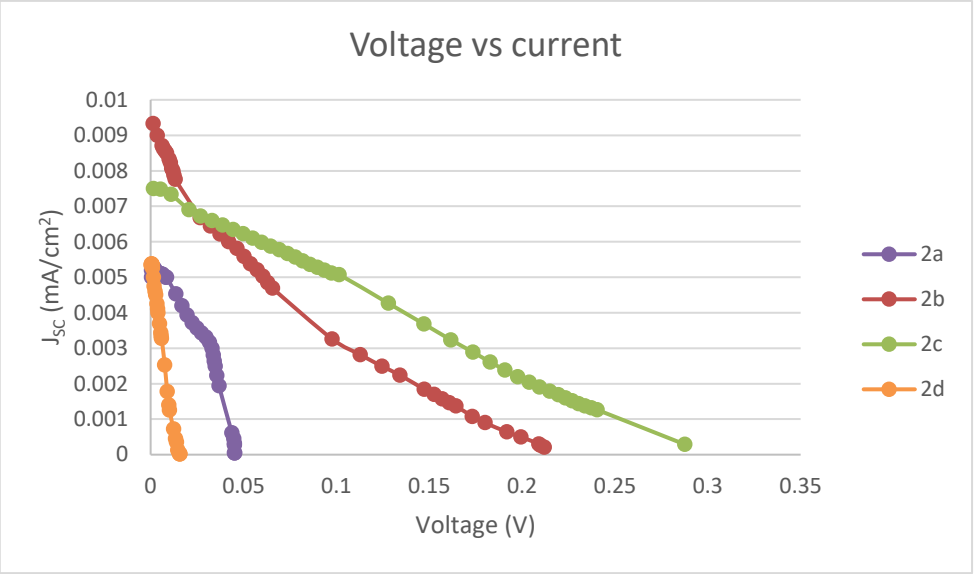

Figure 4.37: J/V measurement of series 1 compounds (above) and series 2 compounds (below)

Furthermore, the effect of different π-spacer at the centre of the molecule also can be observed. Referring to the J/V curves in Figure 4.38, compound with phenyl ring bridge at the centre (**1c** and **2c**) showed higher conversion efficiency compared to compounds with linear bridge (**3c** and **4c**). Compounds **3c** and **4c** are connected by a -N=CHCH=N- and -N=C(CH_3)C(CH_3)=N-, respectively, meanwhile compounds **1c** and **2c** connected by an aromatic ring in *para*- and *ortho*- positions of a central benzene ring into an entire conjugate system. The conjugate effect and the flexibility in coordination structures are the major factors influencing the catalytic activity of a compounds (Wang et al., 2003). A fused aromatic ring system is preferred over a linear chain system with rotatable single bonds to maintain strong contact through the π-conjugated system (Houjou et al., 2017).

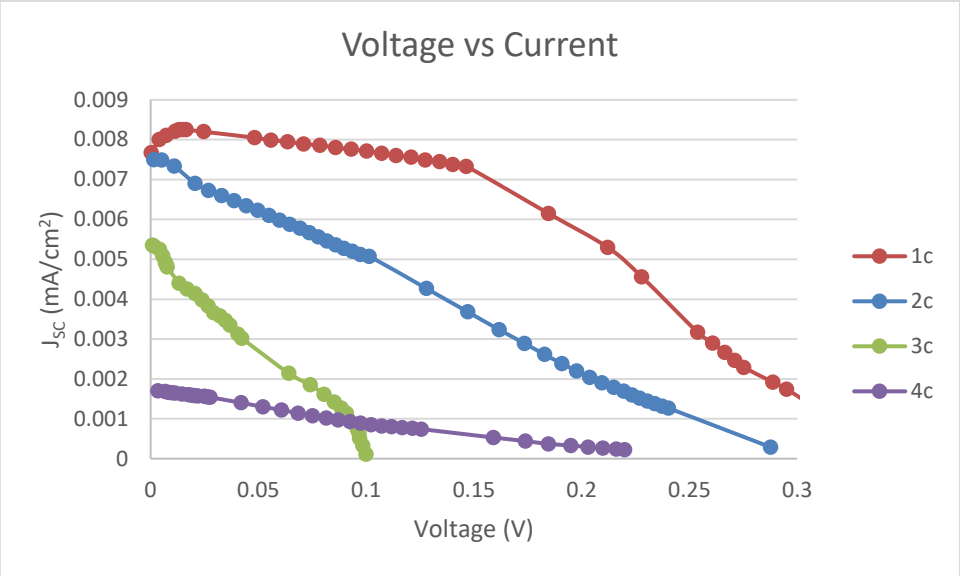

Figure 4.38: J/V measurement of symmetrical bis-Schiff base with different π-spacer

Indeed, there have been some literatures that have compared the π-conjugation effect in *ortho*-, *para*- and *meta*- position phenyl backbone of a molecule (Figure 4.39). It is reported that the strength of electron delocalisation through para-position phenyl bridge is better followed by *ortho*-position and then lastly *meta*-position phenyl bridge (Ruiz-Carretero et al., 2014).

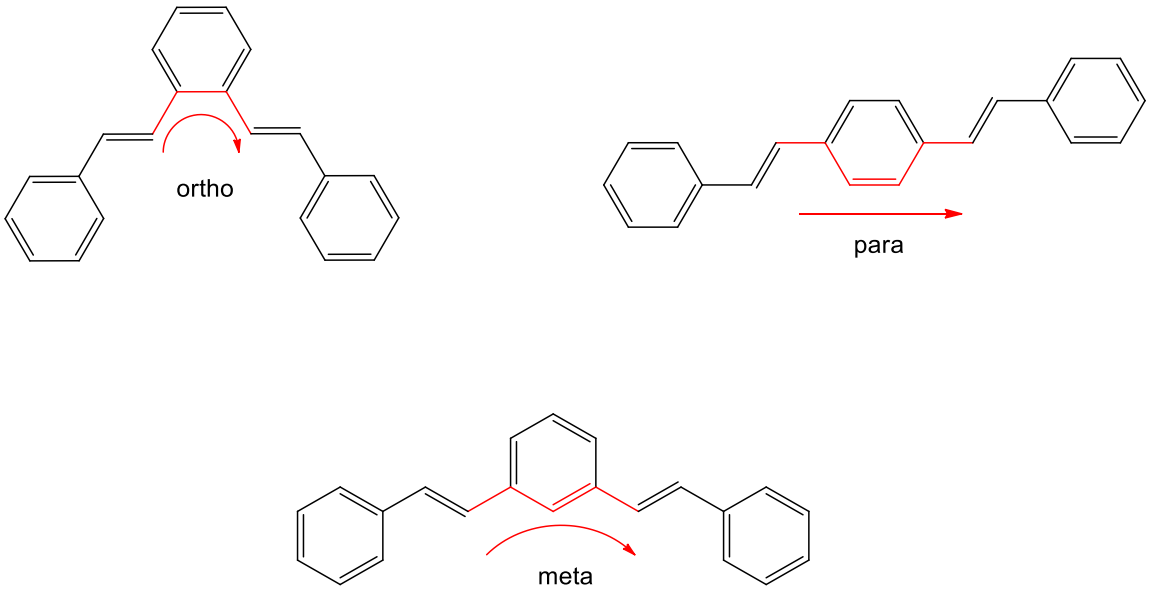

Figure 4.39: Illustrations of *ortho-*, *para-* and *meta-* conjugation paths

The efficiency of electron delocalisation through an ortho-position phenyl bridge is as almost efficient as through para-position phenyl bridge if the π-conjugated backbone does not have large torsion angles and torsional motions (Huang et al., 2011; Ali & Alvi, 2020). Meta-position phenyl bridge on the other hand, destroy the π-conjugation system in the molecule causing the localisation of electron-hole pair as well as electronic decoupling (Figure 4.40). This affects the efficiency of facilitating the electron movement throughout the molecule (Teo et al., 2017).

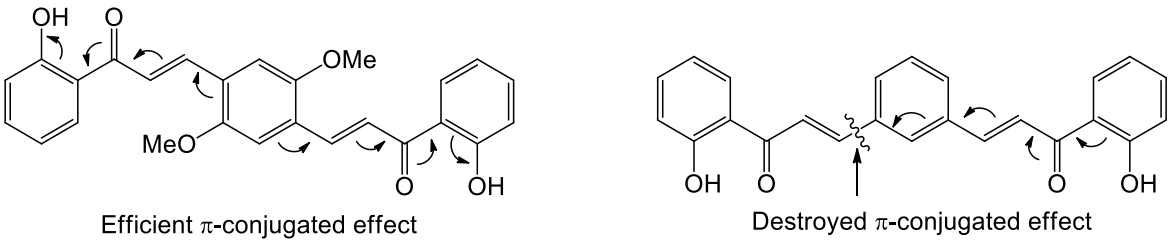

Figure 4.40: The electron delocalisation pathway in *para*-position and *meta*-position phenyl bridge

Therefore, in this project, only phenyl bridge spacer of *ortho*- and *para*- positions were used to see if the difference in conjugation effect strength have effect on the DSSC efficiencies. As reported, *para*- position phenyl bridge dominates over *ortho*- and *meta*- positions (*para* > *ortho* > *meta*). The difference between the strength of *para*- and *ortho*- positions might be because of the steric hindrance of *ortho*- substituents or chains which is then decrease the conjugation effects of the molecule (Ruiz-Carretero et al., 2014; Serafini et al., 2021).

Based on the efficiencies results, it is true that compound **1c** shows higher efficiency by almost double efficiencies than compound **2c**. Both compounds (**1c** and **2c**) have almost the same structure with same substituent (-OMe) except for compound **1c** which contains aromatic π-spacer with *para*- position meanwhile compound **2c** contains aromatic π-spacer with *ortho*- position. Thus, this confirm that the strength of π-conjugation system in a molecule plays a role and can affect the efficiencies of DSSC device.

Therefore, based on the overall PCE results, compound that contain aromatic π-spacers are better in facilitating electron delocalisation within a molecule compared to aliphatic π-spacers. In addition, aromatic π-spacers that are in *para*- positions are more preferrable in terms of strength of their π-conjugation system due to steric hindrance. Furthermore, different substituents also affect the overall efficiencies in terms of their strength in electron donating effects whereby -OMe substituent shows the best results compare to -OH substituent. Thus, since compound 1c have all of the best characteristics in its molecule (Figure 4.41), it gives the highest efficiencies overall.

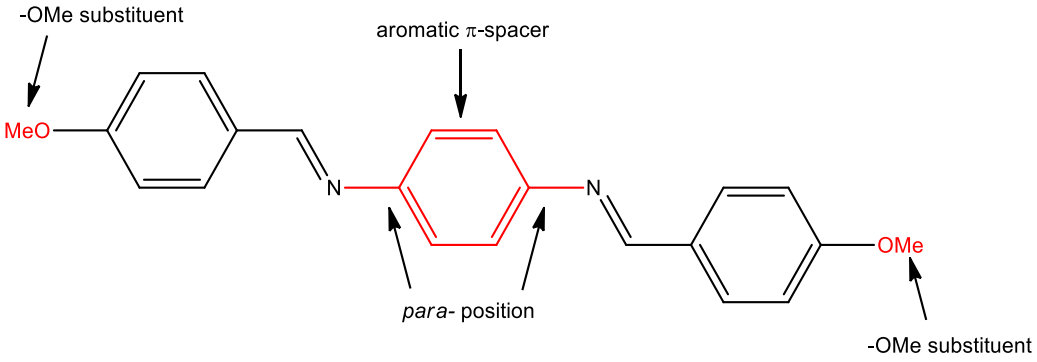

Figure 4.41: The structure of **1c** with its characteristics

CHAPTER 5

CONCLUSION AND SUGGESTION FOR FUTURE WORK

5.1 Conclusion

A total of eleven symmetrical bis-Schiff base compounds and complexes have been synthesised and characterised by using Fourier-transform infra-red (FT-IR), NMR, UV-visible spectroscopy, gas chromatogram mass spectroscopy (GCMS) and CHN analysis. The formation of symmetrical bis-Schiff base compounds (**1a - 4c**) was confirmed mainly by the disappearance of C=O peak at 1750 – 1700 cm^{-1} and the appearance of imine (C=N) peak at 1630 – 1500 cm^{-1} in IR spectra. In addition, NMR spectra also confirmed that the CHO peak at δH 10 ppm was disappeared whereas C=N peak at δH 7.88 – 9.03 ppm was found. Other characterisation results also support the confirmation of those compounds. Meanwhile, for boron difluoride complexes, **1d** and **2d**, the peak that attributed to the υ(OH) vibration was disappeared due to the coordination of the OH group to become complex. Furthermore, a new peak at 1044 cm^{-1} & 1218 cm^{-1} and 1085.85 cm^{-1} & 1153.56 cm^{-1} was found that correspond to the B-F and B-O bonds respectively. In addition, in UV-Visible spectra also shows new peak at 442 – 449 nm of the intramolecular charge transfer due to the presence of boron difluoride in the structure.

The conversion efficiency of all compounds and complexes as a dye in DSSC were tested and recorded. Compound **1c** achieved the highest conversion efficiency of 0.0691% due to the presence of good electron donor (-OMe) substituents as well as aromatic rings in *para*- position as the π-spacer followed by compound **2c** (0.0329%) which have almost similar structure except for the aromatic rings of its π-spacer is in *ortho*- position. The presence of conjugation system in the molecule as well as -OMe substituent as the electron

donor allow sufficient electron delocalisation along the molecule resulting in effective charge transfer within the molecule which is then transported to the TiO_2 layer on the working electrode. Conversely, boron difluoride Schiff base compounds, **1d** and **2d**, recorded the lowest PCE of 0.0017% and 0.0012% respectively. The poor solubility in solvent system of both boron difluoride compounds could be the reason causing the low efficiency because the dye was difficult to be absorbed by the TiO_2 surface.

Based on the data obtained, compound with better electron donors property, with aromatic rings as the π-spacer in *para*- position can give a higher conjugation effect which is ideal for the application in DSSC.

5.2 Suggestion for future work

Based on the overall results from this study, the symmetrical bis-Schiff base compound **1c** bearing the -OMe as the electron donating group gives the highest efficiency of 0.0691%. In addition, compound **1c** also have an aromatic π-spacer in *para*- position in their structure which further helps to facilitates the electron movements throughout the structure. However, there are still several aspects that can be further improved. The following ideas can be looked into in order to accomplish this goal:

i. The introduction of electron donating substituents can enhance the HOMO energy in the compound compared to compound with weaker electron donor (Tai et al., 2011). As seen in this study, compound with -OMe substituent shows the highest efficiency (0.0691%) compared to compound with -OH (0.0200%) and -H (0.0166%) substituent. Other compound that contain stronger electron donating groups such as tertiary amine (diethylaminoaniline, $-NEt_2$ and

dimethylaminoaniline, -NMe_2), furfural (-C_4H_3O) or vanillin which have both -OH and -OMe substituents can be introduced to enhance the efficiencies.

ii. In addition, introducing a better anchoring group can also enhance the power conversion efficiency as it can anchor to the surface of TiO_2 as an effective binding site which is then can allow better electronic communication between the dye and TiO_2 (Ladomenou et al., 2014; Zhang & Cole, 2015). In this study, only -H were used in the compounds which gives <0.07% efficiencies overall. Thus, by introducing strong anchoring group such as -COOH, phosponic acids (-$PO(OH)_2$) and sulphonic acids in the compound can greatly optimise the conversion efficiencies.

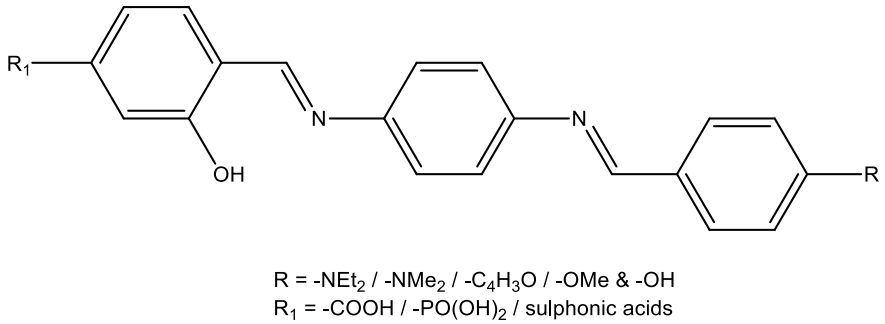

Figure 5.1: Recommended Schiff base structure for future work

iii. According to the study by Phan (2019), comparing the dye sensitiser bonded to the ruthenium metal and dye sensitiser of boron difluoride, compound that bonded with boron difluoride shows greater efficiency with better π-electron delocalisation in the structure which helps in push-pull effects despite the N3 standard dye is a sensitiser of ruthenium metal. In addition, it also has been reported that complexation with boron difluoride have shown an excellent effect on electrochemical properties of a molecules as it can lower the energy gap of a

compound after complexation (Chaabene et al., 2019). Therefore, it is worth to explore more of boron difluoride complexes and investigate the efficiencies when paired with more variety of substituents and anchoring groups.

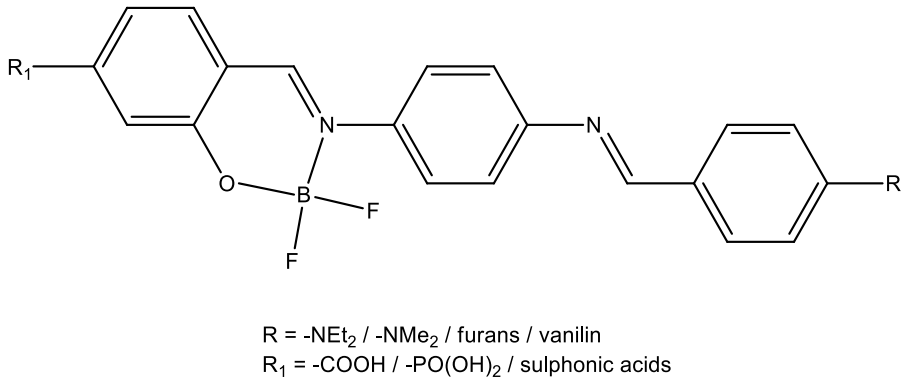

Figure 5.2: Recommended Schiff base boron difluoride structure for future work

REFERENCES

Abdalhadi, S. M., Al-Baitai, A. Y., & Al-Zubaidi, H. A. (2020). Synthesis and characterization of 2, 3-diaminomaleonitrile derivatives by one-pot schiff base reaction and their application in dye synthesized solar cells. *Indonesian Journal of Chemistry*, *21*(2), 443-451.

Abu-Dief, A. M., & Mohamed, I. M. (2015). A review on versatile applications of transition metal complexes incorporating Schiff bases. *Beni-Suef University Journal of Basic and Applied Sciences*, 4(2), 119-133.

Agren, S., Chaabene, M., Allouche, A. R., Ben Chaabane, R., Lahcinie, M., & Baouab, M. H. V. (2020). Blue highly fluorescent boranil derived from anil ligand: Synthesis, characterization, experimental and theoretical evaluation of solvent effect on structures and photophysical properties. *Applied Organometallic Chemistry*, *34*(9), Article e5764.

Akila, E., Usharani, M., Vimala, S., & Rajavel, R. (2012). Synthesis, spectroscopic characterization and biological evaluation studies of mixed ligand schiff base with metal (II) complexes derived from o-phenylenediamine. *Chemical Science Review and Letters*, *1*(4), 181-194.

Al Zoubi, W., Al-Hamdani, A. A. S., Ahmed, S. D., & Ko, Y. G. (2018). A new azo-Schiff base: Synthesis, characterization, biological activity and theoretical studies of its complexes. *Applied Organometallic Chemistry*, *32*(1), Article e3895.

Alattar, R. A., Hassan, Z. M., Abass, S. K., & Ahmad, L. M. (2020, December). Synthesis, characterization and study the photodecolorization of Schiff base Fe (III) complex in

ZnO/Uv-A light system. In *AIP Conference Proceedings* (Vol. 2290, No. 1, p. 030032). AIP Publishing LLC.

Alhamed, M., Issa, A. S., & Doubal, A. W. (2012). Studying of natural dyes properties as photo-sensitizer for dye sensitized solar cells (DSSC). *Journal of Electron Devices*, *16*(11), 1370-1383.

Alhorani, S., Kumar, S., Genwa, M., & Meena, P. L. (2021). Dye extracted from Bael leaves as a photosensitizer in dye sensitized solar cell. *Materials Research Express*, *8*(11), Article 115507.

Ali, R., & Alvi, S. (2020). The story of π-conjugated isotruxene and its congeners: From syntheses to applications. *Tetrahedron*, *76*(35), Article 131345.

Ambrozic, G., Crnjak Orel, Z., & Zigon, M. (2011). Microwave-assisted non-aqueous synthesis of ZnO nanoparticles. *Materials and Technologies*, *45*(3), 173–177.

Ashraf, M. A., Mahmood, K., Wajid, A., Maah, M. J., & Yusoff, I. (2011). Synthesis, characterization and biological activity of Schiff bases. *IPCBEE*, *10*(1), 1-7.

Chaabene, M., Agren, S., Allouche, A. R., Lahcinie, M., Ben Chaabane, R., & Baouab, M. H. V. (2019). Theoretical and experimental investigations of complexation with BF_3. Et_2O effects on electronic structures, energies and photophysical properties of Anil and tetraphenyl (hydroxyl) imidazol. *Applied Organometallic Chemistry*, *33*(11), Article e5218.

Chouk, R., Aguir, C., Haouanoh, D., Bergaoui, M., Tala-Ighil, R., Stathatos, E., & Khalfaoui, M. (2019). A first-principles computational and experimental investigation

on Schiff base cobalt complex towards designing solar cells. *Journal of Molecular Structure, 1196*, 676-684.

Çınar, E. B., Yeşilbağ, S., Doğan, O. E., Ağar, E., Dege, N., & Saif, E. (2020). Synthesis, crystal structure and Hirshfeld surface analysis of 1, 7-dimethyl-5a, 6, 11a, 12-tetrahydrobenzo [b] benzo [5, 6][1, 4] oxazino [2, 3-e][1, 4] oxazine. *Acta Crystallographica Section E: Crystallographic Communications*, *76*(9), 1472-1475.

Cozzi, P. G. (2004). Metal–Salen Schiff base complexes in catalysis: practical aspects. *Chemical Society Reviews*, *33*(7), 410-421.

Da Silva, C. M., da Silva, D. L., Modolo, L. V., Alves, R. B., de Resende, M. A., Martins, C. V., & de Fátima, Â. (2011). Schiff bases: A short review of their antimicrobial activities. *Journal of Advanced Research*, *2*(1), 1-8.

Deshineni, R., Velpula, R., Ragi, R., & Chellamella, G. K. (2016). One-pot multi-component synthesis of 4-substituted thiazole Schiff base derivatives and their antibacterial activity. *Indian Journal of Chemistry*, *55B*(11), 1415–1419.

Dong, B., Xu, G., Luo, X., Cai, Y., & Gao, W. (2012). A bibliometric analysis of solar power research from 1991 to 2010. *Scientometrics*, *93*(3), 1101-1117.

Ebrahimi, S. M., Mahdavi, M., Emami, S., Saeedi, M., Asadi, M., Firoozpour, L., Divsalar, K., Shafiee, A., & Foroumadi, A. (2014). Green and catalyst-free one-pot synthesis of anthranilamide Schiff bases: An approach toward sirtinol. *Synthetic Communications*, *44*(5), 665-673.

Elemike, E. E., Nwankwo, H. U., & Onwudiwe, D. C. (2019). Synthesis and comparative study on the anti-corrosion potentials of some Schiff base compounds bearing similar backbone. *Journal of Molecular Liquids, 276*, 233-242.

Farfán, N., Santillan, R. L., Castillo, D., Cruz, R., Joseph-Nathan, P., & Daran, J. C. (1992). Fused heterocycles derived from pseudoephedrine and ephedrine. *Canadian Journal of Chemistry, 70*(11), 2764-2770.

Gencer Imer, A., Syan, R. H. B., Gülcan, M., Ocak, Y. S., & Tombak, A. (2018). The novel pyridine based symmetrical Schiff base ligand and its transition metal complexes: Synthesis, spectral definitions and application in dye sensitized solar cells (DSSCs). Journal of Materials Science: *Materials in Electronics, 29*(2), 898-905.

Goel, P., Kumar, D., & Chandra, S. (2014). Schiff's Base ligands and their transition metal complexes as antimicrobial agents. *Journal of Chemical Biological and Physical Sciences, Section A, 4*, 1946-1964.

Gondia, N. K., & Sharma, S. K. (2019). Comparative optical studies of naphthalene based Schiff base complexes for colour tunable application. *Materials Chemistry and Physics, 224*, 314-319.

Grätzel, M. (2003). Dye-sensitized solar cells. *Journal of Photochemistry and Photobiology C: Photochemistry Reviews*, *4*(2), 145-153.

Green, M. A. (2000). Photovoltaics: technology overview. *Energy Policy*, *28*(14), 989-998.

Gul, M., Kotak, Y., & Muneer, T. (2016). Review on recent trend of solar photovoltaic technology. *Energy Exploration & Exploitation*, *34*(4), 485-526.

Gupta, C. K., & Sutar, A. K. (2008). Catalytic activities of Schiff base transition metal complexes. *Coordination Chemistry Reviews*, *252*(12-14), 1420-1450.

Haddleton, D. M. (2001). *Polymerisation catalyst and process*. (European Patent No. EP09 06342B1). European Patent Office.

Hagfeldt, A., Boschloo, G., Sun, L. C., Kloo, L., & Pettersson, H. (2010). *Dye-sensitized solar cells*. *Chemical Reviews*, *110*(11), 6595-6663.

Hai-Yan, Z., Xiao-Hang, Q., & Pan-Wen, S. (2004). 5A,6,11a,12-tetrahydro-5a,11a-dimethyl-1,4-benzoxazino[3,2-b][1,4]benzoxazine. *Acta Crystallographica Section E Structure Reports Online*, *60*(9), 01619–01621.

Hajji, C., Zaballos-García, E., & Sepulveda-Arques, J. (2003). Synthesis of 1, 3-Oxazolidines and 1, 3-Dioxolanes by Reaction of (2 R, 3 R)-3-Methylamino-3-phenyl-1, 2-propanediol with Electrophiles. *Synthetic communications*, *33*(24), 4347-4354.

Haque, J., Srivastava, V., Chauhan, D. S., Lgaz, H., & Quraishi, M. A. (2018). Microwave-induced synthesis of chitosan Schiff bases and their application as novel and green corrosion inhibitors: experimental and theoretical approach. *ACS Omega*, *3*(5), 5654-5668.

Hou, Q., Zhao, L., Zhang, H., Wang, Y., & Jiang, S. (2007). Synthesis and luminescent properties of two Schiff-base boron complexes. *Journal of Luminescence*, *126*(2), 447-451.

Houjou, H., Yagi, K., Yoshikawa, I., Mutai, T., & Araki, K. (2017). Effects of interaction between the chelate rings and π-conjugated systems in fused salphen complexes on UV-Vis-NIR spectra. *Journal of Physical Organic Chemistry*, *30*(6), Article e3635.

Huang, H. H., Prabhakar, C., Tang, K. C., Chou, P. T., Huang, G. J., & Yang, J. S. (2011). Ortho-branched ladder-type oligophenylenes with two-dimensionally π-conjugated electronic properties. *Journal of the American Chemical Society*, *133*(20), 8028-8039.

Iftikhar, H., Sonai, G. G., Hashmi, S. G., Nogueira, A. F., & Lund, P. D. (2019). Progress on electrolytes development in dye-sensitized solar cells. *Materials*, *12*(12), Article 1998.

Ikpesu, J. E., Iyuke, S. E., Daramola, M., & Okewale, A. O. (2020). Synthesis of improved dye-sensitized solar cell for renewable energy power generation. *Solar Energy*, *206*, 918-934.

Kabir, E., Kumar, P., Kumar, S., Adelodun, A. A., & Kim, K. H. (2018). Solar energy: Potential and future prospects. *Renewable and Sustainable Energy Reviews*, *82*, 894-900.

Kassim, K., Hamali, M. A., & Yamin, B. (2019). A new alternative synthesis of salicylaldazine via microwave irradiation method. *Journal of Chemistry*, *2019*, Article 9546373

Kilinc, D., Şahin, Ö., & Horoz, S. (2019). Use of low-cost Zn (II) complex efficiently in a dye-sensitized solar cell device. *Journal of Materials Science: Materials in Electronics*, *30*(12), 11464-11467.

Kuan, S. H. C. (2021). *The amine-carbonyl reaction and their role in catalysis*. *Master Thesis*. Universiti Malaysia Sarawak.

Kuddushi, M. M. Y., Malek, M. A. H., Patidar, V. L., Patel, M. S., Patel, R. K., & Dave, R. H. (2018). Synthesis and characterization of Schiff base aniline with 5-bromo-2-hydroxyl benzaldehyde and their metal complexes. *International Journal of Recent Scientific Research, 9*(4(G)), 26026-26030.

Kukharenko, A. V., & Avramenko, G. V. (2001). Synthesis of Boron-containing complexes of 1-(2-hydroxyphenyl)-3-phenyl-2-propen-1-one. *Russian Journal of General Chemistry, 71*(10), 1562-1564.

Kumar, D. K., Kříž, J., Bennett, N., Chen, B., Upadhayaya, H., Reddy, K. R., & Sadhu, V. (2020). Functionalized metal oxide nanoparticles for efficient dye-sensitized solar cells (DSSCs): A review. *Materials Science for Energy Technologies, 3*, 472-481.

Kwak, D. J., Moon, B. H., Lee, D. K., Park, C. S., & Sung, Y. M. (2011). Comparison of transparent conductive indium tin oxide, titanium-doped indium oxide, and fluorine-doped tin oxide films for dye-sensitized solar cell application. *Journal of Electrical Engineering and Technology*, *6*(5), 684-687.

Ladomenou, K., Kitsopoulos, T. N., Sharma, G. D., & Coutsolelos, A. G. (2014). The importance of various anchoring groups attached on porphyrins as potential dyes for DSSC applications. *RSC Advances*, *4*(41), 21379-21404.

Laman Web Rasmi Jabatan meteorologi Malaysia. MetMalaysia: Utama. Retrieved February 14, 2022, from https://www.met.gov.my/

Lee, J. K., & Yang, M. (2011). Progress in light harvesting and charge injection of dye-sensitized solar cells. *Materials Science and Engineering: B, 176*(15), 1142-1160.

Lei, Y., Liu, H., & Xiao, W. (2010). First principles study of the size effect of TiO_2 anatase nanoparticles in dye-sensitized solar cell. *Modelling and Simulation in Materials Science and Engineering*, *18*(2), Article 025004.

Lokhande, P. K. M., Sonigara, K. K., Jadhav, M. M., Patil, D. S., Soni, S. S., & Sekar, N. (2019). Multi-dentate carbazole based Schiff base dyes with chlorovinylene group in spacer for dye-sensitized solar cells: A combined theoretical and experimental study. *ChemistrySelect*, *4*(14), 4044-4056.

Mahadevi, P., & Sumathi, S. (2020). Mini review on the performance of Schiff base and their metal complexes as photosensitizers in dye-sensitized solar cells. *Synthetic Communications*, *50*(15), 2237-2249.

Michael, P. R., Johnston, D. E., & Moreno, W. (2020). A conversion guide: solar irradiance and lux illuminance. *Journal of Measurements in Engineering*, *8*(4), 153-166.

Milichko, V. A., Shalin, A. S., Mukhin, I. S., Kovrov, A. E., Krasilin, A. A., Vinogradov, A. V., Belov, P. A., & Simovski, C. R. (2016). Solar photovoltaics: current state and trends. *Physics-Uspekhi*, *59*(8), 727-772.

Mohan, J., & Kumar, A. (2005). Novel bridgehead nitrogen bisheterocyclic systems: Synthesis, stereochemistry and antimicrobial activity of p-bis [2H, 5H-4-oxo-thiazol-3-yl] phenylenes and p-bis [cis-5H-3, 3a-dihydropyrazolo [3, 4-d] thiazol-6-yl] phenylenes. *Indian Journal of Chemistry, 44B*, 631-634.

Mohanta, P. R., Patel, J., Bhuva, J., & Gandhi, M. (2015). A review on solar photovoltaics and roof top application of it. *International Journal of Advanced Research in Science, Engineering and Technology*, *2*, 2394-2444.

Murase, I. (1959). On the structure of condensation products of o-aminophenols with α-dicarbonyl compounds. I. *Bulletin of the Chemical Society of Japan*, *32*(8), 827-832.

Naik, P., Su, R., Elmorsy, M. R., El-Shafei, A., & Adhikari, A. V. (2018). Investigation of new carbazole based metal-free dyes as active photo-sensitizers/co-sensitizers for DSSCs. *Dyes and Pigments*, *149*, 177-187.

Nain, P., & Kumar, A. (2021). Theoretical evaluation of metal release potential of emerging third generation solar photovoltaics. *Solar Energy Materials and Solar Cells*, *227*, Article 111120.

Nartop, D., & Öğütcü, H. (2020). Synthesis of new unsymmetrical Schiff bases as potential antimicrobial agents. *Sinop Üniversitesi Fen Bilimleri Dergisi*, *5*(1), 13-25.

National Renewable Energy Laboratory. (2022). *Best research cell efficiencies*. Retrieved from https://www.nrel.gov/pv/.

Niklas, J. E., Hunter, K. M., & Gorden, A. E. (2019). Bonding Interactions in Uranyl α-Diimine Complexes: A Spectroscopic and Electrochemical Study of the Impacts of Ligand Electronics and Extended Conjugation. *Inorganic Chemistry*, *58*(22), 15088-15100.

Noh, S. I., Ahn, H. J., & Riu, D. H. (2012). Photovoltaic property dependence of dye-sensitized solar cells on sheet resistance of FTO substrate deposited via spray pyrolysis. *Ceramics International*, *38*(5), 3735-3739.

Nourmohammadian, F., & Gholami, M. D. (2012). Two novel push-pull series of benzothiazole-based dyes: Synthesis and characterization. *Helvetica Chimica Acta*, *95*(9), 1548-1555.

Pan, M., Huang, N., Zhao, X., Fu, J., & Zhong, X. (2013). Enhanced efficiency of dye-sensitized solar cell by high surface area anatase-TiO_2-modified P25 paste. *Journal of Nanomaterials*, *2013*, Article 760685.

Pandey, A. K., Tyagi, V. V., Jeyraj, A., Selvaraj, L., Rahim, N. A., & Tyagi, S. K. (2016). Recent advances in solar photovoltaic systems for emerging trends and advanced applications. *Renewable and Sustainable Energy Reviews, 53*, 859-884.

Pansuriya, P. B., Dhandhukia, P., Thakkar, V., & Patel, M. N. (2007). Synthesis, spectroscopic and biological aspects of iron (II) complexes. *Journal of Enzyme Inhibition and Medicinal Chemistry*, *22*(4), 477-487.

Panwar, N. L., Kaushik, S. C., & Kothari, S. (2011). Role of renewable energy sources in environmental protection: A review. *Renewable and Sustainable Energy Reviews*, *15*(3), 1513-1524.

Pavia, D. L., Lampman, G. M., Kriz, G. S., & Vyvyan, J. A. (2014). *Introduction to Spectroscopy*. Cengage learning.

Pervaiz, M., Sadiq, S., Sadiq, A., Younas, U., Ashraf, A., Saeed, Z., Zuber, M., & Adnan, A. (2021). Azo-Schiff base derivatives of transition metal complexes as antimicrobial agents. *Coordination Chemistry Reviews*, *447*, Article 214128.

Phan, T. P. (2019). *Synthesis and characterization of unsymmetrical α,β-conjugated keto derivatives and their complexes for dye sensitizer solar sell (DSSC) application*. *Master Thesis*. Universiti Malaysia Sarawak.

Phan, T. P., Teo, K. Y., Liu, Z. Q., Tsai, J. K., & Tay, M. G. (2019). Application of unsymmetrical bis-chalcone compounds in dye sensitized solar cell. *Chemical Data Collections*, *22*, Article 100256.

Radi, S., Tighadouini, S., Feron, O., Riant, O., Mabkhot, Y. N., Al-Showiman, S. S., Hadda. T. B., El-Youbi, M., Benabbes, R., & Saalaoui, E. (2015). One pot synthesis, antitumor, antibacterial and antifungal activities of some Sciff base heterocycles. *International Journal of Pharmacy*, *5*(1), 39-45.

Rawal, N., Vaishaly, A. G., Sharma, H., & Mathew, B. B. (2015). Dye sensitized solar cells: the emerging technology. *Energy and Power Engineering Science EPES*, *2*(2), 46-52.

Richhariya, G., & Kumar, A. (2018). Fabrication and characterization of mixed dye: Natural and synthetic organic dye. *Optical Materials*, *79*, 296-301.

Roth, A., Spielberg, E. T., & Plass, W. (2007). Kit for unsymmetric dinucleating double-Schiff-base ligands: Facile access to a versatile new ligand system and its first heterobimetallic copper− zinc complex. *Inorganic Chemistry*, *46*(11), 4362-4364.

Ruiz-Carretero, A., Noguez, O., Herrera, T., Ramírez, J. R., Sánchez-Migallón, A., & de La Hoz, A. (2014). Microwave-assisted selective synthesis of mono-and bistriazines with π-conjugated spacers and study of the optoelectronic properties. *The Journal of Organic Chemistry*, *79*(11), 4909-4919.

Salve, P. S., Alegaon, S. G., & Sriram, D. (2017). Three-component, one-pot synthesis of anthranilamide Schiff bases bearing 4-aminoquinoline moiety as Mycobacterium tuberculosis gyrase inhibitors. *Bioorganic & Medicinal Chemistry Letters*, *27*(8), 1859-1866.

Samani, Z. R., & Mehranpour, A. (2021). Synthesis of new allylidene amino phenol-containing Schiff bases and metal complex formation using trimethinium salts. *RSC Advances, 11*(35), 21695-21701.

Schmidt, M., Görls, H., & Plass, W. (2016). Facile high-yield synthesis of unsymmetric end-off compartmental double Schiff-base ligands: Easy access to mononuclear precursor and unsymmetric dinuclear complexes. *RSC Advances, 6*(79), 75844-75854.

Semalti, P., & Sharma, S. N. (2020). Dye sensitized solar cells (DSSCs) electrolytes and natural photo-sensitizers: a review. *Journal of Nanoscience and Nanotechnology, 20*(6), 3647-3658.

Sen, P. (2019). A highly fluorescent tri-nuclear boron complex with large Stokes shifts based on tripodal Schiff base: synthesis and photophysical properties. *Journal of Chemical Sciences, 131*(7), 1-7.

Sen, P., Mpeta, L. S., Mack, J., & Nyokong, T. (2020). New difluoroboron complexes based on N, O-chelated Schiff base ligands: Synthesis, characterization, DFT calculations and photophysical and electrochemical properties. *Journal of Luminescence, 224*, Article 117262.

Serafini, P., Milani, A., Tommasini, M., Bottani, C. E., & Casari, C. S. (2021). Topology-dependent conjugation effects in graphdiyne molecular fragments. *Carbon, 180*, 265-273.

Shafie, S. M., Mahlia, T. M. I., Masjuki, H. H., & Andriyana, A. (2011). Current energy usage and sustainable energy in Malaysia: A review. *Renewable and Sustainable Energy Reviews, 15*(9), 4370-4377.

Shakdofa, M. M., Labib, A. A., Abdel-Hafez, N. A., & Mousa, H. A. (2018). Synthesis and characterization of VO^{2+}, Co^{2+}, Ni^{2+}, Cu^{2+} and Zn^{2+} complexes of a Schiff base ligand derived from ethyl 2-amino-6-ethyl-4, 5, 6, 7-tetrahydrothieno [2, 3-c] pyridine-3-carboxylate and their investigation as fungicide agents. *Applied Organometallic Chemistry*, *32*(12), Article e4581.

Shalini, S., Prasanna, S., Mallick, T. K., & Senthilarasu, S. (2015). Review on natural dye sensitized solar cells: Operation, materials and methods. *Renewable and Sustainable Energy Reviews*, *51*, 1306-1325.

Shalini, S., Balasundaraprabhu, R., Kumar, T. S., Prabavathy, N., Senthilarasu, S., & Prasanna, S. (2016). Status and outlook of sensitizers/dyes used in dye sensitized solar cells (DSSC): a review. *International Journal of Energy Research*, *40*(10), 1303-1320.

Shanmugapriya, J., Rajaguru, K., Sivaraman, G., Muthusubramanian, S., & Bhuvanesh, N. (2016). Boranil dye based “turn-on” fluorescent probes for detection of hydrogen peroxide and their cell imaging application. *RSC Advances*, *6*(89), 85838-85843.

Sharma, K., Sharma, V., & Sharma, S. S. (2018). Dye-sensitized solar cells: fundamentals and current status. *Nanoscale Research Letters*, *13*(1), 1-46.

Sheehan, S., Surolia, P. K., Byrne, O., Garner, S., Cimo, P., Li, X., Dowling, D. P., & Thampi, K. R. (2015). Flexible glass substrate based dye sensitized solar cells. *Solar Energy Materials and Solar Cells*, *132*, 237-244.

Shelke, R. S., Thombre, S. B., & Patrikar, S. R. (2013). Status and perspectives of dyes used in dye sensitized solar cells. *International Journal of Renewable Energy Resources*, *3*(2), 54-61.

Shntaif, A. H., & Rashid, Z. M. (2016). The synthesis of Schiff bases under microwave Irradiation: Review. *Journal of Chemical and Pharmaceutical Science*, *9*(3), 1066-1068.

Shubbak, M. H. (2019). Advances in solar photovoltaics: Technology review and patent trends. *Renewable and Sustainable Energy Reviews*, *115*, Article 109383.

Sinha, D., Tiwari, A. K., Singh, S., Shukla, G., Mishra, P., Chandra, H., & Mishra, A. K. (2008). Synthesis, characterization and biological activity of Schiff base analogues of indole-3-carboxaldehyde. *European Journal of Medicinal Chemistry*, *43*(1), 160-165.

Sinthuja, S. A., Shaji, Y. C., & Rose, G. L. (2018). Synthesis, characterization and evaluation of biological properties of transition metal chelates with schiff base ligands derived from glutaraldehyde with L-leucine. *International Journal of Scientific Research in Science and Technology*, *4*(2), 587-593.

Sofyan, N., Ridhova, A., Yuwono, A. H., & Udhiarto, A. (2018). Preparation of anatase TiO_2 nanoparticles using low hydrothermal temperature for dye-sensitized solar cell. In IOP Conference Series: *Materials Science and Engineering*, *316*(1), Article 012055

Su'ait, M. S., Rahman, M. Y. A., & Ahmad, A. (2015). Review on polymer electrolyte in dye-sensitized solar cells (DSSCs). *Solar Energy*, *115*, 452-470.

Suhaimi, S., Shahimin, M. M., Alahmed, Z. A., Chyský, J., & Reshak, A. H. (2015). Materials for enhanced dye-sensitized solar cell performance: Electrochemical application. *International Journal of Electrochemical Science*, *10*(4), 2859-2871.

Sun, D., & Yao, Y. (2011). Synthesis of three novel phosphorus-containing flame retardants and their application in epoxy resins. *Polymer Degradation and Stability*, *96*(10), 1720-1724.

Sun, J., Sun, J., Mi, W., Xue, P., Zhao, J., Zhai, L., & Lu, R. (2017). Self-assembling and piezofluorochromic properties of tert-butylcarbazole-based Schiff bases and the difluoroboron complex. *Dyes and Pigments*, *136*, 633-640.

Sönmez, M., Celebi, M., & Berber, I. (2010). Synthesis, spectroscopic and biological studies on the new symmetric Schiff base derived from 2, 6-diformyl-4-methylphenol with N-aminopyrimidine. *European Journal of Medicinal Chemistry*, *45*(5), 1935-1940.

Tai, C. K., Chen, Y. J., Chang, H. W., Yeh, P. L., & Wang, B. C. (2011). DFT and TD-DFT investigations of metal-free dye sensitizers for solar cells: Effects of electron donors and π-conjugated linker. *Computational and Theoretical Chemistry*, *971*(1-3), 42-50.

Tauer, E., Grellmann, K. H., Kaufmann, E., & Noltemeyer, M. (1986). The condensation product of 2-aminophenol and glyoxal. Structure and photochemistry. *Chemische Berichte*, *119*(11), 3316-3325.

Tay, M. G., Chia, Y. Y., Kuan, S. H. C., & Phan, T. P. (2019). The formation of dinuclear trichloro-bridged and mononuclear ruthenium complexes from the reactions of dichlorotris (p-tolylphosphine) ruthenium (II) with diazabutadiene ligands. *Transition Metal Chemistry*, *44*(3), 293-301.

Teo, K. Y., Tiong, M. H., Wee, H. Y., Jasin, N., Liu, Z. Q., Shiu, M. Y., Tang, J. Y., Tsai, J. K., Rahamathullah, R., Khairul. W. M., & Tay, M. G. (2017). The influence of the push-pull effect and a π-conjugated system in conversion efficiency of bis-chalcone compounds in a dye sensitized solar cell. *Journal of Molecular Structure*, *1143*, 42-48.

Tong, G. S. M., Chow, P. K., To, W. P., Kwok, W. M., & Che, C. M. (2014). A Theoretical Investigation into the Luminescent Properties of d8-Transition-Metal Complexes with Tetradentate Schiff Base Ligands. *Chemistry–A European Journal*, *20*(21), 6433-6443.

Tsaturyan, A., Machida, Y., Akitsu, T., Gozhikova, I., & Shcherbakov, I. (2018). Binaphthyl-containing Schiff base complexes with carboxyl groups for dye sensitized solar cell: An experimental and theoretical study. *Journal of Molecular Structure*, *1162*, 54-62.

Ugi, I., Dömling, A., & Hörl, W. (1994). Multicomponent reactions in organic chemistry. *Endeavour*, *18*(3), 115-122.

Ugi, I., Almstetter, M., Bock, H., Dömling, A., Ebert, B., Gruber, B., Hanusch-Kompa, C., Heck, S., Kehagia-Drikos, K., Lorenz, K., Papathoma, S., Raditschnig, R., Schmid, T., Werner, B., & von Zychlinski, A. (1998). MCR XVII. Three types of MCRs and the libraries–Their chemistry of natural events and preparative chemistry. *Croatica Chemica Acta*, *71*(3), 527-547.

Venkatesan, S., Lin, W. H., Teng, H., & Lee, Y. L. (2019). High-efficiency bifacial dye-sensitized solar cells for application under indoor light conditions. *ACS Applied Materials & Interfaces*, *11*(45), 42780-42789.

Vignati, S. (2012). *Solutions for indoor light energy harvesting*. *Master Thesis*. KTH Information and Communication Technology, Stockholm, Sweden.

Wang, M., Zhu, H., Jin, K., Dai, D., & Sun, L. (2003). Ethylene oligomerization by salen-type zirconium complexes to low-carbon linear α-olefins. *Journal of Catalysis*, *220*(2), 392-398.

Wang, H., Liu, Y., Huang, H., Zhong, M., Shen, H., Wang, Y., & Yang, H. (2009). Low resistance dye-sensitized solar cells based on all-titanium substrates using wires and sheets. *Applied Surface Science, 255*(22), 9020-9025.

Wang, H. J., Lu, J., & Zhang, Z. H. (2010). Highly efficient three-component, one-pot synthesis of dihydropyrano [3, 2-c] chromene derivatives. *Monatshefte für Chemie-Chemical Monthly, 141*(10), 1107-1112.

Wang, X., Fan, R., Dong, Y., Su, T., Huang, J., Du, X., Wang, P., & Yang, Y. (2017). Metal (II)-induced synthesis of asymmetric fluorescence benzimidazoles complexes and their dye-sensitized solar cell performance as cosensitizers. *Crystal Growth & Design*, *17*(10), 5406-5421.

Wesela-Bauman, G., Urban, M., Luliński, S., Serwatowski, J., & Woźniak, K. (2015). Tuning of the colour and chemical stability of model boranils: a strong effect of structural modifications. *Organic & Biomolecular Chemistry*, *13*(11), 3268-3279.

Wesley Jeevadason, A., Kalidasa Murugavel, K., & Neelakantan, M. A. (2014). Review on Schiff bases and their metal complexes as organic photovoltaic materials. *Renewable and Sustainable Energy Reviews, 36,* 220–227.

Xavier, A., & Srividhya, N. (2014). Synthesis and study of Schiff base ligands. *IOSR Journal of Applied Chemistry*, *7*(11), 06-15.

Xing, J., & Jia, J. (2021). Reversible mechanofluorochromic properties of phenothiazine-based DAD′ aza-N, O-chelated boron difluoride complexes. *Tetrahedron Letters, 78,* Article 153275.

Xu, S. C., Zhu, S. J., Wang, J., Bi, L. W., Chen, Y. X., Lu, Y. J., Gu, Y., & Zhao, Z. D. (2017). Design, synthesis and evaluation of novel cis-p-menthane type Schiff base compounds as effective herbicides. *Chinese Chemical Letters*, *28*(7), 1509-1513.

Yahya, M., Bouziani, A., Ocak, C., Seferoğlu, Z., & Sillanpää, M. (2021). Organic/metal-organic photosensitizers for dye-sensitized solar cells (DSSC): Recent developments, new trends, and future perceptions. *Dyes and Pigments*, *192*, Article 109227.

Yang, L., Guo, L., Chen, Q., Sun, H., Yan, H., Zeng, Q., Zhang, X., Pan, X., & Dai, S. (2012). Substituent effects on zinc phthalocyanine derivatives: A theoretical calculation and screening of sensitizer candidates for dye-sensitized solar cells. *Journal of Molecular Graphics and Modelling*, *38*, 82-89.

Ye, M., Wen, X., Wang, M., Iocozzia, J., Zhang, N., Lin, C., & Lin, Z. (2014). Recent advances in dye-sensitized solar cells: from photoanodes, sensitizers and electrolytes to counter electrodes. *Materials Today*, *18*(3), 155-162.

Ye, Z., Xie, S., Cao, Z., Wang, L., Xu, D., Zhang, H., Matz, J., Dong, P., Fang, H., Shen, J., & Ye, M. (2021). High-rate aqueous zinc-organic battery achieved by lowering HOMO/LUMO of organic cathode. *Energy Storage Materials*, *37*, 378-386.

Yoo, B., Kim, K., Lee, D. K., Ko, M. J., Lee, H., Kim, Y. H., Kim, W. M., & Park, N. G. (2010). Enhanced charge collection efficiency by thin-TiO_2-film deposition on FTO-coated ITO conductive oxide in dye-sensitized solar cells. *Journal of Materials Chemistry*, *20*(21), 4392-4398.

Yu, Z., Gorlov, M., Nissfolk, J., Boschloo, G., & Kloo, L. (2010). Investigation of iodine concentration effects in electrolytes for dye-sensitized solar cells. *The Journal of Physical Chemistry C*, *114*(23), 10612-10620.

Yu, Z. Y., Zhou, J., Fang, Q. S., Chen, L., & Song, Z. B. (2016). Chemoselective synthesis of 1, 2-disubstituted benzimidazoles in lactic acid without additive. *Chemical Papers*, *70*(9), 1293-1298.

Zhang, L., & Cole, J. M. (2015). Anchoring groups for dye-sensitized solar cells. *ACS Applied Materials & Interfaces*, *7*(6), 3427-3455.

Zhang, X., Liao, C., Cao, J., Yang, L., & Li, Q. (2015). Synthesis and characterization of schiff base-substituted zinc porphyrin dye for sensitized solar cells. *Journal of Computational and Theoretical Nanoscience*, *12*(9), 2745-2750.

Zhang, J., Xu, L., & Wong, W. Y. (2018). Energy materials based on metal Schiff base complexes. *Coordination Chemistry Reviews*, *355*, 180-198.

Zhao, J., Peng, J., Chen, P., Wang, H., Xue, P., & Lu, R. (2018). Mechanofluorochromism of difluoroboron β-ketoiminate boron complexes functionalized with benzoxazole and benzothiazole. *Dyes and Pigments*, *149*, 276-283.

Zhao, N., Ma, C., Yang, W., Yin, W., Wei, J., & Li, N. (2019). Facile construction of boranil complexes with aggregation-induced emission characteristics and their specific lipid droplet imaging applications. *Chemical Communications*, *55*(58), 8494-8497.

Zhu, X., Wang, C., Dang, Y., Zhou, H., Wu, Z., Liu, Z., Ye, D., & Zhou, Q. (2000). The Schiff base N-salicylidene-O, S-dimethylthiophosphorylimine and its metal complexes: synthesis, characterization and insecticidal activity studies. *Synthesis and Reactivity in Inorganic and Metal-Organic Chemistry*, *30*(4), 625-636.

Zulkifli, Z. (2021), 'Malaysia Country Report', in Han, P. and S. Kimura (eds.), *Energy Outlook and Energy Saving Potential in East Asia 2020*, Jakarta: ERIA, 170-190.

APPENDICES

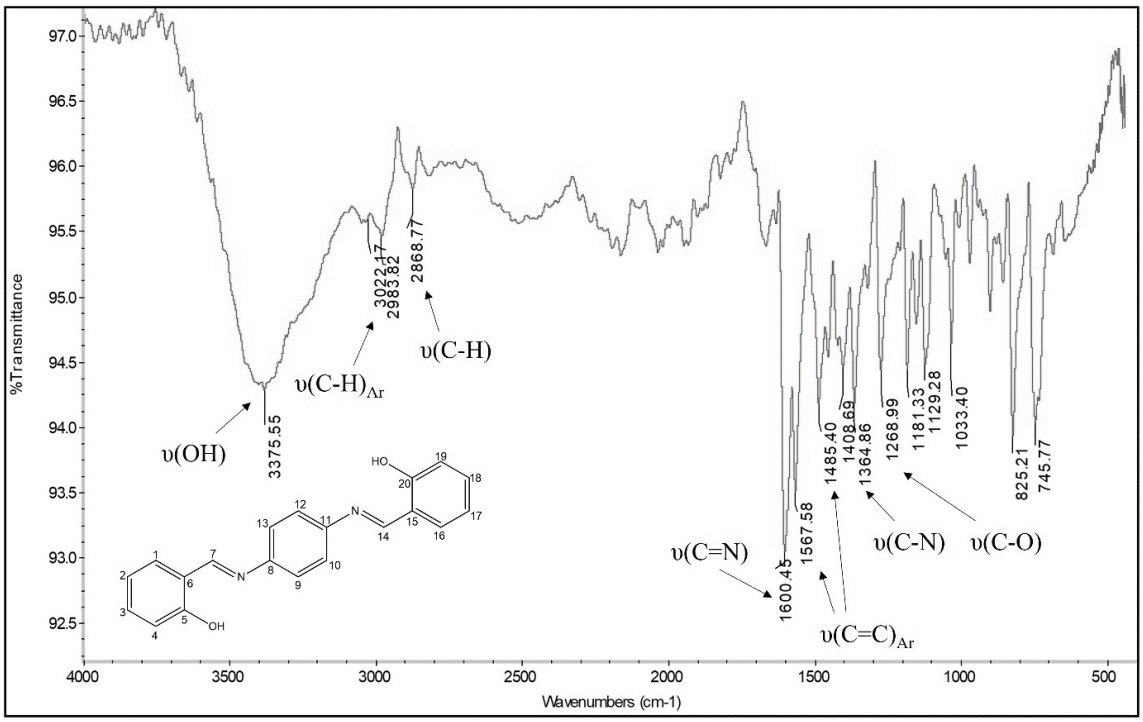

Appendix 1: IR spectrum of **1b**

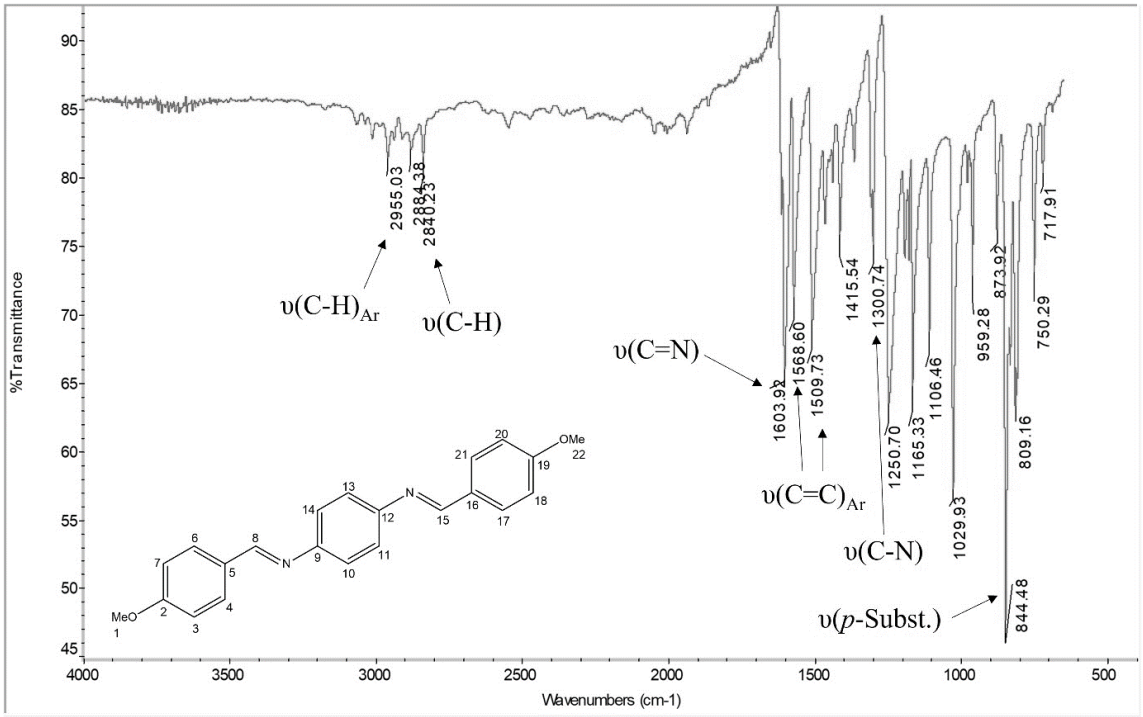

Appendix 2: IR spectrum of **1c**

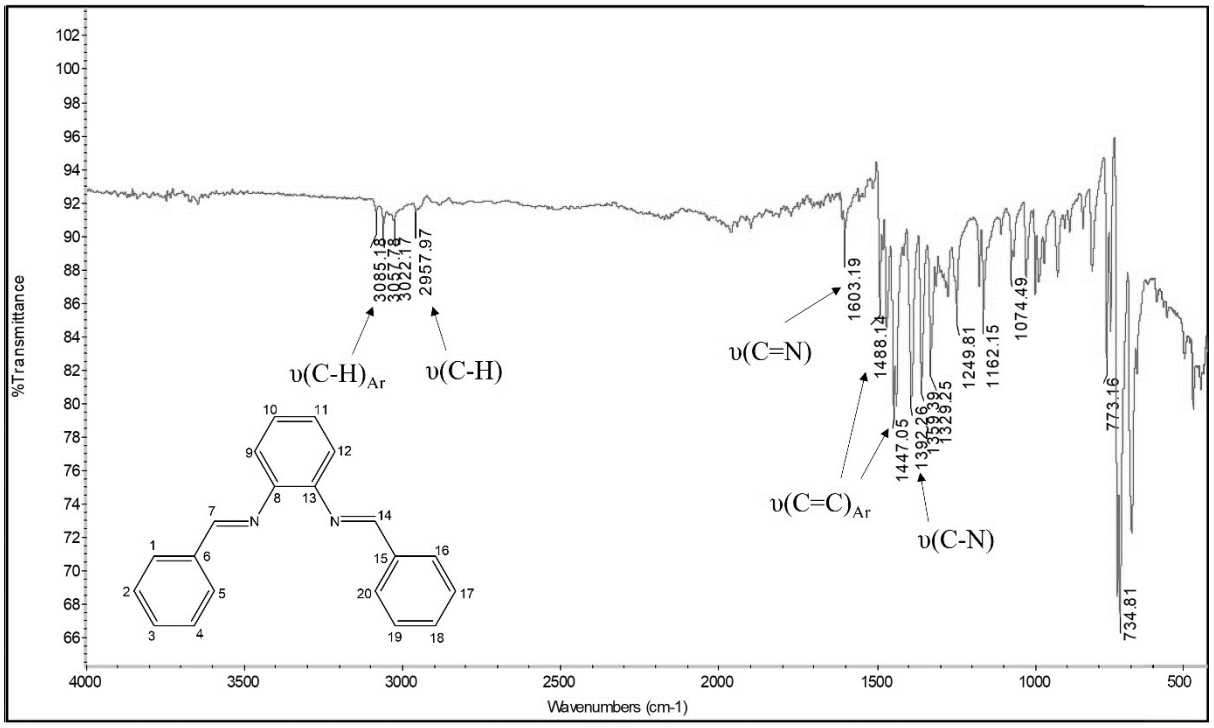

Appendix 3: IR spectrum of **2a**

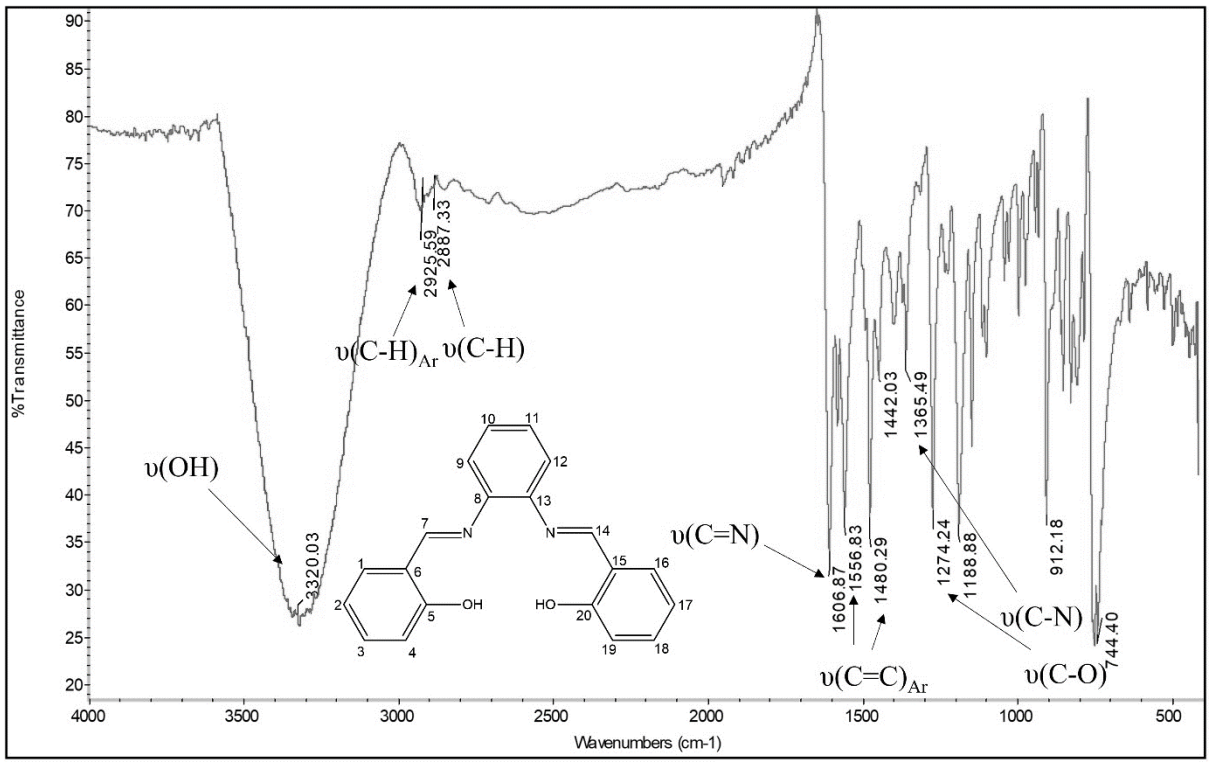

Appendix 4: IR spectrum of **2b**

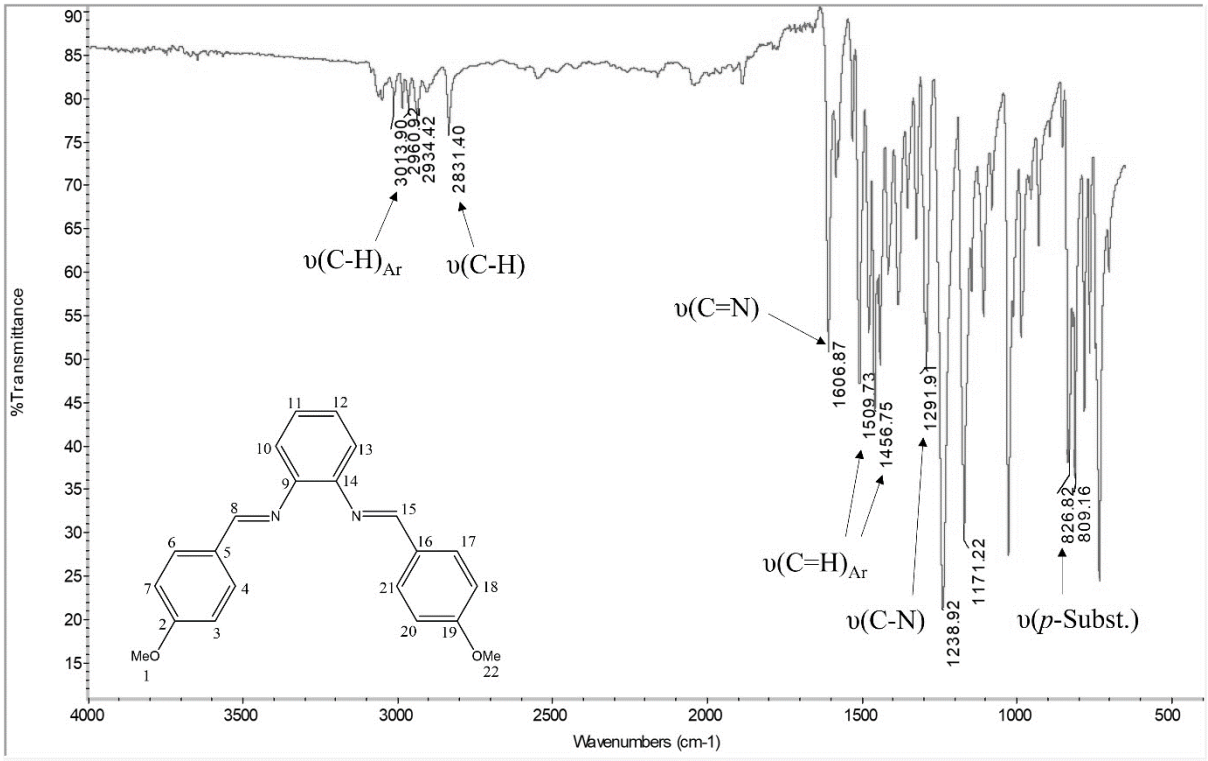

Appendix 5: IR spectrum of **2c**

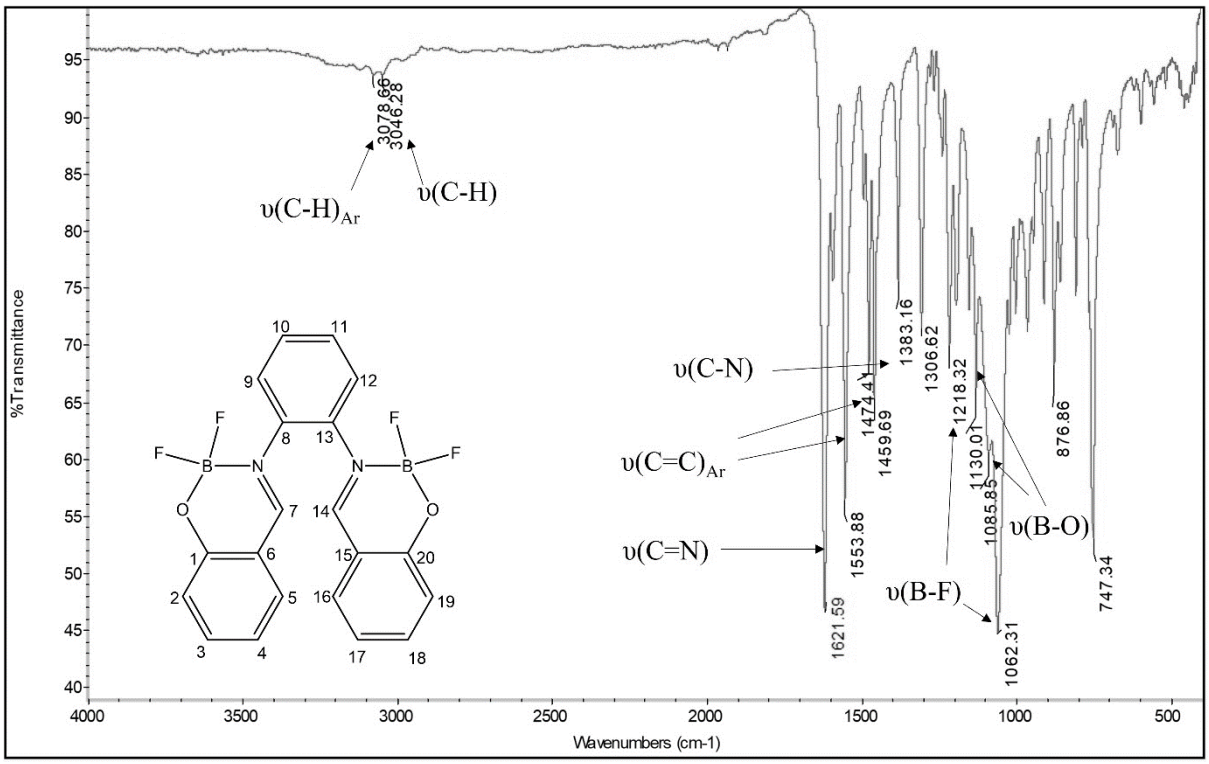

Appendix 6: IR spectrum of **2d**

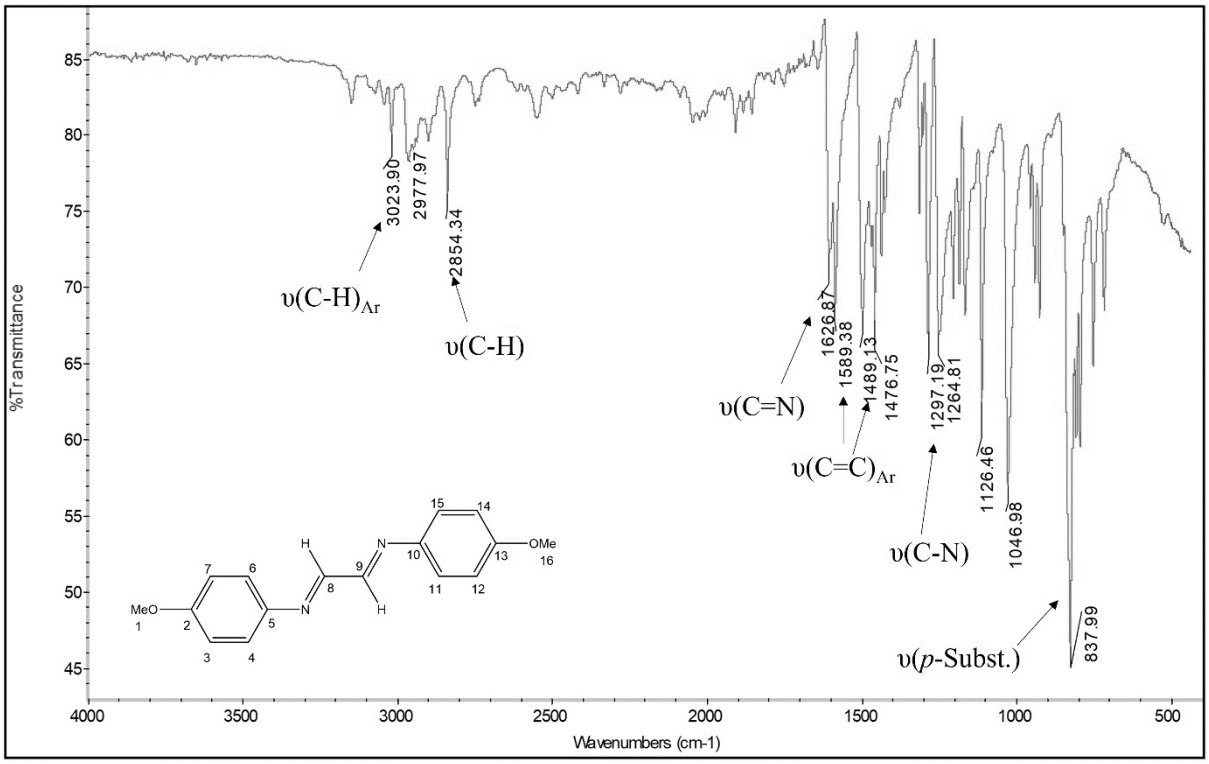

Appendix 7: IR spectrum of **3c**

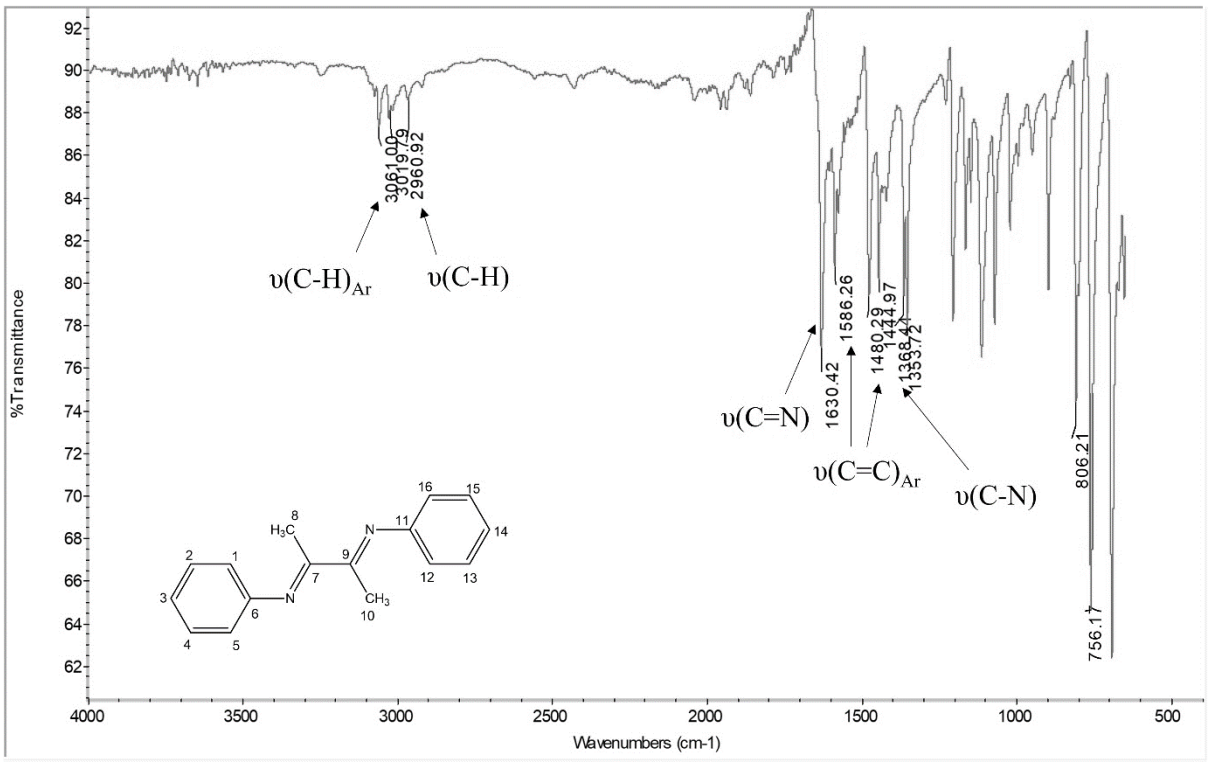

Appendix 8: IR spectrum of **4a**

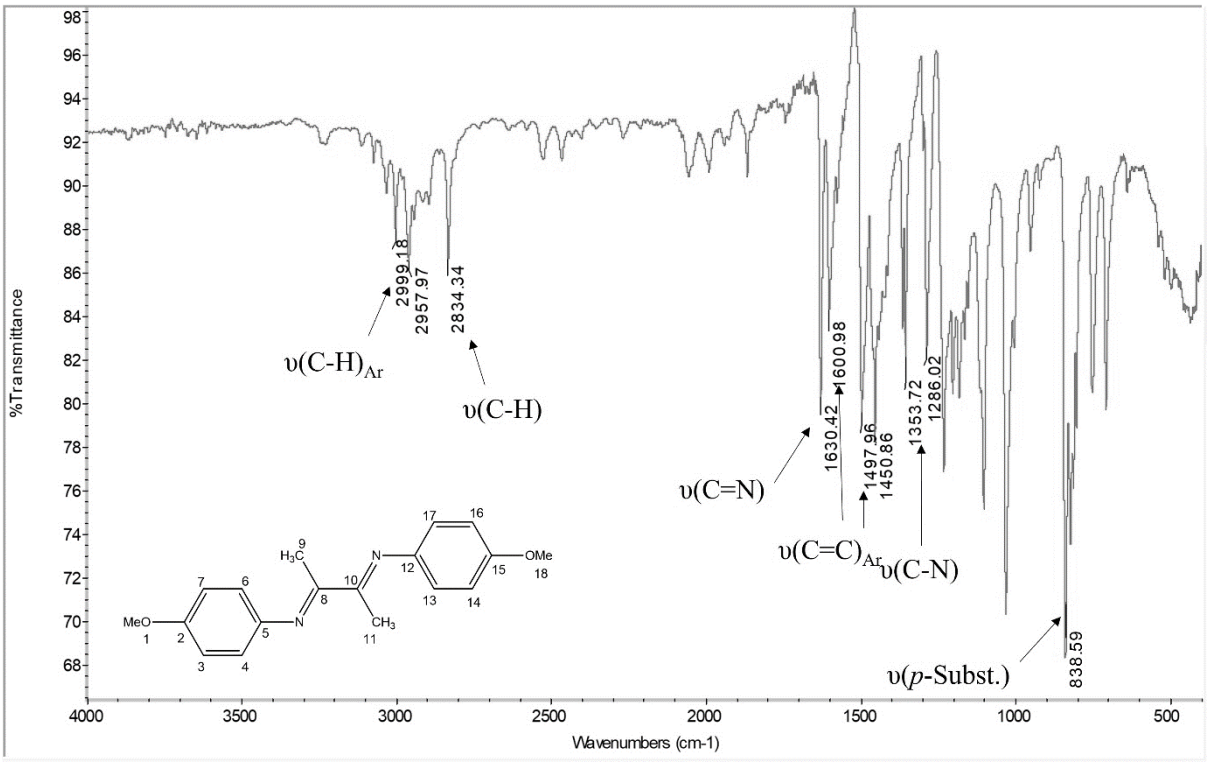

Appendix 9: IR spectrum of **4c**

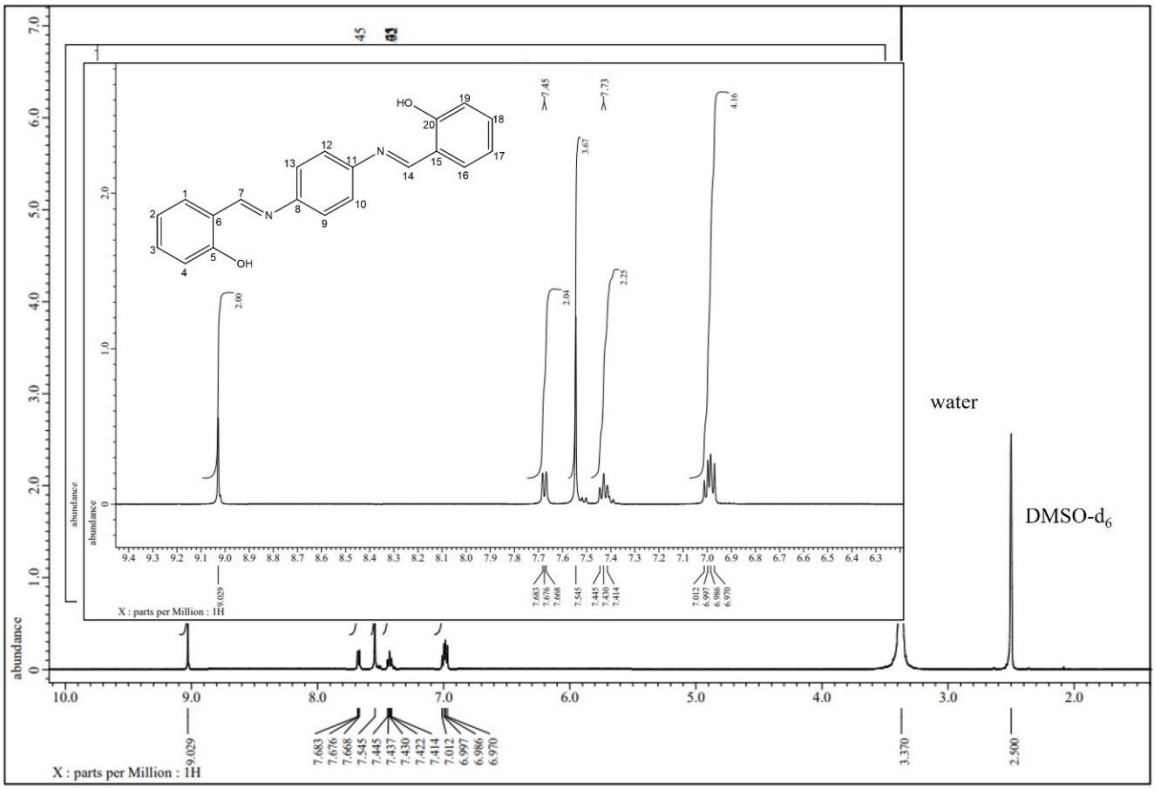

Appendix 10: ^{1}H NMR spectrum of **1b**

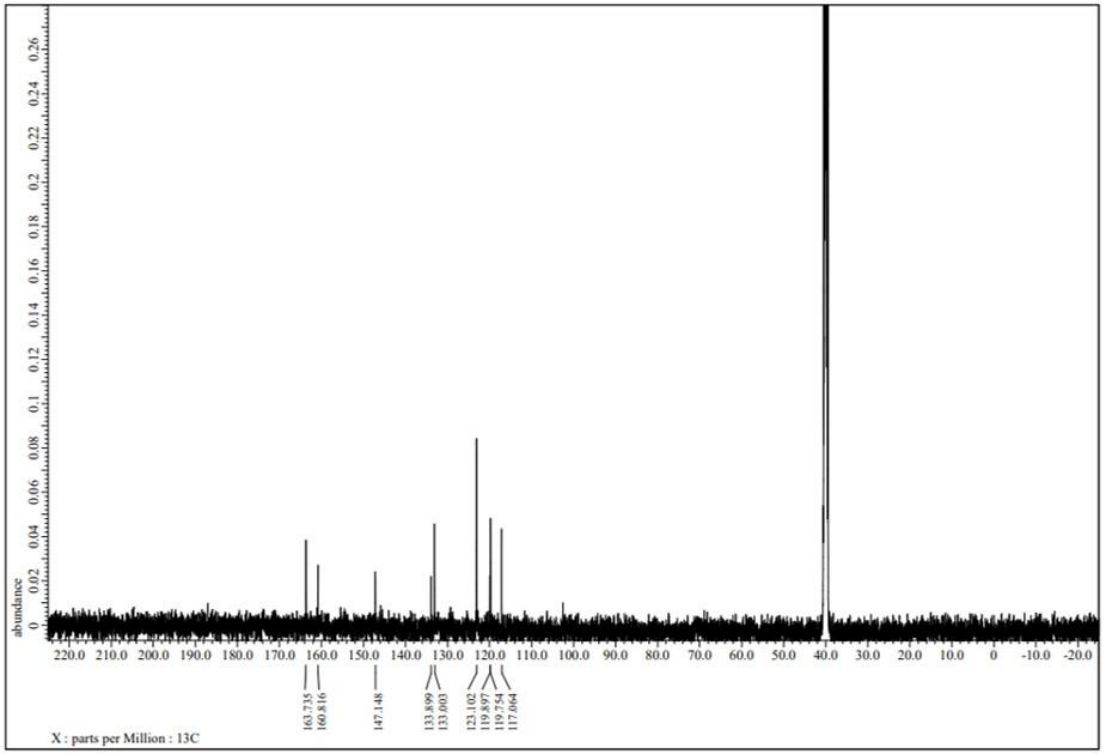

Appendix 11: ^{13}C NMR spectrum of **1b**

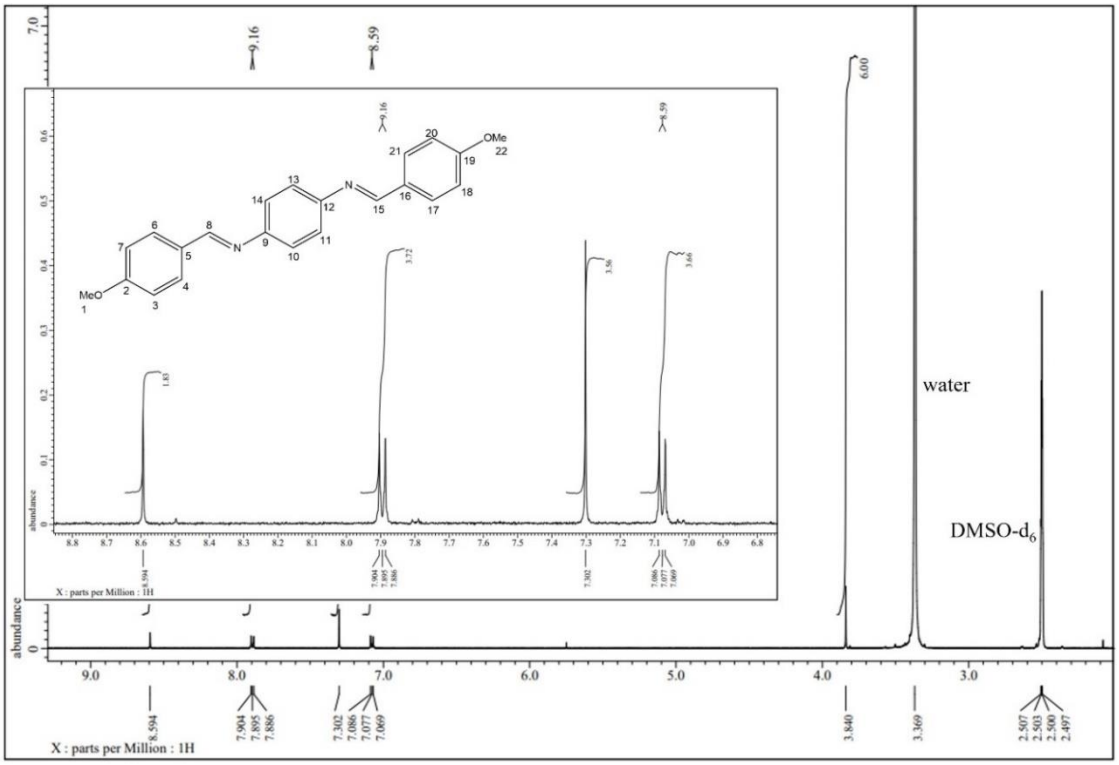

Appendix 12: ^{1}H NMR spectrum of **1c**

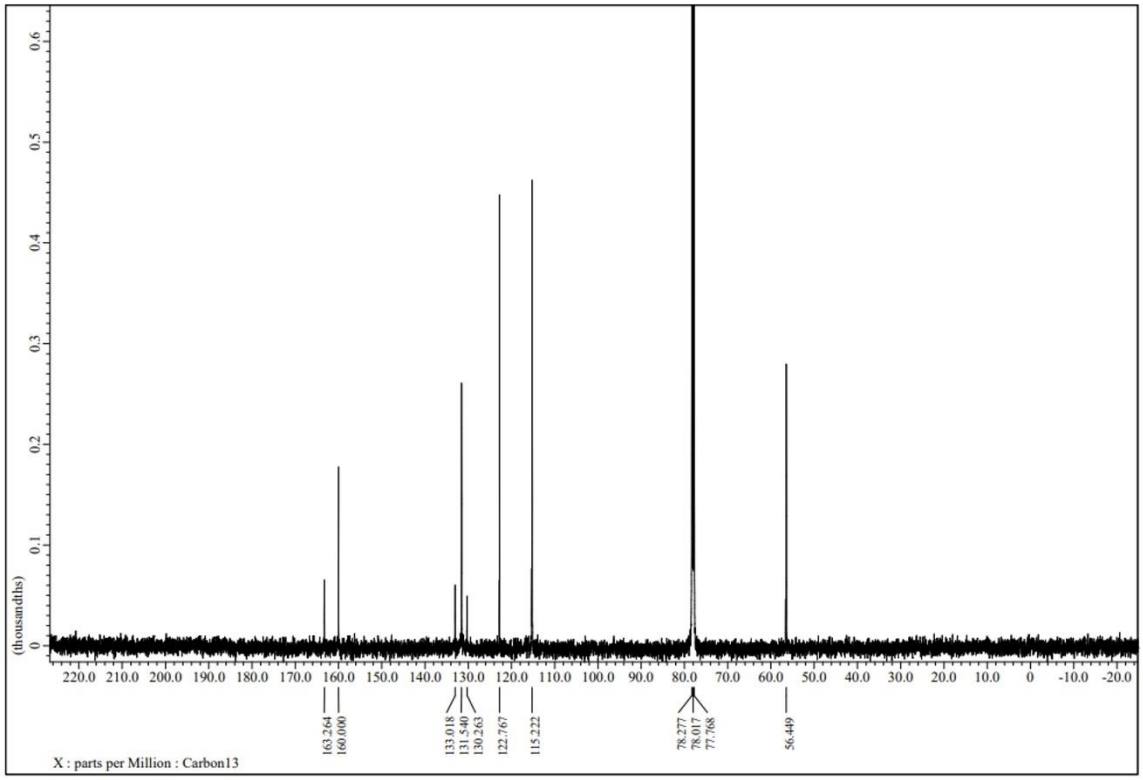

Appendix 13: ^{13}C NMR spectrum of **1c**

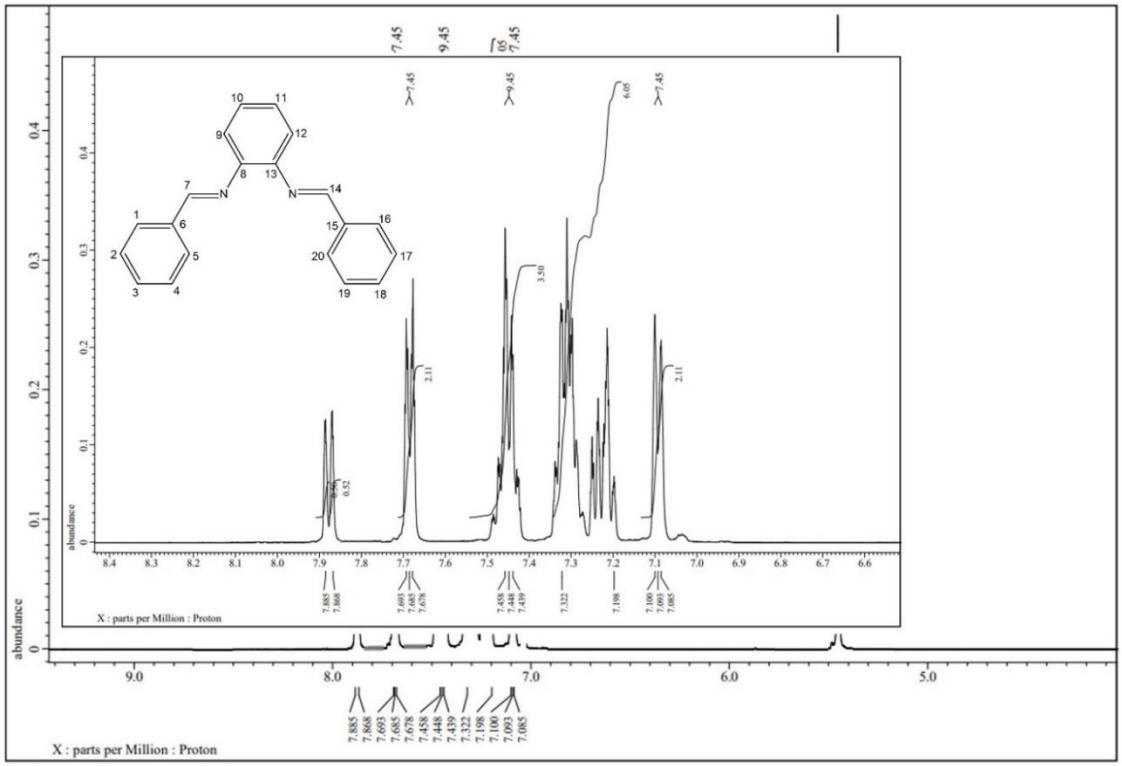

Appendix 14: ^{1}H NMR spectrum of **2a**

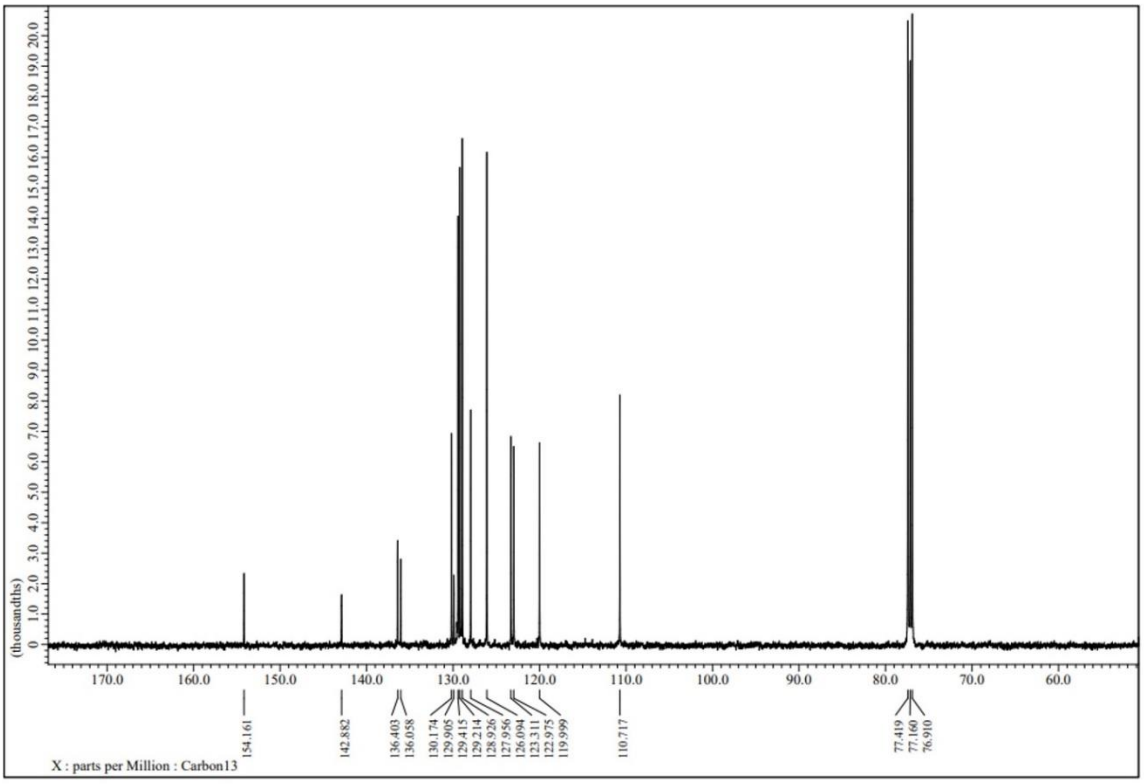

Appendix 15: ^{13}C NMR spectrum of **2a**

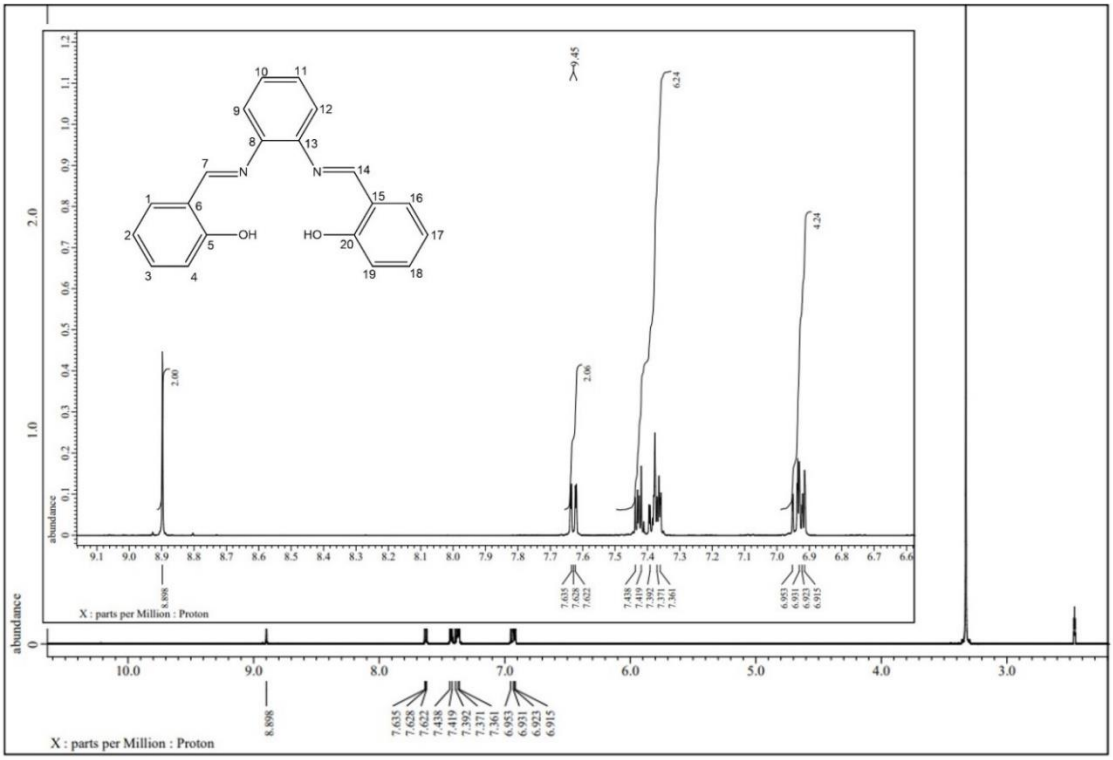

Appendix 16: ^{1}H NMR spectrum of **2b**

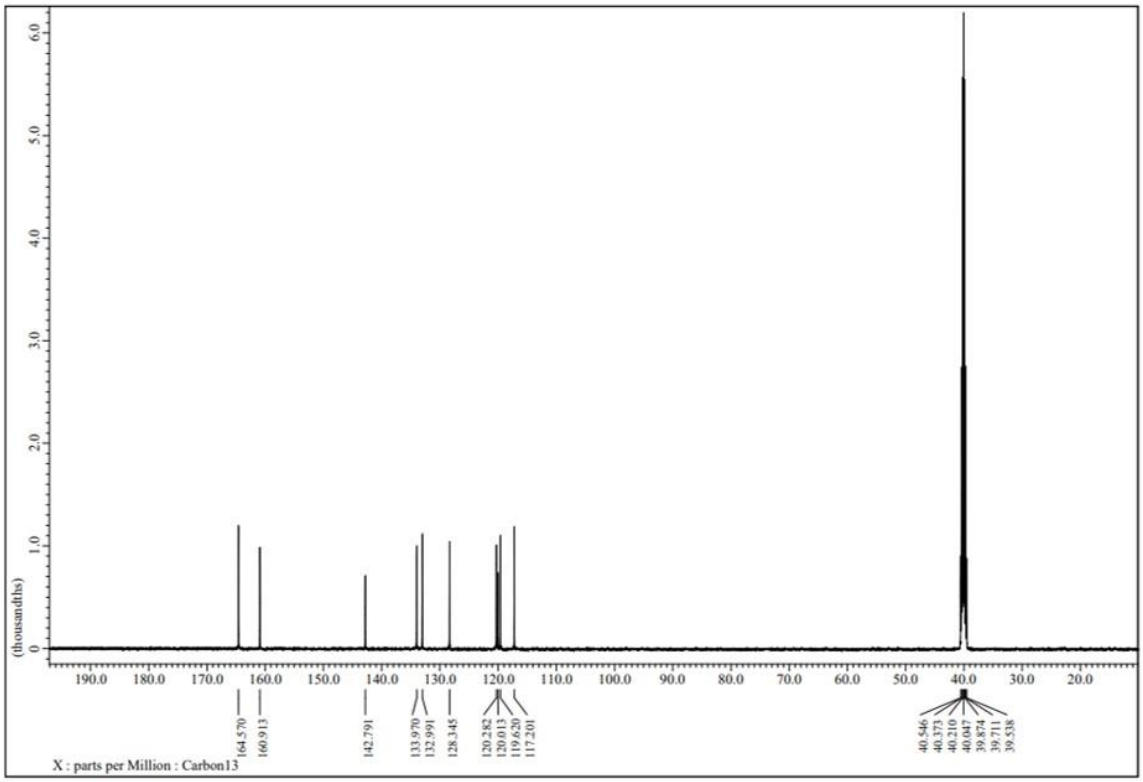

Appendix 17: ^{13}C NMR spectrum of **2b**

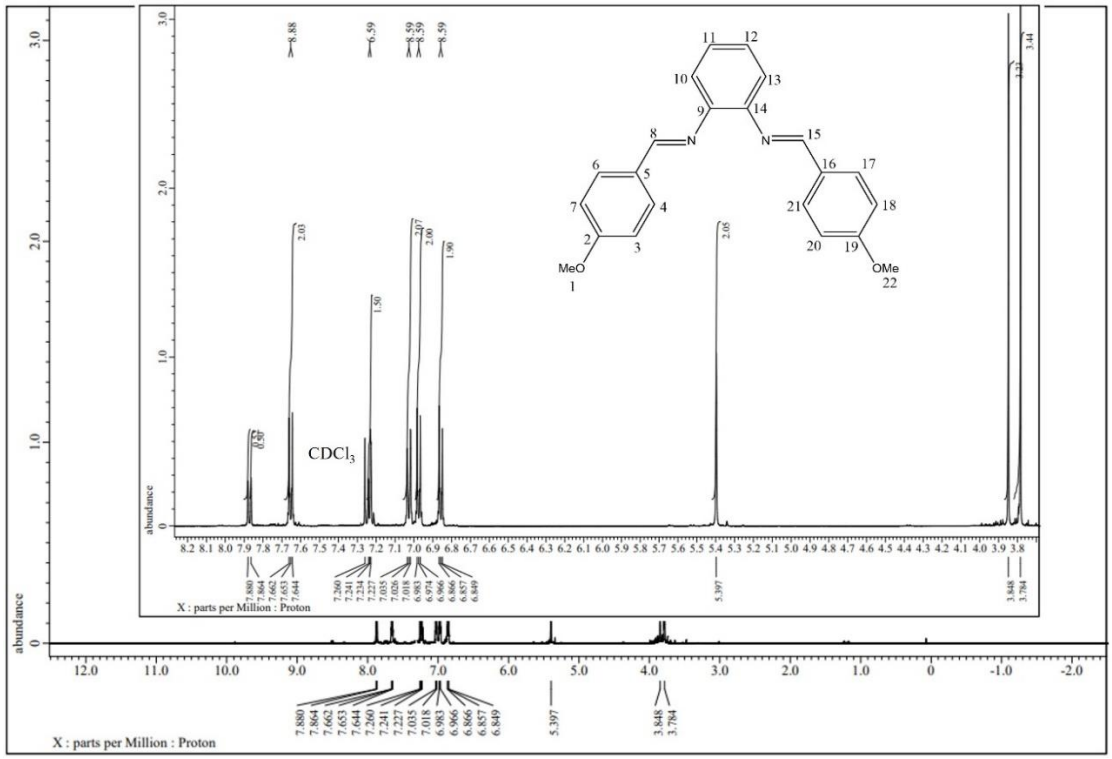

Appendix 18: ^{1}H NMR spectrum of **2c**

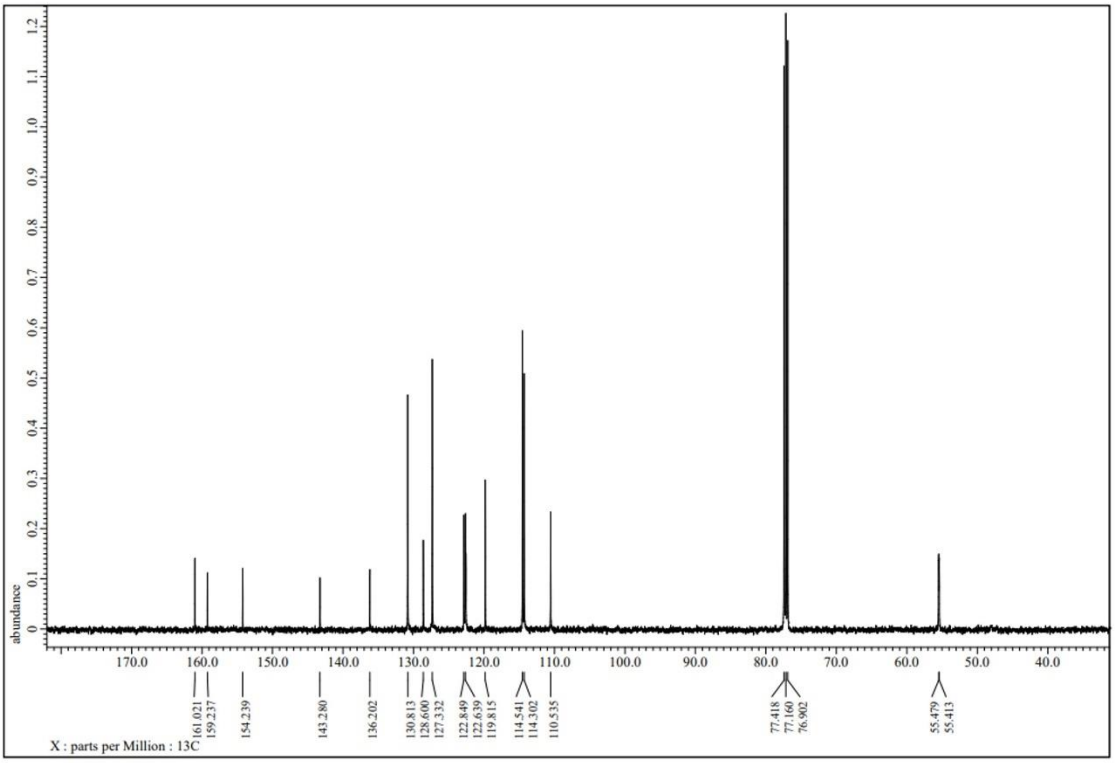

Appendix 19: ^{13}C NMR spectrum of **2c**

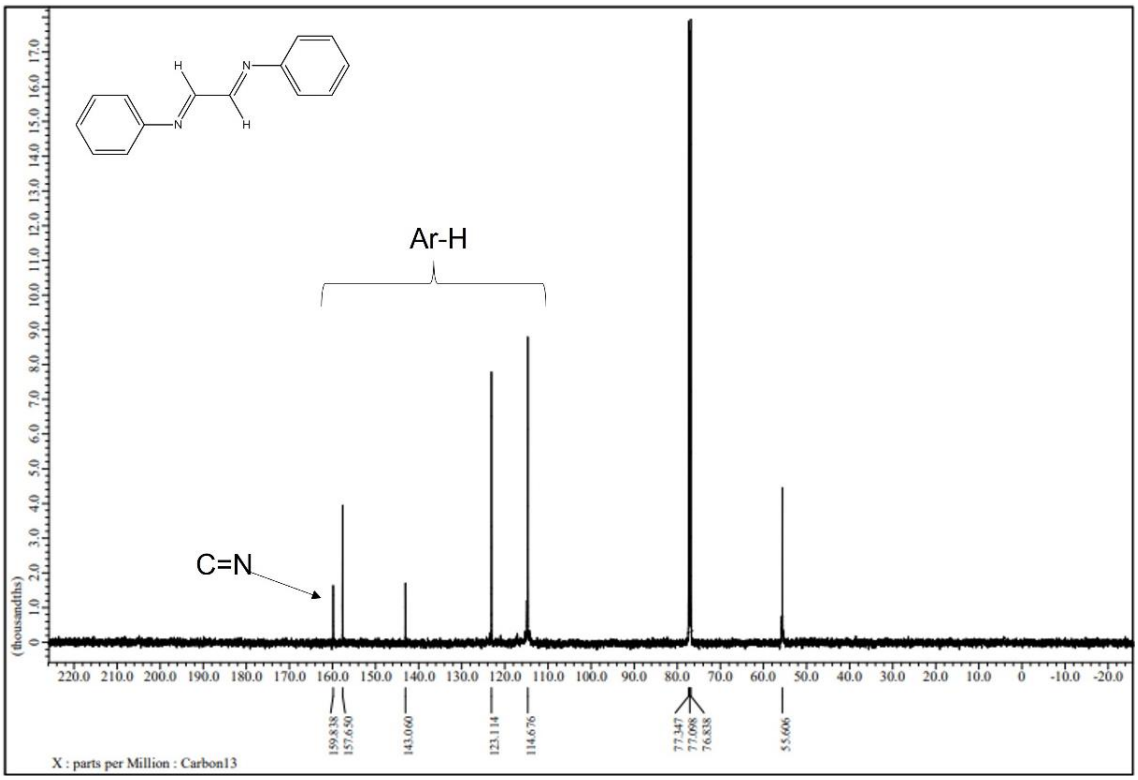

Appendix 20: ^{13}C NMR spectrum of **3a**

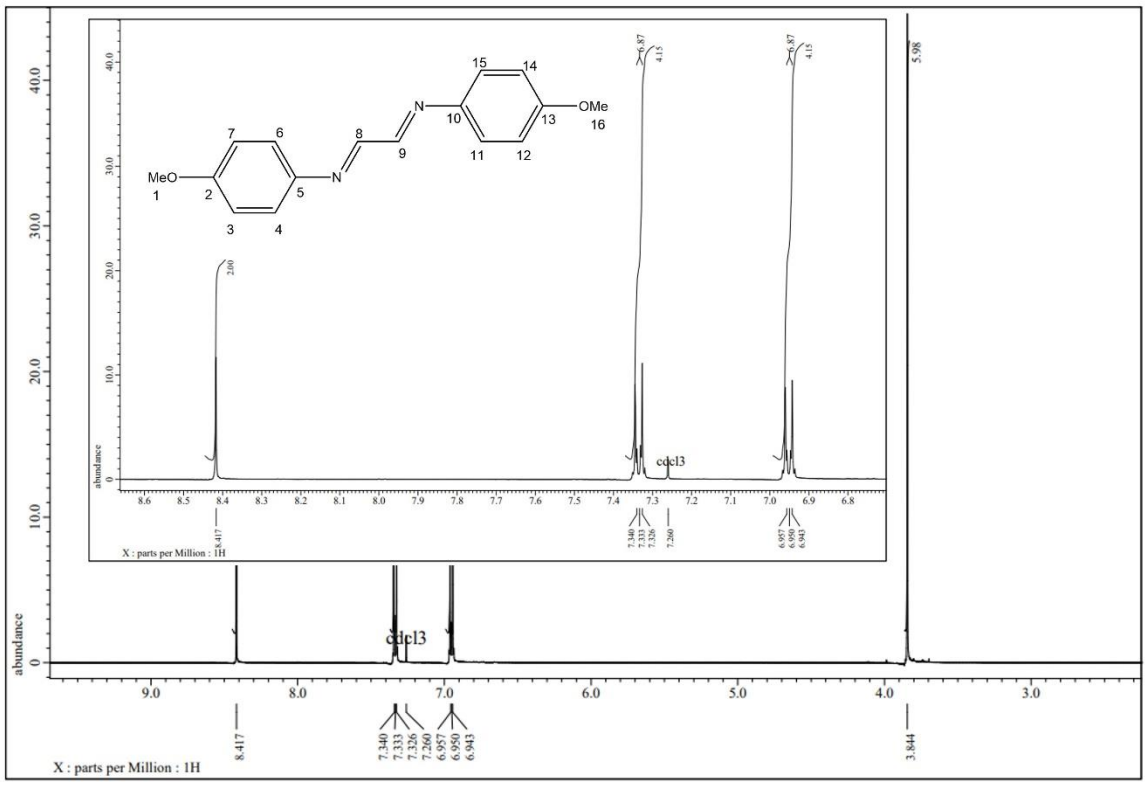

Appendix 21: ^{1}H NMR spectrum of **3c**

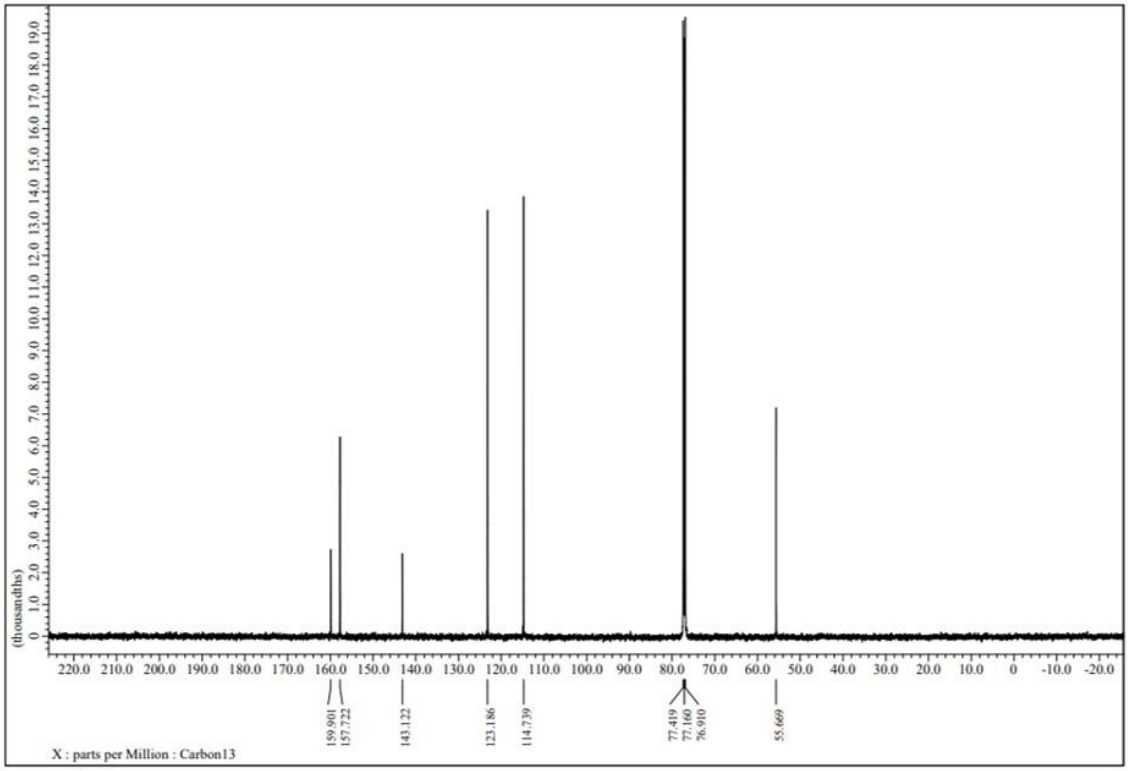

Appendix 22: ^{13}C NMR spectrum of **3c**

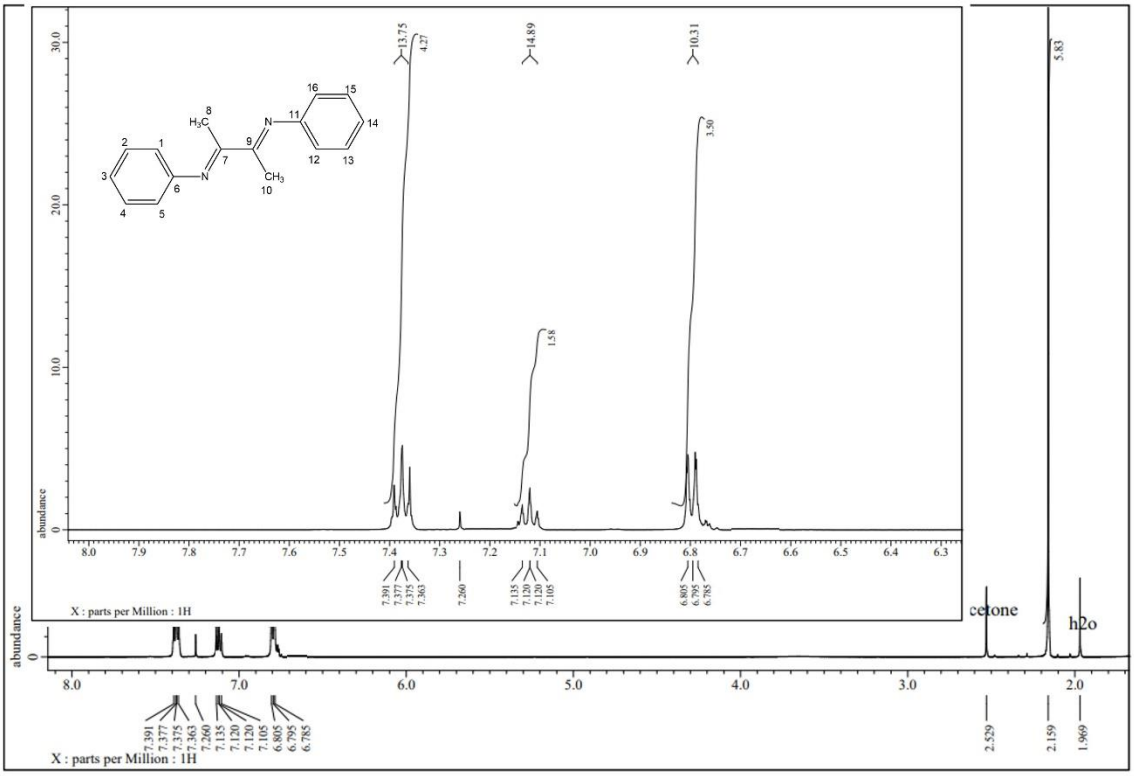

Appendix 23: ^{1}H NMR spectrum of **4a**

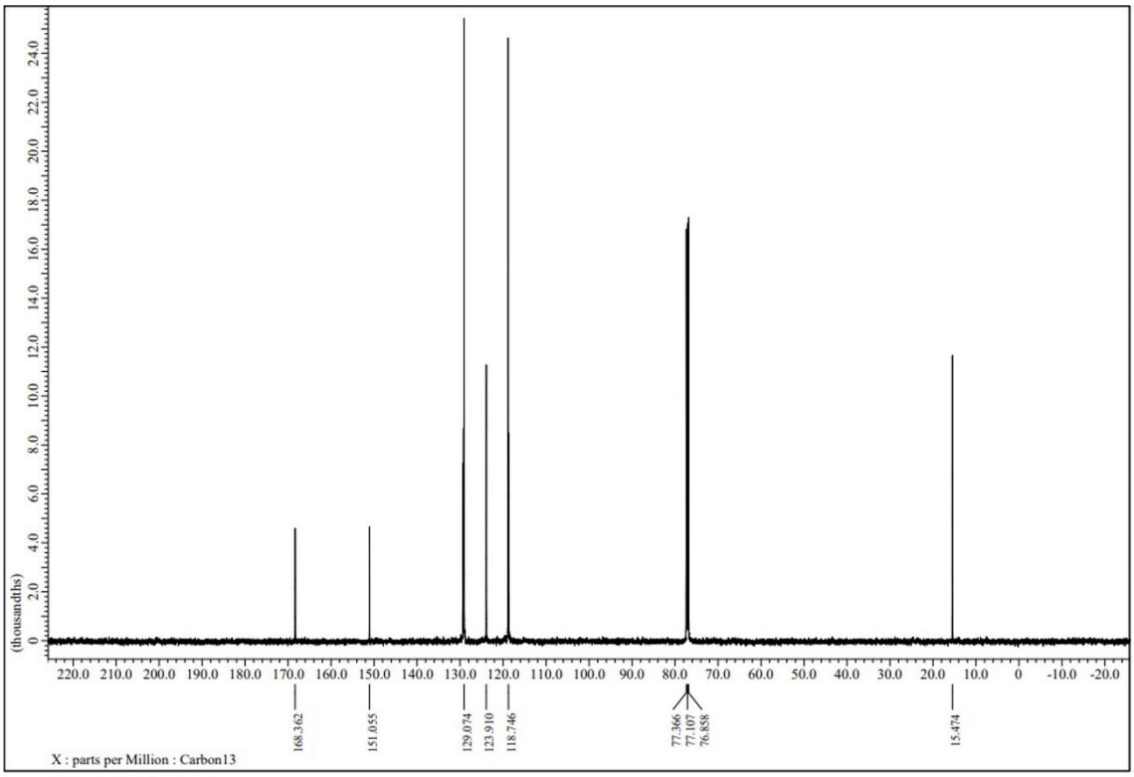

Appendix 24: ^{13}C NMR spectrum of **4a**

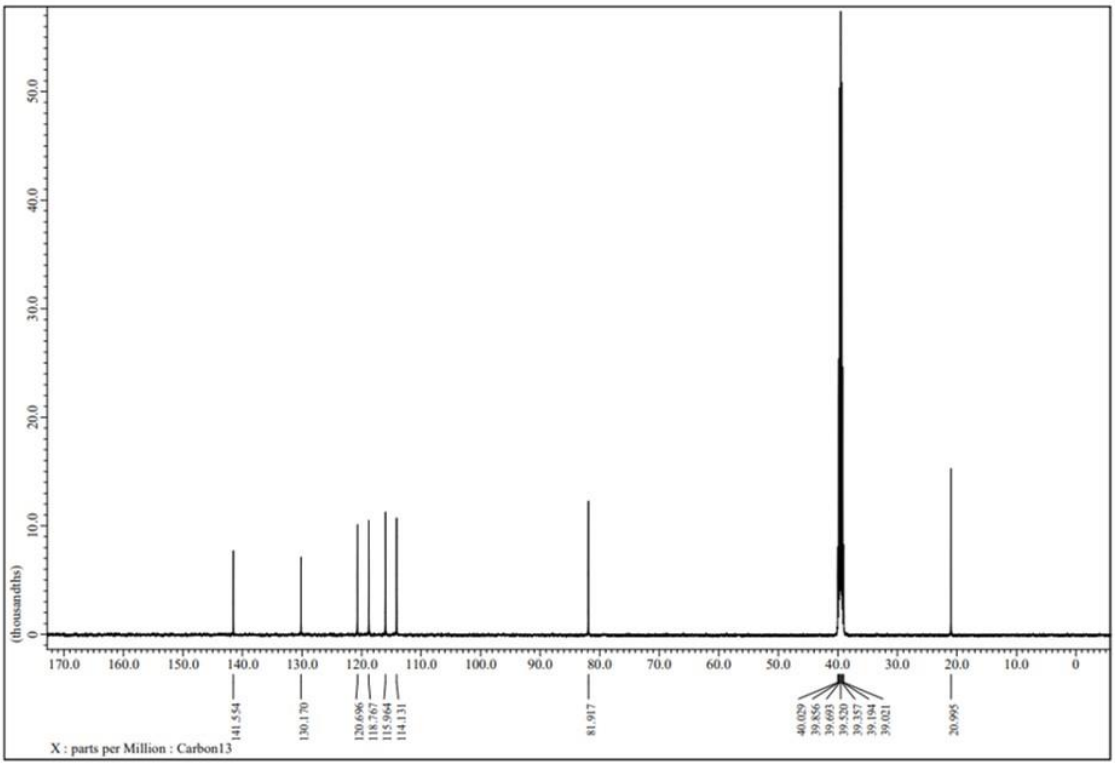

Appendix 25: ^{13}C NMR spectrum of **4b**

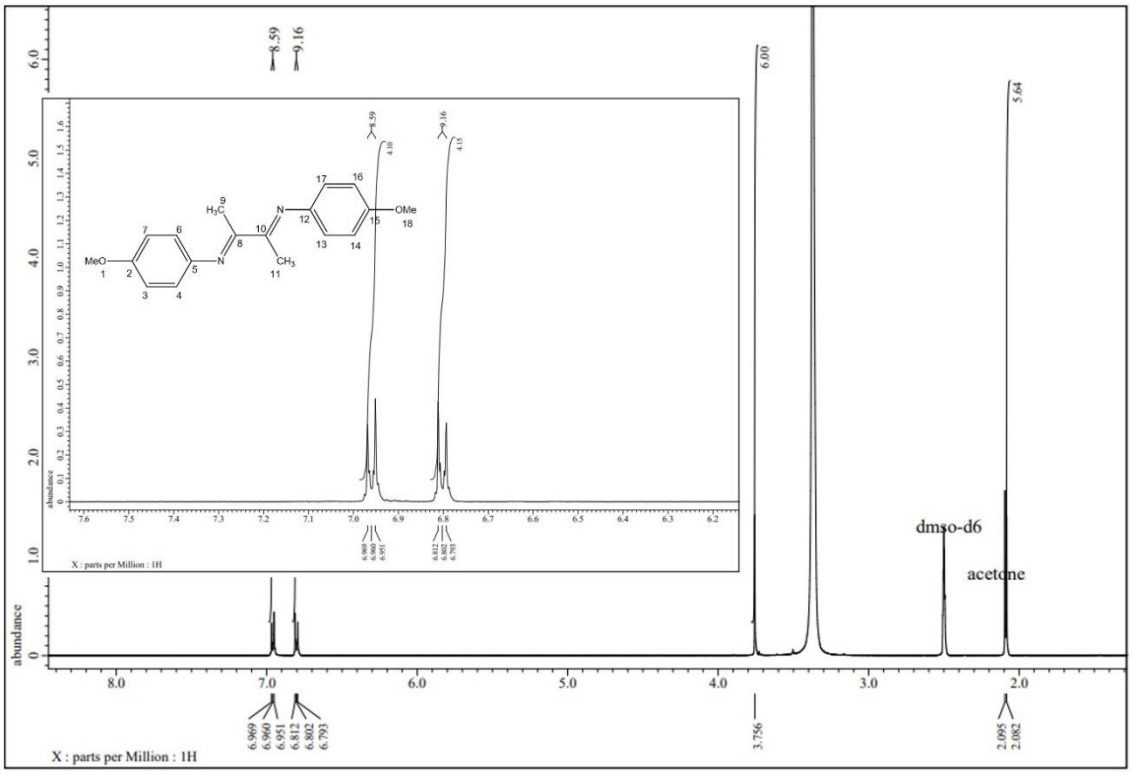

Appendix 26: ^{1}H NMR spectrum of **4c**

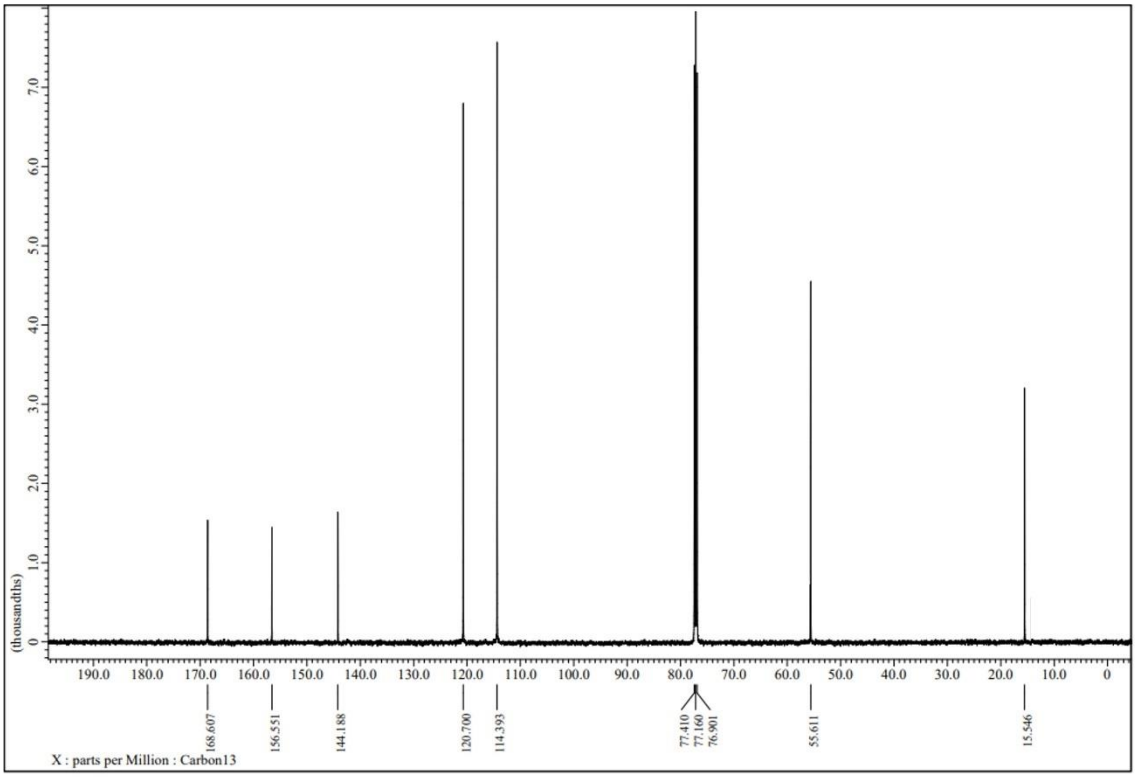

Appendix 27: ^{13}C NMR spectrum of **4c**

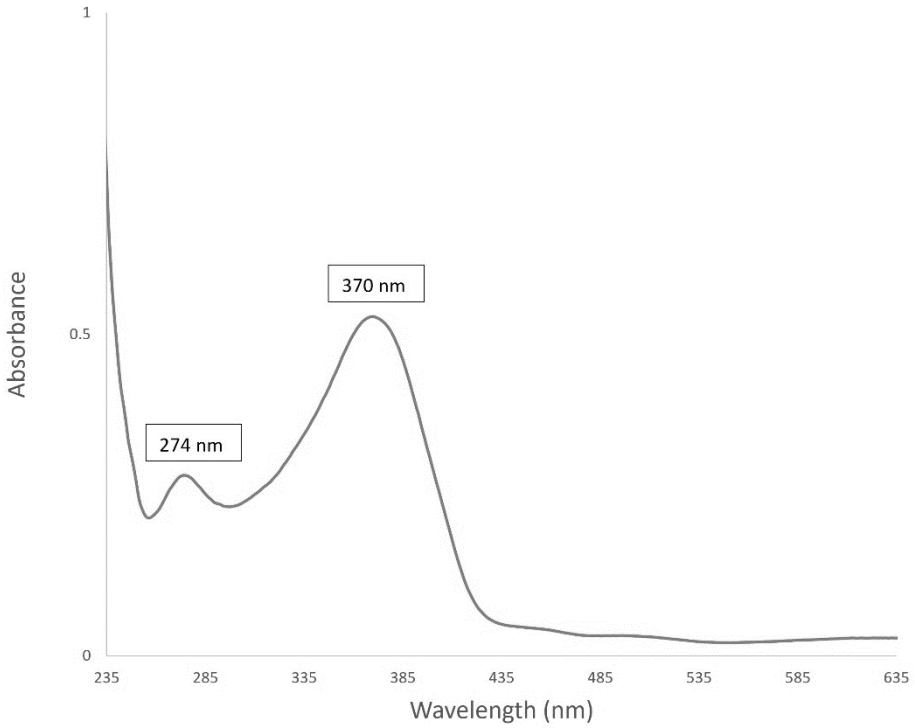

Appendix 28: UV-visible spectrum of **1b**

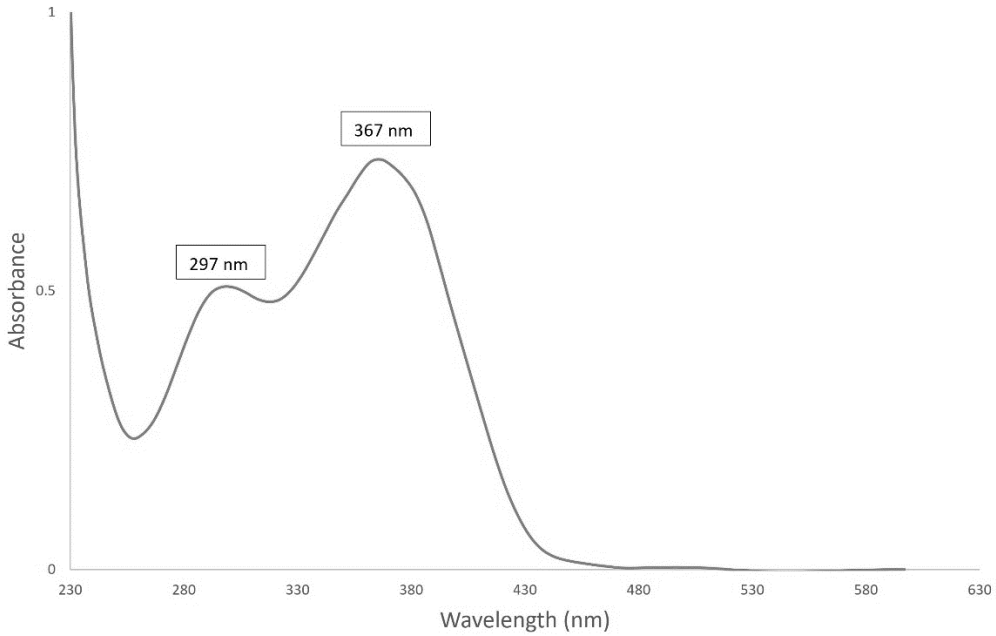

Appendix 29: UV-visible spectrum of **1c**

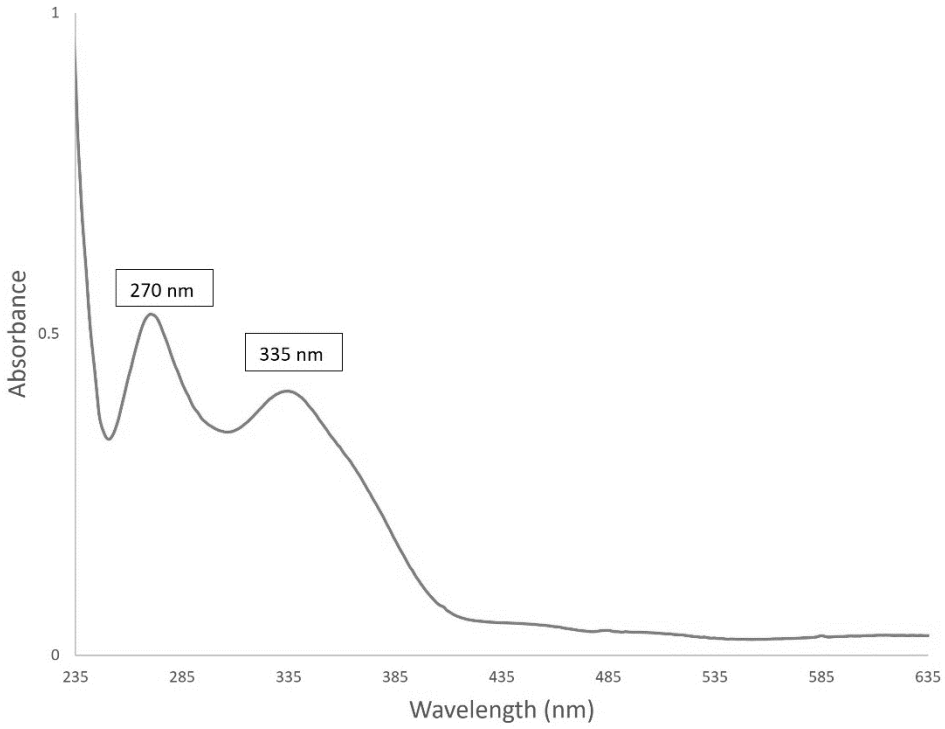

Appendix 30: UV-visible spectrum of **2a**

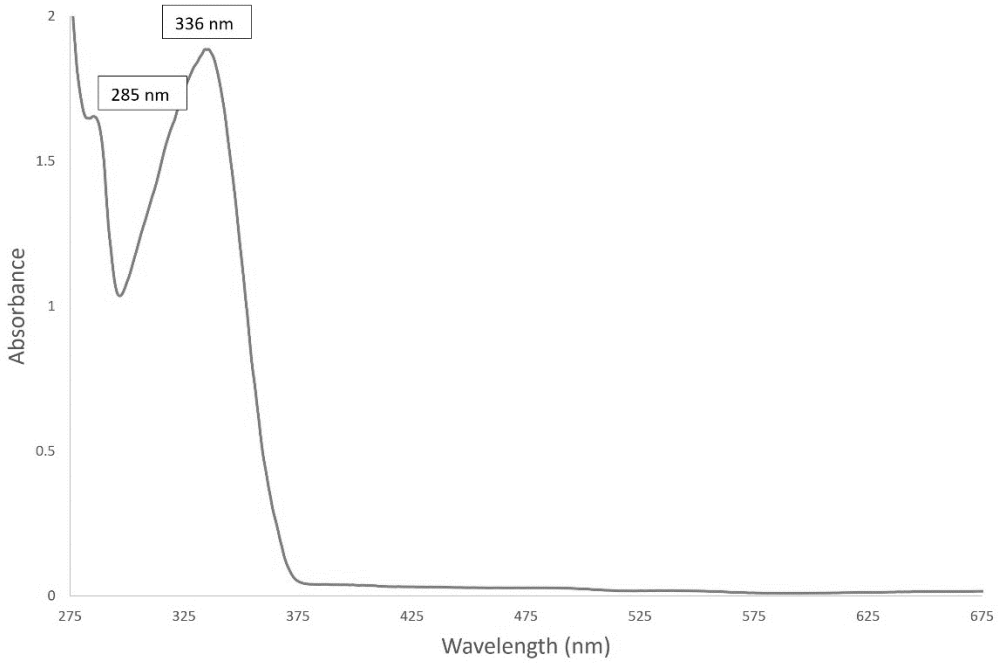

Appendix 31: UV-visible spectrum of **2b**

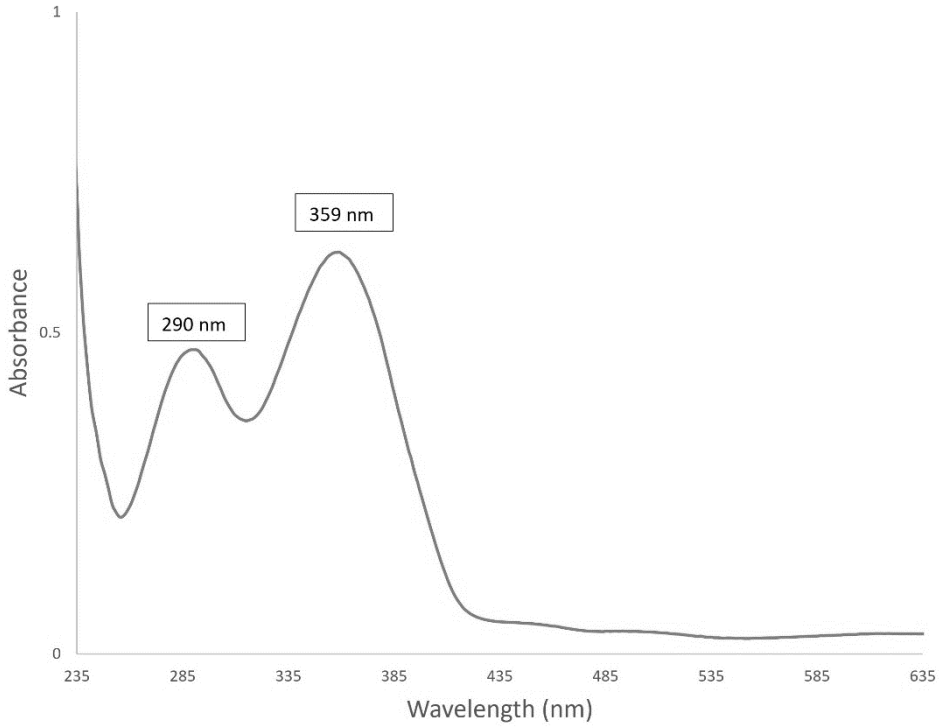

Appendix 32: UV-visible spectrum of **2c**

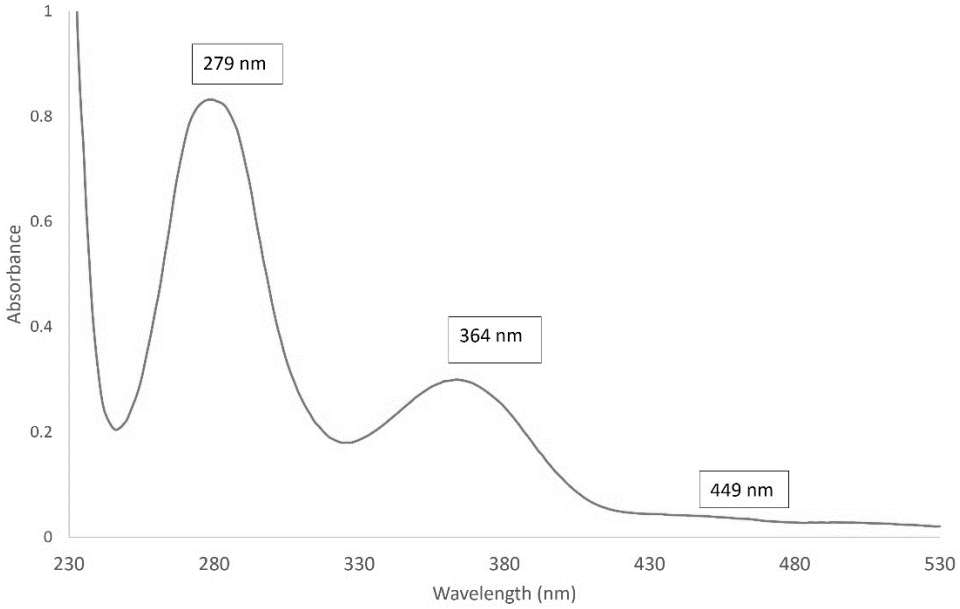

Appendix 33: UV-visible spectrum of **2d**

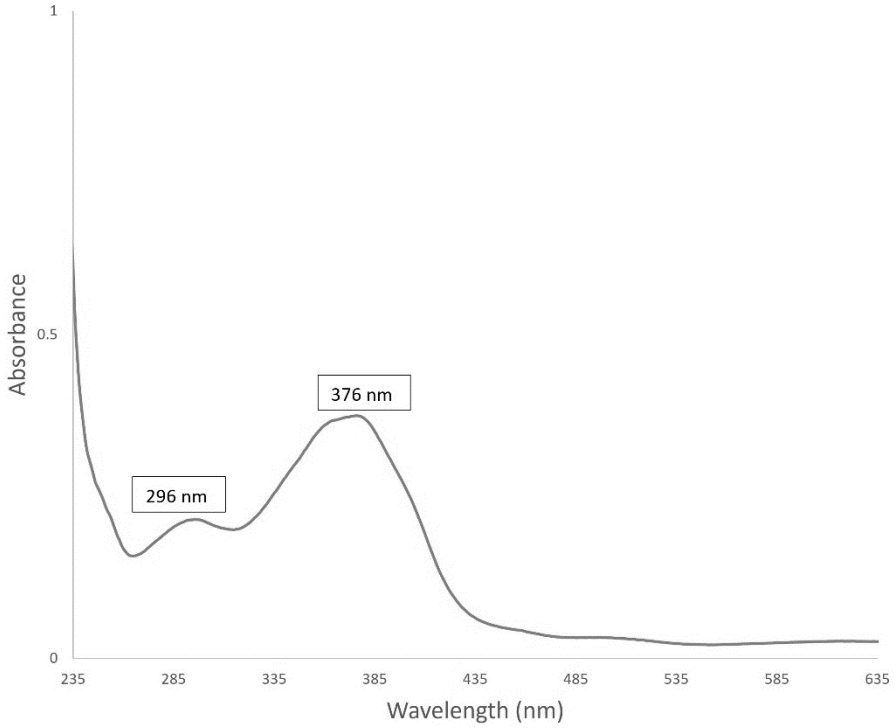

Appendix 34: UV-visible spectrum of **3c**

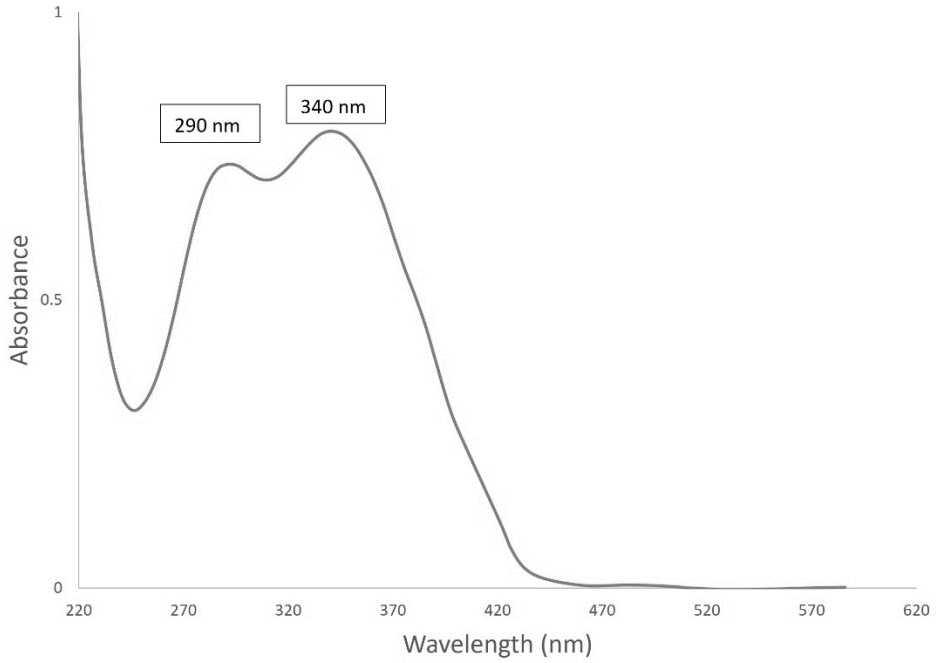

Appendix 35: UV-visible spectrum of **4a**

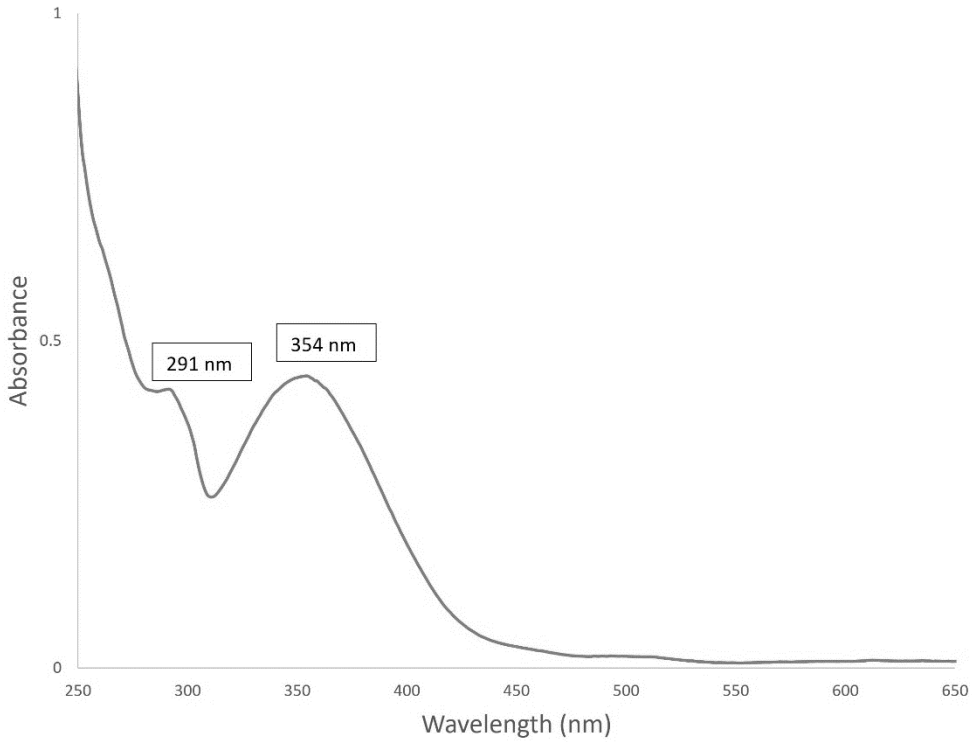

Appendix 36: UV-visible spectrum of **4c**

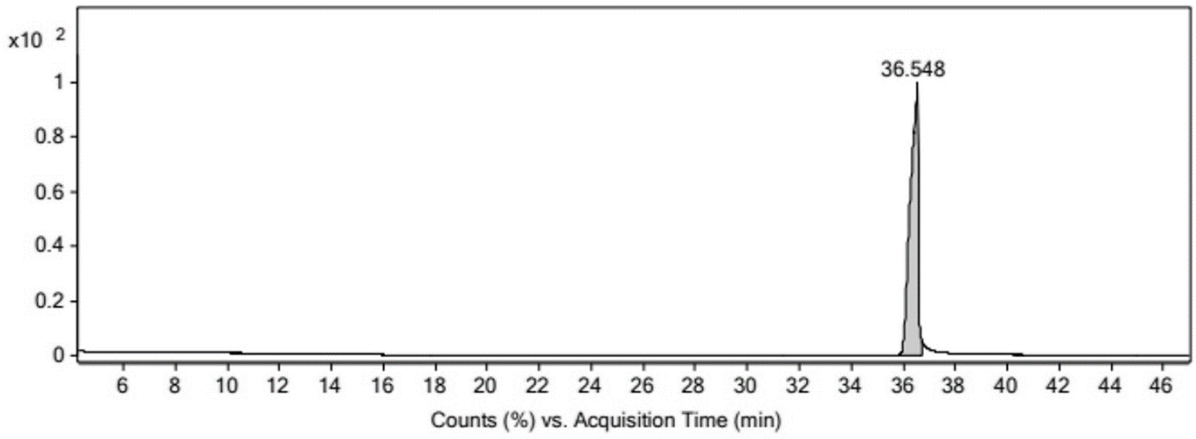

Appendix 37: Gas chromatogram of **1b**

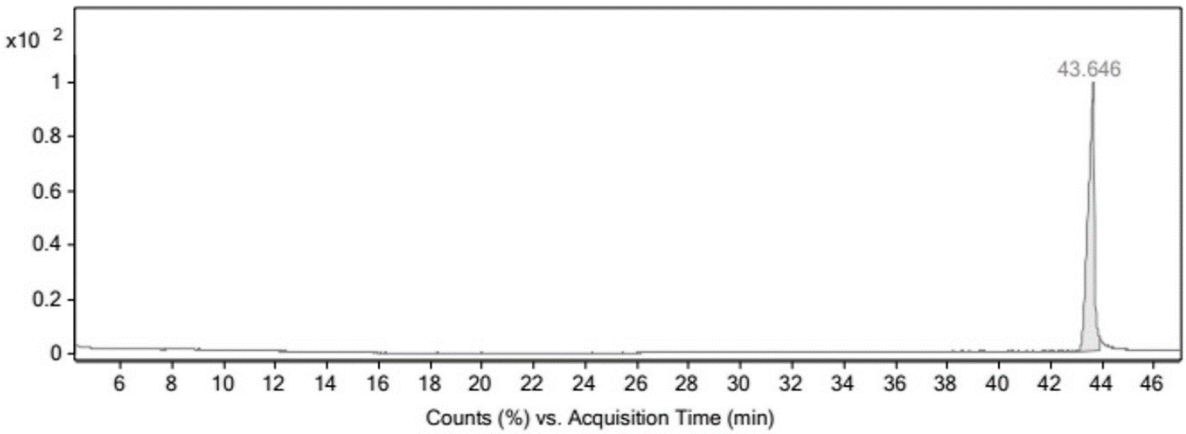

Appendix 38: Gas chromatogram of **1c**

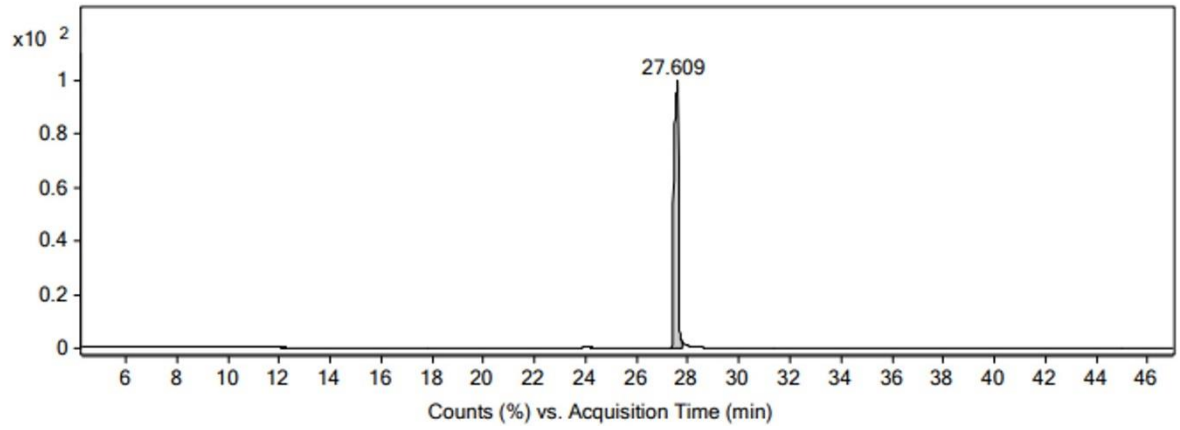

Appendix 39: Gas chromatogram of **2a**

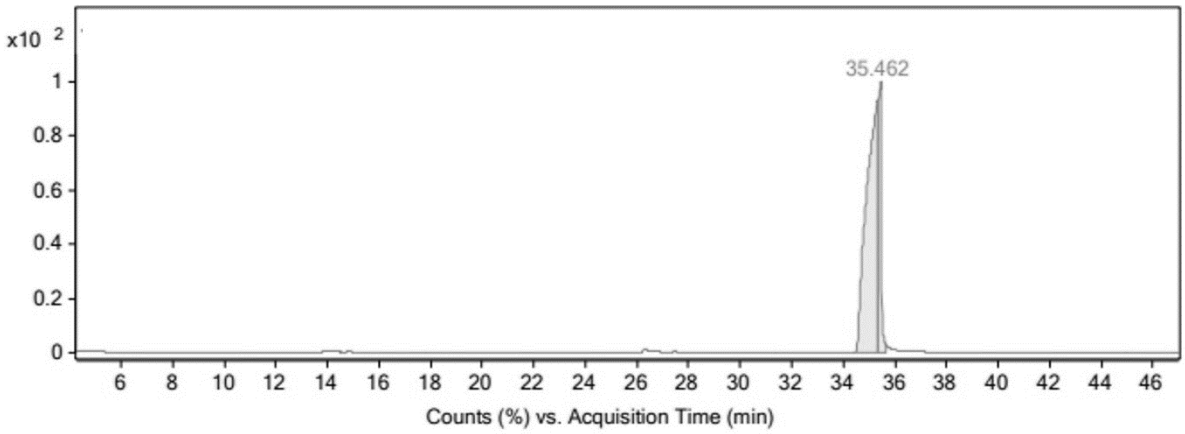

Appendix 40: Gas chromatogram of **2c**

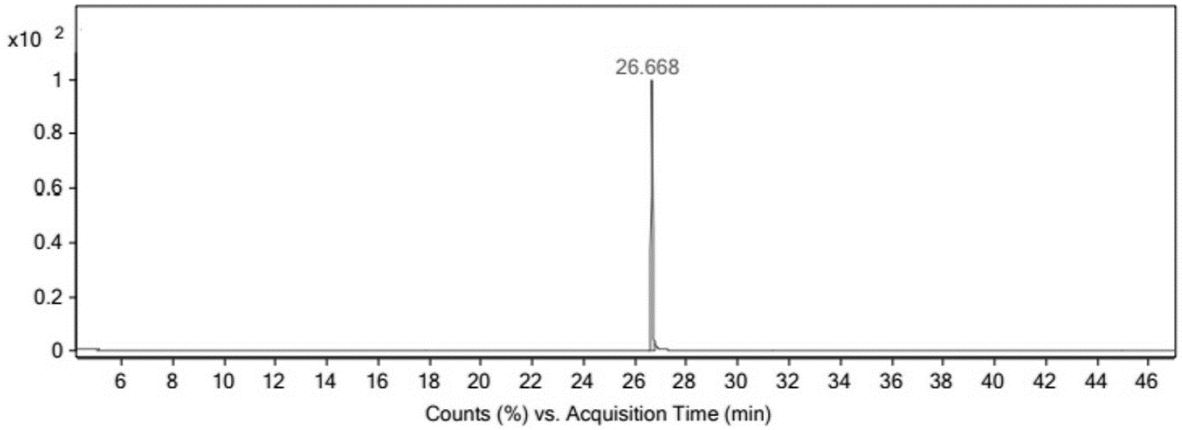

Appendix 41: Gas chromatogram of **3c**

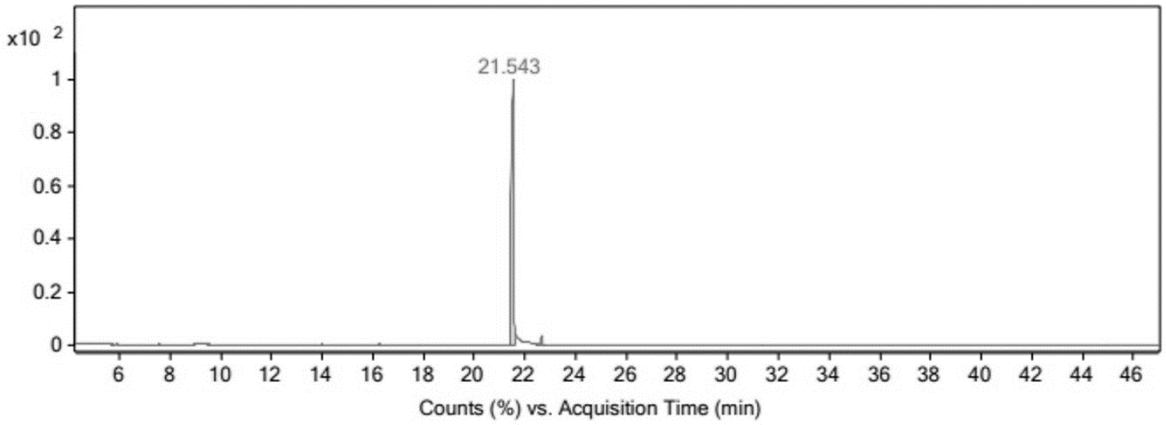

Appendix 42: Gas chromatogram of **4a**

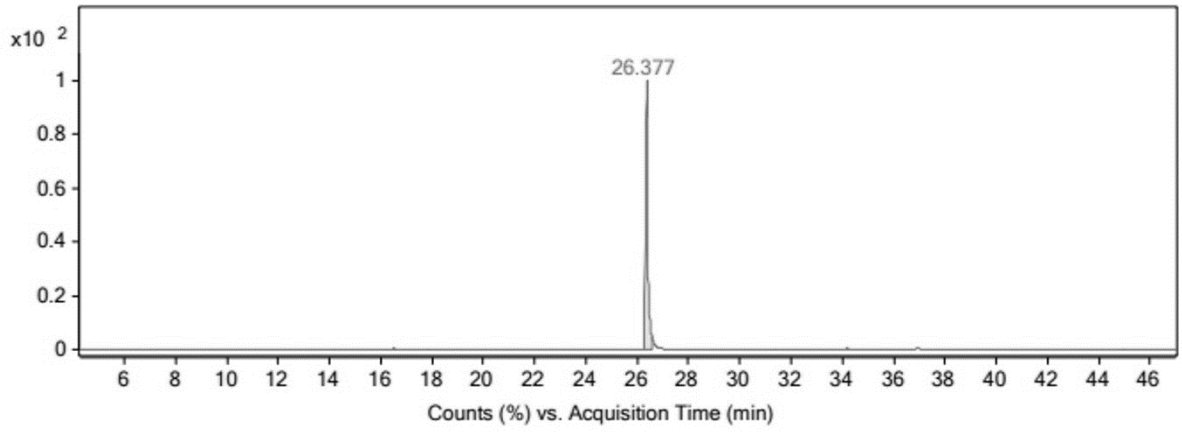

Appendix 43: Gas chromatogram of **4c**

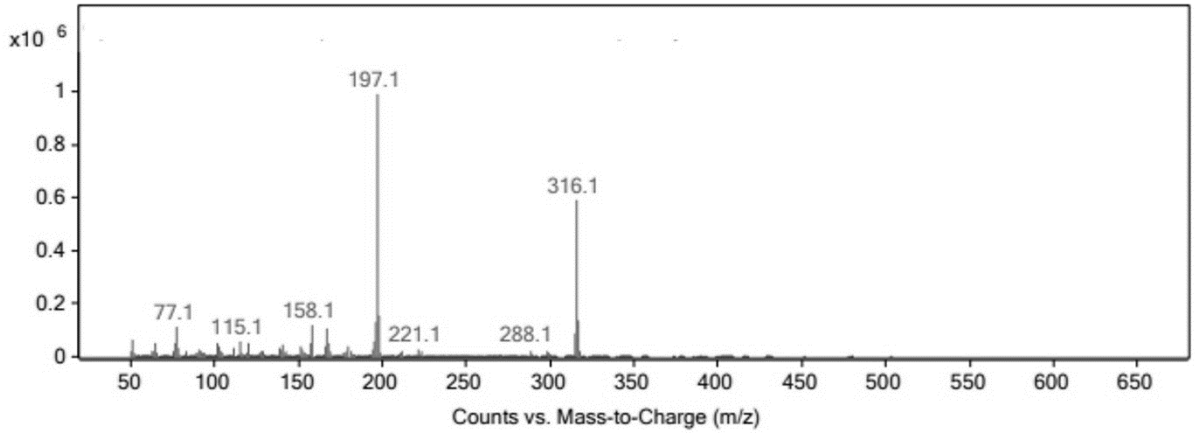

Appendix 44: Mass spectrum of **1b**

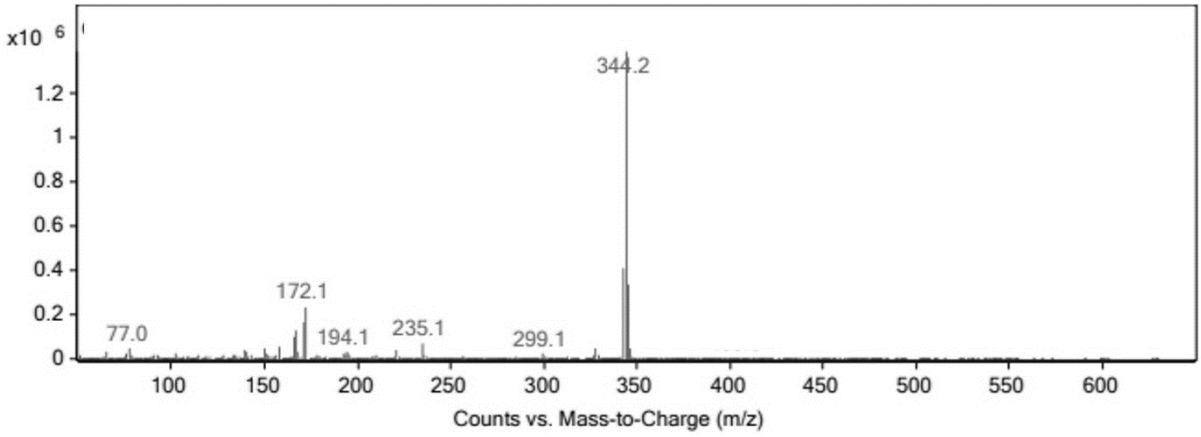

Appendix 45: Mass spectrum of **1c**

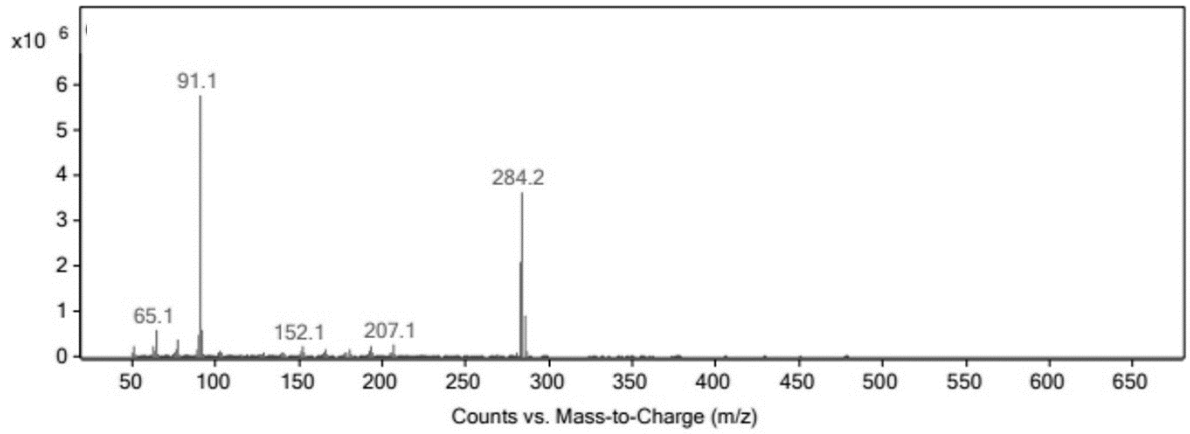

Appendix 46: Mass spectrum of **2a**

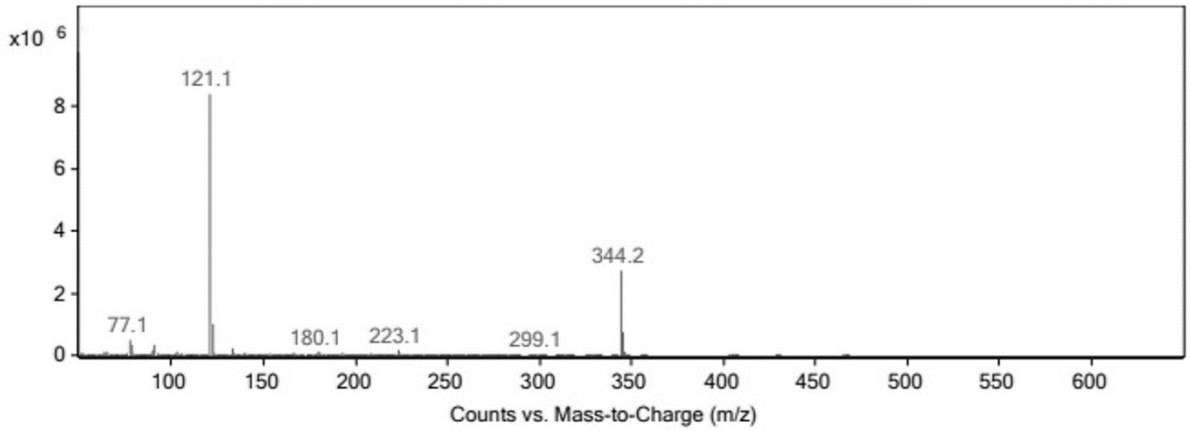

Appendix 47: Mass spectrum of **2c**

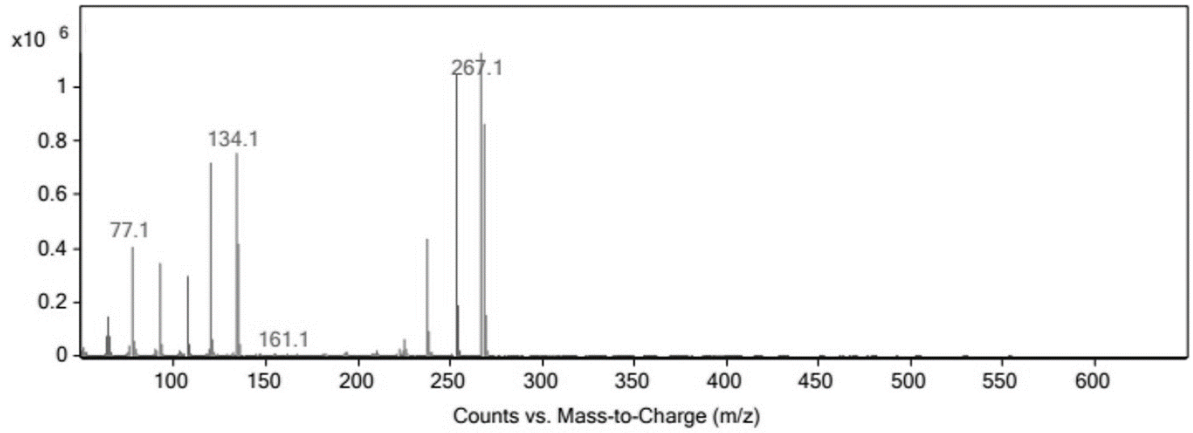

Appendix 48: Mass spectrum of **3c**

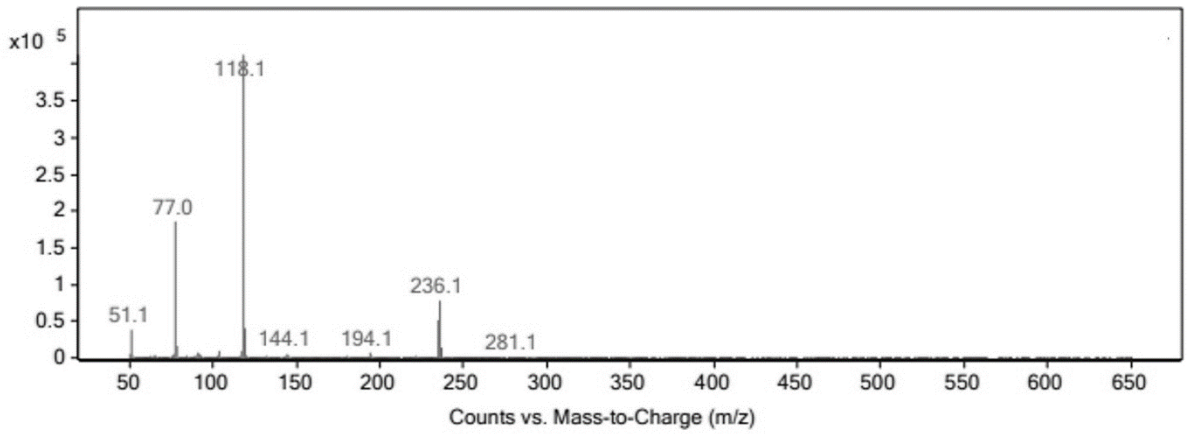

Appendix 49: Mass spectrum of **4a**

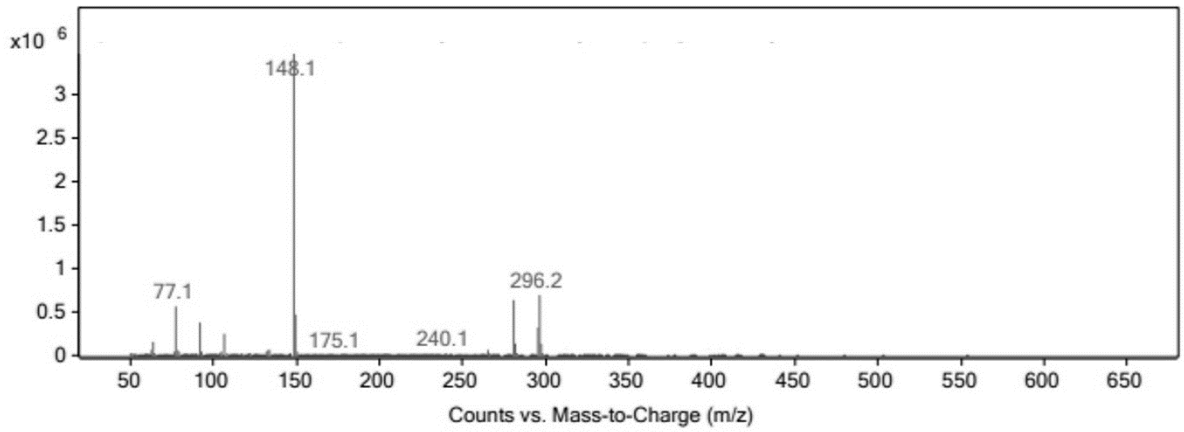

Appendix 50: Mass spectrum of **4c**